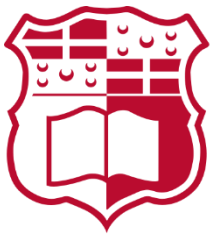

L-Università ta' Malta

Overexpression of PP2A inhibitory subunits promotes expression and activation of oncogenic signatures

PhD Manuscript

Maria Pia Grixti

July 2021

Supervisor: Professor Godfrey Grech

Co-supervisor: Professor Christian Scerri

LIST OF ABBREVIATIONS vii

LIST OF FIGURES xi

LIST OF TABLES xv

ACKNOWLEDGEMENTS xii

ABSTRACT xix

CONTENTS

CHAPTER I- INTRODUCTION 1

1.1 THE PHOSPHATASE ENZYME PP2A 2

1.1.1 Molecular Structure and Diversity of the PP2A Complex 2

1.1.2 PP2A Mutations and Cancer Occurrence 6

1.2 INHIBITION OF THE PP2A COMPLEX 9

1.2.1 IGBP1 10

1.2.2 SET and SETBP1 10

1.2.3 CIP2A 12

1.3 CELLULAR PATHWAYS AND TARGETS OF PP2A 13

1.3.1 PI3K/Akt and p70 S6K/mTOR Pathways 14

1.3.2 Mediation of Cap-Dependent Translation 16

1.3.3 Effect of PP2A on Akt Pathway 17

1.3.4 c-MYC as a PP2A Target 18

1.3.5 Wnt/Beta-Catenin Pathway as a PP2A Target 19

1.3.6 RAF, MAPK, ERK Pathway as a PP2A Target 20

1.4 PP2A ACTIVATION AS A POTENTIAL THERAPEUTIC TARGET 20

1.4.1 Targeting Kinases 20

1.4.2 Targeting Phosphatases 20

1.4.3 Targeting PP2A Catalytic Subunit for Drug Development 21

1.5 OBJECTIVES OF THE INVESTIGATION 25

CHAPTER II- EXPERIMENTAL METHODOLOGY 26

2.1 EXPERIMENTAL OUTLINE 27

2.2 SELECTION OF SUITABLE BREAST CANCER CELL LINES 28

2.2.1 Preparation of cDNA from Various Cell Lines 28

2.2.2 Gene Expression by Real-Time PCR (RT-PCR) 29

2.2.3 Analysis of Real-Time PCR (RT-PCR) data 31

2.2.4 Confirmation of Which Cell Lines Have Lowest Levels of Inhibitors Using Immunocytochemistry (ICC) Techniques 32

2.3 ISOLATION AND CLONING OF PP2A INHIBITORS 34

2.3.1 Primer Design 34

2.3.2 Optimization of Double Digest Experiment 40

2.3.3 Primer Optimisation by Gradient PCR 44

2.3.4 PCR for Each PP2A Inhibitor 44

2.3.5 DNA Extraction from 1 % Agarose Gel 47

2.3.6 Ligation of PP2A Inhibitors with Linearised pIRES2-AcGFP1 48

2.3.7 Transformation of Bacterial Cells 49

2.4 TRANSFECTION OF SELECTED CELL LINES 50

2.4.1 Preparation of RPMI Medium 50

2.4.2 Culturing of Selected Cell Lines 50

2.4.3 Transfection Experiment 51

2.5 WESTERN BLOTTING 53

2.5.1 Preparation of Cell Pellets 53

2.5.2 Preparation of Protein Lysates 53

2.5.3 Bradford Protein Assay 54

2.5.4 Polyacrylamide Gel Electrophoresis 55

2.5.5 Gel Transfer 58

2.5.6 Exposure to Primary and Secondary Antibody 58

2.6 QUANTIGENE™ ASSAY 60

2.7 POLYSOME BOUND RNA PROFILING 61

2.7.1 Preparation of Cell Pellets 62

2.7.2 Preparation of Sucrose Gradients 62

2.7.3 Lysis of Cell Pellets 64

2.7.4 Sucrose Gradient Centrifugation 64

2.7.5 Harvesting The Gradient 66

2.7.6 Percent Polysome Recruitment Studies 67

2.8 DIGITAL WESTERN TECHNOLOGY 69

2.8.1 Analysis of DigiWest Data 71

2.8.2 Comparison of DigiWest Results to Patient Material 72

2.8.3 Statistical Analysis 75

CHAPTER III – RESULTS 76

3.1 SELECTION OF CELL LINES FOR ECTOPIC EXPRESSION OF CIP2A, SET AND IGBP1 77

3.2 THE PP2A ACTIVATOR, FTY720, DOES NOT AFFECT TRANSCRIPTION LEVEL OF PP2A DOWNSTREAM TARGETS 81

3.3 CIP2A, SET AND IGBP1 OVEREXPRESSED IN SELECTED CELL LINES 83

3.4 DIFFERENTIAL GENE EXPRESSION USING POLYSOME BOUND RNA 86

3.5 EIF4E, PKC, ERK AND BETA-CATENIN ARE REGULATED BY PP2A INHIBITORY SUBUNITS 93

3.6 COMPARISON TO PATIENT MATERIAL 107

3.8 OPTIMISATION EXPERIMENTS 121

3.8.1 Isolation of Transfected Cells 121

3.8.2 Optimization of Polysome Bound Methodology 123

CHAPTER IV- DISCUSSION 124

4.1 OVERVIEW 125

4.2 RESEARCH OUTCOMES 129

4.2.1 Overexpression of PP2A Inhibitory Subunits Result in a Common Protein Signature and Phospho-profile 130

4.2.2 PP2A Inhibitory Subunits Promote Translation Initiation 130

4.2.3 PP2A Inhibitory Subunits Modulate ERK Expression 120

4.2.4 PP2A Inhibitory Subunit Overexpression Results in Phosphorylation of PKC Alpha 133

4.2.5 PP2A Inhibitory Subunits Dephosphorylate Ribosomal Protein p70 S6 Kinase 134

4.2.6 PPP2R2A Correlates with Beta-Catenin (CTNNB1) Protein Levels 135

4.2.7 PP2A may be Involved in Metastatic Disease 138

4.3 SELECTION OF RESOURCES AND METHODS 139

4.3.1 Selection of Suitable Breast Cancer Cell Lines 139

4.3.2 Isolation and Cloning of PP2A Inhibitors 140

4.3.3 Transfection of Selected Cell Lines 141

4.3.4 Western Blotting 142

4.3.5 Polysome Bound RNA Profiling 142

4.3.6 Digital Western Technology 144

4.3.7 Limitations of TCGA dataset 144

4.4 SUMMARY AND CONCLUSION 146

4.5 FUTURE EXPERIMENTATION 148

REFERENCES 152

APPENDIX A: RAW DATA 162

APPENDIX B: ETHICAL APPROVAL 178

APPENDIX C: PUBLICATION 180

LIST OF ABBREVIATIONS

4E-BP1	eukaryotic translation factor 4E-binding protein 1
ADT	Anethole dithiolethione
AFI	Average Fluorescence Intensity
Akt	v-akt murine thymoma viral oncogene homolog kinase
AML	Acute myeloid leukaemia
AMP	High adenosine monophosphate
AMPK	AMP-activated kinases
ApoE	Apolipoprotein E
APS	Ammonium Persulfate
ATP	Adenosine triphosphate
AURKA	Aurora Kinase A
bp	Base pairs
BSA	Bovine Serum Albumin
CDH1	E cadherin
CIP2A	Cancerous Inhibitor of PP2A
CTNNB1	Beta Catenin
CML	Chronic myeloid leukaemia
CRC	Colorectal cancer

CsA	Cyclosporin A
DTT	Dithiothreitol
DFS	Disease Free Survival
EC	Endothelial cell
eIF2	Eukaryotic translation initiation factor 2
eIF3	Eukaryotic translation initiation factor 3
eIF4B	Eukaryotic translation initiation factor 4B
eIF4E	Eukaryotic translation initiation factor 4E
eIF4F	Eukaryotic translation initiation factor 4F
EMT	Epithelial and mesenchymal transition
EPCAM	Epithelial and cellular adhesion molecule
eNOS	Endothelial NO synthase
ER	Oestrogen receptor
FBS	Foetal Bovine Serum
FFPE	Formalin-fixed paraffin embedded
FTY720	Fingolimod
FK506	Tacrolimus
FN1	Fibronectin
FTY720	Fingolimod
GFP	Green Fluorescent Protein

GβL	G-protein β-subunit
HER2	Human epidermal growth factor receptor 2
hnRNP	Heterogeneous ribonucleoproteins
IGBP1	Immunoglobulin Binding Protein 1
ICC	Immunocytochemistry
IF	Immunofluorescence
IL-2	Interleukin-2
IRES	Internal Ribosome Entry Site
kDa	Kilo Daltons
LB	Luria-Bertani broth
LCMT-1	Leucine carboxyl methyltransferase 1
MCS	Multiple cloning site
MCL1	Myeloid cell leukemia-1
MFI	Mean Fluorescence Intensity
mRNRps	Messenger ribonucleoprotein particles
mTOR	Mammalian target of rapamycin
NO	Nitric oxide
NRQs	Normalised Relative Quantities
ORF	Open reading frame
pb RNA	Polysome bound RNA

PBS	Phosphate Buffered Saline
PDK1	Pyruvate dehydrogenase kinase 1
PgR	Progesterone receptor
PI3K	Phosphoinositol-3 kinase
PKC	Protein kinase C
PLB	Passive Lysis Buffer
PME-1	Phosphatase methylesterase
PME-1	Phosphatase methylesterase 1
PMSF	Phenylmethylsulfonyl fluoride
PP2A	Protein Phosphatase 2A
PP2A-A	A subunit of PP2A
PP2A-B	B subunit of PP2A
PP2A-C	C subunit of PP2A
(p70) S6K	Ribosomal protein S6 kinase / (p70) S6 kinase
RIN	RNA integrity number
Rheb	RAS-homolog enriched in brain
RICTOR	Rapamycin insensitive companion of mTOR
RT-PCR	Real-Time PCR
SAPE	Streptavidin-conjugated R-phycoerythrin
S.O.C medium	Super Optimal broth with Catabolite repression

SDS	Sodium Dodecyl Sulfate
SETBP1/SEB	SET Binding Protein 1
SG2NA	S/G2 nuclear autoantigen
SV40ST	Simian Virus 40 Small t
TBS	Tris Buffered Saline
TGF - β	Transforming growth factor beta
TNBC	Triple negative breast cancer (cell line)
TNF	Tumour Necrosis Factor
TRIS	Tris (hydroxymethyl) aminomethane
TSC1/TSC2	Tuberous sclerosis protein
UTR	Untranslated region
VEGF	Vascular endothelial growth factor
ΔΔCt	Cycles to Threshold (Ct) Method

LIST OF FIGURES

Chapter 1

Figure 1.1: Structure of PP2A and its subunits

Figure 1.2: Main PP2A inhibitory subunits

Figure 1.3: Targets of PP2A and major cellular pathways

Chapter 2

Figure 2.1: Photographic result of the immunocytochemistry technique, using anti-CIP2A antibody on breast cancer cell line HCC1937

Figure 2.2: pIRES2-AcGFP vector map used for cloning

Figure 2.3: Detail of multiple cloning site (MCS) for pIRES2-AcGFP1, the vector chosen for the cloning experiment

Figure 2.4: Double digestion of pDBLeu using different restriction enzymes

Figure 2.5: PCR-amplified inhibitors CIP2A, SET and IGBP1

Figure 2.6: Transfer assembly set up, according to BIO-RAD instructions

Figure 2.7: Steps involved in DigiWest analysis

Figure 2.8: Diagnosis age for the Breast Invasive Carcinoma (TCGA, Firehose Legacy) dataset.

Chapter 3

Figure 3.1: Expression of CIP2A [A] and SET [B] using real-time PCR

Figure 3.2: The effect of PP2A reactivation in selected cell lines

Figure 3.3: Expression of GFP in MCF-7 and MDA-MB-453 following transfection

Figure 3.4: Measuring expression of CIP2A, SET and IGBP1 using Western Blot analysis

Figure 3.5: Electropherograms of RNA fractions obtained from MDA-MB-453 cell line transfected with CIP2A, following sucrose density gradient centrifugation

Figure 3.6: Capillary electrophoresis of RNA fractions taken from the MDA-MB-453 cell line transfected with CIP2A, following sucrose gradient centrifugation

Figure 3.7: Percent polysome recruitment of c-MYC following overexpression of CIP2A, SET and IGBP1 in MCF-7, HCC1937 and MDA-MB-453

Figure 3.8: CIP2A expression in MDA-MB-453 cells overexpressing SET and CIP2A. The CIP2A antibody #1426 was used in the antibody panel in this DigiWest run

Figure 3.9: Protein quantification bar charts for c-MYC and beta-catenin using the DigiWest technology

Figure 3.10: Protein quantification bar charts for 4E-BP1 phosphoSer65 and 4E-BP1 phosphoThr37/Thr46 using the DigiWest technology

Figure 3.11: Protein quantification bar charts for p70 S6 kinase and p70 S6 kinase phosphoThr389 using the DigiWest technology

Figure 3.12: Protein quantification bar charts for PKC alpha-phosphoThr497 and PKC alpha/beta II-phosphoThr638/Thr641 using the DigiWest technology

Figure 3.13: Protein quantification bar charts for ERK1/2 using the DigiWest technology

Figure 3.14: Total protein expression using DigiWest analysis (protein signature)

Figure 3.15: Co-expression of CIP2A at [A] RNA and [B] protein level using TCGA Breast Invasive Carcinoma dataset

Figure 3.16: Oncoprint generated from cBioPortal using TCGA dataset Breast Invasive Carcinoma

Figure 3.17: Higher expression of AURKA and PPP2R2A is common in lymph node metastasis and may require more advanced surgery

Figure 3.18: Separation of transfected and non-transfected cells using BIOFACS Cell Sorter

Chapter 4

Figure 4.1: PKC alpha activity stabilizes MYC protein

Figure 4.2: Plot showing the correlation between mRNA expression (RNA Seq data) and the Protein expression (z-score level; mass spectrometry) of CIP2A [A] and CTNNB1 (beta-catenin) [B]

LIST OF TABLES

Chapter 1

Table 1.1: The PP2A trimeric enzyme complex has diverse subunits

Table 1.2: Targets of PP2A and their role in the cellular environment

Table 1.3: The therapeutic potential of PP2A (adapted from Chen, et al., 2013)

Chapter 2

Table 2.1: Reaction mixture for RT–PCR for housekeeping gene *RPL13A*, and the target genes *CIP2A* and *SET*

Table 2.2: Information for forward and reverse primers for PP2A inhibitors CIP2A, SET and IGBP1

Table 2.3: Digestion mixture preparation for double digestion of pDBLeu with selected restriction enzyme pairs

Table 2.4: PCR reaction mixture for PP2A inhibitors CIP2A, SET and IGBP1

Table 2.5: Chemicals used to prepare 10 x running buffer for Western Blot gel electrophoresis

Table 2.6: Chemicals used to prepare the 12.5 % resolving gel and 5 % stacking gel for Western Blot gel electrophoresis

Table 2.7: Reagents required for preparation of sucrose gradients, necessary for polysome bound RNA profiling

Table 2.8: Preparation of NP40 buffer, used to lyse the cell pellets and release the RNA

Table 2.9: Clinico-pathological details for the Breast Invasive Carcinoma (TCGA, Firehose Legacy) dataset

Chapter 3

Table 3.1: CIP2A, SET and IGBP1 Immunocytochemistry H-scores, on a panel of breast cancer cell lines

Table 3.2: Normalisation of DigiWest raw data

Table 3.3: Log_2 fold change relative to control, for transfected cell lines

Table 3.4: CIP2A protein co-expression using mass spectrometry data (protein levels)

Table 3.5: Spearman correlation and p-values for a selection of proteins

Table 3.6: Co-occurrence of PP2A inhibitory, regulatory and catalytic subunits, regulators, and protein signature

Table 3.7: Correlation between copy number variations and RNA expression

Table 3.8: Spearman correlation and p-values for PP2A inhibitory and regulatory subunits AURKA CTNNB1 and epithelial markers EPCAM and CDH1

Table 3.9: Bioanalyser Results for non-transfected cell line MDA-MB-453, following sucrose gradient centrifugation, using two different protocols

Chapter 4

Table 4.1: Outcomes resulting from overexpression of PP2A inhibitory subunits

ACKNOWLEDGEMENTS

First of all, I would like to sincerely thank my supervisor Professor Godfrey Grech for his constant patience and advice throughout my research as well as his unfailing enthusiasm. Thanks are extended to my co-supervisor Professor Christian Scerri for having originally encouraged me to pursue this project and for his constant support.

I would also like to heartily thank Dr Christian Saliba, former research officer at the Pathology Department, for having patiently taught me all laboratory techniques. My thanks are extended to Dr Shawn Baldacchino, also a former research officer the Pathology Department, who was always so helpful and supportive in whatever I required.

I am also very grateful to all members of staff at the Allied Research Unit, especially Professor Anthony Fenech and Dr Byron Baron, for offering me their resources and their precious time. I would like to Ms Oriana Mazzitelli, at the Applied Biomedical Science Department, Faculty of Health Services for helping out with the cell-sorting instrumentation. I am thankful to all members of the Molecular Genetics Laboratory, Physiology and Biochemistry Department and the Health Department at the University of Malta, for always being available and supportive.

Finally, I would like to thank my family, primarily my dear mother, who taught me to focus on my goals and pursue them. My thanks are extended to my husband John, and my daughters, Rebekah and Rachel, for their constant love and support throughout these years. Special thanks to my friend Veronica, for her unfailing encouragement. Finally, I would like to thank my dear cousin Anna Marie, as her words, many moons ago, still echo in my ears, triggering me to pursue this dream.

To My Mother,

My Lifelong Admiration

To My Dear Husband,

And My Two Beautiful Daughters

ABSTRACT

The phosphatase enzyme PP2A regulates various signalling pathways, including the mTOR pathway, and is responsible for control of cell growth, proliferation, and apoptosis. In this investigation, the effect of overexpressing the PP2A inhibitory subunits CIP2A, SET and IGBP1 was studied in selected breast cancer cell lines, MCF-7 and MDA-MB-453. Polysome bound RNA studies revealed that recruitment of c-MYC transcript to the polysomes increases significantly upon overexpression of CIP2A, SET and IGBP1 in both MCF-7 and MDA-MB-453. DigiWest technology was then used to measure total protein and phospho-proteins using lysates from MDA-MB-453 cells overexpressing the PP2A inhibitory subunits and compared to the originator cells. A list of proteins that are upregulated upon overexpression (protein signature) as well as a phospho-profile was generated. The protein signature showed upregulation of beta-catenin, MCL1, c-MYC and RICTOR. The shift towards expression of ERK2 upon overexpression of CIP2A, SET and IGBP1 offers an opportunity to further investigate the role of the PP2A inhibitory subunits in Epithelial and Mesenchymal Transition (EMT)-induction. The phospho-profile showed an upregulation of p4E-BP1(phosphoThr37/Thr46) suggesting the release and activation of eIF4E; upregulation of PKC alpha (phosphoThr497/Thr638/Thr641); and dephosphorylation of p70 S6 kinase (phosphoThr389). Correlation of the protein signature with the expression of the PP2A inhibitory subunits was performed using the publicly available patient dataset, namely the Breast Invasive Carcinoma (TCGA), generating an oncogenic signature, also including c-MYC and beta catenin. The results show that the expression of beta-catenin protein is regulated via various components of the PP2A complex and confirm AURKA as the surrogate marker of low PP2A activity.

Chapter I

Introduction

1.1 THE PHOSPHATASE ENZYME PP2A

Protein Phosphatase 2 (PP2 or PP2A) belongs to a group of serine/threonine phosphatases, referred to as the PPP family. PP2A is associated with a variety of signalling pathways, which include DNA replication, transcription, translation, cell growth and apoptosis (Peyssonnaux, et al., 2001; Qi, et al., 2011; Silverstein, 2002; Zhang, et al., 2012). Experiments have shown and proven that an inactive PP2A induces human cell transformation, with inhibition being possible through the Simian virus 40 small t (SV40ST) antigen binding to PP2A. Malignant transformation of human and rat cells can be induced with a variant of the SV40ST, mutated with only the PP2A inactivation domain. Conversely, the SV40ST antigen can no longer induce cellular transformation when it loses its PP2A binding site (Hahn, et al., 2002). Therefore, PP2A can regulate important cell pathways and is responsible for the control of tumorigenesis.

1.1.1 Molecular Structure and Diversity of the PP2A Complex

PP2A consists of several subunits that combine to affect a variety of substrates. In addition, its activity can be regulated through other regulatory subunits that bind to the complex. An understanding of PP2A's structure and its interactions with other compounds shed lights on its activity and mode of regulation.

Essentially, PP2A is a heterotrimer complex composed of a variable B subunit and active core dimer that can occur freely. The latter consists of a structural (scaffolding) subunit (A subunit – 65 kDa) and a catalytic subunit (C subunit – 36 kDa).

Figure 1.1 shows the structure of PP2A as well as its subunits, while Table 1.1 illustrates its heterogeneity. There are four known PPP2A-B subunit families (B, B', B" and B'"). In addition, there are also two slightly different transcripts of the other subunit types (A and C), which are in turn coded for by different genes.

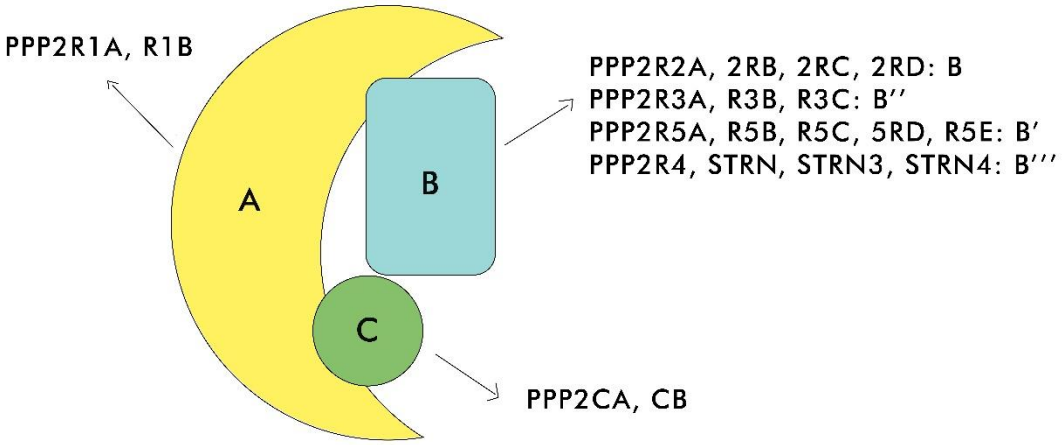

Figure 1.1: Structure of PP2A and its subunits (*Adapted from O'Connor, et al., 2018)*..Structurally, PP2A is a heterotrimer complex composed of a scaffolding subunit **A**, shown in yellow, a catalytic subunit **C**, shown in green, and a regulatory subunit **B**, shown in blue. The figure shows that the **A** and **C** subunits have two isoforms each, while the **B** subunits are diverse. Low expression or loss of function of PPP2R5A and deletion of PPP2R2A are a common occurrence in several cancers of different origin (Besse, et al., 2016; Baldacchino, et al., 2014).

Table 1.1: The PP2A trimeric enzyme complex has diverse subunits

PP2A subunits					
Structural Subunits, A	**Regulatory Subunits, B**				**Catalytic Subunits, C**
	Regulatory Subunit Family B	Regulatory Subunit Family B'	Regulatory Subunit Family B"	Regulatory Subunit Family B"'	
PPP2R1A (Aα or P65α)	PPP2R2A (B55α or PR55α)	PPP2R5A (B'56α or PR61α)	PPP2R3A (B"α or PR72α)	PPP2R4 (B"' or PR53)	PPP2CA
PPP2R1B (Aβ or P65β)	PPP2R2B (B55β or PR55β)	PPP2R5B (B'56β or PR61β)	PPP2R3B (B"β or PR70β)	Striatin (STRN or PR110)	PPP2CB
	PPP2R2C (B55γ or PR55γ)	PPP2R5C (3 isoforms: B'56γ1, B'56γ2 and B'56γ2 or PR61γ1, PR61γ2 and PR61γ3)	PPP2R3B (PR48)	Striatin-3SG2NA (STRN3 or PR93)	
	PPP2R2D (B55δ or PR55δ)	PPP2R5D (B'56δ or PR61δ)	PPP2R3C (B"γ or PR72γ)	Striatin-4 (STRN4)	
		PPP2R5E (B'56ε or PR61ε)			

Adapted from: Janssens, et al., 2005; "GeneCards - The Human Gene Compendium," 2013; Gray, et al., 2013; Laine, 2013; Seshacharyulu, et al., 2013.

In the case of the A structural subunit, there exist two transcripts (PPP2R1A and PPP2R1B) which are share 86 % identity in the primary amino acid sequence (Seshacharyulu, et al., 2013). They are coded by genes that are located on chromosome bands 19q13.41 and 11q23.2. Both genes are expressed, which indicates that they are structurally and functionally very much alike. PPP2R1A is 90 % more abundant than PPP2R1B (10 %). Studies in *Xenopus* have however shown that PPP2R1B occurs at very high levels, from egg formation, to fertilization, to development of the embryo. The ratio between the two transcripts is then restored, implying that there may be a link with primary development (Ruediger, et al., 1994; Seshacharyulu, et al., 2013).

The catalytic subunit C also has two transcripts (PPP2CA and PPP2CB) which are both expressed and share 97 % of their sequence. However, PPP2CA occurs in ten-fold more quantities than PPP2CB. They are coded by chromosome bands 5q23-q31 and 8p12-p11.2 respectively. Although the C subunit transcripts are so similar, removal of the PPP2CA gene results in death of mice embryos, indicating that one transcript does not replace the other (Gu, et al., 2012). The C-terminal of the catalytic subunit is unique and very well conserved, with it serving as the binding site for the A and B subunits (Seshacharyulu, et al., 2013).

The B subunits of PP2A have common or overlapping binding sites, located on the PP2A structural subunit A. Hence, this explains the fact that one B subunit at a time can occur at the binding site located on subunit A (Hendrix, et al., 1993). As a consequence, due to the diversity of B subunits, coded by genes located in various parts of the genome, a multitude of diverse PP2A complexes exist, with different regulatory subunits that are specific to the tissue in question. In the case of the B55 family; the B55α and B55β tend to be expressed in a variety of tissues, but B55γ and B55δ are expressed in brain regions. In addition, each distinct subunit is found in a particular area of the brain, and more specifically, in different

parts of the brain cell (nuclear or cytoplasmic locations). This implies that PP2A activity depends on which B subunit is attached to its binding site, which is supported by the fact that the PP2A active core dimer is present homogeneously in tissues, cytoplasm, and nucleus (Hemmings, et al., 1990).

The B subunit of PP2A (PP2A-B) regulates substrate specificity of the enzyme. Depending on the binding of specific B isoforms, PP2A is localised into different cellular compartments. This restricts activity to specific substrates in the cellular compartment. PPP2R5A, PPP2R5B and PPP2R5E are programmed to leave the nucleus and enter the cytoplasmic regions. On the other hand, PPP2R5C and PPP2R5D do not have this inbuilt program and are therefore restricted to the nucleus (Slupe, et al., 2011).

The PP2A-C subunit has a flexible peptide tail motif at the carboxyl terminus that spans residues 294-309. In this location, there are two main regulatory residues: tyrosine at residue 307 (Y307) and leucine 309 (L309). Phosphorylation at Y307 and demethylation at L309, cause inactivation of PP2A (Chen, et al., 1992; Sontag, et al., 2010; Sents, et al., 2013).

The binding of the B subunits to the PP2A active dimer occurs by post-translational control. This is a result of methylation and phosphorylation, occurring at the residues leucine 309 (L309) and tyrosine 307 (Y307) respectively on both isoforms of the catalytic subunit. Phosphorylation at Y307 prevents the association of the B and B’ subunits with the active core dimer, while B" subunit binding is unaffected. Methylation at L309 affects B55 binding, while other subunits are unaffected (Xu, et al., 2006; Slupe, et al., 2011).

Demethylation of L309 is catalysed by phosphatase methylesterase (PME-1) and methylation is catalysed by leucine carboxyl methyltransferase 1 (LCMT-1). Post-translational modification is therefore of paramount importance as regards the constitution of PP2A (Stanevich, et al., 2011).

1.1.2 PP2A Mutations and Cancer Occurrence

Research has shown that reduced activity of PP2A is a common occurrence in several cancers in various tissues (Baldacchino, et al., 2014; Cristobal, et al., 2014). According to Watt, et al., (2017), deletion of PP2A genes as well as loss of the PP2A regulatory subunits, is observed in breast tumours, supporting the prime importance of PP2A as a breast cancer therapeutic target.

Over the past years, biomarkers used to predict how breast cancer patients will respond to therapy are the oestrogen receptor (ER), progesterone receptor (PgR), and human epidermal growth factor receptor 2 (HER2). Patients that are diagnosed positive for these biomarkers are given a specific therapy, including endocrine treatment in the case of ER and PgR positive patients, and the administration of monoclonal antibody and trastuzumab, for HER2-positive patients. On the other hand, patients who are negative for these three biomarkers, referred to as triple negatives (TNBC), do not respond to these specific therapies, creating a worse scenario. Studies within the group of researchers in the Department of Pathology at the University of Malta have shown that three TNBC cell lines are sensitive to FTY720, a PP2A activator. Therefore, PP2A may be considered as a possible target for cancer therapy, specifically breast cancer (Baldacchino, et al., 2014).

Research has shown that the low level of PP2A activity in cancer patients may be the result of various factors, including mutations, which directly or indirectly

affect the three subunits A, B and C. Mutations in the PP2A scaffold subunit A possibly inhibit the effective binding of both B and C subunits, preventing proper activity of PP2A. Mutations in *PPP2R1A* and *PPP2R1B*, as well as reduction in heterozygosity, is a common occurrence in various cancer types, including malignancies found in the colon, breast, liver and lung (Wang, et al., 1998; Calin, et al., 2000; Takagi, et al., 2000; Janssens, et al., 2005; Chou, et al., 2007; Ruediger, et al., 2011). Somatic missense mutations were also detected in *PPP2R1A* in high-grade serous endometrial tumours (Stebbing, et al., 2013).

A higher frequency of alterations occurs in *PPP2R1B* in lung cancer patients. It has also been proven that *PPP2R1B* is mutated in 13 % breast cancers. The consequence is that the B and C subunits cannot attach correctly. A deletion mutation in PPP2R1B is translated into a truncated protein that prevents attachment to the catalytic subunit of the PP2A complex (Wang, et al., 1998). Correct assembly of the PP2A active core dimer is therefore negatively affected. *PPP2R1B* has in fact been considered as a tumour suppressor gene, since it is absent in human breast cancer patients (Janssens, et al., 2005; Sablina, et al., 2007).

1.2 INHIBITION OF THE PP2A COMPLEX

Since PP2A regulates a diversity of signalling pathways, it also needs to be controlled by inhibitory subunits. The main inhibitory subunits are Immunoglobulin Binding Protein 1 (IGBP1), also referred to as alpha4, SET nuclear oncoprotein (SET) and SET Binding Protein 1 (SETBP1) and Cancerous Inhibitor of PP2A (CIP2A) (**Figure 1.2**).

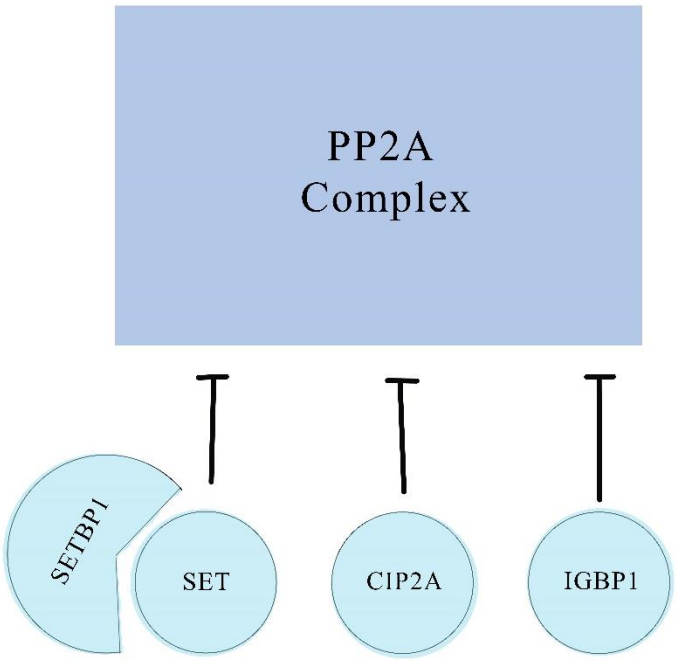

Figure 1.2: Main PP2A inhibitory subunits (*Adapted from: Grech, et al., 2016).* The main inhibitory subunits for the PP2A heterotrimer complex are SET, CIP2A and IBGP1. SETBP1 binds to SET, preventing the latter from degradation.

1.2.1 IGBP1

IGBP1 is an inhibitory subunit that binds with PP2A. As a result of this interaction, PP2A's activity and specificity to substrate becomes modified (Kloeker, et al., 2003). The structural A and variable B PP2A subunits become displaced and IGBP1 binds to the catalytic C PP2A.

IGBP1 was shown to be overexpressed in primary breast cancer when compared to matched adjacent non-tumour tissues (Chen, et al., 2011). Of interest, oestrogen downregulates miRNA-34b (Lee, et al., 2011), a known suppressor of IGBP1 expression, leading to overexpression of IGBP1 in ER+ breast cancer. In addition, the rs4938723 C<T polymorphisms in the promoter region of pri-miR-34b/c results in low miRNA-34b expression and is associated with enhanced IGBP1 expression and low survival rate of triple negative breast cancer patients (Tsiakou, et al., 2019). The proliferative capacity of IGBP1 expression was shown in an erythroid progenitor model. IGBP1 overexpression resulted in a TGFβ-dependent block of erythroid differentiation and enhanced proliferation (Grech, et al., 2008). In addition, expression of IGBP1 is mTOR-dependent and required Stem Cell factor signalling for polysome recruitment of the IGBP1 transcript. Details of the mTOR pathway are documented in Section 1.3.1 of this introductory account.

1.2.2 SET and SETBP1

The oncoprotein, SET (I2PP2A) is a PP2A inhibitory subunit. SETBP1 protects SET from protease cleavage and hence stabilises SET protein (Cristóbal, et al., 2010). In triple negative breast cancer, the miRNA, miR-211-5p is significantly

downregulated resulting in increased expression of SETBP1 and formation of the PP2A/SET complex, promoting proliferation and invasion (Chen, et al., 2017).

The phosphatase activity of PP2A is inhibited by the expression of the PP2A inhibitor SET in chronic myeloid leukaemia (CML) patients (Neviani, et al., 2005). This mechanism has been studied extensively. SET is overexpressed in CML resulting in increased phosphorylation of the BCR-ABL1 fusion protein. Reactivation of PP2A with the activator, FTY720 led to growth suppression, enhanced apoptosis, restored differentiation, and decreased *in vivo* leukaemogenesis of BCR-ABL1 positive cells (Neviani, et al., 2005). BCR-ABL1 has been shown to enhance the mTOR pathway (Markova, et al., 2009) and drives other pathways such as the MAPK/ERK/RAS pathway, responsible for communicating signals from receptors at the cell surface to DNA in the nucleus (O'Hare, et al., 2010). Both pathways are linked to PP2A, and the outcomes are possibly a result of its deregulation. The expression of BCR-ABL1 is also related to the phosphorylation at tyrosine 307 of PPP2CA, resulting in PP2A inhibition (Neviani, et al., 2005). This PP2A inhibition maintains the BCR-ABL kinase activity (Lucas, et al., 2011).

In acute myeloid leukaemia (AML) cases SETBP1 is overexpressed due to a translocation that involves the *ETV6* gene (Barjesteh van Waalwijk et al., 2005). The latter codes for a transcription factor protein responsible for blood cell formation. SETBP1 has been found mutated in colorectal carcinomas or lost in the common chromosomal aberrations at 18q21. In fact, more than 60 % of 18q21 aberrations are deletions (Minakuchi, et al., 2001) and are related to various malignancies such as leukaemia, pancreatic and colorectal cancers, and lymphoma.

1.2.3 CIP2A

CIP2A is a PP2A inhibitory subunit, coded by the *KIAA1524* gene on chromosome 3q13.13, known to inhibit c-MYC protein degradation in cancer cells (Melissa, et al., 2007). Overexpression of CIP2A is commonly found in malignancies located in the colon, ovaries as well as in the upper body regions such as the neck and head areas. In addition, it is associated with more aggressive tumours which are at a very advanced stage (Junttila, et al., 2007; Vaarala, et al., 2010; Böckelman, et al., 2011; Teng, et al., 2012; Laine, 2013). CIP2A is overexpressed in 39 % of breast cancer patients and CIP2A expression correlates with aggressive clinical parameters and lymph node positivity in human breast cancer tissues (Come, et al., 2009). Of interest, CIP2A was shown to promote triple negative breast cancer tumour growth following enhanced AKT/p27Kip1 phosphorylation and cell cycle progression (Liu, et al., 2017).

Although CIP2A is considered as a cytoplasmic protein, membranous expression was also observed in ER+ breast cancer patients. CIP2A expression and distribution in the cellular membrane was detected in 21 % of tamoxifen resistant ER+ breast cancer patients and strongly predicts a worse overall survival and disease-free survival in ER+ breast cancer patients (Baldacchino, et al., 2017).

CIP2A depletion suppresses cell growth in human breast tumour and leukaemic cellular models, with no effect on PP2A activity. It has been suggested that CIP2A binds allosterically to PP2A at its B subunit binding interface, thus altering substrate specificity and/or limiting activity (Junttila, et al., 2007; Wang, et al., 2011).

1.3 CELLULAR PATHWAYS AND TARGETS OF PP2A

As mentioned previously, PP2A influences a variety of cellular processes and regulates a number of signalling pathways. Table 1.2 lists the pathways of interest. Pathways that are particularly implicated in breast cancer are discussed in Sections 1.3.3, 1.3.4, 1.3.5 and 1.3.6.

Table 1.2: Targets of PP2A and their role in the cellular environment

Targets of PP2A	Cellular Role	Reference
p70 S6K, mTOR	Cell Proliferation and survival, initiation of the translation process	(Hahn, et al., 2010; Ismail et al., 2013)
PI3K/Akt	Cell Proliferation and Survival	(Alessi, et al., 1996; Sablina, et al., 2010)
RAF, MAPK, ERK	Cell Proliferation and Survival	(Puustinen, et al., 2009; Silverstein, 2002; Stebbing, et al., 2013)
c-MYC	Tumourigenesis	(Mumby, 2007; Sablina, et al., 2010)
Wnt/beta-catenin	Tumourigenesis	(Sablina, et al., 2010; Zhang, et al., 2012)
FoxM1	Transcription factor that controls cell cycle gene expression genes	(Alvarez-Fernandez, et al., 2011)
Bcl-2, caspase-3	Apoptosis	(Silverstein, 2002)
p53, CDC25	Cell cycle key stages and regulation	(Zhang et al., 2012)

1.3.1 PI3K/Akt and p70 S6K/mTOR Pathways

The mTOR (mammalian target of rapamycin) pathway mediates multiple cellular functions critical to tumour initiation, progression, and outcomes, including growth and proliferation. PP2A is responsible for regulating this pathway and keeping it in check, hence, reducing the risk of tumour development. In turn, PP2A inhibitory subunits IGBP1, SET, and CIP2A regulate PP2A.

The basis of the mTOR pathway is as follows. PI3K (Phosphoinositol-3 kinase) is responsible for activation of Akt (v-akt murine thymoma viral oncogene homolog kinase) by phosphorylation at residue threonine 308 (T308) followed by phosphorylation at residue serine 473 (S473). As a result, phosphorylation of Akt results in activation of the mTOR complex (consisting of mTOR, Raptor, G-protein β-subunit like (GβL) and Deptor) by inhibiting the tuberculin sclerosis 1 and 2 complexes (TSC1/TSC2), which act as tumour suppressors. The TSC1/TSC2 complex in turn disables the GTP-binding protein called Ras homolog enriched in brain (Rheb) (**Figure 1.3**).

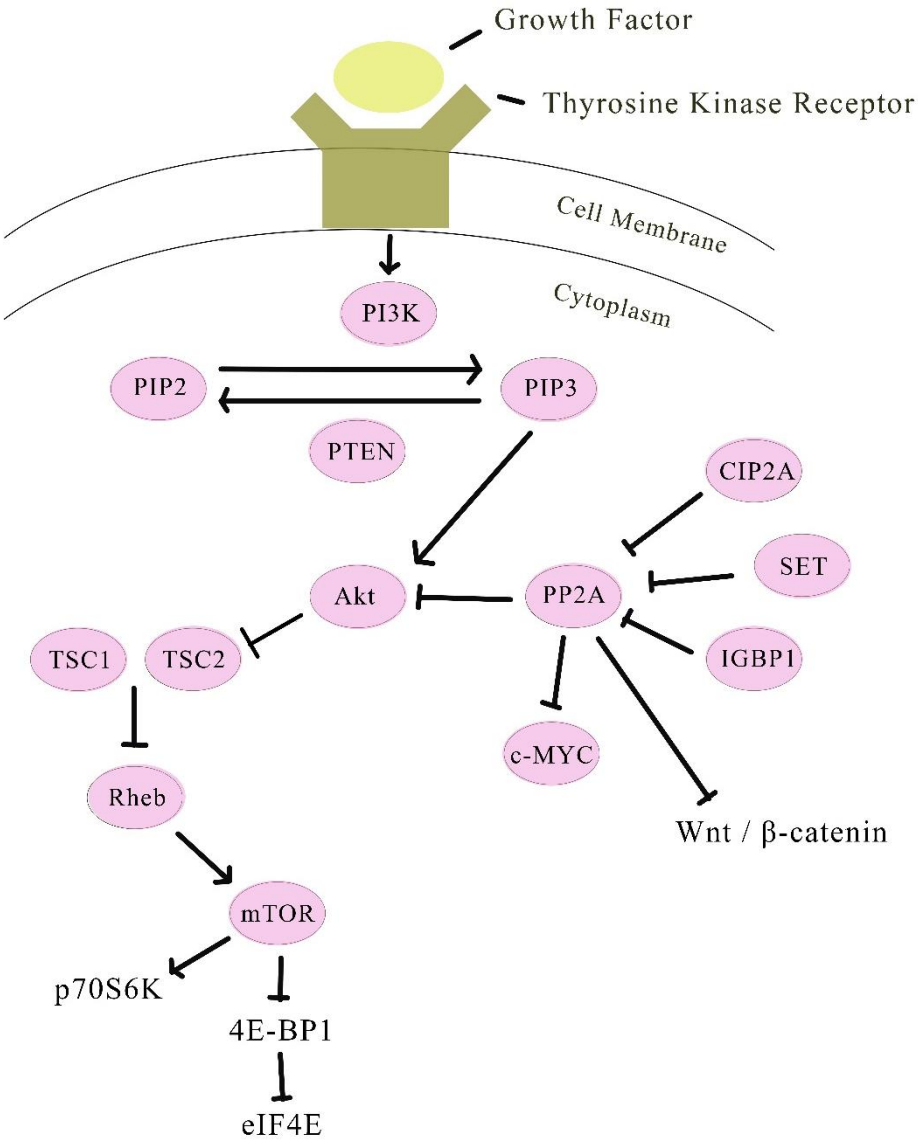

Figure 1.3: Targets of PP2A and major cellular pathways *(Adapted from Zhang, et al,, 2012).* PIP2 and PIP3 are phospholipid pools which can be interconverted through PI3K and PTEN. The latter is a multifunctional tumour suppressor. PP2A directly affects the mTOR pathway, via Akt, automatically affecting p70 S6K and 4E-BP1. PP2A also targets c-MYC and the Wnt/beta-catenin pathway. CIP2A, SET and IGBP1 are PP2A's inhibitory subunits.

1.3.2 Mediation of Cap-Dependent Translation

Cap-dependent translation involves various steps, including translation initiation as the rate limiting step of this process. Translation initiation is regulated through multiple eukaryotic initiation factors (eIFs) that bind together to form a ternary complex which attaches to the mRNA cap through the cap-binding protein, eIF4E. Recruitment of this complex requires the availability of eIF4E which is tightly regulated via the PI3K/AkT/mTOR pathway and the PP2A feedback mechanisms, through phosphorylation of 4E-BP1. PP2A is involved in dephosphorylation of multiple translation initiation factors and their effectors/sequestering complexes. Experimental evidence shows that PP2A dephosphorylates p70 S6K at Thr389 (Westphal, et al., 1999), eIF4E at Ser209 (Li et al, 2010), eIF4B at Ser422 (Xu, et al., 2020) and 4E-BP1 (Nien, et al., 2007). Hence binding of regulatory subunits and inhibitory subunits to the PP2A complex is crucial for cap-dependent translation initiation.

The best measurement of cap-dependent translation initiation efficiency is eIF4E activity. This can be measured as a function of eIF4E expression and 4E-BP1 phosphorylation state. Interestingly, eIF4E expression and p4E-BP1 was found to be positively associated with breast cancer tumour grade in a study using 424 patients (Coleman, et al., 2009). In addition, high eIF4E expression was found to be an indicator of poor prognosis associated with luminal B breast cancers (Pettersson, et al., 2011), supporting the observations that increased eIF4E availability, through loss of PP2A feedback on the mTOR-dependent 4E-BP1 hyperphosphorylated state, is associated with aggressive breast cancer phenotypes. In fact, deregulation of PP2A activity or PP2A substrate selection, collectively representing states of increased inhibitory PP2A subunits or loss of PP2A regulatory subunits, is a common event in breast cancer reaching 59.6 %

of basal breast cancer (Baldacchino, et al., 2014). Loss of regulatory subunits is exemplified by deletion of PPP2R2A (B55α). PPP2R2A is known to target the PP2A complex to dephosphorylate phosphatidylinositol-3-kinase (PI3K)/AkT effectors and eIF4B (Xu, et al., 2020], with a direct effect on translation initiation.

In addition to eIF4E, p70 S6K is an mTOR-dependent kinase with a central role in cap dependent translation initiation. Phosphorylated p70 S6K phosphorylates the eukaryotic translation initiation factor 4B (eIF4B), promoting its binding with eIF3 (Holz, et al., 2005; Mamane, et al., 2006; Ismail, et al., 2013). Hence low PP2A activity or altered PP2A substrate specificity, has a direct effect on p70 S6K phosphorylation and also on eIF4B. Indirectly, eIF3 is not recruited to the complex. Decreased eIF3 is observed in breast cancer and studies using cellular models show that decreased eIF3 expression induce a shift from cap-dependent translation to translation mediated by internal ribosome entry sites, a process shown to be associated with Epithelial Mesenchymal Transition in breast cancer (Han, et al., 2020).

1.3.3 Effect of PP2A on Akt Pathway

Previous studies have shown that TNBC patients have elevated p-Akt which was further supported by evidence showing that tumour suppressor BRCA1 negatively regulates the phosphorylation status of Akt (Xiang, et al., 2008). High levels of p-Akt commonly occur in most breast tumours and human breast cell lines. These findings were accompanied and correlated with a low expression of the BRCA1 protein (Stål, et al., 2003; Al-Bazz, et al., 2009; Xiang, et al., 2011). Possibly Akt activation by BRCA1 is PP2A mediated or accompanied by PP2A downregulation that allows p-Akt overexpression. Similarly, studies carried out on breast cancer cell lines show higher sensitivity of TNBC and BRCA1-deficient

cancers to mTOR inhibitors (Xiang, et al., 2011). This suggests that deregulation of the mTOR effectors and/or regulators plays an important role in the pathology of TNBC.

Increased expression of a mutant PP2A-C at the phosphorylation site Y307 has been identified in individuals with HER2 positive breast tumours. This results in acceleration of disease and loss of PP2A activity. When PP2A activity is restored, cells entered apoptosis (Stebbing, et al., 2013).

Studies have shown that an aggressive melanoma occurs when PPP2R5C is truncated, and as a result, PP2A becomes delocalised. The regulatory B subunit recruited by PP2A is mediated by growth factor signals. This then leads to the dephosphorylation of S6K (Petritsch, et al., 2000; Kloeker, et al., 2003; Sablina, et al., 2010). It is therefore possible that dephosphorylation of S6K by PPP2R5C plays an important role in this phenotype (Hahn, et al., 2010; Slupe, et al., 2011).

1.3.4 c-MYC as a PP2A Target

Figure 1.3 and Table 1.2 illustrate that PP2A inhibits c-MYC oncoprotein. Deregulation of c-MYC has been implicated in breast cancer development and progression, with poor clinical outcomes. Its deregulation results in the loss of tumour suppressors such as BRCA1 and the activation of oncogenic pathways (Grushko, et al., 2004).

Stabilization and accumulation of the c-MYC protein (Zhang, et al., 2012) and amplification of the c-MYC gene (Chrzan, et al., 2001) are two separate events that overexpress the c-MYC protein in breast cancer. Accumulation of c-MYC protein is dependent on PP2A activity, initiated by the phosphorylation of c-MYC

at threonine 58, followed by binding of glycogen synthase kinase-3 (GSK3) (Sears, et al., 2000). In breast cancer patients, 8.6 % have a high expression of CIP2A or SET and 60 % of the basal phenotype is associated with PP2A deregulation (Baldacchino, et al., 2014). CIP2A binds c-MYC protein at serine 62 inhibiting PPP2R5A activity and hence its degradation (Junttila, et al., 2007), resulting in the stabilization and accumulation of the MYC protein (Denk, et al., 2012; Arnold, et al., 2020). Knockdown of CIP2A leads to increased PP2A activity which in turn reduces MYC levels protein (Come, et al., 2009; Junttila, et al., 2007; Mannava, et al., 2011; Niemelä, et al., 2012).

1.3.5 Beta-catenin as a PP2A Target

Figure 1.3 and Table 1.2 also shows that PP2A targets the Wnt/beta-catenin pathway. Beta catenin is a highly conserved and versatile molecule, associated with various functions, including cell adhesion processes. Wnt signalling is responsible for cell fate decisions as well as cancer pathogenesis. The main effector of this signalling pathway is beta-catenin (Polakis, et al., 2012). The latter is regulated via adherins, which recruit beta-catenin to the cell membrane, hence preventing its translocation to the nucleus. Another regulatory mechanism involves the destruction of beta-catenin by phosphorylation. This is achieved through kinases, including GSK3 (Liu, et al., 2002).

Beta-catenin regulation is a complex process. It is interesting to note that destabilization of the membrane bound beta-catenin, possibly by the destruction through kinases results in overall reduction in the amount of beta-catenin present in the cell. However, the beta-catenin in the cytoplasm is now free to translocate to the nucleus, where it serves as a transcription factor for beta-catenin target genes (Orsulic, et al., 1999). As a result of this, Wnt signalling may be enhanced

in the cell. It is highly unlikely that PP2A inhibits the Wnt signalling pathway directly by dephosphorylation of beta-catenin since when the latter is dephosphorylated, it is stabilized (Liu, et al., 2002). Studies have in fact shown that PP2A dephosphorylated GSK3, thus activating it. As a consequence, this kinase will phosphorylate and destroy beta-catenin (Li, et al., 2016).

Although the Wnt/beta-catenin signalling pathway has been implicated in mammary oncogenesis, the link between beta-catenin and breast cancer may still be unclear. A study by Sefidbakht, et al. (2021) showed that cytoplasmic beta-catenin is associated with high grade tumours and ER and HER2 patients. A study by Geyer, et al. (2011) was conducted to determine whether the distribution of beta-catenin is altered in breast cancer patients. In the study, it was shown that reduction of beta-catenin membranous expression and nuclear accumulation occurred in TNBC phenotypes. Nuclear accumulation of beta-catenin, due to incorrect Wnt signalling or mutation of the CTNNB1 gene, actually results in breast cancer, because genes that induce mammary hyperplasia, such as that coding for cyclin D1 are activated (Hatsell, et al., 2003).

An interesting occurrence resulting from changes in cell-to-cell adhesion is Epithelial and Mesenchymal Transition (EMT). In this case, epithelial cells change their morphology and become highly motile, resulting in very rapid metastasis. It is interesting to note that in EMT, E-cadherin is reduced. The latter is responsible for stabilization of membrane-bound beta catenin. As a result, beta-catenin accumulates in the cytoplasm, if it resists degradation (Heuberger, et al., 2010).

1.3.6 RAF, MAPK, ERK Pathway as a PP2A Target

The major function of this signalling pathway is to regulate cell proliferation and apoptosis. PP2A is a negative regulator of the ERK pathway, brought about by dephosphorylation of the ERK kinase (Stebbing, et al., 2013). This kinase has two isoforms, ERK1 and ERK2, which are considered to exhibit functional redundancy. This means that the total ERK quantity, rather than isoform specificity, is required for ERK function (Buscà, et al., 2016).

ERK is a downstream target for the proto-oncogene Ras, which is often mutated in many cancers, including breast cancer. It was discovered that elevated ERK1 or ERK2 activity is a common occurrence in TNBC patients with a short disease-free period (Bartholomeusz, et al, 2012). Thus, levels of ERK may be relevant to determine survival period in the patient.

1.4 PP2A ACTIVATION AS POTENTIAL THERAPEUTIC TARGET

Studies on structure, function and regulation of protein kinases (which catalyse phosphorylation) and phosphatases (which catalyse dephosphorylation) has been thorough and such studies have concluded that both kinases and phosphatases need to be regulated in order to maintain a healthy cellular environment (Bauman, et al., 2002). Drugs have been developed that target both kinases and phosphatases (McConnell, et al., 2009).

1.4.1 Targeting kinases

Using protein kinases as drug targets is becoming increasingly popular. An example of a drug which targets kinases is rapamycin (Sirolimus). This is produced by the bacterium *Streptomyces hygroscopicus*. It acts as an immunosuppressant and is used to prevent organ rejection in transplantation surgery. It prevents activation of T cells and B cells by inhibiting their response to interleukin-2 (IL-2). Rapamycin also has anti-cancer benefits, as it inhibits mTOR, thus suppressing cell transformation. (McConnell, et al., 2009).

1.4.2 Targeting phosphatases

Although targeting kinases has been found effective for cancer therapy, this also affects non-malignant cells, and one must proceed with caution. Growth signals are still important for the maintenance of cells and cannot be eliminated from the cellular environment. Clinical trials as well as thorough research on kinases has automatically led to the possibility of using phosphatases as plausible drug targets (Lyon, et al., 2002; Lazar et al., 2006; Tonks, 2006). FDA approved drugs include the immunosuppressants Cyclosporin A (CsA) and Tacrolimus (FK506). FK506 has immunosuppressant properties and prevents organ transplant rejection. Similarly, FK506 blocks the activation of calcineurin through the formation of complexes with immunophilins (Liu, et al., 1991). CsA is a fungal metabolite (from the fungus *Tolypocladium inflatum*) which was approved for clinical use eight years before its mode of action was deciphered (Cohen, 2002a).

Targeting phosphatases directly makes use of the innate growth suppression mechanism and enhances these processes to attenuate excessive growth. Furthermore, negative feedback pathways often regulate several major molecules

in central pathways involved in cancer development. Therefore, targeting a phosphatase should directly affect cell growth and survival.

1.4.3 Targeting PP2A Catalytic Subunit for Drug Development

As described previously, within the PPP family, the catalytic domains are highly conserved, with functional diversity being a consequence of the regulatory domains and subunits (Barford, et al., 1998). A common structure within the PPP family members is the beta 12 and beta 13 loop. This loop is critical for the binding selectivity of various compounds and is close to the catalytic domain (Connor, et al., 1999). Based on this evidence, it is plausible to design selective regulators for serine/threonine phosphatases, which have an effect on this catalytic subunit region.

Oestrogen receptor (ER) negative breast cancers have recently been associated with the fact that nitric oxide (NO) activates certain pathways and accelerates the cancer process. A common pathway affected in this way is the P13K/Akt signalling pathway (Switzer, et al., 2011). As mentioned previously, this pathway is negatively regulated by PP2A.

Fingolimod (FTY720) is a low molecular weight immunosuppressant commonly found to be effective during organ transplantation and multiple sclerosis (Neviani, et al., 2007). It mirrors myriocin, a natural amino fatty acid antibiotic obtained from the thermophylic fungus *Mycelia sterilia*. FTY720 decreases the movement of T-lymphocytes towards the organ which has been transplanted and thus reduced the possibility of rejection (Chiba, 2005).

Studies have also been carried out using FTY720 *in vitro* in human bladder cancer cells. At a concentration of 10 µM, this drug induced selective apoptosis in these

cells, including fragmented nuclei and condensed chromatin. *In vivo*, decreased cancer growth was also observed using FTY720, since reduction in tumour growth was observed. Thus, FTY720 may be a potential anti-cancer drug (Azuma, et al., 2003).

Angiogenesis (formation of new blood vessels from pre-existing ones) is a natural process that occurs in mammals. However, in pathologic situations, such as tumour development, angiogenesis also occurs. Another characteristic of FTY720 is that it becomes phosphorylated *in vivo* and interacts with vascular endothelial growth factor (VEGF). When this occurs, both tumour-associated angiogenesis and tumour cell proliferation decreases, accompanied by increased apoptosis (LaMontagne, et al., 2006).

FTY720 also causes apoptosis by changing PP2A activity in certain human B- and T-cell leukaemia situations but does not cause apoptosis in normal cells of the bone marrow. FTY720-treated leukemia cells show that the activity of PP2A is actually increased, causing dephosphorylation of various compounds, including Akt, ultimately resulting in cell death (Neviani, et al., 2007). FTY720 therefore resists leukemogenesis, which gives hope to leukemia patients where the common kinase inhibitors for this condition have failed.

It has recently been proven that PP2A activity is reduced in colorectal cancer (CRC) patients. However, restoration of PP2A activity occurs, using the PP2A activator drug FTY720 and as a consequence, reduction of cell proliferation in these patients. Thus, PP2A has been proven to be a strong target for cancer suppression (Christobal, et al., 2014).

The mechanism underlying the effect of FTY720 on PP2A activation is unclear. The waxy lipid molecule ceramide interacts with SET, within the cell

(Mukhopadhyay, et al., 2009). As a result, PP2A activity is increased. Perhaps FTY720 interacts in a similar way within the cell environment. Ceramide could possibly be used as a pharmacological agent, although this molecule is very quickly metabolised. However, using agents that stimulate ceramide biosynthesis, including Vitamin D3, should theoretically enhance PP2A activation. (Switzer, et al., 2011).

1.5 OBJECTIVES OF THE INVESTIGATION

The previous sections have shown that research so far has been directed mainly towards PP2A and the PI3K/Akt/mTOR pathway, with interesting discoveries, which have shed light on possible solutions for human cancer treatment. Research has also been directed towards inhibitors of PP2A , such as IGBP1, SET and CIP2A. To study the effects of these inhibitors in this research, breast cancer cell lines having low levels of the three inhibitors need to be transfected. The main objectives of this research are to:

- Generate cell lines overexpressing PP2A endogenous inhibitors CIP2A, SET and IGBP1 and confirm their expression by Western Blotting.
- Use DigiWest analysis to compare originator cell lines with those overexpressing CIP2A, IGBP1 and SET, in terms of expression and activity of proteins, to generate a protein signature and phospho-profile respectively.
- Use the findings to generate an oncogenic signature related to PP2A activity.
- Correlate the findings with publicly available datasets.

Chapter II

Experimental Methodology

2.1 EXPERIMENTAL OUTLINE

The experimental research has many components and one set of findings led to the design and execution of the next set of experiments. The flow chart given below is an overview of experimental outline, which serves to facilitate understanding of the methodology sequence adopted in this investigation.

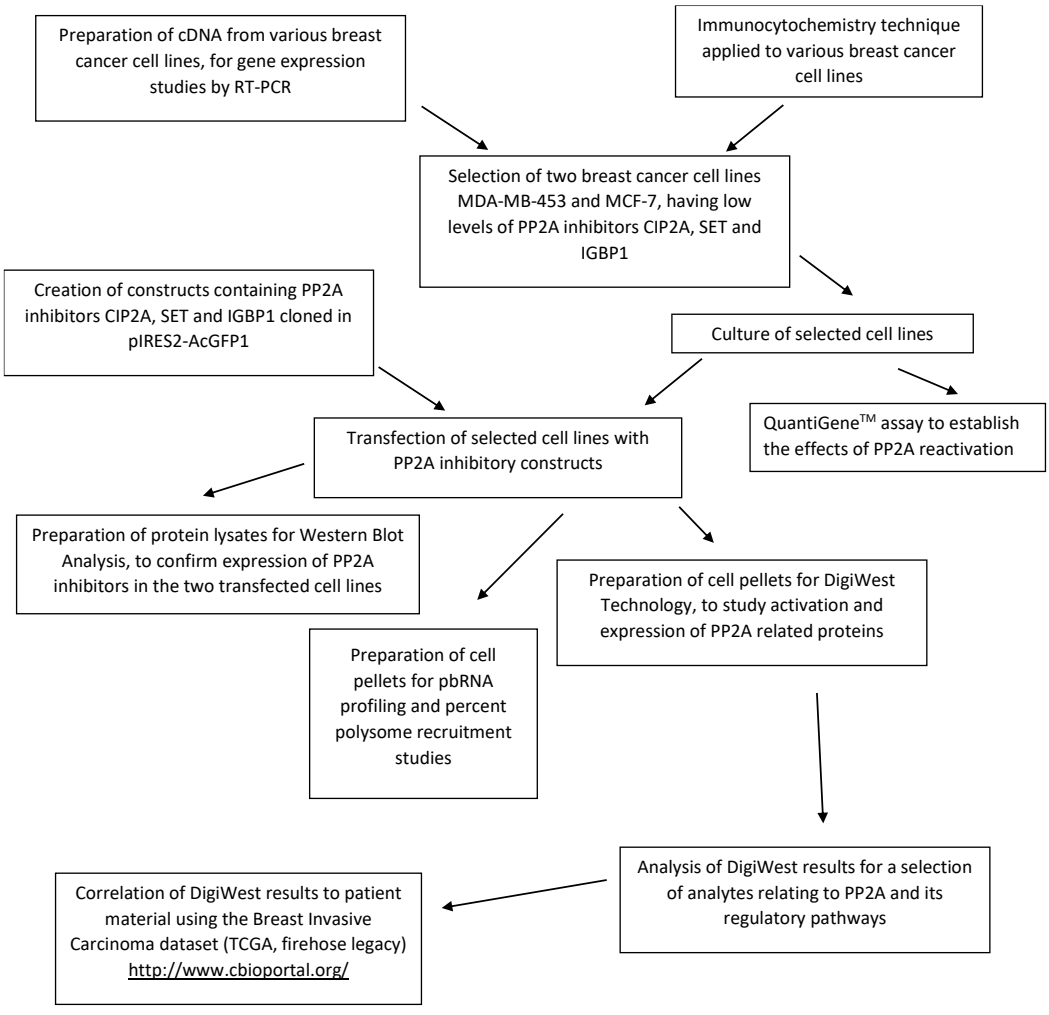

2.2 SELECTION OF SUITABLE BREAST CANCER CELL LINES

In order to investigate the effect of inhibitors CIP2A, IGBP1 and SET on PP2A, two cell lines having low levels of the mentioned inhibitors were identified, using the procedures described below.

2.2.1 Preparation of cDNA from Various Cell Lines

The Pathology Laboratory (University of Malta) houses a panel of breast cancer cell lines, stored as pellets in liquid nitrogen, at -80 ^{o}C. In order to prepare these pellets, each cell line was cultured in its respective medium, as indicated in databases ATTC®, 2012; DSMZ, 2013. The cell lines include ER+ MCF-7, HER2+ MDA-MB-453 and SK-BR-3 as well as ER+/HER2+ BT-474 and the triple negative breast cancer cell lines (TNBC) BT-20, Hs578T, MDA-MB-468, MDA-MB-436, and HCC1937. Cells were counted using an electronic cell counter (CASY 1 TTC Cell Counter and Analyser) to prepare pellets containing approximately 4 x 10^6 cells. The latter were freshly lysed in QIAzol (QIAGEN Cat: 79306), to preserve the released RNA. These were then stored in liquid nitrogen at -80 ^{o}C until further use.

In order to prepare cDNA, RNA was extracted from the cell pellets using the QIAGEN RN*easy* Mini Kit (QIAGEN Cat: 74104). When handling RNA, benches and equipment were cleaned using RNAZap (Sigma Cat: R2020) to protect RNA from RNase degradation. The quality of the RNA was then validated by spectrophotometry, using the NanoDrop™ 2000/2000c. The acceptable 260/280 ratio is 2.

RNA (1 µg for each cell pellet) was reverse transcribed into cDNA *in vitro*, using the Quantitect Reverse Transcription Kit (QIAGEN Cat: 205310). This kit provides high cDNA yields even from low abundance transcripts and eliminates genomic DNA contamination effectively.

2.2.2 Gene Expression by Real-Time PCR (RT-PCR)

Real-Time PCR (RT-PCR) is an efficient laboratory technique used to quantify gene expression. It makes use of a fluorescent dye, which binds to double stranded DNA, emitting a signal of a specific wavelength in the process. A common fluorescent dye used in RT-PCR is SYBR green. The latter has excitation and emission wavelength of 494 nm and 521 nm respectively. Detection occurs during the extension step of RT-PCR. This means that the amount of fluorescence depends on the amount of PCR product obtained. The signal intensity therefore increases with increasing cycle number, since the PCR product accumulates.

RT-PCR was carried out on the cDNA prepared from the various cell lines, using the Rotor-Gene QIAGEN Real-Time PCR System. The reaction mixture was prepared as described in Table 2.1. A blank sample was also set up, containing the entire mix, except for the cDNA. This served as the no template control (NTC); detection of fluorescence in the NTC would indicate contamination. Housekeeping gene *RPL13A* was used as an internal control gene, and the inhibitors *CIP2A* and *SET* as the target genes. Initial denaturation was carried out at 95 ^{o}C for 10 minutes. Then 40 cycles of denaturation (95 ^{o}C for 15 seconds), followed by annealing (57 ^{o}C for 30 seconds) and finally, extension (72 ^{o}C for 30 seconds) were carried out. The annealing temperature of 57 ^{o}C was used for all primers, determined by previous optimisation experiments in the Pathology laboratory, using the RAJI cell line.

Table 2.1: Reaction mixture for RT-PCR for housekeeping gene *RPL13A*, and the target genes *CIP2A* and *SET*

Component	Volume (µl)	Final Concentration
2 x Maxima SYBR Green / ROX qPCR Master mix (Thermo Scientific, Cat: K0221)	12.5	1 x
10 µM forward primer	0.5	0.2 µM
10 µM reverse primer	0.5	0.2 µM
Template cDNA (0.25 ng/µl)	1.0	0.25 ng
Nuclease-free water	10.5	
TOTAL REACTION VOLUME	25.0	

The table shows the constituents for the RT-PCR reaction mixture for housekeeping gene *RPL13A* and target genes *CIP2A* and *SET*. *IGBP1* was omitted for this experiment as previous investigations have established that there is translational control of this transcript (Grech, et al., 2008). Template cDNA was obtained from the following cell lines: ER+ MCF-7, HER2+ MDA-MB-453 and SK-BR-3, ER/HER2+ BT-474 and TNBC BT-20, Hs578T, MDA-MB-468, MDA-MB-436, and HCC1937. The blank sample (NTC) lacked cDNA and therefore served as the negative control.

2.2.3 Analysis of Real-Time PCR (RT-PCR) Data

Gene expression can be analysed by RT-PCR using the Comparative Cycles to Threshold (Ct) Method, also referred to as the ΔΔCt Method. Assuming 100 % PCR efficiency, the difference in quantification cycle value between two samples can be calculated by the following equation:

$$\Delta\Delta Ct = C_t \text{ (target gene)} - C_t \text{ (reference gene)}$$

The RT-PCR software then converts this value to Normalised Relative Quantities (NRQs) by the equation:

$$NRQ = 2^{-\Delta\Delta Ct}$$

The NRQ values obtained in this experiment are represented graphically in Figure 3.1. The values have been normalised to MCF 10-A, a human epithelial cell line commonly used in the laboratory as an *in-vitro* model for normal breast cell function and the housekeeping gene *RPL13A* was used as the reference gene as it is highly stable.

Three independent biological experiments were conducted for RT-PCR. Each experiment had a triplicate analytical measurement.

2.2.4 Confirmation of Which Cell Lines Have Lowest Levels of Inhibitors using the Immunocytochemistry (ICC) Technique

A panel of breast cancer cell lines, located on cover slips and fixed in paraformaldehyde is available at the Pathology Laboratory. Immunocytochemistry (ICC) using CIP2A, SET and IGBP1 antibodies, was carried out on these cell lines and photographic images of the results obtained were taken (refer to Appendix A). The ICC technique provides information on the protein's cellular localisation as well as its expression, both being significant to relate the protein's role in cellular processes. The ICC protocol applied was CSA II Biotin-Free Tyramide Signal Amplification System. This employs a highly sensitive ICC staining procedure incorporating a signal amplification method based on the peroxidase-catalysed deposition of a fluorescein-labelled phenolic compound, followed by a secondary reaction with a peroxidase-conjugated secondary antibody. The experimental photographic results were inspected (**Figure 2.1**) and H-scores were calculated. The H-score is a method of assessing the extent of immunoreactivity and is obtained by the formula:

3 x % of strong staining cells + 2 x % of moderate staining cells + 1 x % of weak staining cells

giving a range of 0 to 300. Therefore, the minimum H-score is 0, where 100 % cells show zero intensity, while the maximum H-score is 300, where 100 % cells show strong intensity. For each breast cancer cell line, H- scores were calculated for three fields of view and an average taken. H-scores were also calculated independently by another researcher and results were in concordance. The calculated H-scores are shown in Table 3.1. They were compared to RT-PCR results shown in Figure 3.1.

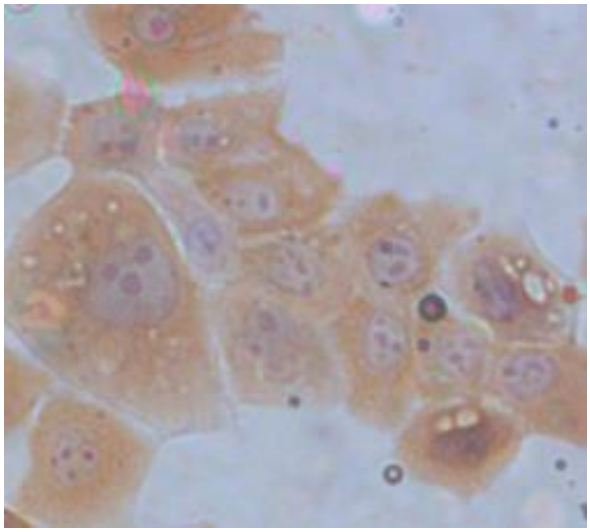

Figure 2.1: Photographic result of the immunocytochemistry technique, using anti-CIP2A antibody on breast cancer cell line HCC1937. A panel of breast cancer cell lines, located on cover slips and fixed in paraformaldehyde were subjected to the immunocytochemistry (ICC) technique, using the protocol documented by the CSA II Biotin-Free Tyramide Signal Amplification System. The cell lines were subjected to anti-CIP2A, SET and IGBP1 antibodies. Photographic images of the results obtained were taken and inspected. The presence and location of the protein of interest is indicated by a brown stain.

2.3 ISOLATION AND CLONING OF PP2A INHIBITORS

Once the cell lines having lowest levels of PP2A inhibitors CIP2A, SET and IGBP1 were identified, the next step was to prepare constructs with the coding sequences, for subsequent transfection into the cell lines.

2.3.1 Primer Design

In order to clone PP2A inhibitors CIP2A, IGBP1 and SET into the vector pIRES2-AcGFP1, specific primers were designed. The cDNA sequence for each inhibitor was obtained from the programme Ensembl Genome Browser 97 (www.ensembl.org). Each sequence was then imported into another programme, Primer3Plus (www.bioinformatics.nl). Finally, 24 bases from each end of the coding sequence were selected. This size was chosen to obtain a good specificity for each coding sequence but also to keep a relatively similar melting temperature for both primers and in the ideal primer melting temperature range.

The primers were then converted to In-Fusion primers, since the In-Fusion® HD Cloning System (www.clontech.com) was used for cloning. For each forward primer, the KOZAK sequence (CACC) was inserted after the restriction enzyme site, and before the start codon, as this facilitates ribosome recruitment and hence translation of the fragment. For each reverse primer, a c-MYC tag (CAGATCTTCTTCAGAAATAAGTTTTTGTTC) was inserted, just after the restriction enzyme site and stop codon. The MYC tag will allow the use of Western Blotting to quantify and determine the presence and size of the translated insert using an anti-MYC antibody.

The primer sequences were then inputted into another programme, NEBcutter V2.0 (www.labtools.us/nebcutter-v2-0/), in order to determine which restriction enzymes do not cut though them. Finally, a pair of different restriction enzymes that are active in the same restriction enzyme buffer were selected. For both CIP2A and SET, EcoR I and Sal I were selected, while for IGBPI, Bgl II and Sal I were used. Using different enzymes minimizes re-annealing of vector to itself, hence increasing cloning efficiency. Furthermore, these enzymes did not have any secondary restriction sites on the pIRES2, other than the multiple cloning site (MCS). Using this enzyme pair, the three inhibitors can be re-excised out of the vector and introduced into different vectors if needed. (**Table 2.2, Figure 2.2 and Figure 2.3**).

Table 2.2: Information for forward and reverse primers for PP2A inhibitors CIP2A, SET and IGBP1

CIP2A	Forward Primer Sequence: GACTCCACTGCCTGCTT
	Restriction enzyme cutting site (EcoR I): GAATTC
	In-Fusion Primer Sequence: CTCAAGCTTC GAATTCACCATGGACTCCACTGCCTGCTT
	Melting Temperature Tm = 77.9 °C
	Reverse Primer Sequence: TATACTGAGATTCACA
	Restriction enzyme cutting site (Sal I): GTCGAC
	In-Fusion Primer Sequence: CCGCGGTACCGTCGACCTACAGATCTTCTTCAGAAATAAGTTTTTGTTCTATAC TGAGATTCACA
	Melting Temperature Tm = 80.5 °C
SET	Forward Primer Sequence: GCCCCTAAACGCCAGTC
	Restriction enzyme cutting site (EcoR I): GAATTC
	In-Fusion Primer Sequence: CTCAAGCTTCGAATTCACCATGGCCCCTAAACGCCAGTC
	Melting Temperature Tm = 79.0 °C
	Reverse Primer Sequence: GTCATCTTCTCCTTCA
	Restriction enzyme cutting site (Sal I): GTCGAC
	In-Fusion Primer Sequence: CCGCGGTACCGTCGACTTACAGATCTTCTTCAGAAATAAGTTTTTGTTC GTCATCTTCTCCTTCA
	Melting Temperature Tm = 82.6 °C
IGBP1	Forward Primer Sequence: GCTGCTGAGGACGAGTT
	Restriction enzyme cutting site (Bgl II): AGATCT
	In-Fusion Primer Sequence: TACCGGACTCAGATCTCACCATGGCTGCTGAGGACGAGTT
	Melting Temperature Tm = 78.9 °C
	Reverse Primer Sequence: GCCCATGTTCTGTCGG
	Restriction Enzyme Cutting Site (Sal I): GTCGAC
	In-Fusion Primer Sequence: CCGCGGTACCGTCGACTCACAGATCTTCTTCAGAAATAAGTTTTTGTTCGCCCA TGTTCTGTCGG
	Melting Temperature Tm = 86.8 °C

The table shows the forward and reverse primer sequences for each PP2A inhibitor CIP2A, SET and IGBP1, as well as their melting temperatures. These primers were converted to In-Fusion primers, since the In-Fusion® HD Cloning System (www.clontech.com) was used for cloning. This was achieved by the insertion of the KOZAK sequence (CACC) after the restriction enzyme site, and before the start codon, for each forward primer. For each reverse primer, a c-MYC tag (CAGATCTTCTTCAGAAATAAGTTTTTGTTC) was inserted, just after the restriction enzyme site and stop codon. Melting temperatures (T_m) were taken from the Bioneer Oligo Synthesis Report (Bioneer Corporation).

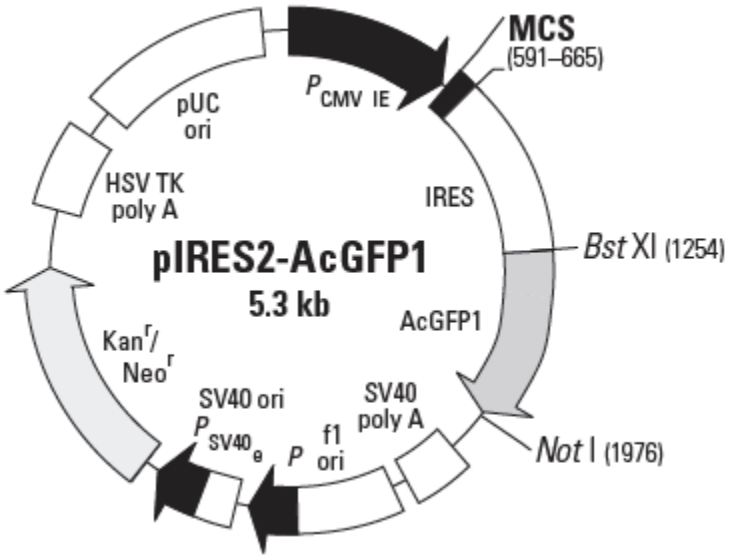

Image source: https://www.takarabio.com/documents/Vector%20Documents/PT3743-5.pdf

Figure 2.2: pIRES2-AcGFP1 vector map used for cloning. The vector map shown in Figure 2.2 has the following features:

CMV/IE Promoter: Immediate cytomegalovirus promoter sequence
MCS: Multiple cloning site, where the insert was introduced
IRES: Internal Ribosomal entry site gene that mediates translation of the inserted fragment
AcGFP1: *Aequorea coerulescens* Green Fluorescent Protein that is also translated into protein when the vector is transfected. Detecting this protein would imply successful transfection through translation of the inserted protein of interest
SV40 polyA tail, promoter and SV40 origin: for replication in mammalian cells expressing the SV40 T antigen
Neomycin phosphotransferase CDS with Kan(R) promoter: for conferring kanamycin-resistance to transformed bacteria
HSV TK - polyadenylation signals from *Herpes simplex* virus thymidine kinase: to allow stably transfected cells to be selected using G418 (3)
pUC origin of replication: for propagation in *E. coli* (cells used to clone construct)
f1 origin: for single-stranded DNA production.

bp	591	601	611	621	631	641	651	661	
5’	GCTAGCGCTA	CCGGACTCAG	ATCTCGAGCT	CAAGCTTCGA	ATTCTGCAGT	CGACGGTACC	GCGGGCCCGG	GATCC	3’

Figure 2.3: Detail of multiple cloning site (MCS) for pIRES2-AcGFP1, the vector chosen for the cloning experiment. The figure shows location of the selected restriction enzymes used for this experiment, namely Bgl II (AGATCT), EcoR I (GAATTC) and Sal I (GTCGAC), on the multiple cloning site of the pIRES2-AcGFP1 vector.

2.3.2 Optimization of Double Digest Experiment

In order to ensure that the enzyme pairs selected were working efficiently, two separate double digest reactions (using EcoR I/Sal I and Bgl II/Sal I) were carried out using pDBLeu vector as a positive control. With EcoR I and Sal I, pdDBLeu is digested into three fragments of sizes 4580 bp, 2747 bp and 2576 bp. The latter two fragments are very similar in size and do not appear as separate bands on an agarose gel. However, the first band is clearly distinct. Therefore, two distinct bands appear if the digestion is successful. In the case of Bgl II and Sal I, two fragments are obtained, of sizes 7174 bp and 2729 bp, clearly distinct on an agarose gel.

The digestion mixture was prepared according to Table 2.3 and incubated at a temperature of 37 ^{o}C for 3 hours. A blank sample (NTC) was also set up, containing the entire mix, except for the cDNA. The products of digestion were separated by gel electrophoresis using a 1 % agarose gel and viewed under ultraviolet light (**Figure 2.4**).

Since pIRES2-AcGFP1 has restriction enzyme sites only in its MCS, a double digestion as described with pDBLeu would produce a linearised vector, and therefore one fragment, of approximate size 5300 bp, would be obtained on an agarose gel (Refer to Section 2.3.5).

Table 2.3: Digestion mixture preparation for double digestion of pDBLeu with selected restriction enzyme pairs

A: EcoR I/Sal I

Component	Volume (µl)	Final Concentration
Restriction Enzyme 10 x buffer	2.0	1 x
Acetylated BSA (10 µg/µl)	0.2	2.0 µg
Restriction Enzyme **EcoR I** (10 U/µl)	0.2	2.0 U
Restriction Enzyme **Sal I** (10 U/µl)	0.5	5.0 U
DNA (pDBLeu) (1µg/µl)	4.0	4.0 µg
Sterile Deionised water	12.8	
TOTAL REACTION VOLUME	20.0	

B: Bgl II/Sal I

Concentration	Volume (µl)	Final Concentration
Restriction Enzyme 10 x buffer	2.0	1 x
Acetylated BSA (10 µg/µl)	0.2	2.0 µg
Restriction Enzyme **Bgl II** (10 U/µl)	0.2	2.0 U
Restriction Enzyme **Sal I** (10 U/µl)	0.5	5.0 U
DNA (pDBLeu) (1µg/µl)	4.0	4.0 µg
Sterile Deionised water	12.8	
TOTAL REACTION VOLUME	20.0	

The above reaction mixtures were prepared for the two double digest experiments: EcoR I/Sal I (A) and Bgl II/Sal I (B). Both mixtures were incubated for 3 hours at 37 ^{o}C and then run on a 1 % agarose gel. The NTC lacked cDNA and therefore served as the negative control.

A: Double digestion of pdBLeu using EcoR I/Sal I

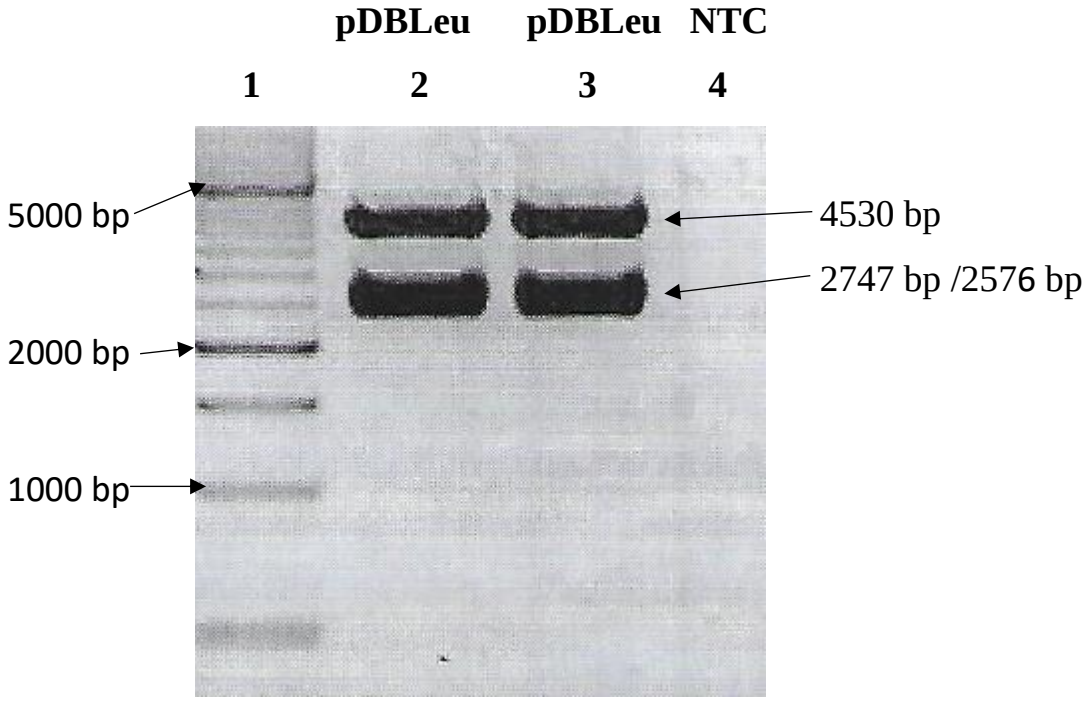

B: Double digestion of pdBLeu using Bgl II/Sal I

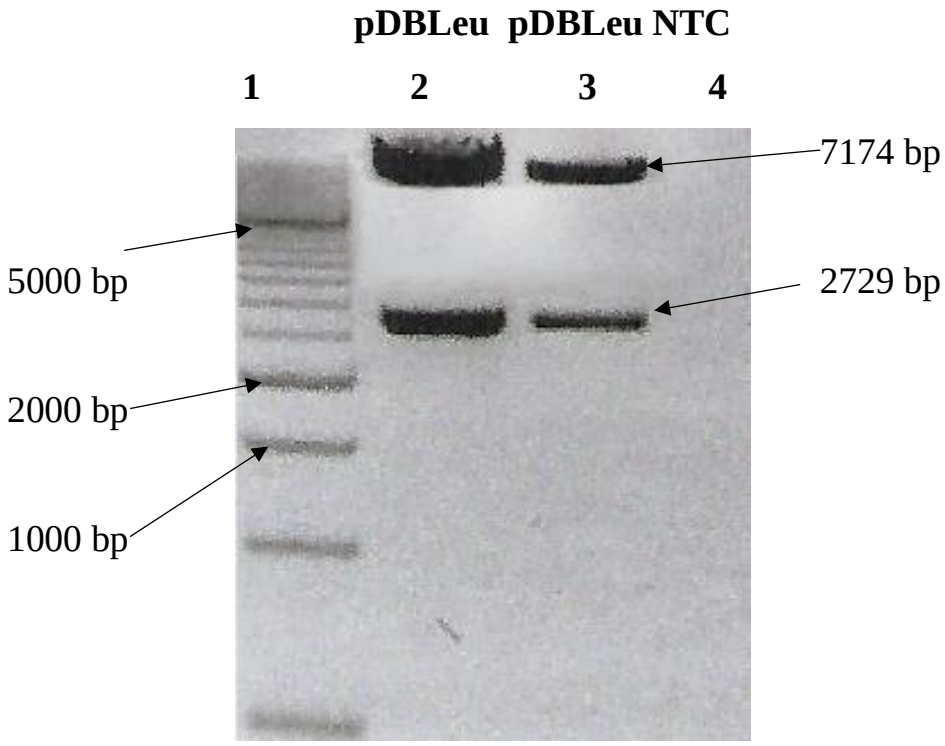

Figure 2.4: Double digestion of pDBleu using different restriction enzymes. Figures **A** and **B** show a photograph of the gel electrophoresis experiment, obtained following double digestion of pDBLeu using the different enzyme pairs (EcoR I/Sal I in **A** and Bgl II/Sal I in **B**). Lane 1 shows the DNA molecular weight marker (ProMega-Marker® Lambda Ladder). Lanes 2 and 3 show the digestion mix (2 µl) and lane 4 is the control which lacked DNA (NTC). In both cases the bands of expected sizes were obtained and the NTC did not show any bands. The experiment therefore proved successful.

2.3.3 Primer Optimisation by Gradient PCR

The three sets of primers for the three PP2A inhibitors required optimisation for the ideal annealing temperature, number of PCR cycles as well as which template cDNA which gives maximum yield of product. Such optimisation was carried out using Gradient PCR in the TProfessional Basic Thermal Cycler (Biometra). The instrument produces a gradient of temperatures, ranging horizontally from temperatures of 50.0 ^{o}C to 62.0 ^{o}C. A low annealing temperature can produce non-specific products, while if the temperature is too high, the PCR yield can be low. This experiment was also repeated with various template cDNA samples, as well as using various cycle durations, again to determine the best yield of product. Once PCR was complete, the PCR products were visualised using gel electrophoresis (1 % agarose gel) and the optimum conditions were established. A blank sample lacking cDNA (NTC) was prepared as the control experiment, for any PCR experiment.

2.3.4 PCR for Each PP2A Inhibitor

Once the ideal conditions for the amplification of each inhibitor were established, as described in Section 2.3.3, the PCR experiment was conducted. The reaction mixture is shown in Table 2.4. The PCR conditions for each inhibitor were as follows: Initial denaturation was carried out at 95 ^{o}C for 10 minutes. Then 40 cycles of denaturation (95 ^{o}C for 15 seconds), annealing (57 ^{o}C for 30 seconds) and extension (72 ^{o}C for 30 seconds) were conducted. For all inhibitors, template cDNA HL60 was used. Annealing temperatures were however, set as follows: 53.8 ^{o}C for CIP2A, 52.5 ^{o}C for SET and 56.5 ^{o}C for IGBP1. The PCR products were then run on a 1 % agarose gel as described in Section 2.3.3. The expected

sizes of products were obtained: 2783 bp for CIP2A, 938 bp for SET and 1086 bp for IGBP1 (**Figure 2.5**).

Table 2.4: PCR reaction mixture for PP2A inhibitors CIP2A, SET and IGBP1

Component	Volume (µl)	Final Concentration
5 x PCRBIO Reaction Buffer	2.0	1 x
10 µM In-Fusion forward primer	0.4	0.4 µM
10 µM In-Fusion reverse primer	0.4	0.4 µM
PCRBIO HiFi Polymerase 2U/ µl	0.1	0.2 U
Template cDNA HL60 (0.25 ng/µl)	1.0	0.25 µg
PCR Grade water	6.1	
TOTALREACTION VOLUME	10.0	

The table shows the PCR reaction mix used to prepare the three PP2A inhibitors, using template cDNA HL60. The PCR conditions for each inhibitor were as follows: Initial denaturation was carried out at 95 ^{o}C for 10 minutes. Then 40 cycles of denaturation (95 ^{o}C for 15 seconds), annealing (57 ^{o}C for 30 seconds) and extension (72 ^{o}C for 30 seconds) were conducted. Annealing temperatures were, however, as follows: 53.8 ^{o}C for CIP2A, 52.5 ^{o}C for SET and 56.5 ^{o}C for IGBP1.

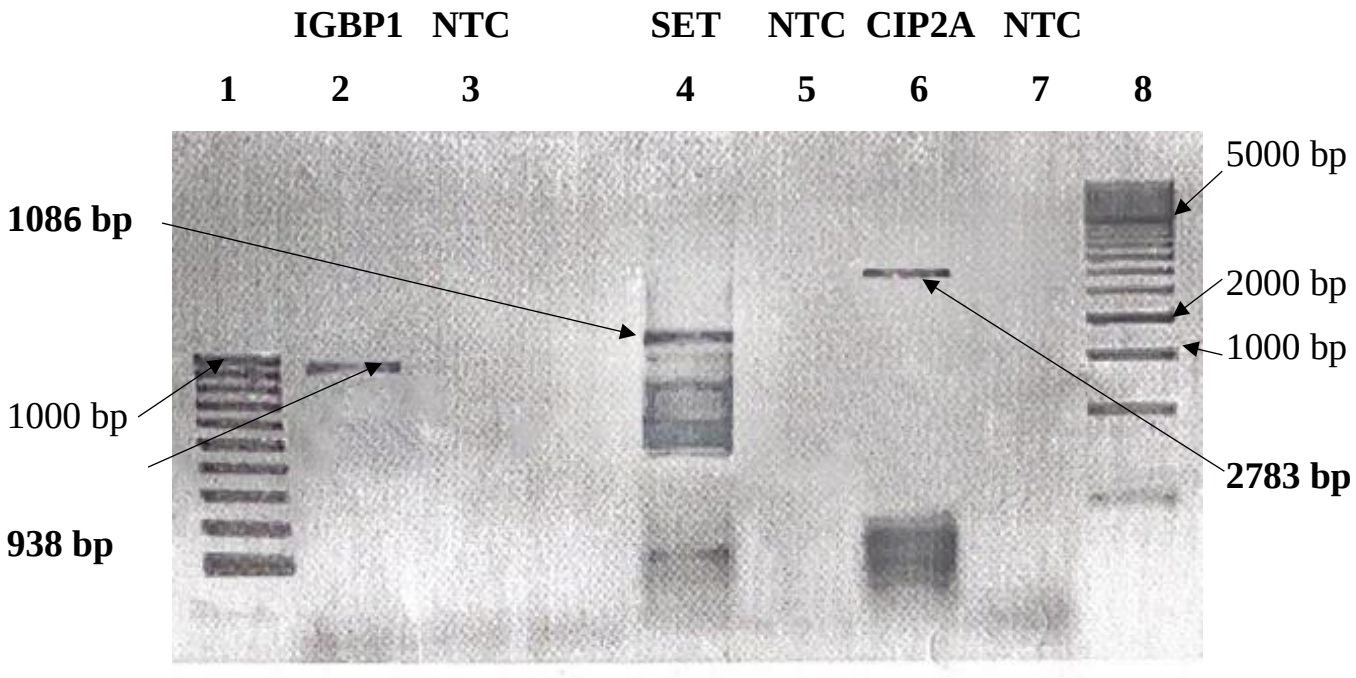

Figure 2.5: PCR-amplified inhibitors CIP2A, SET and IGBP1. The figure shows a photograph of the gel electrophoresis experiment, obtained following the PCR reaction (**Table 2.4**). Lanes 1 and 8 show the DNA molecular weight marker (ProMega-Marker® Lambda Ladder). Lanes 3, 5 and 7 show the control (NTC), where the PCR experiment lacked DNA. Lanes 2, 4 and 6 show the PCR products (2 µl of reaction mixture), for each PP2A inhibitor. The gel shows PCR products having the expected and hence correct sizes. These are 2783 bp for CIP2A, 1086 bp for SET and 938 bp for IGBP1, confirming the accuracy of the experiment. The NTC does not show any bands, as expected.

2.3.5 DNA Extraction from 1 % Agarose Gel

The PCR-amplified inhibitors, were excised from the agarose gel, using a clean scalpel blade, and purified using the Nucleospin Gel and PCR Clean-up. The gel fragments were weighed, and for every 100 mg of gel, 200 µl of buffer NTI were added, according to the protocol. The Nucleospin Gel and PCR Clean-up makes use of a silica membrane incorporated in a column. By a series of washings, the purified DNA is eluted and collected in a microcentrifuge tube.

A double digestion according to Section 2.3.2 was then carried out on the three PCR products, using EcoR I/Sal I for CIP2A and SET, and Bgl II/Sal I for IGBP1. This was also carried out on pIRES2-AcGFP1, using EcoR I/Sal I and Bgl II/Sal I and pdBLeu as the control (refer to Appendix A). The digestion mixture contents were run on a 1 % agarose gel, excised from the gel and purified using the Nucleospin Gel and PCR Clean-up protocol. Ligation of vector and PCR products was then carried out as described in the next section.

2.3.6 Ligation of PP2A Inhibitors with Linearised pIRES2-AcGFP1

The PCR-amplified and purified fragments were then ligated into the linearised pIRES2-AcGFP1 vector using the In-Fusion® HD Plus Cloning kit (Clontech Cat: 638910). The protocol recommends using 50 ng of vector and insert respectively, regardless of their length. The In-Fusion mix was therefore prepared and incubated at 50 ^{o}C for 15 minutes, then placed on ice. A negative control lacking the purified PCR fragment was also prepared.

The pIRES2-AcGFP1 was selected for its Internal Ribosome Entry Site (IRES) and for the Green Fluorescent protein gene (GFP) (**Figure 2.2**). The coding sequence of interest is inserted into the multiple cloning site (MCS) of the vector. This is located upstream of the IRES. This site will allow the insert to be translated from the same mRNA transcript as the GFP. The IRES mediates recruitment on ribosomes when successfully transfected into mammalian cells, resulting in a higher translational efficiency. The AcGFP is a modified alternative to the monomeric GFP and is more stable than other counterparts. It can be detected by fluorescence over a period of time after transfection. Its detection confirms successful transfection and subsequent translation of the protein of interest.

Following the cloning procedure, the sequence of the constructs was verified (www.ensembl.org; please refer to Appendix A for cDNA information). The constructs were used to transform bacterial cells, as described in the next section.

2.3.7 Transformation of Bacterial Cells

Each construct (5 ng DNA) was transformed into 50 µl of thawed Stellar™ bacterial cells by heat shock (60 seconds at 42 °C). This was followed by placing the tubes on ice for 1 to 2 minutes. A volume of 500 µl S.O.C medium (Super Optimal broth with Catabolite repression) was added to the transformed cells, which were then incubated by shaking for 1 hour at 37 °C at 225 rpm (horizontal shaking). Approximately 10 µl of transformed bacteria was inoculated on LB agar with 50 µg/mL kanamycin antibiotic and incubated overnight. Growth was assessed and colonies were picked using the aseptic technique. They were then expanded in Kanamycin supplemented Luria-Bertani (LB) broth and the construct was extracted and purified using the QIAprep Spin Miniprep Kit and a Microcentrifuge (QIAGEN Cat: 27104). These constructs were then sequenced by BIONEER Corporation to confirm that the appropriate sequence was inserted and was clear of any mutations that may have occurred during amplification. Orientation of insert to vector was not an issue as two different restriction enzymes were used allowing only insertion in the correct 5'- 3' orientation.

2.4 TRANSFECTION OF SELECTED CELL LINES

Selected cell lines MDA-MB-453 and MCF-7 were grown in RPMI-1640 medium (Sigma Cat: R6504) containing 10 % Foetal Bovine Serum (FBS, Sigma Cat: F9665) and 1 % penstrep (Sigma Cat: P0781). The culture methods are described below.

2.4.1 Preparation of RPMI Medium

In a clean glass beaker, 900 ml of distilled water at a temperature of about 15 to 30 ^{o}C were added. The beaker was placed on a magnetic stirrer and the RPMI powder was emptied into it. This was stirred until completely dissolved. To the solution, 2 grams of sodium bicarbonate were added. The pH was adjusted to 0.2 units below the required pH 8, using 1N hydrochloric acid or sodium hydroxide as required. Distilled water was added up to 1 litre. The medium was the filtered using a 0.2 µm filter, into sterile bottles. After filtration, the pH will rise to the correct value. FBS and penstrep (10 % and 1 %) were added.

2.4.2 Culturing of Selected Cell Lines

The two frozen selected cell lines MDA-MB-453 and MCF-7, were allowed to thaw slowly on ice. Ten mls of 1 x phosphate buffered saline (PBS, ThermoFisher Cat: AM9625) were added by gentle pipetting and the contents were transferred to a Falcon centrifuge tube. After a four-minute centrifugation at 100 x g at 4 ^{o}C, the supernatant was discarded and 6 mls RPMI were added.

The cells were placed in a T-25 flask and incubated for 2 days. Following successful growth, the cells were transferred to a T-75 flask containing 12 ml RPMI medium.

2.4.3 Transfection Experiment

Transfection of the selected cell lines with the three constructs CIP2A, SET and IGBP1 was carried out using the FuGENE HD protocol and FuGENE HD Transfection Reagent (Promega Cat: E2311). After a trial transfection in 24-well plates and 6-well plates, the experiment was scaled up for a T-25 flask and 6 ml RPMI medium. The cells were seeded at a density of 2.42 x 10^6 cells/flask for MCF-7 and 3.03 x 10^6 cells/flask for MDA-MB-453. Concentrations were measured using an electronic cell counter (CASY 1 TTC Cell Counter and Analyser). A 100 µl aliquot was taken from the cell suspension and placed in a CASY bottle and 10 ml of CASYton dilution fluid (Cat: 551808001) was added. Cell count could then be recorded at a minimum of 90 % viability.

After 24 hours incubation at 37 ^oC, the FuGENE complex was prepared using 8.8 µg DNA in 414 µl total volume RPMI medium. To this, 26 µl of FuGENE reagent was added (FuGENE:DNA ratio of 3.0:1). The complex was mixed by pipetting 15 times and incubated for 10 minutes at room temperature. Finally, 400 µl of complex was added to each flask and mixed thoroughly. The flasks were incubated at 37 ^pC. A positive control experiment was set up using pmaxGFP vector. After 48 hours, the flasks were observed using the Nikon Eclipse T_i Fluorescent Microscope under both bright field and dark field (using the green filter set-up) and the transfection efficiency was estimated (**Figure 3.3**).

An attempt to separate transfected from non-transfected cells using the BIOFACS Cell Sorter (FACSDiva Version 6.1.3), available at the Applied Biomedical Science Department, Faculty of Health Services, was also made use of in a preliminary experiment. Optimisation of the FACS medium and flow rate, for the adherent MCF-7 cell line, transfected with IGBP1, was conducted and proved successful on a small scale. However, sorting of cells using this technique resulted in a very low yield of transfected product, as shown in Figure 3.18. The idea of sorting the cells prior to further investigation was therefore discarded as, on a larger scale, it was not practical in terms of chemicals, laboratory ware as well as handling of the experiment itself. As a consequence, the investigation proceeded to the next step, extraction of protein from the transfected cell lines.

2.5 WESTERN BLOTTING

This laboratory technique is useful to visualise and approximately quantify a protein of interest. By means of gel electrophoresis, a mixture of proteins of varying molecular weight can be separated. Using an antibody specific to the desired protein, the latter's presence can be confirmed.

2.5.1 Preparation of Cell Pellets

Following the transfection experiment according to Section 2.3.1, the cells in each T25 flask were treated with 3 ml 1x Trypsin EDTA (Sigma Cat: T4174) and incubated for 3 minutes at 37 ^{o}C, to remove them from the base of the flask. After addition of 3 ml RPMI, the contents were centrifuged at 200 x g for 5 minutes. The supernatant was discarded, and the pellet was washed with 1 ml PBS (Phosphate Buffered Saline, Sigma Cat: P4417). The centrifugation step was repeated, and the supernatant was again removed. The pellets, containing over 5 x 10^6 cells, were stored at -80 ^{o}C.

2.5.2 Preparation of Protein Lysates

In order to lyse the cell pellets and release the protein, 5x PLB (Passive Lysis Buffer, Promega Cat: E1941) was diluted using 4 parts sterile water (as per Dual-Luciferase® Reporter Assay and Dual-Luciferase® Reporter 1000 Assay Systems-Promega protocol). To each cell pellet, 1x PLB was added (approx 20 µl for every 1 x 10^6 cells). The contents were mixed by vortexing and placed on

ice for 30 minutes. They were then centrifuged at 10 000 to 15 000 x g, for 15 minutes at 4°C. Cold temperatures are necessary to prevent denaturation of proteins. The supernatant was collected into a fresh tube and quantified using the Bradford Protein Assay.

2.5.3 Bradford Protein Assay

Following protein extraction, protein concentration was determined using Bradford Protein Assay. This is an important step as the amount of protein being loaded on the gel is necessary, and protein expression levels can be compared. The assay involves the binding of the dye Brilliant Blue G to proteins in solution. As a result of the binding, a blue protein-dye complex is formed, the intensity of which is proportional to the amount of protein present. The complex is detected at 595 nm, using a spectrophotometer.

Bradford Reagent (Sigma Cat: B6916) and Bovine Serum Albumin (BSA, Sigma Cat: A3608) are both required, to prepare a calibration curve which can then be used to quantify the protein lysates. BSA standards (1500, 1000, 500, 250, 125, 62.5 µg/ml) were prepared. For each standard, 5 µl of solution was added to 245 µl of Bradford Reagent. They were mixed well and left on ice for at least 5 minutes, for the colour to develop. A blank was also prepared, using 5 µl of 1x PLB instead of the standard. The calibration curve was then obtained by Nanodrop Spectrophotometry at 595 nm (refer to Appendix A). Samples were read in duplicate. Finally, absorbance values were obtained for the protein lysates, using 5 µl lysate and 245 µl Bradford reagent and the concentrations deduced from the calibration curve.

2.5.4 Polyacrylamide Gel Electrophoresis

The next step in Western blotting is polyacrylamide gel electrophoresis. The glass panes for the gel electrophoresis chamber were rinsed with deionized water, followed by 70 % ethanol. The mould was then set up and the running and stacking gels were prepared according to Table 2.5. The proteins of interest were of sizes 100 kDa for CIP2A and 39 kDa for both SET and IGBP1. Therefore, a 12.5 % resolving gel was used, which was allowed to run at 150 V for at least 1.5 hours, ensuring that the larger protein is resolved, while the smaller proteins are not lost, by keeping a close eye at the marker.

The running gel was pipetted into the mould below the comb groove and water-saturated butanol was placed at the surface. This was then removed, once the gel was set, and the surface was rinsed with deionized water. The stacking gel was then pipetted on top of the resolving gel and the plastic comb was inserted. It was removed when the gel was set. The mould was then placed in the electrophoresis chamber, containing 1x Running Buffer (**Table 2.6**).

While the gel was setting, the samples were prepared for loading. For each inhibitor, 35 µg of lysate were loaded, in a maximum volume of 15 µl. To each sample, 5 µl of loading dye (NuPAGE LDS Sample Buffer 4x, Thermo-Fisher Cat: NP0007) was added (dye:sample ratio of 1:3). The samples were heated at 95 ^{o}C for 3 minutes, to denature the proteins, then mixed well and placed on ice.

The samples, each containing 4 µl of molecular weight marker (BIO-RAD Protein Ladder Cat: 1610374) were then loaded into the wells. The gel was then run at 150V, as described previously.

Table 2.5: Chemicals used to prepare 10 x running buffer for Western Blot gel electrophoresis

Tris (hydroxymethyl) aminomethane (Tris Base, 25 mM-MW 121.14 g/mol)	15.18 g
Glycine (190 mM-MW 75.066 g/mol)	71.31 g
10 % Sodium Dodecyl Sulfate (SDS)	5 ml
Deionized water	500 ml

The above table shows the mixture of reagents required to prepare the stock running buffer for Western blotting. A 1 in 10 dilution was then made for the electrophoresis chamber buffer. The pH was adjusted to 8.3-8.8 using hydrochloric acid. All chemicals were available at the Pathology Laboratory for common use.

Table 2.6: Chemicals used to prepare the 12.5 % resolving gel and 5 % stacking gel for Western Blot gel Electrophoresis

12.5 % Resolving Gel:

TEMED	10 µl
Deionized water	3.80 ml
1M Tris HCl (pH 8.8)	3.72 ml
30 % acrylamide	3.12 ml
10 % SDS	0.10 ml
Ammonium Persulfate (APS)	100 µl

5 % Stacking Gel

TEMED	7.5 µl
Deionized water	2.3 ml
1M Tris HCl (pH 6.8)	0.4 ml
30 % acrylamide	0.5 ml
10 % SDS	15 µl
Ammonium Persulfate (APS)	50 µl

The above table shows the mixture of reagents required to prepare the resolving gel and stacking gel for Western blotting. Both resolving gel and stacking gel contain ammonium persulfate (APS), which needs to be added as the last reagent, to activate the mixture and initiate the solidification. All chemicals were available at the Pathology Laboratory for common use.

2.5.5 Gel Transfer

After the electrophoresis run, the separated proteins required to be transferred onto a nitrocellulose membrane. The latter was cut to the size of the gel and soaked in 1 x Running Buffer. Two thick filter papers were also soaked in the same buffer. The transfer assembly was then set up as shown in Figure 2.6 and transfer was carried out for 1 hour at a constant current of 0.5A, using the BIO-RAD apparatus.

After the transfer, the membrane was placed in deionized water for a few minutes, then in Ponceau S for 3 to 5 minutes, to confirm efficient transfer and presence of protein. It was then left for 1 hour in blocking agent (3 % Odyssey Blocking Buffer, LI-COR, Cat: 927-40000) and then washed three times with 1x Tris Buffered Saline (TBS).

2.5.6 Exposure to Primary and Secondary Antibody

The next step involved overnight exposure to primary antibody at 4 ^{o}C. The antibody used was Myc-Tag 9B11 (Cell Signalling Technology Cat: 22765) and was diluted 1:1000 (5 µl in 5 ml 1 x TBS). This antibody recognizes the c-MYC present in the constructs (**Table 2.2**).

Following the overnight exposure, the membrane was washed three times using 1 x TBS, for five minutes each and then exposed to secondary antibody (IRDye 800CW Conjugated goat Anti-mouse IgG, LI-COR) diluted 1:10,000 in 1x TBS,

for 1 hour. After three 5-minute washes with 1 x TBS, the membrane was scanned and visualised using the Odyssey Infrared Scanner and its software (**Figure 3.3**).

Figure 2.6: Transfer assembly set up, according to BIO-RAD instructions

Image Source:
http://www.biorad.com/webroot/web/images/lsr/solutions/technologies/protein_electrophoresis_blotting_and_imaging/western_blotting/technology_detail/pet21_gel_membrane_setup.gif

In order to transfer the separated proteins onto a nitrocellulose membrane after the electrophoresis run, the 'blotting sandwich' was prepared as shown in the diagram. The membrane was cut to the size of the gel and soaked in 1 x Running Buffer. Two thick filter papers were also soaked in the same buffer. The transfer assembly was then set up as shown in the figure and transfer was carried out for 1 hour at a constant current of 0.5 A.

2.6 QUANTIGENE™ ASSAY

This experiment was conducted to determine whether beta-catenin transcription is regulated by PP2A reactivation using the chemical inducer, FTY720, in concentrations of 100 pM, 1 nM and 5 nM. Beta-catenin is the main effector of the Wnt pathway as described in Section 1.3.5. Cell pellets were prepared as described in Section 2.5.1 for the cell lines MCF-7, HCC1937 and MDA-MB-453. The cell lines were treated with the various concentrations of FTY720, and the RNA level measured using QuantiGene™ 12-plex assay (Thermo Fisher Scientific) and prepared according to the instructions on the protocol. The samples were prepared on a 96-well plate and were incubated overnight at 54 °C at 600 rpm, in a previously calibrated VorTemp™ 56 shaking incubator (Labnet International, Corning, NY).

On the second day of the procedure, the 96-well plate was centrifuged at 240 x *g* for one minute at room temperature and placed into a hand-held magnetic separation plate, where it was left for one minute to allow the magnetic beads to settle at the bottom of each well. After the plate was emptied, 100µL of streptavidin-conjugated R-phycoerythrin (SAPE) working reagent was added and the plate was incubated for 30 minutes on a shaking platform at a speed of 600 rpm at room temperature. A further three washing steps were carried out using SAPE wash buffer, followed by the addition of 130µL of SAPE wash buffer to each well.

The plate was finally read on both the Luminex® 200 and MAGPIX® instruments (Luminex, Thermo Fisher Scientific) and data was obtained using FlexMAP 3D. The results (median fluorescence intensities, MFIs, of 50 values)

were analysed by first subtracting the mean background signal (blank MFI) for each gene from the mean MFI of the samples. Finally, $\log_2$ fold change was calculated as described in Section 2.8.1 for each sample and results are shown in Figure 3.2.

2.7 POLYSOME BOUND RNA PROFILING

Polysome bound RNA (pbRNA) profiling is a laboratory technique used to study the association of mRNAs with ribosomes. This technique allows determination of the fraction of a specific mRNA bound to ribosomes as well as the fraction of existing free messenger ribonucleoprotein particles (mRNRps), giving an accurate estimate of translation efficiency.

Prior to isolation of polysome bound RNA from transfected cell lines, optimization of the methodology was carried out using two different techniques. One technique made use of the QIAGEN RNeasy Mini Kit (QIAGEN Cat: 74104), while the other technique was that proposed by Grech, et al., 2008. Results were analysed using the Agilent 2100 Bioanalyser. Both methods yielded good quality RNA, with RNA Integrity Numbers (RIN) of 8.6 and 9.1 respectively. RIN values range from 0 to 10. A RIN value of 7 or more, indicates good quality RNA. However, concentrations of RNA were higher in the case of that proposed by Grech, et al, 2008. (**Table 3.9**) This method was therefore selected for further experimentation and is documented below.

2.7.1 Preparation of Cell Pellets

The procedure for preparation of cell pellets to be used in pbRNA profiling is identical to that described in Section 2.5.1. However, for each experiment, cell pellets were prepared from two T-25 flasks were used, a total of 1 x 10^7 cells per sucrose gradient.

2.7.2 Preparation of Sucrose Gradients

In order to prepare the sucrose gradients, two basic sucrose solutions are required, 15 % and 40 % sucrose (w/v), prepared as described in Table 2.7. Just before use, for every millilitre of sucrose, 10 µl of 1M dithiothreitol (DTT), 10 µl of cycloheximide (10 mg/ml) and 20 µl heparin (50 mg/ml) were added. The latter chemicals are important to prevent degradation of the RNA.

From the two basic sucrose solutions (15 % and 40 % (w/v)) two more solutions containing 23.3 % and 31.6 % (w/v) sucrose were prepared (by mixing the 15 % solution with the 40 % stock at ratios of 2:1 and 1:2, respectively).

In order to prepare the gradients, 2.5 ml of 40 % glucose was placed in a centrifuge tube, and snap-frozen in liquid nitrogen. On top of this layer, 2.5 ml of 31.6 % sucrose was added, and snap-frozen again. This was repeated using 23.3 % and 15 % sucrose. The gradients were stored at -80 ^{o}C and thawed slowly overnight before use.

Table 2.7: Reagents required for preparation of sucrose gradients, necessary for polysome bound RNA profiling

10 mM Tris-HCl pH7.5	5 ml 1M stock
140 mM NaCl	14 ml 5M stock
1.5 mM $MgCl_2$	0.75 ml 1M stock
15 % sucrose	75 g
40 % sucrose	200 g
Add water up to 500 ml	

The above table lists what is required to prepare the two basic sucrose solutions (15 % and 40 % (w/v). From these solutions, two more solutions with 23.3 %and 31.6 % (w/v) sucrose were prepared (by mixing the 15 % solution with the 40 % stocks at ratios of 2:1 and 1:2, respectively).

2.7.3 Lysis of Cell Pellets

Each cell pellet was lysed in 1 ml NP40 buffer (containing RNase inhibitors), and maintained at 4 ^{o}C (**Table 2.8**). The lysed contents were centrifuged at 3000 x g for 3 minutes. This removes the nuclei. The supernatant was then placed in a new microfuge tube and centrifuged at 10 000 to 15 000 x g for 10 minutes, to remove the mitochondria and membrane particles.

2.7.4 Sucrose Gradient Centrifugation

The supernatant from the final centrifugation was loaded onto the sucrose gradient. Each gradient was weighed and equilibrated with NP40 buffer prior to the final centrifugation step, to ensure that the rotor was balanced. Centrifugation was then carried out in a cold SW28 rotor for 2 hours at 141 000 x g at 4 ^{o}C.

Table 2.8: Preparation of NP40 buffer, used to lyse the cell pellets and release the RNA

NP40 buffer:	**Before use (for every 913 µl NP40 buffer, add the following:**
0.5 % NP40 (Thermofisher Cat: 1557027)	12 µl RNAsin (500U/ml, Promega Cat: N2111)
10 mM Tris HCl pH 8.0	15 µl cycloheximide (10 mg/ml)
140 mM NaCl	20 µl DTT (1M)
1.5 mM $MgCl_2$	10 µl phenylmethylsulfonyl fluoride (PMSF, 0.1M), or any other protease inhibitor

The left column of the table lists the chemicals required to prepare NP40 buffer. Just before use, RNase inhibitors listed in the right column were added, for every 913 µl NP40 buffer.

2.7.5 Harvesting the Gradient

Following centrifugation, for each gradient, 20 microfuge tubes containing 30 µl SDS (20 %), 12 µl EDTA (0.5 M) and 10 µl proteinase K (10 mg/ml) were prepared. To each tube, 620 µl fractions of the gradient were aliquoted, and tube contents were mixed immediately. The microfuge tubes were incubated at 37 ^{o}C for 30 minutes. Following this step, 750 µl of cold phenol:chloroform (1:1) were added, the mixture was vortexed for 1 minute, followed by a 5 minute centrifugation at 10 000 to 15 000 x g. To the upper phase, 1 ml of cold ethanol was added, the contents were mixed and left to precipitate for 1 hour on ice. Finally, a 30 minute centrifugation at 10 000 to 15 000 x g was carried out and the pellet was washed with 70 % ethanol and dissolved in 15 µl water. The contents were stored at a temperature of -80^{o}C, until they were analysed using the Aligent 2100 Bioanalyser (following the Aligent RNA 6000 Nano Kit Protocol). Results are shown in Figure 3.5.

However, some difficulties were encountered as regards repeatability of the procedure as shown in Figure 3.6. The probable source of error was the fact that the SW28 rotor available at the laboratory did not reach the speed dictated by the protocol according to Grech, et al. (2008), which specifies using an SW40/SW41 rotor at a speed of 284 000 x g.

2.7.6 Percent Polysome Recruitment Studies

Although repeatability of the polysome bound RNA experiment was being questioned, further investigations using this technique were still carried out at this stage. Cell pellets were prepared as described in Section 2.5.1 for the cell lines MCF-7, HCC1937 and MDA-MB-453, containing the plasmid pIRES2-AcGFP1 (as control experiments), as well as the same cell lines transfected with the plasmid cloned with the three inhibitors CIP2A, SET and IGBP1(as described in Section 2.4). Percent polysome recruitment was determined using an algorithm as described below.

The algorithm generates a ratio of ΔCt of free RNA and pb RNA. The derivation also involves the calculation of a factor based on the RNA concentration of the pooled free RNA and pooled pb RNA. The RNA input into cDNA synthesis is standardised to 1µg, but the percent polysome recruitment must account for the RNA concentrations between the pooled pb RNA and free RNA, hence the generated factor. This factor is multiplied to the fold change, followed by the calculation of the percent polysome recruitment. Due to this multiplier factor, it is important to have comparable distribution of free and pb RNA fractions, hence the use of the Bioanalyser data analysis of each fraction from the sucrose gradient.

Following the data analysis, percent polysome recruitment between the pIRES2-AcGFP1 vector and the over-expressors (one construct per bulk experiment) was investigated. The polysome recruitment of c-MYC, known to be negatively regulated by active PP2A was measured (**Figure 3.7**). In a separate experiment, the cells were treated with 10nM rapamycin, the latter being an inhibitor of the

mTOR pathway, to determine whether polysome recruitment was mTOR dependant (**Figure 3.7**).

For this experiment, a parametric test, namely a paired t-test was carried out to determine whether there is a significant difference between the means of two sets of paired (matched) data which are assumed to be in normal distribution. The pairs considered were the control cell line and the transfected cell line, as well as the transfected cell line and the same cell line treated with rapamycin (refer to Appendix A). The paired t-test generates a p-value; a p-value of 0.05 is considered of borderline significance. A result is considered statistically significant if the p-value less than 0.01.

The application of the paired t-test showed that significant statistical differences between the means of the separate experimental datasets were obtained (refer to Appendix A). This prompted us to investigate alternative ways to measure the differential expression in the cellular models upon overexpression of the PP2A regulators. In the meantime, the possibility of carrying out DigiWest experimentation on the protein lysates became the obvious next step.

2.8 DIGITAL WESTERN TECHNOLOGY

The next phase of experimentation was dedicated to generating samples required for the differential expression of control MDA-MB-453 breast cancer cell lines as compared to those having ectopic expression of CIP2A, SET and IGBP1. These samples were prepared as described in Section 2.5.1 and were frozen as cell pellets in the -80^{o}C freezer, until it was possible to send them for analysis using a novel technology developed at the Natural and Medical Science Institute at the University of Tübingen in Germany (NMI), one of the Pathology Department's collaborators.

Digital Westerns (DigiWest) is a novel technology that allows the interrogation of 200-500 antibodies using one protein lysate. The method involves the separation of proteins on a standard SDS-polyacrylamide gel and transfer of the separated protein fractions onto a blotting membrane (**Figure 2.7**). The proteins are biotinylated on the membrane. The lanes are cut into 0.5mm strips, and the biotinylated proteins eluted into a 96-well plate. Avidin coated beads are placed in the wells ensuring that different wells have different beads that are read in specific regions on the Luminex analyser. The 96 well plate contents are pooled, subjected to antibody coupling, and read using the FlexMAP 3D Luminex instrument. The results obtained appear as protein quantification bar graphs, specific to each antibody (referred to as analyte) showing the intensity of the signal against the molecular weight of the protein. For each analyte, the expected weight of the protein (in kDa) is inputted into the analyser software, in order to ensure that the correct peak is selected.

DigiWest technology provides a bigger insight than using polysome bound RNA profiling, since it can measure the difference in protein activation, rather than indicate protein expression as a function of quantity of transcripts on polysomes.

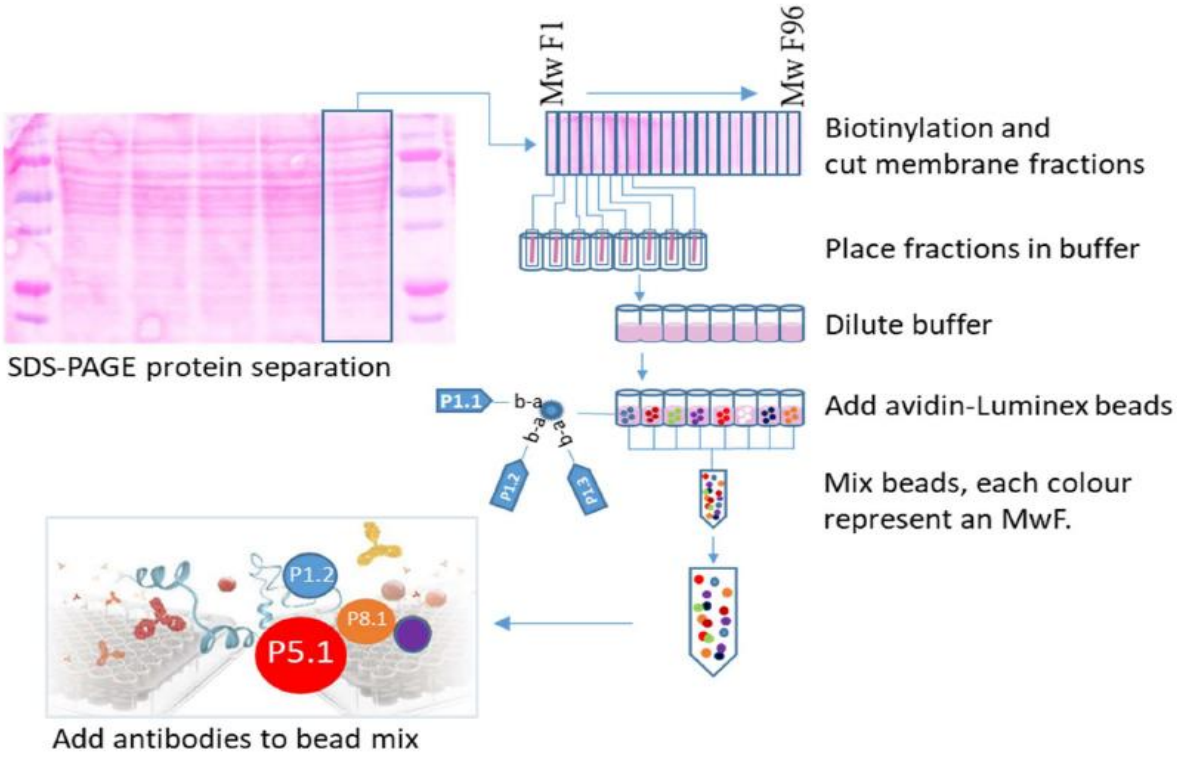

Figure 2.7: Steps involved in DigiWest analysis. Proteins are separated using SDS-polyacrylamide gel electrophoresis and transferred to a blotting membrane, where they are biotinylated. The lanes are cut into 0.5mm strips, and the biotinylated proteins eluted into a 96-well plate. Avidin coated beads are placed in the wells ensuring that different wells have different beads that are read in specific regions on the Luminex analyser. The 96 well plate contents are pooled, subjected to antibody coupling, and read using the FlexMAP3D Luminex instrument.

2.8.1 Analysis of DigiWest Data

Once DigiWest results were available from NMI, the data was analysed thoroughly. The raw data consists of a numerical value for the peak signal (average [median] fluorescence intensity (AFI)), for every analyte used, for control MDA-MB-453 as well as the same cell line transfected with CIP2A, SET and IGBP1. The AFI value is derived from at least 50 data points per analyte. A total of 45 analytes were investigated. As standard procedure, the data is first normalised to the data obtained for the analyte 'strep'. This refers to streptavidin which is bonded to the magnetic beads. Normalisation is done by dividing the peak value obtained for each analyte by the correction factor. The latter is the peak value for strep divided by the median.

When a peak signal was not obtained, it was assigned a value of 50 AFI (This was below any minimum value obtained in the raw data). The normalised data is shown in Table 3.2.

Next, $\log_2$ fold change was calculated using the normalised peak signal values (AFI) obtained in MDA-MB-453 ectopically expressing the three PP2A inhibitors, divided by the normalised peak value signals (AFI) measured in the originator cell lines. Fold change is shown in Table 3.3.

The data in the Table 3.3 was analysed carefully and analytes which showed upregulation or downregulation in the three transfected cell lines were inspected thoroughly. A selection of analytes, relating to PP2A and its regulating mechanisms were also investigated. For each selected analyte, the protein

quantification bar charts generated by DigiWest (peak signal [AFI] against molecular weight [kDa]) were investigated. These are shown in Figures 3.9 to 3.13. A comparison of the results obtained using the CIP2A analyte on MDA-MB-453 transfected cell lines containing SET and CIP2A respectively is shown in Figure 3.8.

2.8.2 Comparison of DigiWest Results to Patient Material

The last step for data analysis involved looking for trends and patterns by comparison of the DigiWest results to patient material available at cBioPortal for Cancer Genomics (https://www.cbioportal.org/). This public website utilises data from The Cancer Genome Atlas (TCGA), an NIH-sponsored research project. The dataset used for this particular study is Breast Invasive Carcinoma (TCGA, Firehose Legacy) and contains a total of 1108 samples (Cerami, et al., 2012; Gao, et al., 2013). Data is obtained from primary and untreated breast tumours. Information about mutations, copy number alterations, mRNA expression and protein levels are available for the dataset. The basic clinic-pathological characteristics and diagnosis age of the cohort are shown in Table 2.9 and Figure 2.8. Results obtained in the analysis are documented in Figures 3.15 to 3.17 and Tables 3.4 to 3.7.

Table 2.9: Clinico-pathological details for the Breast Invasive Carcinoma (TCGA, Firehose Legacy) dataset

	#	Freq ▾
Breast Invasive Ductal Carcinoma	814	73.5%
Breast Invasive Lobular Carcinoma	207	18.7%
Breast Mixed Ductal and Lobular Carcinoma	28	2.5%
Breast Invasive Mixed Mucinous Carcinoma	16	1.4%
Metaplastic Breast Cancer	14	1.3%
Breast	7	0.6%
Invasive Breast Carcinoma	6	0.5%
NA	5	0.5%
Paget Disease of the Nipple	3	0.3%
Adenoid Cystic Breast Cancer	2	0.2%
Malignant Phyllodes Tumor of the Breast	2	0.2%
Solid Papillary Carcinoma of the Breast	2	0.2%
Basal Cell Carcinoma	1	<0.1%
Breast Invasive Carcinoma, NOS	1	<0.1%

Adapted from cBioPortal for Cancer Genomics (https://www.cbioportal.org/)

The data in the table gives details regarding the number of patients diagnosed with a specific breast cancer type, out of the total of 1108 samples. The largest number of patients have been diagnosed with breast invasive ductal carcinoma (814 patients and therefore 73.5 % of the cohort).

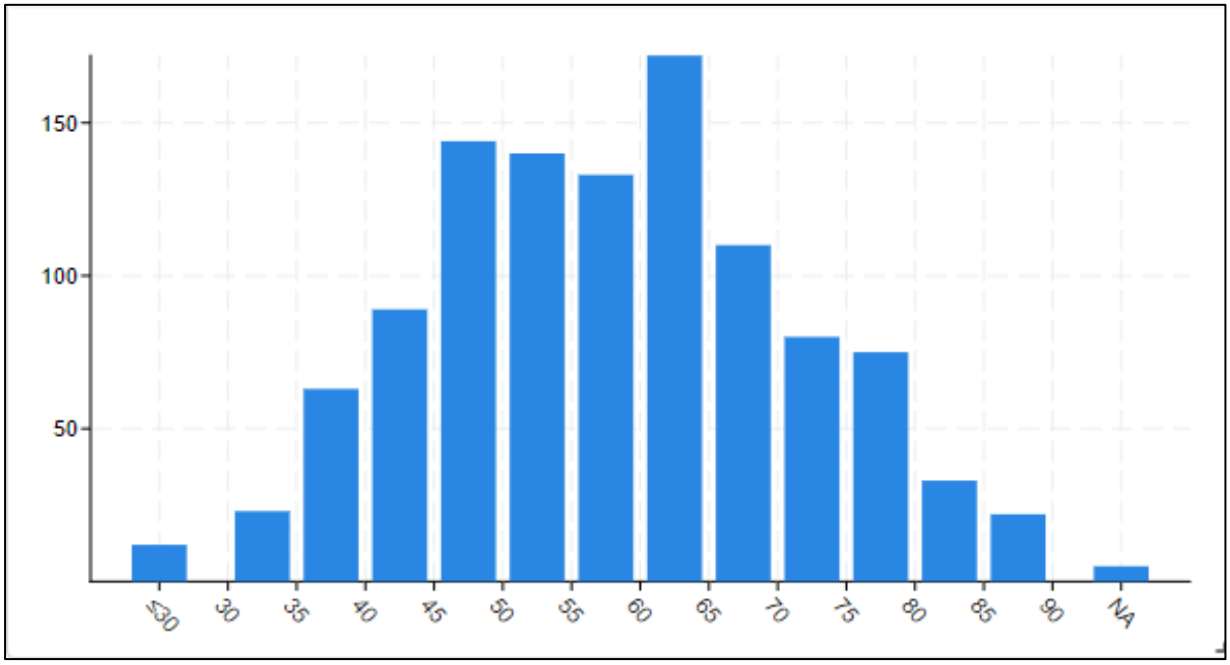

Figure 2.8: Diagnosis age for the Breast Invasive Carcinoma (TCGA, Firehose Legacy) dataset. The figure gives details regarding the diagnosis age of the patients in the cohort. The highest diagnosis age is between 60 to 65, with a total of more than 150 individuals.

2.8.3 Statistical Analysis

Comparison of DigiWest results to the TCGA dataset requires the application of statistical analysis, namely the application of Spearman Rank-order Correlation, a non-parametric test used to measure the degree of association between two variables. This means that the data is not necessarily in normal distribution. The correlation is quantified by means of a value: the Spearman Correlation. There is a perfect positive correlation between the variables with a Spearman of +1 and a perfect negative correlation with a Spearman of -1.

The Spearman Correlation is applicable to both linear and non-linear relationships and generates a p-value. As stated in Section 2.7.6, a p-value of 0.05 is considered of borderline significance. A result is considered statistically significant if the p-value less than 0.01.

Chapter III

Results

3.1 SELECTION OF CELL LINES FOR ECTOPIC EXPRESSION OF CIP2A, SET AND IGBP1

To investigate the effect of ectopic expression of the PP2A inhibiting subunits, CIP2A, SET and IGBP1, the endogenous expression in breast cancer cell lines was measured to select cellular models to study the effect of overexpression studies. First we measured the transcript level of CIP2A and SET using real-time PCR analysis (**Figure 3.1**). IGBP1 was not measured at RNA level, since it was shown previously that the RNA level of this gene is ubiquitously expressed and the level of expression control is at the level of polysome recruitment. Secondly, immunocytochemistry was used to measure the protein expression, including IGBP1, in the cell lines (**Table 3.1**). Hence the aim was to identify breast cancer cell lines that express the endogenous inhibitory subunits at a low level, making them eligible for ectopic expression studies.

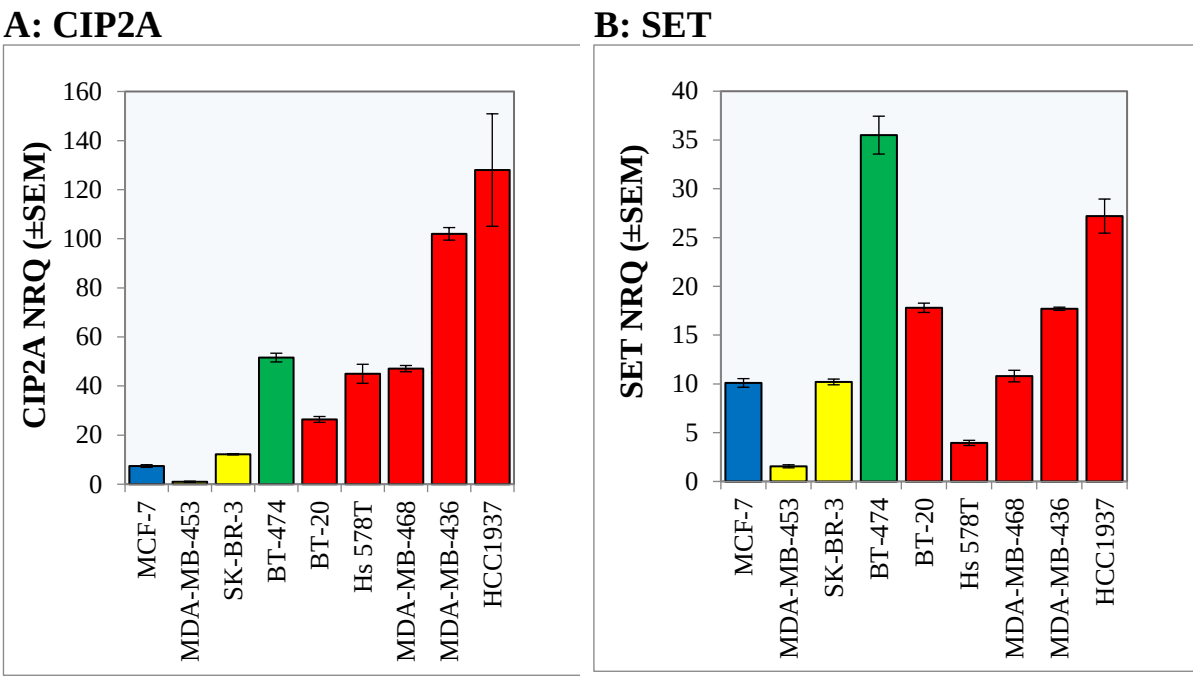

Figure 3.1: Expression of CIP2A [A] and SET [B] using real-time PCR. Cells were cultured in recommended medium and RNA extracted from cultures at high percent viability. The real-time PCR results were measured in normalised relative quantities (NRQ), using housekeeping gene *RPL13A* and MCF-10A as the control breast cancer cell line. Each bar represents an average of three independent biological experiments, with triplicate analytical measurement for each experiment. The standard error is indicated using error bars. The blue bar represents an ER+ cell line, yellow bars represent HER+ cell lines, green bar represents a triple positive cell line and the red bars represent triple negative breast cancer cell lines. The triple negative breast cancer cell lines had a high expression of CIP2A (**Figure 3.1A**) and SET (**Figure 3.1B**), taking an NRQ value of 10 as a threshold for low expression, except for SET expression in Hs578T. The triple positive cell line, BT474 had a high expression of both CIP2A and SET. The ER+ cell line MCF-7 and the HER+ cell lines MDA-MB-453 and SKBR3 showed low expression of both CIP2A and SET when compared to the other subtypes. Of interest, the HER+ cell line MDA-MB-453 had the lowest expression of both CIP2A and SET. The triple negative breast cancer cell line, HCC1937 expressed CIP2A and SET at very high levels and shall be considered as a control with high expression of endogenous inhibitory subunits in further experiments.

Next we measured the protein expression of CIP2A, SET and IGBP1 using immunocytochemistry. IGBP1 was included in this analysis.

Following the immunocytochemistry technique and inspection of the cells, H-scores were calculated for each cell line (Section 2.2.4), stained with antibodies for the PP2A inhibitors CIP2A, SET and IGBP1 (**Table 3.1**). Cell lines MCF-7 and MDA-MB-453 had the lowest H-scores, hence supporting the real-time PCR results. Excluding Hs578T, which represent the lowest H-scores in both SET and IGBP1 at 87 and 15 respectively, MCF-7 and MDA-MB-453 had the lowest H-scores when compared to the other cell lines. The H-scores in HCC1937 support the use of this cell line as a control for high endogenous expression of PP2A inhibitory subunits.

Hence, MCF-7 and MDA-MB-453 cell lines were selected on the basis of low endogenous expression of CIP2A, SET and IGBP1 for the overexpression study.

Table 3.1: CIP2A, SET and IGBP1 Immunocytochemistry H-scores, on a panel of breast cancer cell lines

CIP2A:

Cell line	MCF-7	MDA-MB-453	SK-BR3	BT-474	BT-20	Hs578T	MDA-MB-468	MDA-MB-436	HCC-1937
H-Score	67	0	116	130	175	136	93	235	179

IGBP1:

Cell line	MCF-7	MDA-MB-453	SK-BR3	BT-474	BT-20	Hs578T	MDA-MB-468	MDA-MB-436	HCC-1937
H-Score	73	0	115	87	79	15	98	150	179

SET:

Cell line	MCF-7	MDA-MB-453	SK-BR3	BT-474	BT-20	Hs578T	MDA-MB-468	MDA-MB-436	HCC-1937
H-Score	140	108	126	170	159	87	165	248	160

3.2 THE PP2A ACTIVATOR, FTY720, DOES NOT AFFECT TRANSCRIPTION LEVEL OF PP2A DOWNSTREAM TARGETS

Before carrying out transfection experiments on the selected cell lines, we used the RNA bead-based QuantiGene™ Assay to measure the surrogate marker of PP2A activity, Aurora Kinase A (*AURKA*) and the effect of the PP2A activator, FTY720 on the transcript level of *AURKA*, beta-catenin (*CTNNB1*), fibronectin 1 (*FN1*) and the endogenous inhibitors CIP2A and SET at a transcript level.

The selected cell lines MDA-MB-453 and MCF-7, representing low endogenous levels of PP2A inhibitors, as well as HCC1937 (as a control cell line) were exposed to varying concentrations of the PP2A activating drug, FTY720. Figure 3.2 **[A]** shows AURKA expression in MCF-7, MDA-MB-453 and HCC1937, compared to other cell lines and Figure 3.2 **[B]** shows the effect of PP2A reactivation on the selected genes, in the three cell lines. As expected, the expression of AURKA is low in MCF-7 and MDA-MB-453 predicting a high PP2A activity. Surprisingly the expression of AURKA in the control cell line, HCC1937 was also low. Addition of FTY720 did not result in a decreased AURKA expression. Although there was a 1 $\log_2$ fold decrease in CIP2A following exposure to 5nM of FTY720, this suppression is on the basis of a low expression of CIP2A in MDA-MB-453. There is no effect on *CTNNB1* transcription in both MDA-MB-453 and MCF-7 upon addition of FTY720 (**Figure 3.2**). In the control cell line HCC1937, a 1.5 $\log_2$ fold change is observed for *CIP2A* following exposure to various concentrations of FTY720, indicating that upon activation of PP2A, transcription of *CIP2A* is induced. The increase in CIP2A transcript level does not correlate with the transcription of AURKA and is only seen in the control cell line that expresses CIP2A at high levels when

compared to MCF-7 and MDA-MB-453. Of interest, although it was shown in other studies that FN1 expression is associated with high levels of CIP2A (Gao, et al., 2017), this was not observed in the HCC1937 cell line. The unexpected results following FTY720 exposure on transcription regulation of PP2A targets indicate clearly that the regulation of PP2A through its endogenous inhibitors is complex and requires investigation using overexpression studies of PP2A endogenous inhibitors and measurement at the level of polysome recruitment of transcripts or protein analysis.

[A]:

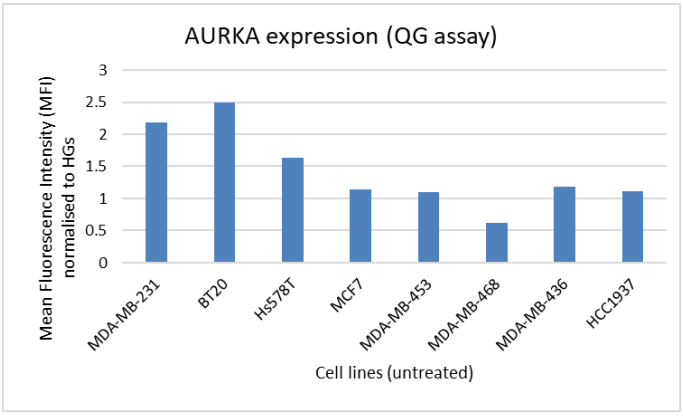

[B]:

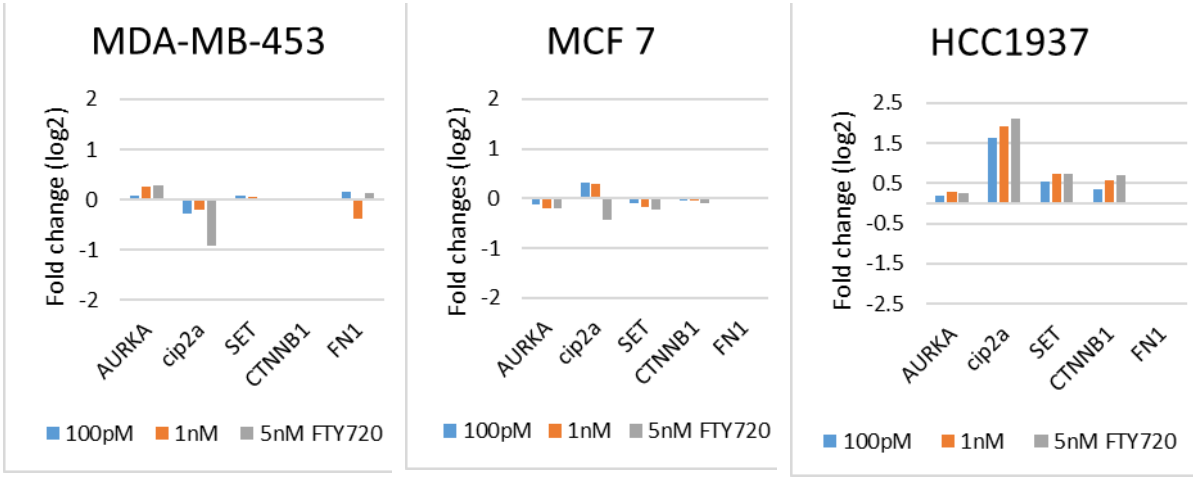

Figure 3.2: The effect of PP2A reactivation in selected cell lines. Figure 3.2 **[A]** shows AURKA expression in various cell lines, MCF-7, while Figure 3.2 **[B]** shows $\log_2$ fold change for RNA levels obtained using QuantiGene™ assay, for a selection of genes, in the cell lines, MDA-MB-453, MCF-7 and HCC1937, using different concentrations of FTY720: 100 pM (blue), 1 nM (orange) and 5 nM (grey).

3.3 CIP2A, SET AND IGBP1 OVEREXPRESSED IN SELECTED CELL LINES

Studying the effect on gene expression of the PP2A inhibitory subunit, CIP2A, SET and IGBP1 required the ectopic expression of the inhibitory subunits in the selected cell lines known to have low endogenous expression. Hence we generated constructs with coding sequences (cds) in a pIRES2-AcGFP1 vector, transcribing a mRNA including reading frames of target and GFP, resulting in expression of both proteins using an internal ribosome entry site to express the GFP protein. First the expression of the proteins was assessed using fluorescent microscopy to show transfection efficiency using GFP (**Figure 3.3**) as an endpoint measurement and Western Blotting to detect the expression of the target of interest (**Figure 3.4**).

The pictures in Figure 3.3 show the transfection experiment carried out. These were grown in a T-25 flask and transfected with the three PP2A inhibitors CIP2A, SET and IGBP1 (one construct per bulk experiment). The control experiment using pmaxGFP empty vector, for both cell lines, is also shown. The green fluorescence is due to the presence of the GFP protein, which is expressed in the cell lines. Both MCF-7 (**Figure 3.3A**) and MDA-MB453 (**Figure 3.3B**) successfully expressed the GFP protein. Transfection efficiency in MCF-7 was higher than in MDA-MB-453 for all constructs, approximately at 70% and 50% respectively. Although the efficiency was the same in all constructs transfected in MDA-MB-453, the intensity of GFP was low upon transfection with the SET-pIRES-GFP construct. To ensure that the presence of GFP driven by the pIRES2, equates to the expression of the target coding sequence, we next analyzed cell lysates using Western blotting.

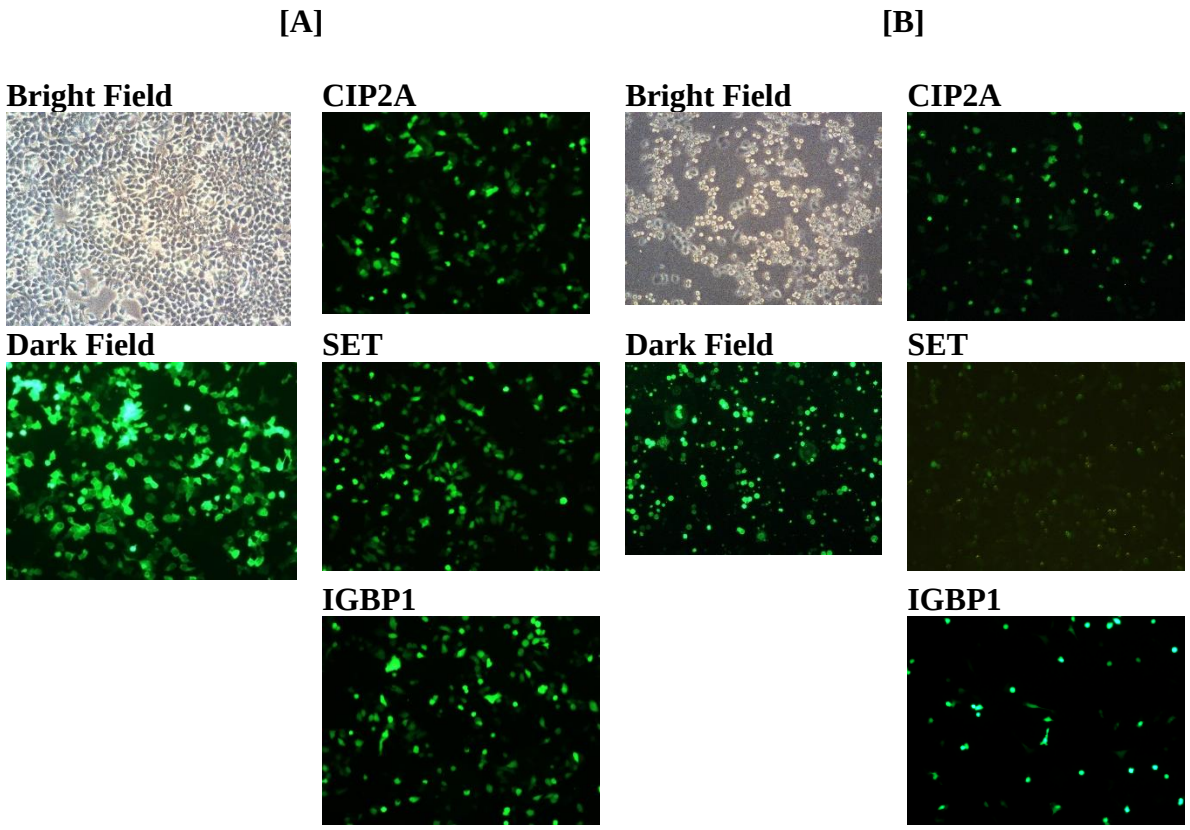

Figure 3.3: Expression of GFP in MCF-7 and MDA-MB-453 following transfection. MCF-7 **[A]** and MDA-MB-453 **[B]** were transfected using FuGENE HD. The frames show a bright field and a dark field (green fluorescence filter) following transfection with the vector only, and three frames showing the expression of GFP following transfection using the CIP2A, SET and IGBP1 construct starting from top to bottom.

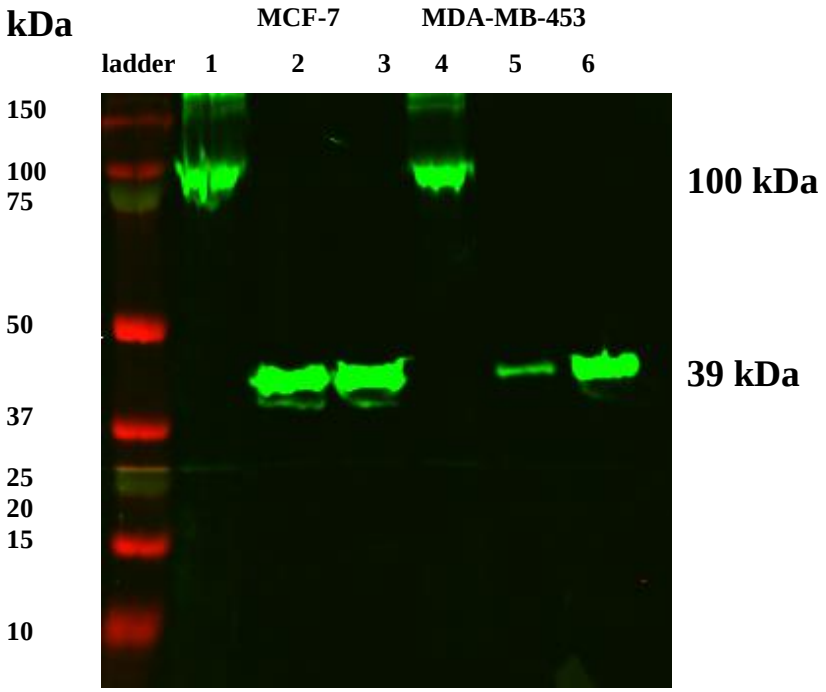

Figure 3.4: Measuring expression of CIP2A, SET and IGBP1 using Western Blot analysis. The Ladder (BIO-RAD Protein Ladder Cat: 1610374) was loaded in the left well. Lanes 1,2,3: 35 µg of lysates from MCF-7 transfected with CIP2A, SET, IGBP1; Lanes 4,5,6: Lysates of MDA-MB-453 transfected with CIP2A, SET, IGBP1. Expression was measured using antibody Myc-Tag 9B11 which recognises the c-MYC tag present in the constructs. The Western blot confirms that both cell lines MCF-7 and MDA-MB-453 are expressing the three inhibitors: CIP2A (100 kDa), SET (39 kDa) and IGBP1 (39 kDa) as bands are obtained in the expected positions. Interestingly, the expression of SET in MDA-MB-453 is lower than the other inhibitory subunits, supporting the GFP results.

3.4 DIFFERENTIAL GENE EXPRESSION USING POLYSOME BOUND RNA

Following successful expression of ectopic CIP2A, SET and IGBP1 in both selected cell lines, bulk transfections were subjected to the extraction of polysome bound RNA. The fractions generated following sucrose gradient density centrifugation were analysed using Agilent Bioanalyser to measure the ratio of 28S:18S. Once the fractions with a 2:1 ratio were identified, these were pooled and further analysed using known translation controlled genes, exemplified by c-MYC. Translation efficiency is driven by mTOR signalling and hence following overexpression of the PP2A inhibitory subunits, which is expected to release PP2A-dependent mTOR negative feedback, polysome recruitment of c-MYC was observed. Enhanced mTOR-dependent polysome recruitment is inhibited by rapamycin, which was also used in this experiment.

Following RNA extraction of twelve fractions from the sucrose gradient centrifugation, the RNA was analysed using capillary electrophoresis (Agilent, Bioanalyser).

[A]:

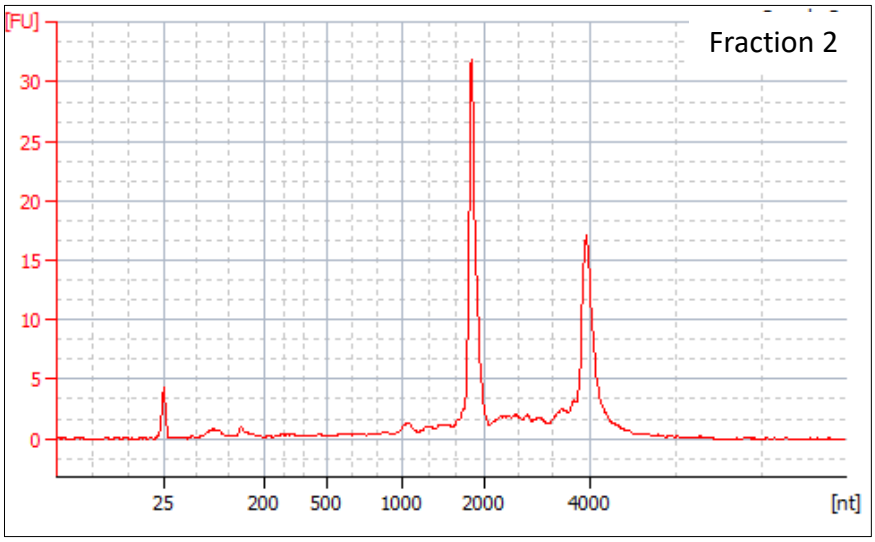

[B]:

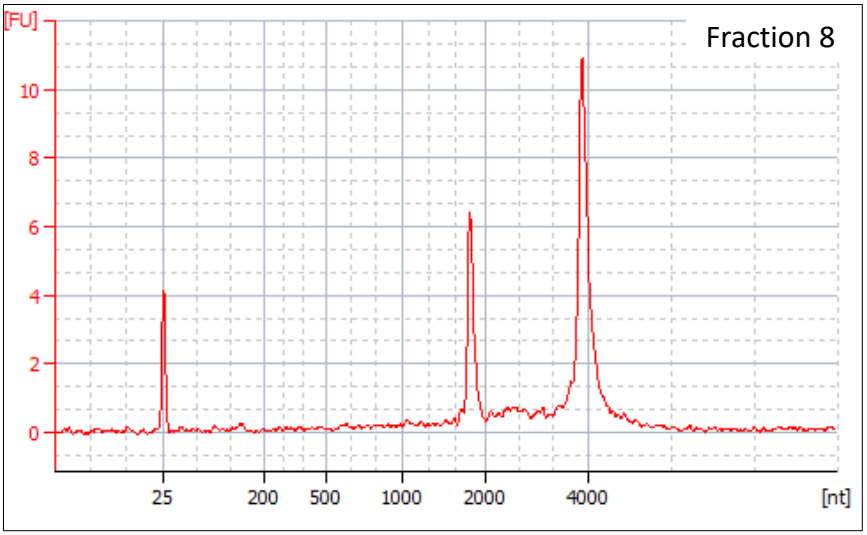

Figure 3.5: Electropherograms of RNA fractions obtained from MDA-MB-453 cell line transfected with CIP2A, following sucrose density gradient centrifugation. This procedure generates 12 fractions. Fraction 2 [A] and fraction 8 [B] are shown here. The 28S resolves at 4000nt, the 18S resolves at around 1800nt and the 5S at 25nt. The quantity is measured in FU. Ratio of 28S:18S were derived from the FU values of the peaks. The results indicate clearly that fraction 2 represents free RNA (**Figure 3.5A**) and fraction 8 (**Figure 3.5B**) represents polysome bound RNA, with a ratio of 2:1 (28S:18S, sample 8).

Each sucrose density gradient centrifugation experiment generates twelve electropherograms that can be visualised as a gel electrophoresis (**Figure 3.6**). The results show that the transition from free RNA to polysome bound at fractions 2 and 3 is consistent, but it is important to measure all samples and fractions to identify samples with proper distribution of RNA. All samples were subjected to this analysis and polysome bound RNA fractions were pooled and further analysis compared to pooled free RNA fractions.

[A]:

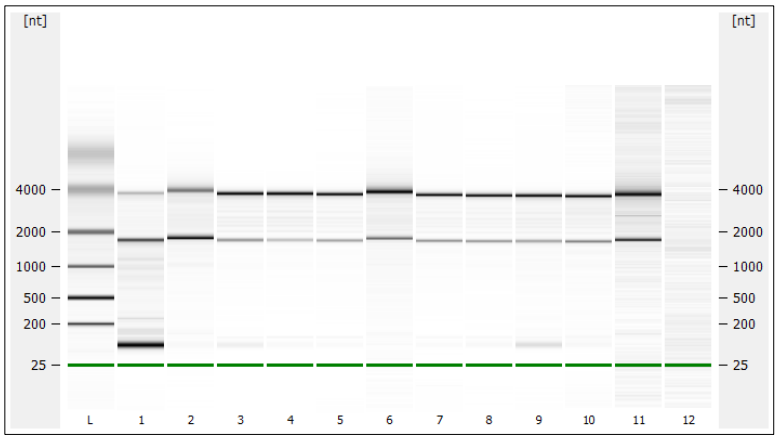

[B]:

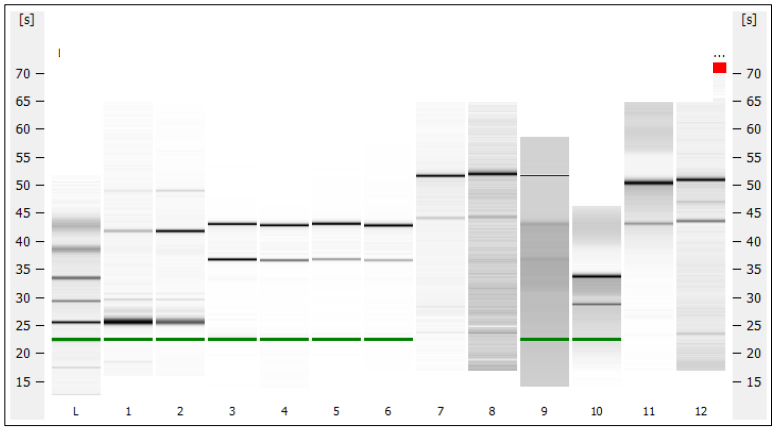

Figure 3.6: Capillary electrophoresis of RNA fractions taken from the MDA-MB-453 cell line transfected with CIP2A, following sucrose gradient centrifugation. The figure shows **[A]** sample with a proper distribution of free and polysome bound RNA fractions with fractions 3-11 showing a 28:18S ratio of 2:1, free RNA in fractions 1 and 2 with the 5S in fraction 1, while **[B]** sample shows a sucrose gradient with a proper transition from free to polysome bound, which is disrupted from fractions 7 to 12.

Prior to differential gene expression analysis using polysome bound RNA, we wanted to measure the effect of the ectopic expression of the PP2A inhibitory subunits on the polysome recruitment of a known translationally controlled transcript, c-MYC. Hence, using the pooled polysome bound fractions and separately the pooled free fractions from each sample, we performed real-time PCR to quantify c-MYC in the various RNA compartments following addition of empty vector, or CIP2A, or SET or IGBP1 transfected cells. To show that this is a PP2A-dependent, mTOR activity (and hence inhibited with rapamycin), the transfected cells were also treated with rapamycin. Percent polysome recruitment was determined by the ΔCT ratio of free RNA and pbRNA. The cell line HCC1937 was included since it has high levels of endogenous expression for CIP2A and SET (refer to Figure 3.7).

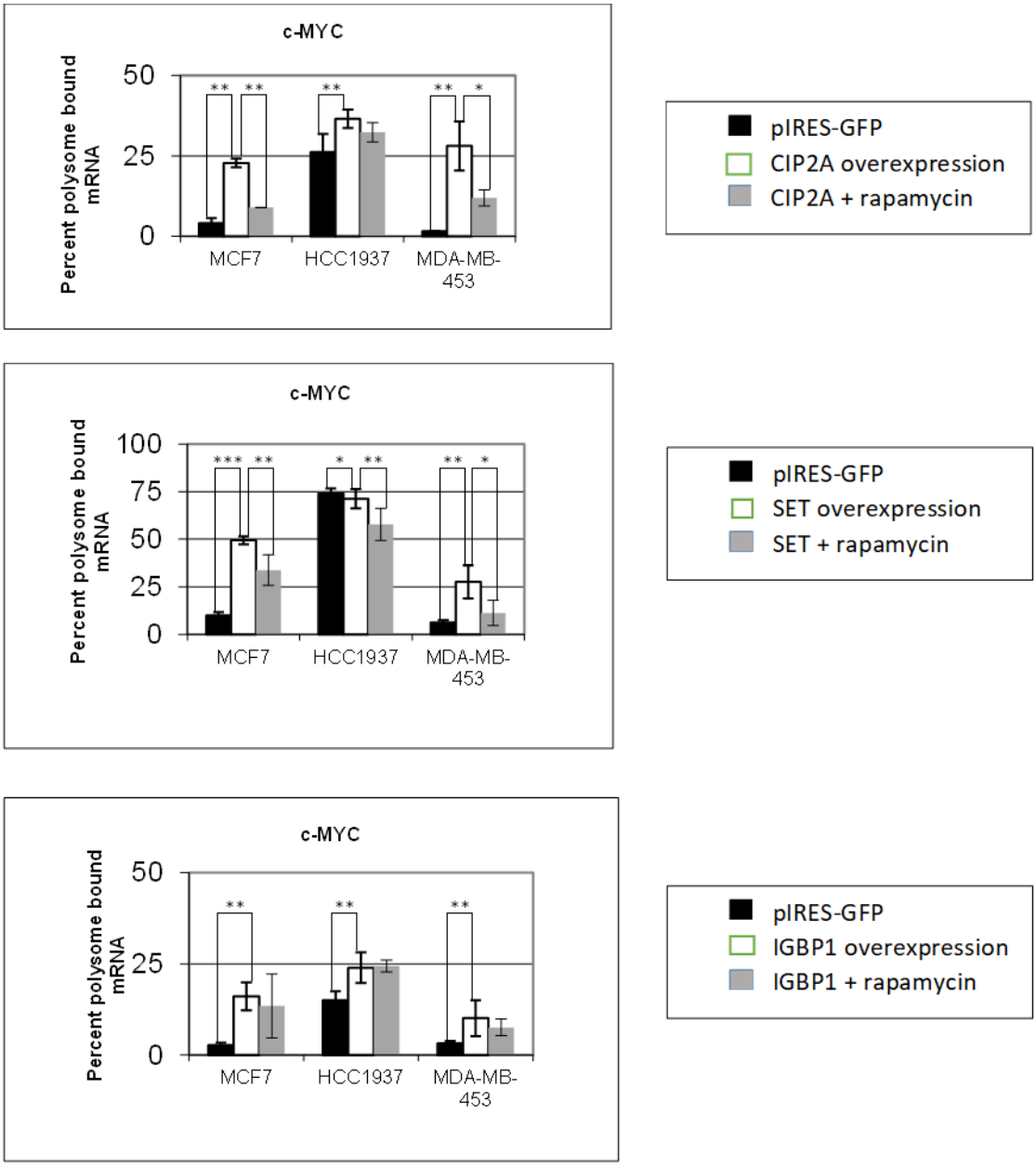

Figure 3.7: Percent polysome recruitment of c-MYC following overexpression of CIP2A, SET and IGBP1 in MCF-7, HCC1937 and MDA-MB-453. Cells were transfected with pIRES2-AcGFP1 (black bars; vector control) or the pIRES constructs to overexpress CIP2A, SET and IGBP1 in the absence (white bars) or presence (grey bars) of 10nM rapamycin. Each data point is an average of three independent experiments, with triplet analytic measurement for each experiment. The application of a paired t-test generates p-values; significant p-values (0.05 or less) are indicated as shown: ***: <0.05; **: < 0.01; ***: < 0.001.**

The results in Figure 3.7 show that recruitment of c-MYC transcript to the polysomes increases upon overexpression of CIP2A, SET and IGBP1 in both MCF-7 and MDA-MB-453. There is no increase in HCC1937 since this cell line express high endogenous levels of the PP2A inhibitory subunits, and the polysome recruitment of c-myc was high in the absence of ectopic expression. As expected, there is a decrease in polysome recruitment upon addition of the mTOR inhibitor rapamycin when CIP2A and SET were overexpressed.

Of interest, although we have shown previously that SET ectopic expression is the lowest, SET resulted in a high degree of enhanced polysome recruitment when compared to CIP2A and IGBP1 in the MCF-7 cell line. The increase in polysome recruitment was the lowest following IGBP1 overexpression. In fact the decrease in polysome recruitment following rapamycin was minimal in the IGBP1-overexpressing cells.

When we compared the pIRES2-AcGFP1 vector control in HCC1937 in the different experiments, it was evident that the magnitude of polysome recruitment was not constant, giving percentages of 75 %, 25 % and 20 %. To our knowledge this should be constant between experiments since we used the same passage and vector control. This was confirmed by conducting a paired t-test between the separate experiments, and comparison of the means gave p-values of 0.05 or less (Refer to Appendix A). This observation prompted us to explore other ways of investigating differential expression in the cellular models, and hence we opted for the DigiWest Technology.

3.5 EIF4E, PKC, ERK AND BETA-CATENIN ARE REGULATED BY PP2A INHIBITORY SUBUNITS

We have shown that the known PP2A targets are not regulated at the level of transcription using the PP2A activator, FTY720. Using polysome bound RNA measurements, we showed that the translationally controlled transcript, c-MYC is recruited to polysomes following overexpression of the PP2A inhibitory subunits, CIP2A, SET and IGBP1. The control cell line HCC1937 showed variable polysome recruitment between repeated measures. The option of Digital Westerns (DigiWest) became available as an innovative technique during this study. We utilised DigiWest analysis to measure protein expression and activation (phospho-profile) following overexpression of the PP2A inhibitory subunits CIP2A, SET and IGBP1 in MDA-MB-453.

The DigiWest multiplex bead-based assay utilised 45 antibodies, including 18 total protein antibodies and 27 specific phospho-proteins. These antibodies, referred to as analytes, are epitope specific. DigiWest analysis was carried out on the control MDA-MB-453 cell line, as well as the same cell line transfected with the PP2A inhibitory subunits CIP2A, SET and IGBP1. This cell line has the lowest level of inhibitors, as proven by RT-PCR and ICC (**Figure 3.1 and Table 3.1**). As described in Section 2.8, the weight of the protein is inputted into the DigiWest software, to ensure that the target peak (shown as a dark grey peak on the protein quantification bar chart) is the protein of interest.

In order to ensure that the DigiWest technology was yielding satisfactory results, preliminary investigations were conducted on the MDA-MB-453 cell line,

transfected with SET and CIP2A. Figure 3.8 shows the protein quantification bar chart obtained using the analyte CIP2A #1426, for the SET (**A**) and CIP2A (**B**) transfected cell lines.

A: SET **B: CIP2A**

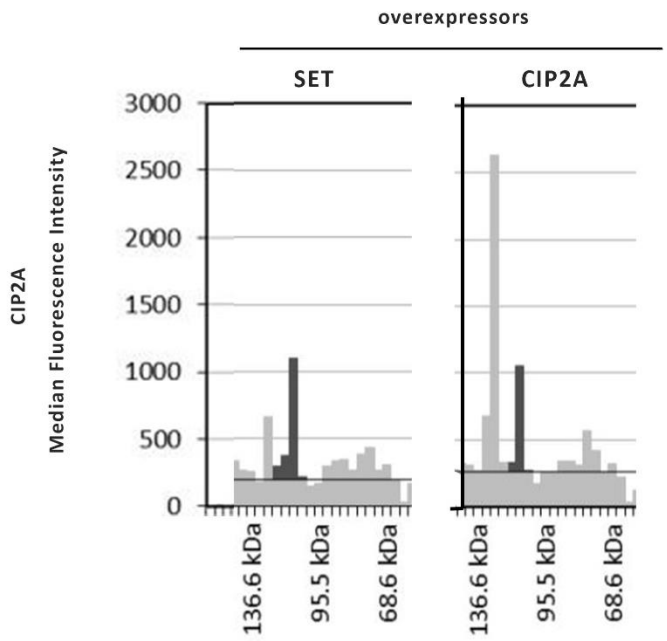

Figure 3.8: CIP2A expression in MDA-MB-453 cells overexpressing SET and CIP2A. The CIP2A antibody #1426 was used in the antibody panel in this DigiWest run. The y-axis represents the Average (Median) Fluorescence Intensity (AFI) and the x-axis the kDa distribution. The peaks in dark grey represent signify the position of the CIP2A protein. A peak at approximately 100 kDa (dark grey) is present in both transfected cell lines. Hence both bulk transfections express endogenous CIP2A at a low level (approx. 1000 AFI). Typically, an endogenously expressed protein, exemplified by eIF4E has an AFI value of 18,000 (**Table 3.2**). Comparing the peaks obtained following SET overexpression and CIP2A overexpression, the CIP2A antibody generated another peak of significant intensity (> 2500 AFI) in MDA-MB-453 expressing ectopic CIP2A. This peak has a molecular weight value of approximately 140 kDa. The 140 kDa peak represents the ectopic CIP2A including the MYC tag that is in frame with the coding sequence.

The raw data obtained from the DigiWest analysis was normalised against strep, as described in Section 2.7.1 and shown in Table 3.2.

Table 3.2: Normalisation of DigiWest raw data

	CONTROL	IGBP1	SET	CIP2A
ANALYTE	[AFI]	[AFI]	[AFI]	[AFI]
4E-BP1 - phosphoSer65# 1202	200.0	196.8	243.6	228.8
4E-BP1 - phosphoThr37/Thr46# 1203 P1	737.5	451.1	626.1	475.4
4E-BP1 - phosphoThr37/Thr46# 1203 P2	50.0	473.1	626.1	636.3
4E-BP1 - phosphoThr70# 2345 P1	572.5	195.1	385.5	372.0
4E-BP1 - phosphoThr70# 2345 P2	287.5	249.2	280.0	350.0
beta-Catenin# 1783	2215.1	7483.5	7639.4	9604.9
beta-Catenin - phosphoSer552# 1862	135.0	293.1	245.5	486.9
beta-Catenin (non-pospho Ser33/37/Thr41; active) # 2323	50.0	673.3	590.7	836.9
c-myc# 1717	937.5	27208.1	19614.8	33336.7
c-myc - phosphoThr58# 2398	1955.1	1021.3	1124.8	1197.3
c-myc - phosphoThr58/Ser62# 1240	50.0	87.9	59.5	56.4
CREB# 1827	125.0	50.0	50.0	50.0
CREB - phosphoSer133# 1920	50.0	79.4	295.3	118.1
DEPTOR/DEPDC6# 2355	775.0	465.4	697.1	392.8
eIF4B# 2189	440.0	50.0	50.0	50.0
eIF4B - phosphoSer406# 2356	50.0	50.0	50.0	54.3
eIF4B - phosphoSer422# 2188	300.0	50.0	85.3	50.0
eIF4E# 1820	18048.4	11277.2	11708.9	10066.7
eIF4E - phosphoSer209# 1904	435.0	638.6	645.3	414.8
Erk1/2 (MAPK p44/42) P1 + P2	43163.6	15168.9	13701.3	15265.5
GRB10 - phosphoSer476# 2365	50.0	50.0	50.0	90.9
GSK3 beta# 1835	8727.9	4626.6	7080.4	7345.0
GSK3 beta - phosphoSer9# 2073	50.0	50.0	50.0	133.7
Mcl-1# 0702 P1	50.0	104.7	50.0	50.0
Mcl-1# 0702 P2	50.0	187.5	543.7	572.6
Mcl-1 - phosphoSer159/Thr163# 0698	50.0	50.7	50.0	50.0
p70 S6 kinase# 1566 P1	165.0	50.0	81.5	117.0
p70 S6 kinase# 1566 P2	2780.1	751.0	782.4	644.6
p70 S6 kinase - phosphoThr389# 1211	157.5	50.0	50.0	50.0
PKC (pan) - phosphoSer660# 1218	1247.6	261.0	198.5	361.5
PKC (pan) gamma - phosphoThr514# 2378 P1	4480.2	2198.0	2047.2	2655.9
PKC (pan) gamma - phosphoThr514# 2378 P2	2302.6	1574.6	1475.7	1152.4
PKC alpha# 1583	50.0	50.0	50.0	72.1
PKC alpha - phosphoSer657# 2340	570.0	234.8	291.5	300.9
PKC alpha - phosphoThr497# 2341	50.0	1302.6	1324.2	1346.8
PKC alpha/beta II - phosphoThr638/Thr641TK # 092	50.0	385.2	466.0	492.1
PRAS40# 2081	3775.2	2459.9	3672.5	3195.0
PRAS40 (AKT1S1) - phosphoThr246# 2487	50.0	59.1	50.0	50.0
Raptor# 1167	632.5	585.4	780.5	467.0
Raptor - phosphoSer792# 1467	50.0	129.2	122.7	57.5
Rictor# 1468	50.0	174.9	167.8	103.4
S6 ribosomal protein# 1836	6192.8	14820.9	12758.8	12085.3
S6 ribosomal protein - phosphoSer235/236# 2079	24163.7	16136.1	22334.2	25950.9
S6 ribosomal protein - phosphoSer240/Ser244BG/MP # 055	8430.4	5738.3	7506.1	9514.0
SGK1 - phosphoSer78# 2387	870.0	120.0	62.3	94.0

Table 3.2 shows normalised DigiWest data (average fluorescent intensity (AFI)) for every analyte used, for the control MDA-MB-453 cell line, as well as the same cell line transfected with IGBP1, SET and CIP2A. The raw data is normalised to the data obtained for the analyte 'strep' as described in Section 2.7.1. When a peak signal was not obtained, it was assigned a value of 50 AFI (This was below any minimum value obtained in the raw data).

Fold change $\log_2$ values were also calculated as described in Section 2.7.1 and are shown in Table 3.3.

Table 3.3: Log_2 fold change relative to control, for transfected cell lines

	CONTROL	IGBP1	SET	CIP2A
ANALYTE				
4E-BP1 - phosphoSer65# 1202	0.00	-0.02	0.28	0.19
4E-BP1 - phosphoThr37/Thr46# 1203 P1	0.00	-0.71	-0.24	-0.63
4E-BP1 - phosphoThr37/Thr46# 1203 P2	0.00	3.24	3.65	3.67
4E-BP1 - phosphoThr70# 2345 P1	0.00	-1.55	-0.57	-0.62
4E-BP1 - phosphoThr70# 2345 P2	0.00	-0.21	-0.04	0.28
beta-Catenin# 1783	0.00	1.76	1.79	2.12
beta-Catenin - phosphoSer552# 1862	0.00	1.12	0.86	1.85
beta-Catenin (non-pospho Ser33/37/Thr41; active) # 2323	0.00	3.75	3.56	4.07
c-myc# 1717	0.00	4.86	4.39	5.15
c-myc - phosphoThr58# 2398	0.00	-0.94	-0.80	-0.71
c-myc - phosphoThr58/Ser62# 1240	0.00	0.81	0.25	0.17
CREB# 1827	0.00	-1.32	-1.32	-1.32
CREB - phosphoSer133# 1920	0.00	0.67	2.56	1.24
DEPTOR/DEPDC6# 2355	0.00	-0.74	-0.15	-0.98
eIF4B# 2189	0.00	-3.14	-3.14	-3.14
eIF4B - phosphoSer406# 2356	0.00	0.00	0.00	0.12
eIF4B - phosphoSer422# 2188	0.00	-2.59	-1.81	-2.59
eIF4E# 1820	0.00	-0.68	-0.62	-0.84
eIF4E - phosphoSer209# 1904	0.00	0.55	0.57	-0.07
Erk1/2 (MAPK p44/42) P1 + P2	0.00	-1.51	-1.66	-1.50
GRB10 - phosphoSer476# 2365	0.00	0.00	0.00	0.86
GSK3 beta# 1835	0.00	-0.92	-0.30	-0.25
GSK3 beta - phosphoSer9# 2073	0.00	0.00	0.00	1.42
Mcl-1# 0702 P1	0.00	1.07	0.00	0.00
Mcl-1# 0702 P2	0.00	1.91	3.44	3.52
Mcl-1 - phosphoSer159/Thr163# 0698	0.00	0.02	0.00	0.00
p70 S6 kinase# 1566 P1	0.00	-1.72	-1.02	-0.50
p70 S6 kinase# 1566 P2	0.00	-1.89	-1.83	-2.11
p70 S6 kinase - phosphoThr389# 1211	0.00	-1.66	-1.66	-1.66
PKC (pan) - phosphoSer660# 1218	0.00	-2.26	-2.65	-1.79
PKC (pan) gamma - phosphoThr514# 2378 P1	0.00	-1.03	-1.13	-0.75
PKC (pan) gamma - phosphoThr514# 2378 P2	0.00	-0.55	-0.64	-1.00
PKC alpha# 1583	0.00	0.00	0.00	0.53
PKC alpha - phosphoSer657# 2340	0.00	-1.28	-0.97	-0.92
PKC alpha - phosphoThr497# 2341	0.00	4.70	4.73	4.75
PKC alpha/beta II - phosphoThr638/Thr641TK # 092	0.00	2.95	3.22	3.30
PRAS40# 2081	0.00	-0.62	-0.04	-0.24
PRAS40 (AKT1S1) - phosphoThr246# 2487	0.00	0.24	0.00	0.00
Raptor# 1167	0.00	-0.11	0.30	-0.44
Raptor - phosphoSer792# 1467	0.00	1.37	1.30	0.20
Rictor# 1468	0.00	1.81	1.75	1.05
S6 ribosomal protein# 1836	0.00	1.26	1.04	0.96
S6 ribosomal protein - phosphoSer235/236# 2079	0.00	-0.58	-0.11	0.10
S6 ribosomal protein - phosphoSer240/Ser244BG/MP # 055	0.00	-0.55	-0.17	0.17
SGK1 - phosphoSer78# 2387	0.00	-2.86	-3.80	-3.21

Table 3.3 shows log_2 fold change normalised to the originator cell line was calculated for each analyte as described in Section 2.7.1, using the normalised peak signal values (AFI) obtained in MDA-MB-453 ectopically expressing IGBP1, SET and CIP2A the originator normalised peak value signals (AFI) measured in the originator cell lines. The data in this table was analysed carefully and analytes of interest were selected and investigated further (Refer to Figures 3.9 to 3.14).

Of interest, 4E-BP1 phosphoThr37/Thr46 shows an increase in AFI in peak 2 that represents the hyperphosphorylation state of the protein, also seen as a shift in size to a higher kDa distribution. A fold change (log_2) of 3.2 was measured following overexpression of IGBP1, and 3.6 for both SET and CIP2A overexpression. Beta-catenin and c-MYC show an increase in total protein with a fold change of 1.8 and 4.5, respectively. This was seen in CIP2A, SET and IGBP1 with CIP2A overexpression showing the highest fold change for both proteins. Interestingly phospho-ERK showed a decrease in phosphorylation when considering the summation of both p44 and p42 isoforms. The advantage of DigiWest is that one can also investigate the different subunits separately by defining the peaks. In fact, analysis of the ratio of the p44: p42 isoform ratio shows a regulation on the basis of ERK isoform distribution (**Figure 3.13**). We also see an increase in protein expression of MCL1 (log_2 of 3 in CIP2A and SET) and RICTOR (log_2 of 1 to 1.8). The regulation of PKC alpha and p70 S6K show variable regulations at the different phosphorylated sites. Upon overexpression of CIP2A, SET and IGBP1 we show a decrease in the total and phosphorylation of p70 S6K. PKC alpha shows an increase in phosphorylation at Threonine 487 (#2341) and Threonine 638/642 (#092) following overexpression of CIP2A (log_2 of 4.7 and 3.3 respectively), SET (log_2 of 4.7 and 3.2 respectively) and IGBP1 (log_2 of 4.7 and 2.9 respectively). The AFI of PKC alpha total antibody, measured by the antibody #1583, did not give signals above the threshold and hence we

could not derive phospho: total ratios. This was possible using the S6 ribosomal protein data. There is an increase (log_2 fold change of 1 to 1.2) in total protein expression when overexpressing the three PP2A inhibitory subunits. Taking the phospho: total ratios, there is a decrease in S6 ribosomal protein Ser 235/236 phosphorylation. The control cells have a phospho: total ratio of 3.9 and this value decreases to 1.1, 1.8 and 2.2 in cells overexpressing IGBP1, SET and CIP2A respectively.

Following this analysis, we selected the following analytes to present the detailed results, which are summarised in this paragraph. Figures 3.9 to 3.12 show protein quantification bar charts for analytes c-myc# 1717, beta-catenin# 1783, 4E-BP1 PhosphoSer65# 1202, 4E-BP1 PhosphoThr37/Thr46# 1203, p70 S6 kinase# 1566, p70 S6 kinase phosphoThr 389# 1211, PKC alpha-phosphoThr497# 2341 and PKC alpha/beta II-phosphoThr638/Thr641TK# 092. The results in Table 3.3 and Figure 3.9 show that there is a log_2 of 4.9, 4.4 and 5.2 in the cell lines transfected with IGBP1, SET and CIP2A respectively for c-MYC. A similar trend is seen in beta-catenin (log_2 of 1.8, 1.8 and 2.1) and hyperphosphorylated 4E-BP1 (log_2 of 3.2, 3.7 and 3.7) (**Table 3.3** and **Figure 3.10**). Table 3.3 and Figure 3.11 show that overexpression of the PP2A inhibitory subunits has inhibited the expression of p70 S6 kinase. Table 3.3 and Figure 3.12 also show that show that presence of the three inhibitors in the transfected cell lines increases the presence of both phosphorylated PKC proteins significantly (log_2 of 4.7, 4.7 and 4.8; log_2 of 2.9, 3.2 and 3.3).

Figure 3.13 shows the protein quantification chart for ERK1/2 MAPK (p44/42). Interestingly, the expression of the two ERK isoforms is significantly different in the transfected cell lines.

The figure below shows the DigiWest result obtained for c-MYC and beta-catenin, in the control and transfected MDA-MB-453 cell line. Both c-MYC and beta-catenin are downstream targets of PP2A. Both require eIF4E for translation. The latter becomes available when the mTOR pathway is not inhibited by PP2A (Refer to Sections 1.3.4 and 1.3.5).

[A]: **[B]:**

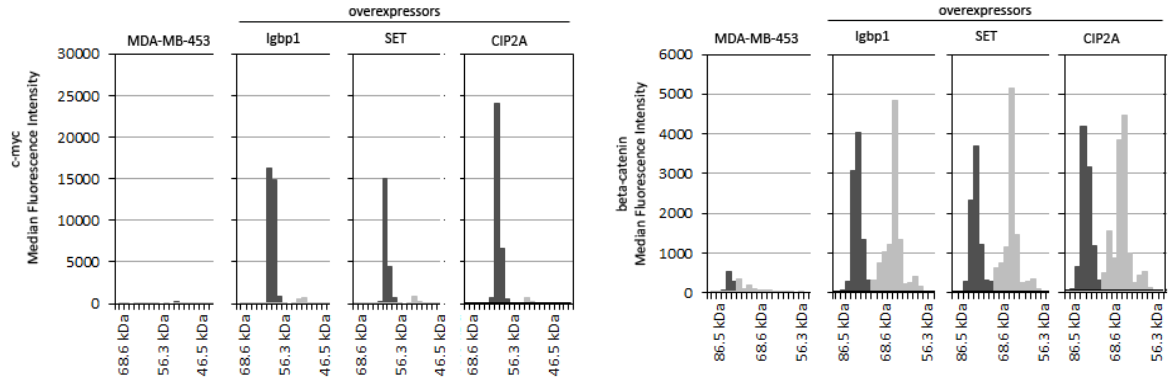

Figure 3.9: Protein quantification bar charts for c-MYC and beta-catenin using the DigiWest technology. The bar charts show the peak signal value (AFI) for c-MYC **[A]** and beta-catenin **[B]**, each represented by a dark grey peak. In both bar charts, the x-axis represents the protein size in kDa and the y-axis shows the Average Fluorescence Intensity (AFI) generated by the Luminex read-out. The expected size of c-MYC is 65 kDa and that of beta-catenin is 85 kDa. From left to right the bar charts represent the control (originator cell line MDA-MB-453) and the transfected MDA-MB-453 with IGBP1, SET and CIP2A (far right).

The figure on page 102 (**Figure 3.10**) shows the DigiWest result obtained for phosphorylated 4E-BP1 in the control and transfected MDA-MB-453 cell line. 4E-BP1 is a downstream effector of the mTOR pathway. When 4E-BP1 is phosphorylated at various locations, such as serine and threonine, it releases eIF4E, making the latter available for polysome recruitment of a number of transcripts, including c-MYC and beta-catenin. This occurs when the mTOR pathway is not inhibited by PP2A (Refer to Sections 1.3.4 and 1.3.5).

The figure on page 103 (**Figure 3.11**) shows the DigiWest result obtained for p70 S6 kinase and phosphorylated p70 S6 kinase, in the control and transfected MDA-MB-453 cell line. As described in section 1.3.2, is an mTOR-dependent kinase with a central role in cap dependent translation initiation. Phosphorylated p70 S6 kinase phosphorylates eIF4B, promoting its binding with eIF3. Hence low PP2A activity has a direct effect on both p70 S6 kinase and eIF4B.

The figure on page 104 (**Figure 3.12**) shows the DigiWest result obtained for phosphorylated PKC alpha in the control and transfected MDA-MB-453 cell line. Previous investigations have shown that the regulatory subunit PPP2R2A dephosphorylates and inactivates PKC alpha (Ruvolo, et al., 2014). Phosphorylated PKC alpha is active and suppresses the PPP2R5A regulatory subunit, therefore c-MYC is stabilized.

The figure on page 105 (**Figure 3.13**) shows the DigiWest result obtained for ERK 1 and ERK 2, two isoforms in the ERK pathway. The major function of this signalling pathway is to regulate cell proliferation and apoptosis. PP2A is a negative regulator of the ERK pathway, as described in Section 1.3.6.

[A]: **[B]:**

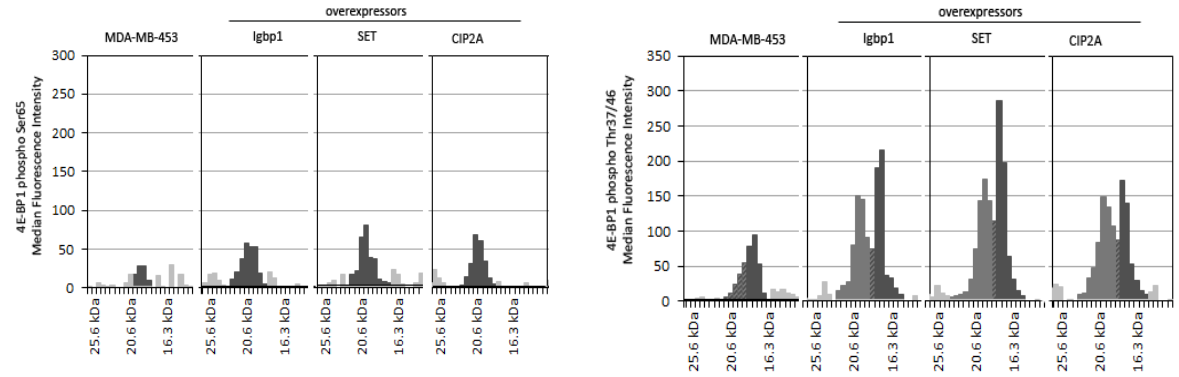

Figure 3.10: Protein quantification bar charts for 4E-BP1 phosphoSer65 and 4E-BP1 phosphoThr37/Thr46 using the DigiWest technology. The bar charts show the peak signal value (AFI) for 4E-BP1 phosphorylated at serine 65 (#1202; dark grey peak) **[A]** and at threonine 37/46 (#1203) **[B]**. In the latter figure, two peaks are observed. The dark grey peak represents hypophosphorylated 4E-BP1 (P1) while the light grey peak is the hyperphosphorylated 4E-BP1 (P2). The difference between the two phosphorylated states becomes visible since 4E-BP1 is a low molecular weight protein. In both bar charts, the x-axis represents the protein size in kDa and the y-axis shows the Average Fluorescence Intensity (AFI) generated by the Luminex read-out. The expected size of hypophosphorylated 4E-BP1 is about 17 kDa while the hyperphosphorylated 4E-BP1 is about 20 kDa. From left to right the bar charts represent the control (originator cell line MDA-MB-453), cell line MDA-MB-453 transfected with IGBP1, followed by SET and at the far right the CIP2A.

[A]: **[B]:**

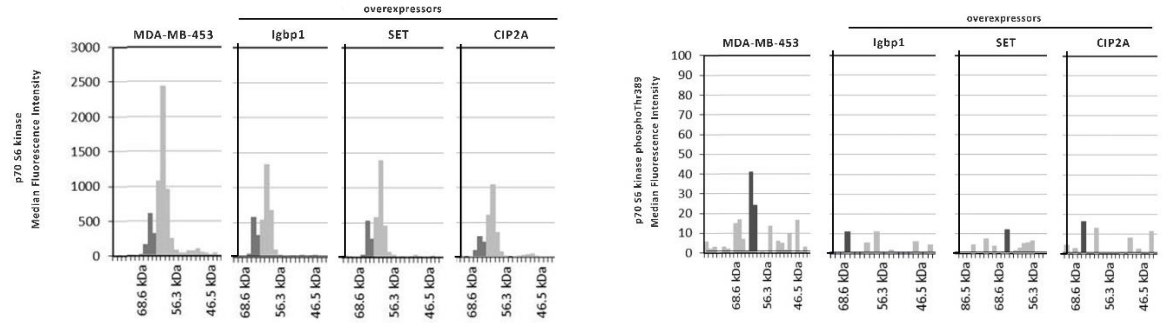

Figure 3.11: Protein quantification bar charts for p70 S6 kinase and p70 S6 kinase phosphoThr389 using the DigiWest technology. The bar charts show the peak signal value (AFI) for p70 S6 kinase (#1566) **[A]** and p70 S6 kinase phosphorylated at threonine 389 (#1211) **[B]**. In both bar charts, the x-axis represents the protein size in kDa and the y-axis shows the Average Fluorescence Intensity (AFI) generated by the Luminex read-out. The expected size of p70 S6 kinase is about 70 kDa. From left to right the bar charts represent the control (originator cell line MDA-MB-453), cell line MDA-MB-453 transfected with IGBP1, followed by SET and at the far right the CIP2A. A peak at approximately 70 kDa would be expected in these bar graphs, showing the expression of p70 S6 kinase, but this is not present.

[A]: **[B]:**

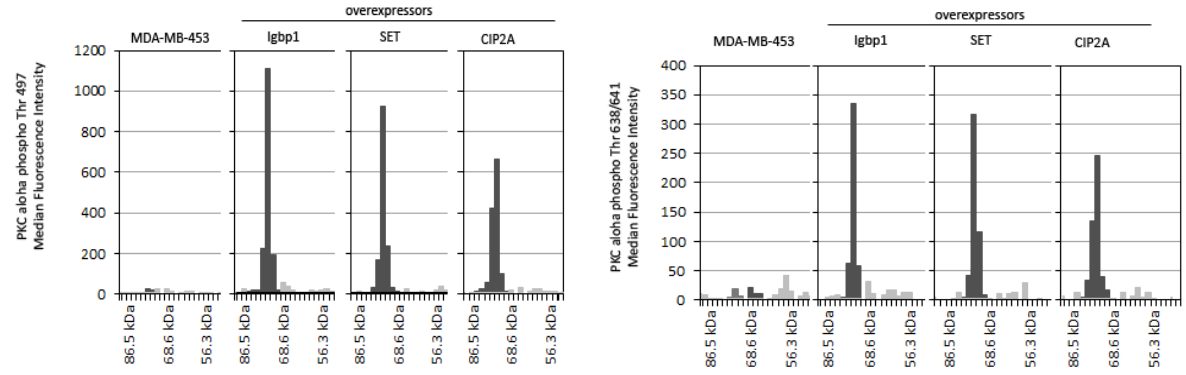

Figure 3.12: Protein quantification bar charts for PKC alpha-phosphoThr497 and PKC alpha/beta II-phosphoThr638/Thr641 using the DigiWest technology. The bar charts show the peak signal value (AFI) for protein kinase C (PKC) phosphorylated at threonine 497 (#2341) **[A]** and at threonine (#092) **[B]**. In both bar charts, the x-axis represents the protein size in kDa and the y-axis shows the Average Fluorescence Intensity (AFI) generated by the Luminex read-out. The expected size of PKC is about 77 kDa. From left to right the bar charts represent the control (originator cell line MDA-MB-453), cell line MDA-MB-453 transfected with IGBP1, followed by SET and at the far right the CIP2A.

A:

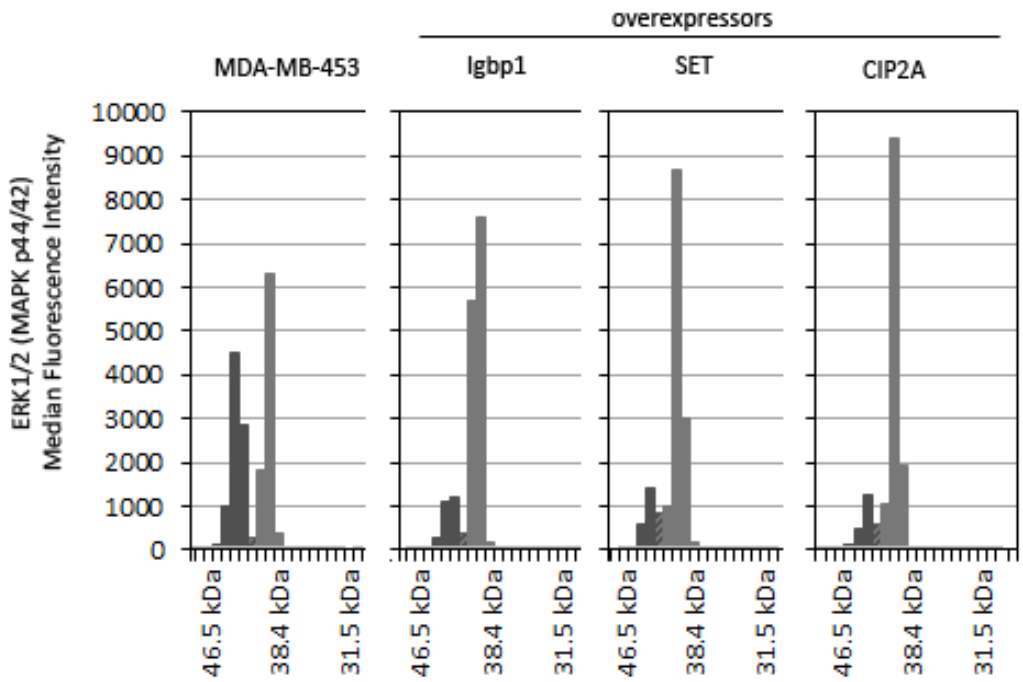

B:

	MDA-MB-453 cell line	$ERK2^{p42}$/ $ERK1^{p44}$ (peak2/peak1) ratio
	CONTROL	1.0031
Transfected cell lines	**IGBP1**	5.3726
	SET	4.8681
	CIP2A	6.0344

Figure 3.13: Protein quantification bar charts for ERK1/2 using the DigiWest technology. The bar charts show the peak signal value (AFI) for ERK1/2 (p44/p42) represented by peak 1 (dark grey) and peak 2 (light grey) **[A]**. The x-axis represents the protein size in kDa and the y-axis shows the Average Fluorescence Intensity (AFI) generated by the Luminex read-out. The expected size of ERK1 (dark grey) is 44 kDa and ERK2 (light grey) is 42 kDa. From left to right the bar charts represent the control (originator cell line MDA-MB-453) and the transfected MDA-MB-453 with IGBP1, SET and CIP2A (far right). Table **[B]** shows the ratio of ERK1 (p44) to ERK2 (p42) normalised peak signal values (AFI) in originator MDA-MB-453 cell line and the MDA-MB-453 cell lines, transfected with the PP2A inhibitors IGBP1, SET and CIP2A. The expression of total ERK1/2 did not show any significant changes upon overexpression of the PP2A inhibitory subunits (Tables 3.2 and 3.3). However, looking at the peak signal values, ERK1 expression decreased in the transfected cell lines, while ERK2 expression increased as shown by the $ERK2^{p42}$/ $ERK1^{p44}$ ratio.

In addition to beta-catenin and c-MYC, the following total protein expression was affected by overexpression of the PP2A inhibitory subunits. The selection of analytes included CREB# 1827, eIF4B# 2189, Mcl-1# 0702 P2 and RICTOR# 1468. Results obtained are shown in Figure 3.14 below:

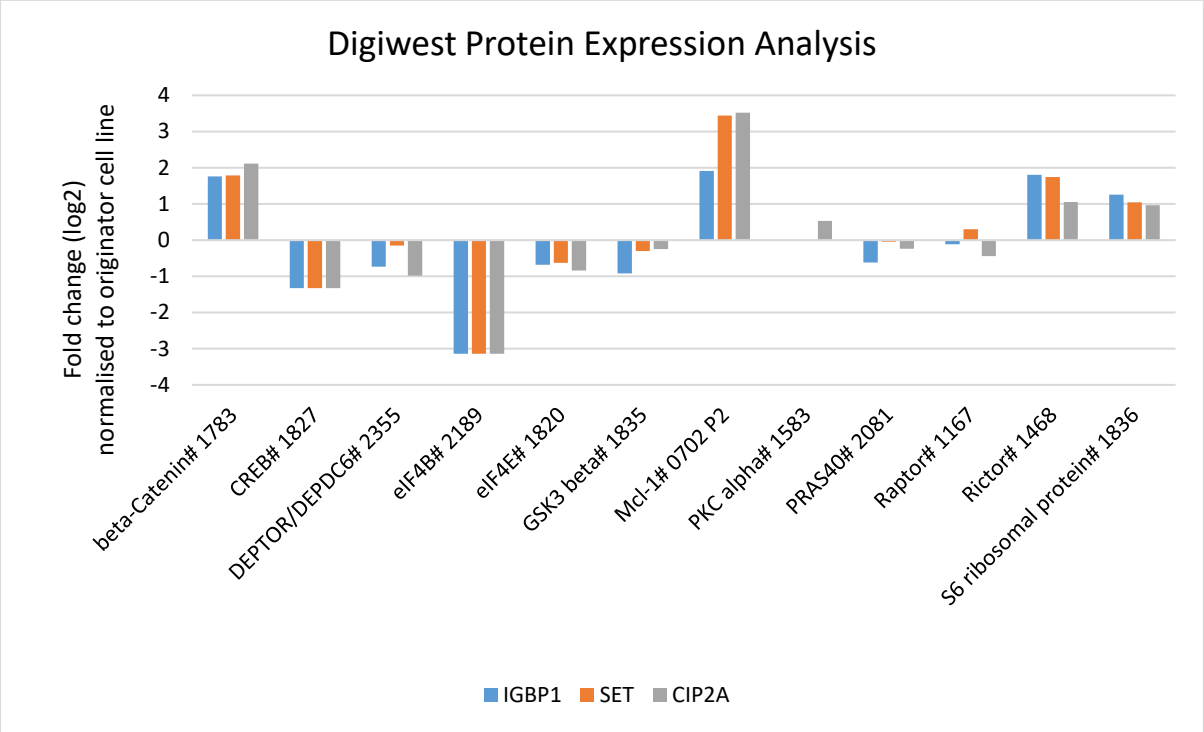

Figure 3.14: Total protein expression using DigiWest analysis (protein signature). The figure shows the $\log_2$ fold change, generated as described in Section 2.7.1, using the normalised peak signal values (AFI) obtained in MDA-MB-453 ectopically expressing IGBP1 (blue), SET (orange) and CIP2A (grey) and the normalised peak value signals (AFI) measured in the originator cell lines, for a selection of analytes. The figure shows more than two-fold increase (value of 1 on a $\log_2$ scale) in total protein levels of beta-catenin, MCL1 and RICTOR and a downregulation of eIF4B and CREB. The accumulation of beta-catenin, MCL1 and RICTOR prompted us to investigate the co-expression of the PP2A inhibitors by utilising the Breast Invasive Carcinoma dataset from TCGA (Firehose Legacy, Cerami, et al., 2012; Gao, et al., 2013). Beta-catenin is a PP2A target, MCL1 is overexpressed in cancer cells while RICTOR has an effect on the mTOR pathway (Refer to Chapter 1).

3.6 COMPARISON TO PATIENT MATERIAL

The oncogenic signature generated from Digiwest analysis (**Figure 3.14**), prompted us to attempt correlation with patient material, by utilising the Breast Invasive Carcinoma dataset from TCGA (Firehose Legacy, Cerami, et al., 2012; Gao, et al., 2013).

The first correlation attempt involved investigating CIP2A coexpression with other proteins, including a selection of proteins derived from the DigiWest oncogenic signature, namely beta catenin (CTNNB1), MCL1 and RICTOR. In order to do so, the genomic profile selected in the TCGA dataset was titled: Protein levels (mass spectrometry by CPTAC), for a sample of 74 patients (**Table 3.4**).

Table 3.4: CIP2A protein coexpression using mass spectrometry data (protein levels)

Correlated protein	Spearman Correlation	p-Value
AURKA	0.711	4.49E-11
TPX2	0.636	1.12E-09
KIF2C	0.602	1.38E-08
MCM2	0.581	5.39E-08
PTEN	-0.402	0.000378
CBX2	0.359	0.002099
SET	0.321	0.005345
Selection from DigiWest analysis		
CTNNB1	-0.012	0.918
MCL1	0.110	0.350
RICTOR	-0.156	0.184

Table 3.4 shows the correlation of CIP2A with a selection of proteins, using the Breast Invasive Carcinoma dataset from TCGA (Firehose Legacy, Cerami, et al., 2012; Gao, et al., 2013). The correlation occurs in the order: AURKA, TPX2, KIF2C, MCM2, PTEN, CBX2 and SET. This correlation was observed in a sample size of 74 patients. The table also includes a selection of proteins from DigiWest analysis (Figure 3.14). The data in the table shows that CIP2A coexpression correlates primarily with AURKA, with a Spearman correlation of 0.711 (p-value = 4.41×10^{-11}). CIP2A protein expression does not correlate with the expression of CTNNB1 (beta-catenin), MCL1 and RICTOR in the patient sample.

From the top correlated proteins, three were selected, namely AURKA, PTEN and SET. Coexpression of CIP2A with these proteins was investigated at mRNA expression level and the genomic profile selected in the TCGA dataset was titled: mRNA expression (RNA Seq V2 RSEM), with a sample of 1100 patients. Coexpression was also investigated at protein level using the genomic profile titled: Protein levels (mass spectrometry by CPTAC), with a sample of 74

patients, in order to determine whether any post-transcriptional mechanisms are involved. Results are shown in Figure 3.15 on the next page. Plot **A** shows the correlation between mRNA expression of CIP2A (RNA Seq data) and that of AURKA, PTEN and SET, while plot **B** shows the correlation between protein expression of CIP2A (z-score level; mass spectrometry) and the protein expression of AURKA, PTEN and SET. The Figure also provides the Spearman correlation, and the p-values. Comparing the correlations using mRNA expression and protein expression datasets shows that CIP2A and AURKA correlate at both RNA and protein level, showing that translation reflects the transcript levels. PTEN correlates at protein level only indicating that the post-transcriptional mechanisms are important in PTEN expression. To a lesser extent, CIP2A and SET correlate at both RNA and protein level.

[A]:

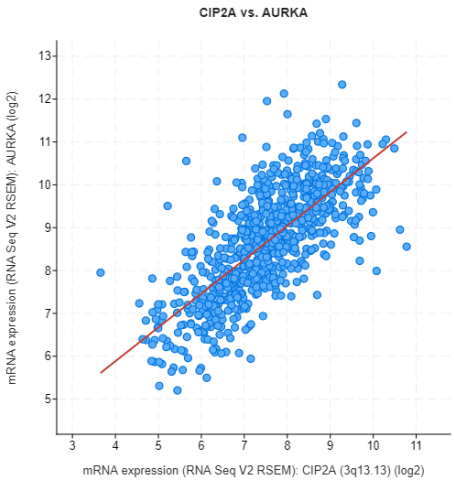

Spearman: 0.75, p-value $3.16X10^{-146}$

[B]:

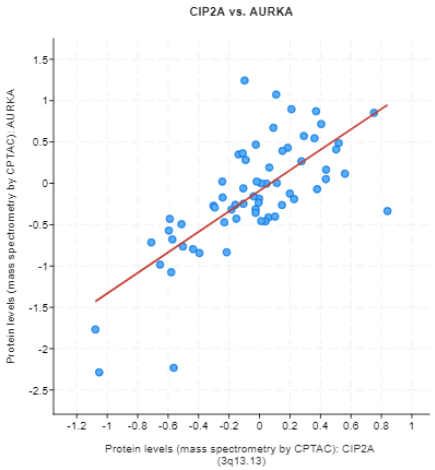

Spearman: 0.71, p-value $4.49X10^{-11}$

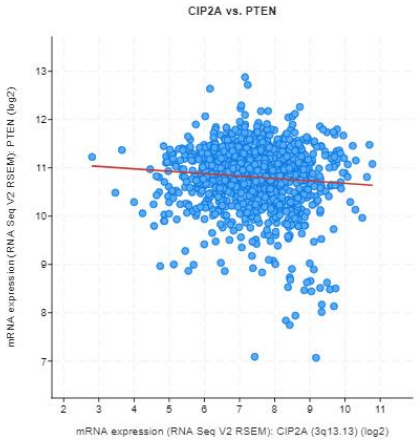

Spearman: -0.08, p-value 0.0641

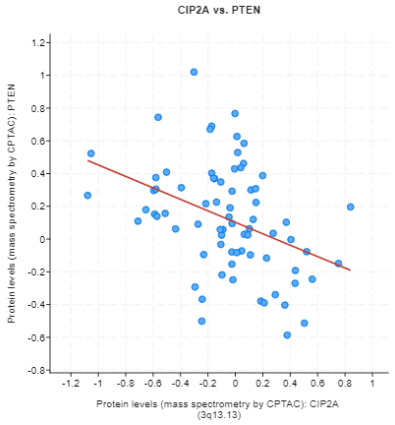

Spearman: -0.40, p-value 3.78×10^{-4}

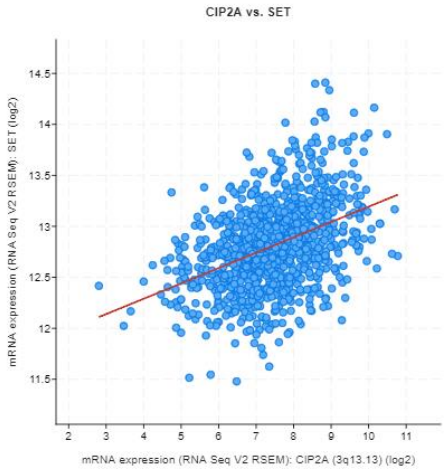

Spearman: 0.43, p-value $5.04X10^{-51}$

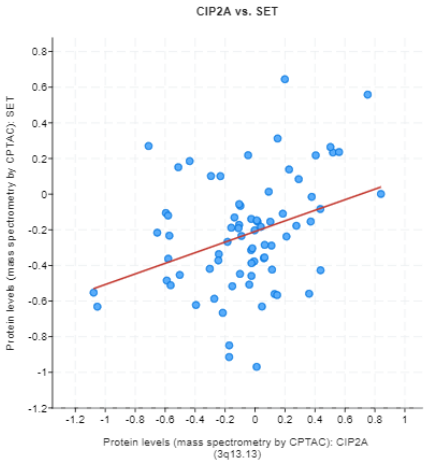

Spearman: 0.32, p-value $5.35X10^{-3}$

Figure 3.15: Co-expression of CIP2A at [A] RNA and [B] protein level using TCGA Breast Invasive Carcinoma dataset.

The TCGA dataset was next used to determine whether there is a correlation between the PP2A regulatory subunits PPP2R2A and PPP2CA, the PP2A inhibitory subunits used in this study (CIP2A, SET and IGBP1) and a selection of proteins from the DigiWest oncogenic signature (CTNNB1, RICTOR and MCL1). AURKA was also included in the investigation, since this kinase has been documented to be a surrogate marker of PP2A activity (Bonello, 2020). The genomic profile used was titled: Protein levels (mass spectrometry by CPTAC), with a sample of 74 patients. Results are shown in Table 3.5:

Table 3.5: Spearman correlation and p-values for a selection of proteins

	PPP2CA		CIP2A		IGBP1		SET		CTNNB1		AURKA	
SET	0.33	0.00375	0.32	0.00535	-0.02	0.856			0.2	0.0929	0.29	0.0224
IGBP1	0.41	2.40E-04	0.00	0.999			-0.02	0.856	-0.14	0.227	-0.19	0.127
CIP2A	-0.04	0.708			0.00	0.999	0.32	0.00535	-0.01	0.919	0.71	4.50E-11
PPP2CA									-0.18	0.119		
PPP2R2A	0.77	8.28E-16	-0.16	0.162	0.31	0.0634	0.12	0.31	-0.31	7.30E-03	-0.28	0.0263
AURKA	-0.15	0.232	0.71	4.50E-11	-0.19	0.127	0.29	0.0224	0.15	0.224		
Selection from DigiWest analysis												
CTNNB1	-0.18	0.119	-0.01	0.919	-0.14	0.227	0.20	0.0929			0.15	0.224
RICTOR	0.25	0.0350	-0.13	0.294	0.06	0.634	0.20	0.0900	0.12	0.34	-0.26	0.420
MCL1	0.13	0.302	0.11	0.350	0.06	0.632	-0.03	0.819	-0.22	0.0561	0.16	0.199

The data in the table shows Spearman correlations (numbers in red) and corresponding p-values (numbers in blue), for a selection of proteins, including those selected from DigiWest analysis. Data in cells highlighted in yellow are of particular importance. This data shows that SET protein levels correlate with expression of CIP2A (Spearman correlation of 0.32; p-value = 0.00535). Both IGBP1 and SET protein levels correlate with the protein expression of PPP2CA showing a Spearman correlation of 0.41 (p-value = 2.40 $X10^{-4}$) and 0.33 (p-value = 0.00375) respectively. Also, the protein level of PPP2R2A inversely correlates with the protein levels of CTNNB1 (beta-catenin) (Spearman correlation of -0.31; p-value = 7.3 $X10^{-3}$). There is also a correlation between PPP2R2A and PPP2CA (Spearman correlation of 0.77; p-value = $8.28x10^{-16}$). High expression of the PP2A inhibitory subunits, CIP2A and SET, was found to correlate with AURKA

expression with a Spearman coefficient of 0.71 (p-value 4.5 $X10^{-11}$) and 0.29 (p-value = 0.0224), respectively. IGBP1 protein expression was not correlated with AURKA expression. AURKA also inversely correlates with PPP2R2A (Spearman correlation of -0.28; p-value = 0.0263) and PPP2CA (Spearman correlation of -0.15; p-value = 0.232). This correlation is supported by previous results showing that AURKA is a surrogate marker of PP2A activity.

The TCGA dataset was next used to generate an oncoprint for a group of genes, selected on the basis of the results obtained (**Figure 3.16**). The gene group consisted of *CIP2A, SET, IGBP1, PPP2R2A, PPP2CA, AURKA, TPX2, MYC, MCL1, CTNNB1* and *RICTOR.* This group therefore consists of the PP2A regulatory and catalytic subunits, and inhibitors, as well as the protein signature generated following overexpression of the inhibitors CIP2A, SET and IGBP1.

In order to generate the oncoprint, the genomic profile was titled: Putative copy number alterations, with a sample size of 1101 patients. Gene alterations manifested in the oncoprint consist of amplifications and deep deletions. Amplifications refer to an increase in the number of gene copies, within the genome. Deletions refer to the loss of all or part of a gene. According to the cBioPortal, a deep deletion is possibly a homozygous deletion.

Alterations may also affect the mRNA and/or protein associated with the gene and this is also shown in the oncoprint. When mRNA and protein expression data are selected in the query, the cBioPortal will determine whether the expression is high or low, for that particular gene in the sample.

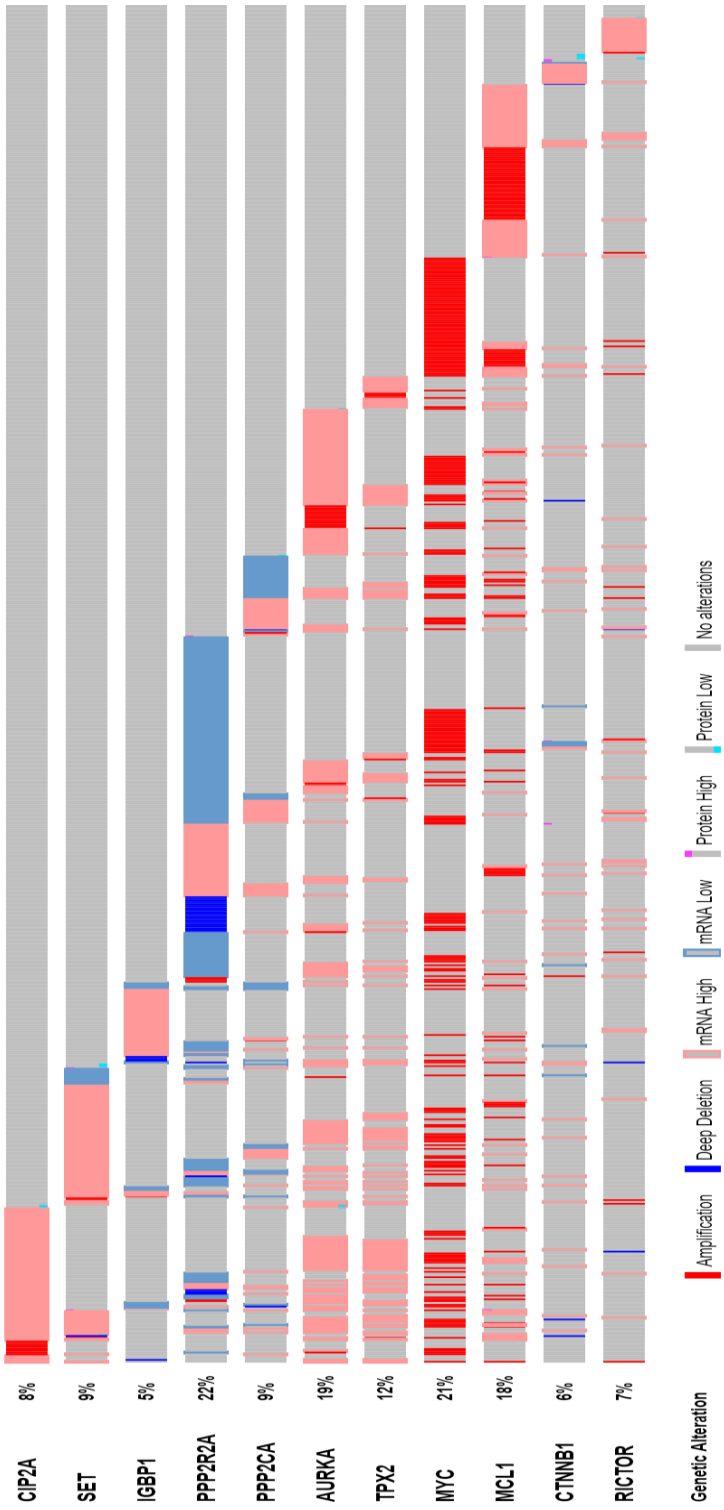

Figure 3.16: Oncoprint generated from cBioPortal using TCGA dataset Breast Invasive Carcinoma (https://www.cbioportal.org/oncoprinter). The figure shows the oncoprint generated for the gene group: *CIP2A, SET, IGBP1, PPP2R2A, PPP2CA, AURKA, TPX2, MYC, MCL1, CTNNB1* and *RICTOR.* It gives a summary of the percent gene

alterations per sample. Each sample is a column, and each gene is a row. Different kinds of gene alterations are highlighted with different colours. The gene alterations include amplifications (red) and deep deletions (blue). No alterations are shown in grey. High or low mRNA and protein content are also included. The main observation in this oncoprint that the highest alterations are shown in PPP2R2A (22 %, with 17 % deletions). The oncoprint also shows that 12/1101 (1 %) of samples show amplified CIP2A, 6 samples have SET amplification and there are no amplifications in IGBP1.

Following the oncoprint, the coefficient of co-occurrence (log_2 odds ratio) was determined for a selection of genes, including those listed in Table 3.4, the PP2A inhibitory, regulatory and catalytic subunits, and the oncogenic signature selection. This ratio quantifies how strongly the presence or absence of alterations in one gene are associated with the presence or absence of alterations in another. This was investigated using the genomic profile titled: Putative copy-number alterations from GISTIC, with a sample of 1080 patients. The results are shown in Table 3.6.

Table 3.6: Co-occurrence of PP2A inhibitory, regulatory and catalytic subunits, and protein signature

A	B	Neither	A Not B	B Not A	Both	Log2 Odds Ratio	p-Value	Tendency
AURKA	*TPX2*	848	124	43	86	>3	<0.001	Co-occurrence
CIP2A	*TPX2*	927	45	88	41	>3	<0.001	Co-occurrence
CIP2A	*AURKA*	854	37	161	49	2.812	<0.001	Co-occurrence
CIP2A	*SET*	938	67	77	19	1.788	<0.001	Co-occurrence
CIP2A	*MYC*	818	54	197	32	1.299	<0.001	Co-occurrence
SET	*TPX2*	912	60	93	36	2.557	<0.001	Co-occurrence
SET	*AURKA*	835	56	170	40	1.811	<0.001	Co-occurrence
SET	*MYC*	810	62	195	34	1.188	<0.001	Co-occurrence
SET	*PPP2CA*	922	76	83	20	1.548	<0.001	Co-occurrence
CTNNB1	*SET*	953	52	85	11	1.246	0.016	Co-occurrence
IGBP1	*PPP2CA*	954	44	92	11	1.374	0.01	Co-occurrence
TPX2	*MYC*	800	72	172	57	1.881	<0.001	Co-occurrence
PPP2R2A	*MYC*	702	170	153	76	1.036	<0.001	Co-occurrence
PPP2CA	*PPP2R2A*	792	63	206	40	1.288	<0.001	Co-occurrence
TPX2	*PPP2CA*	893	105	79	24	1.369	<0.001	Co-occurrence
PPP2CA	*MYC*	804	68	194	35	1.093	<0.001	Co-occurrence
AURKA	*PPP2R2A*	709	146	182	64	0.772	0.001	Co-occurrence
CTNNB1	*MYC*	831	41	207	22	1.107	0.005	Co-occurrence
MCL1	*MYC*	725	147	174	55	0.641	0.009	Co-occurrence
TPX2	*PPP2R2A*	766	89	206	40	0.741	0.01	Co-occurrence
TPX2	*MCL1*	804	95	168	34	0.776	0.011	Co-occurrence
AURKA	*MYC*	747	125	144	85	1.819	<0.001	Co-occurrence

In the table, the $\log_2$ odds ratio quantifies how strongly the presence or absence of alterations in A are associated with the presence or absence of alterations in B in the selected samples. If the odds ratio is greater than 1, then A and B are associated. The odds ratio is calculated using the formula: **odds ratio = (Neither * Both) / (A Not B * B Not A).** As expected, amplifications in *AURKA* and *TPX2* co-occur since the genes are associated with 20q amplifications in breast cancer. *CIP2A* co-occurs with *TPX2*, *AURKA*, *SET*, and *MYC*. *SET* co-occurs with *TPX2*, *AURKA*, *MYC*, *PPP2CA*, and *CTNNB1*, whilst *IGBP1* co-occurs with *PPP2CA* alterations.

The TCGA dataset was also used to determine whether there is a relationship between copy number variations and RNA expression for the PP2A inhibitory, regulatory, and catalytic subunits, AURKA as well as beta-catenin (CTNNB1), RICTOR and MCL1, identified in the oncogenic signature. This was investigated using the genomic profile titled: Putative copy-number alterations from GISTIC, with a sample of 1080 patients. Results are shown in Table 3.7.

Table 3.7: Correlation between copy number variations and RNA expression

		COPY NUMBER VARIATION (CNV)													
		AURKA		SET		IGBP1		CIP2A		PPP2CA		PPP2R2A		MCL1	
RNA EXPRESSION	SET	0.06	0.0498	0.40	9.28E-42	0.02	0.561	-0.01	0.811	-0.15	5.00E-07	-0.18	7.04E-09	-0.02	0.429
	IGBP1	-0.18	6.20E-09	0.13	2.00E-05	0.00	0.930	-0.12	4.80E-05	0.34	6.50E-30	0.17	1.29E-08	0.12	7.60E-05
	CIP2A	0.20	5.60E-11	-0.10	1.40E-03	-0.07	0.0280	0.30	4.97E-24	-0.27	7.00E-20	-0.18	1.44E-09	0.06	0.0374
	PPP2CA	0.13	9.80E-06	0.06	0.0451	-0.01	0.701	-0.01	0.800	0.62	1.10E-116	-0.03	0.399	-0.03	0.409
	PPP2R2A	-0.18	7.24E-09	0.05	0.0773	0.03	0.400	0.01	0.718	0.12	1.08E-04	0.75	3.60E-198	0.15	1.30E-06
	AURKA	0.51	1.37E-71	-0.17	7.70E-09	0.00	0.947	0.18	7.18E-09	-0.26	1.07E-17	-0.27	3.92E-19	0.09	3.10E-03
	Selection from DigiWest analysis														
	CTNNB1	-0.14	4.02E-06	-0.01	0.755	0.05	0.109	0.09	1.90E-03	0.03	0.351	0.12	5.90E-03	0.03	0.343
	RICTOR	0.03	0.308	0.04	0.223	0.00	0.907	-0.01	0.664	1.50E-01	1.02E-06	0.00	9.55E-01	-0.10	9.70E-04
	MCL1	-0.17	2.50E-08	0.02	0.418	0.13	1.05E-05	0.07	2.80E-02	-0.03	3.04E-01	0.25	2.49E-16	0.46	1.90E-57

The table shows Spearman correlations (numbers in red) and corresponding p-values (numbers in blue) to determine whether there is a relationship between copy number variation (CNV) (alteration of the genome: insertions, duplications, deletions) and RNA expression (RNA Seq). Data in cells highlighted in yellow are of particular importance. This data shows that AURKA is inversely correlates with PPP2CA (Spearman coefficient of -0.26, p-value = 1.07 $X10^{-17}$) and PPP2R2A (Spearman coefficient of -0.27, p-value = 3.92 $X10^{-19}$). Another significant result includes the inverse correlation of PPP2R2A with SET (Spearman coefficient of -0.18, p-value = 7.04 $X10^{-9}$) and CIP2A (Spearman coefficient of -0.18, p-value = 1.44 $X10^{-9}$) indicating that this deletion co-occurs with high expression of CIP2A and SET resulting in further inhibitory effect on the phosphatase. The RNA expression of MCL1 positively correlates with the

copy number variation in PP2R2A (Spearman coefficient of 0.25, p-value = 2.5 $X10^{-16}$). There is also a slight correlation of MCL1 copy number variation with RNA expression of PP2R2A (Spearman coefficient of 0.15, p-value = 1.3 $X10^{-6}$) and TPX2 (Spearman coefficient of 0.14, p-value = 7.6 $X10^{-2}$).

Another interesting investigation involved possible correlation of epithelial markers epithelial cellular adhesion molecule (EPCAM) and E-cadherin (CDH1) with the PP2A inhibitory, catalytic and regulatory subunits, AURKA as well as beta catenin (CTNNB1). As mentioned in Section 1.3.5, research has shown that there is an association between beta-catenin, and epithelial and mesenchymal transition (EMT). In order to conduct this investigation, the genomic profile for the TCGA dataset was titled: Protein levels (mass spectrometry by CPTAC), with a sample of 74 patients. Results are shown in Table 3.8.

Table 3.8: Spearman correlation and p-values for PP2A inhibitory and regulatory subunits AURKA CTNNB1 and epithelial markers EPCAM and CDH1.

	PP2CA		CIP2A		IGBP1		SET		CTNNB1		AURKA	
SET	0.33	0.00375	0.32	0.00535	-0.02	0.856			0.2	0.0929	0.29	0.0224
IGBP1	0.41	2.40E-04	0	0.999			-0.02	0.856	-0.14	0.227	-0.19	0.127
CIP2A	-0.04	0.708			0	0.999	0.32	0.00535	-0.01	0.919	0.71	4.50E-11
PP2CA			-0.04	0.708	0.41	0.00025	0.33	0.00375	-0.18	0.119	-0.15	0.232
PPP2R2A	0.77	8.28E-16	-0.16	0.162	0.31	0.0634	0.12	0.31	-0.31	7.30E-03	-0.28	0.0263
EPCAM			0.24	0.0356	-0.25	0.0298	0.33	3.68E-03	0.61	6.30E-09	0.45	1.97E-04
CDH1			0.06	0.616	0.02	0.872	0.38	9.69E-04	0.61	8.96E-09	0.08	0.522

The data in the table shows Spearman correlation (numbers in red) and corresponding p-values (numbers in blue), for PP2A inhibitory and regulatory subunits and epithelial markers EPCAM and CDH1. Data in cells highlighted in yellow are of particular importance. This data shows that beta-catenin (CTNNB1) positively correlates with the expression of epithelial cellular adhesion molecule (EPCAM; Spearman correlation of 0.61; p-value = 6.30 $X10^{-9}$) and E-cadherin (CDH1; Spearman correlation of 0.61; p-value = 8.96 $X10^{-9}$) and while SET positively correlates with the expression of EPCAM (Spearman correlation of 0.33; p-value = 3.68 $X10^{-3}$) and E-cadherin (CDH1; Spearman correlation of 0.38; p-value = 9.69 $X10^{-4}$).

As a final experiment, the TCGA dataset was used to investigate clinical attributes in patients showing gene alterations (identified in Figure 3.16) in *CIP2A*, *SET*, *AURKA*, *IGBP1*, *PPP2CA* and *PPP2R2A*. The clinical attributes selected for each group of patients were Positive Finding Lymph Node Haematoxylin and Eosin Staining Microscopy Count (log_2) (**Figure 3.17A**) and Staging System (**Figure 3.17B**).

Figure 3.17A is a box plot showing the Positive Finding Lymph Node Haematoxylin and Eosin Staining Microscopy Count (log_2) for each group of patients showing the selected gene alterations. The log_2 value is directly related to the occurrence of lymph node metastasis. Figure 3.17B shows Staging System (number of samples) for the same selection. The Staging System is a standard used to classify the aggressivity of the malignancy.

Of interest, higher expression of AURKA and PPP2R2A are associated with an increased likelihood of lymph node metastasis (**Figure 3.17A**) and have a higher likelihood for more advanced surgery, that is *axillary lymph node dissection alone* or *sentinel lymph node biopsy plus axillary dissection* (**Figure 3.17B**). In other words, neoplastic cells of patients who tend to have the highest number of lymph node metastasis and axillary interventions have higher levels of expression of AURKA and deletions in PPP2R2A. Conversely, if a tumour is found to have high expression/deletions of these two markers then one can infer that the patient is likely to have locoregional lymph node metastasis.

Since AURKA expression is correlated with CIP2A and SET (**Table 3.5**) and PPP2R2A deletions are correlated significantly with an increased RNA expression of AURKA, SET, and CIP2A (**Table 3.7**), this result provides the basis to study the role of PP2A regulation in metastatic disease.

A:

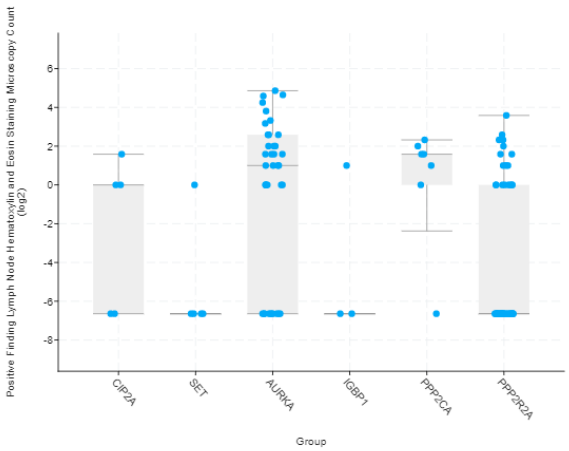

B:

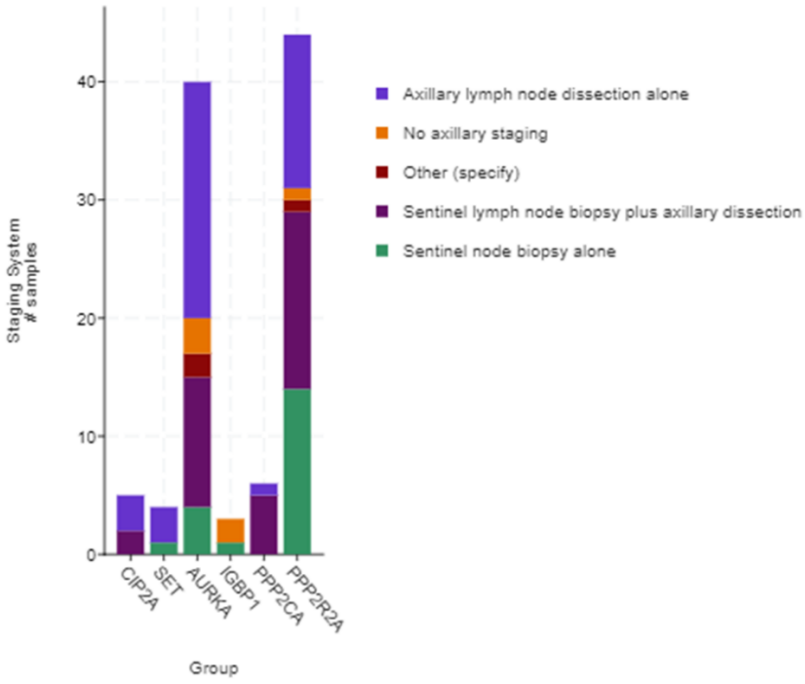

Figure 3.17: Higher expression of AURKA and PPP2R2A is common in lymph node metastasis and may require more advanced surgery. The figures show that high expression of AURKA and PPP2R2A deletions are associated with an increased likelihood of lymph node metastasis (**Figure 3.17A**) and have a higher likelihood for more advanced surgery, that is *axillary lymph node dissection alone* or *sentinel lymph node biopsy plus axillary dissection* (**Figure 3.17B**).

3.7 OPTIMISATION EXPERIMENTS

3.7.1 Isolation of Transfected Cells

An attempt was made to separate transfected from non-transfected cells using the ARIA II Cell Sorter as described in Section 2.4.3. Results obtained are shown below

A:

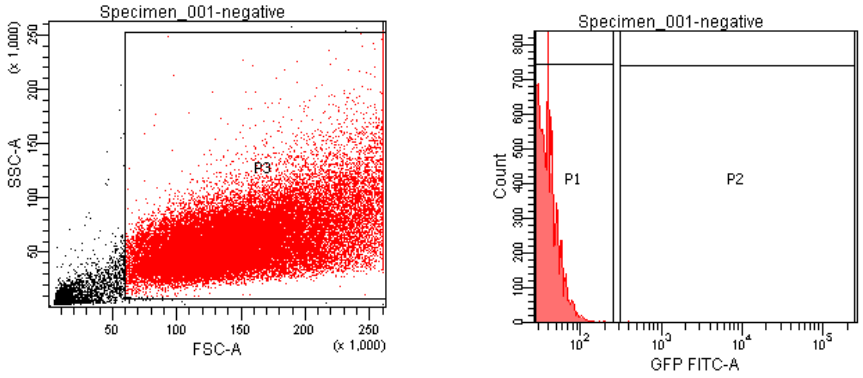

B:

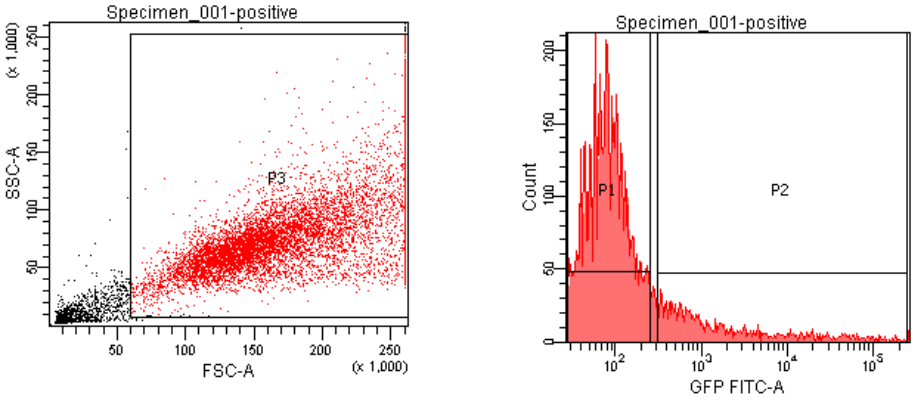

Figure 3.18: Separation of transfected and non-transfected cells using BIOFACS Cell Sorter.

The graphs show side scatter against forward scatter data for the control (negative) and transfected MCF-7 (positive) cell line. The side scatter reading gives an indication of the complexity of the cell while the forward scatter reading gives an indication of the cell size. The instrument was set at high purity. This control result ensures an accurate machine set-up, with a transfection efficiency of 0 %. The high purity setting yielded a 17 % transfection efficiency. This yield is low, therefore the idea of sorting the cells prior to further investigation was discarded as, on a larger scale, it was not practical in terms of chemicals, laboratory ware as well as handling of the experiment itself.

3.7.2 Optimization of Polysome Bound RNA Methodology

Prior to isolation of polysome bound RNA from transfected cell lines, optimization of the methodology was carried out using two different techniques. One technique made use of the QIAGEN RNeasy Mini Kit (QIAGEN Cat: 74104), while the other technique was that proposed by Grech, et al., 2008. Results are shown below:

Table 3.9: Bioanalyser results for non-transfected cell line MDA-MB-453, following sucrose gradient centrifugation, using two different protocols

	PROTOCOL	
	A: QIAGEN RNeasy Mini Kit	**B: Grech, et al. (2008)**
RNA Integrity Number (RIN)	8.6	9.1
RNA concentration ng/μl	142	496
rRNA ratio	2.3	2.2

The table shows the Bioanalyser result obtained, following sucrose density gradient centrifugation, for the second fraction using the QIAGEN RNeasy Mini Kit **[A]** and the protocol by Grech, et al. (2008) **[B]**. Both results show acceptable RIN values (8.6 for A and 9.1 for B). The RNA concentration for A is, however, much less than for **B** (142 ng/μl for A and 496 ng/μl for B). The protocol used for **B** was therefore selected for further experimentation.

Chapter IV

Discussion

4.1 OVERVIEW

In this study, the effect of overexpressing the PP2A inhibitory subunits CIP2A, SET and IGBP1 was studied in selected breast cancer cell lines. Previous investigations show that low activity of the phosphatase enzyme, PP2A is associated with more than 60 % of triple negative breast cancer (TNBC) patients, representing the poor prognostic basal subtype (Bonello, 2020). In this study, we identified two breast cancer cell lines with low expression of CIP2A, SET and IGBP1 using RNA and protein as end-point measurement through real time PCR and immunocytochemistry (ICC) respectively. Although scoring using ICC is subjective, it was imperative to include, since IGBP1 is a translationally controlled transcript at the level of polysome recruitment (Grech, et al., 2008). Low PP2A activity can be reactivated using therapeutic drugs, such as FTY720 or through functional assays following overexpression of the target protein. mTOR is a direct target of PP2A activity. Studying translation initiation and polysome recruitment of competitive RNA molecules is challenging. It was previously shown that IGBP1 is controlled at the level of polysome recruitment (Grech, et al., 2008). In fact, measuring the effect of PP2A modulation by FTY720 and overexpression of inhibitory subunits proved inconclusive when the point measurement was based on RNA extraction. Hence, we opted to use polysome bound RNA and eventually, due to differences in percent polysome recruitment between experiments, we moved to Digital Western (protein) analysis.

Once the constructs that contain the coding sequence of the three inhibitory subunits were prepared, the expression was measured using Western blotting following transfection. The transfection efficiency was determined by measuring GFP fluorescence generated by the bicistronic construct.

The first phase of the study involved the overexpression of the inhibitory subunits in the selected cell lines, MCF-7 and MDA-MB-453. The cell line HCC1937 was used as a positive control since it expresses the inhibitory subunits at high endogenous levels **(Figure 3.1**). Using polysome bound RNA the percent polysome recruitment of c-MYC in the pIRES2-AcGFP vector and in the overexpressors (one construct per bulk experiment), was compared, as shown in Figure 3.7. The polysome recruitment of c-MYC, known to be negatively regulated by active PP2A was measured. The results show that recruitment of c-MYC transcript to the polysomes increases significantly upon overexpression of CIP2A, SET and IGBP1 in both MCF-7 and MDA-MB-453. In addition, the enhanced polysome recruitment of c-MYC was mTOR-dependent when CIP2A and SET were overexpressed, shown as a significant decrease in polysome recruitment upon the addition of rapamycin, an established inhibitor of the mTOR pathway (McConnell, et al., 2009). However, there were significant differences in polysome recruitment of c-MYC in the different experiments when comparing the results obtained from addition of the pIRES2-AcGFP vector alone (**Figure 3.7**).

This prompted us to investigate alternative ways to measure the differential expression in the cellular models upon overexpression of the PP2A inhibitory subunits CIP2A, SET and IGBP1. The use of Digital Western (DigiWest) technology, whereby multiple antibodies can be measured simultaneously in the same lysate, was the method of choice. A panel of antibodies was used to measure total protein and phospho-proteins using lysates from MDA-MB-453 cells overexpressing the PP2A inhibitory subunits and compared to the originator cells (**Figures 3.9 to 3.13**). The comparison generated a list of proteins that are upregulated upon overexpression of the PP2A inhibitory subunits (**Figure 3.14**). The identified proteins are involved in pathways known to be regulated by PP2A as well as others that are associated with cancer progression. The “protein

signature" included beta-catenin (CTNNB1), RICTOR and MCL1. A number of phospho-proteins were also upregulated upon overexpression of CIP2A, IGBP1 and SET. The "phospho-profile" included 4E-BP1(phosphoThr37/Thr46) and PKC alpha (phosphoThr497/Thr638/Thr641).

Correlation of the "protein signature" with the expression of the PP2A inhibitory subunits was then performed using the publicly available patient dataset, namely the Breast Invasive Carcinoma (TCGA, Firehose Legacy) available at cBioPortal for Cancer Genomics (https://www.cbioportal.org/).

Interestingly, the data in Table 3.5 shows that the protein levels of the PP2A regulatory subunit, PPP2R2A inversely correlate with the protein levels of beta-catenin (Spearman correlation of -0.31; p-value = 7.3 $X10^{-3}$). There is also a correlation between PPP2R2A and the PP2A catalytic subunit, PPP2CA (Spearman correlation of 0.77; p-value = 8.28 $X10^{-16}$). This supports the result from our dataset, showing an increase in beta-catenin protein following overexpression of PP2A inhibitory subunits (displacement of PPP2R2A from the PP2A complex). In addition, the low PPP2R2A and PPP2CA protein levels significantly correlated with a high expression of AURKA, the surrogate marker of low PP2A activity (Bonello, 2020) (PPP2R2A: Spearman correlation of -0.28; p-value = 0.0263; PPP2CA: Spearman correlation of -0.15; p-value = 0.232). Table 3.8 shows that beta-catenin also positively correlates with the expression of EPCAM (Spearman correlation of 0.61; p-value = 6.30 $X10^{-9}$) and E-cadherin (CDH1; Spearman correlation of 0.61; p-value = 8.96 $X10^{-9}$) and while SET positively correlates with the expression of EPCAM (Spearman correlation of 0.33; p-value = 3.68 $X10^{-3}$) and E-cadherin (CDH1; Spearman correlation of 0.38; p-value = 9.69 $X10^{-4}$). CIP2A and IGBP1 show no correlation. This suggests that interpretation of differential gene expression should also consider the type of tumour in terms of epithelial or mesenchymal.

The TCGA dataset was also used to determine whether there is a relationship between copy number variations and RNA expression for the PP2A inhibitory, regulatory, and catalytic subunits, as well as AURKA and beta-catenin, RICTOR and MCL1 (identified in the protein signature). The data in Table 3.7 shows that there is a positive correlation between RNA expression of MCL1 and copy number variation in PPP2R2A (Spearman coefficient of 0.25, p-value = 2.49 $X10^{-16}$). AURKA inversely correlated with PPP2CA (Spearman coefficient of -0.26, p-value = 1.07 $X10^{-17}$) and PPP2R2A (Spearman coefficient of -0.27, p-value = 3.92 $X10^{-19}$). Another significant result includes the inverse correlation of deletions in PPP2R2A with SET (Spearman coefficient of -0.18, p-value = 7.04 $X10^{-9}$) and CIP2A (Spearman coefficient of -0.18, p-value = 1.44 $X10^{-9}$) indicating that this deletion co-occurs with high expression of CIP2A, SET resulting in further inhibitory effect on the phosphatase.

Following DigiWest analysis, a detailed investigation of the ERK isoforms, ERK1(p44) and ERK2(p42), showed that the ratio of p42/p44 increased significantly following overexpression of the PP2A inhibitory subunits (**Figure 3.13**). The shift towards expression of ERK2(p42) upon overexpression of CIP2A, SET and IGBP1 offers an opportunity to further investigate the role of the PP2A inhibitory subunits in Epithelial and Mesenchymal Transition (EMT)-induction.

4.2 RESEARCH OUTCOMES

This research supports previous investigations regarding PP2A and its inhibitory subunits. However, it also has a novel nature which provides fresh insight into the current state of the art. The subsequent sections describe the findings, which are also summarized in Table 4.1, for further clarity.

Table 4.1: Outcomes resulting from overexpression of PP2A inhibitory subunits

OUTCOME	REFERENCE SECTION
Generation of a common protein signature, including beta-catenin, MCL1 and RICTOR, and phospho-profile, including 4E-BP1 and PKC alpha	4.2.1
Promotion of translation initiation for c-MYC, MCL1 and beta-catenin due to release of eIF4E	4.2.2
Shift towards expression of ERK2(p42)	4.2.3
Phosphorylation of PKC alpha	4.2.4
Dephosphorylation of p70 S6 kinase	4.2.5
Negative correlation of beta-catenin protein levels with PP2A regulatory subunit PPP2R2A	4.2.6
Possible role of PP2A in metastatic disease	4.2.7

4.2.1 Overexpression of PP2A Inhibitory Subunits Result in a Common Protein Signature and Phospho-profile

The DigiWest multiplex bead-based assay utilised 45 antibodies, including 18 total protein antibodies and 27 specific phospho-proteins, measuring expression and activity of proteins, to generate a protein signature and phospho-profile respectively.

Upon overexpression of the PP2A inhibitory subunits, CIP2A, SET and IGBP1 and setting a threshold of greater than a fold change of 2, the generated protein signature list included beta-catenin, MCL1, and RICTOR (**Figure 3.14**), while the phospho-profile showed upregulation of 4E-BP1(phosphoThr37/Thr46), and upregulation of PKC alpha (phosphoThr497/Thr638/Thr641; **Figure 3.10 and 3.12**). Overexpression of the PP2A inhibitory subunits thus promotes expression and activation of oncogenic signatures.

4.2.2 PP2A Inhibitory Subunits Promote Translation Initiation

The overexpression of the PP2A inhibitory subunits in this study, show significant increase in the phosphorylation of 4E-BP1 (**Figure 3.10**). Phosphorylated 4E-BP1 is a marker of active mTOR signalling, and PP2A is responsible for keeping the mTOR pathway in check. Overexpression of the PP2A inhibitory subunits, as in the case of this investigation, thus causes upregulation of 4E-BP1. Additionally, 4E-BP1 is also known to release eIF4E from the suppressive complex, as described in Section 1.3.2 (Coleman, et al., 2009).

This research has shown that overexpression of the PP2A inhibitory subunits results in an increase in the endogenous expression of c-MYC (**Figure 3.9**). This

result tallies with previous investigations, which have shown that CIP2A regulates MYC mRNA translation through a PP2A dependent translation initiation pathway (Denk, et al., 2012). The MYC 5' untranslated region (UTR) requires an elevated level of eIF4E for translation initiation. The PP2A regulatory subunit, B56α directs the phosphatase complex to the N terminus of c-MYC resulting in dephosphorylation at serine 62, leading to ubiquitination and degradation. Silencing of B56α results in accumulation of c-MYC (Arnold, et al., 2020). Overexpression of CIP2A was shown to inhibit PP2A activity leading to MYC stabilisation, by suppressing the dephosphorylation of c-MYC (Denk, et al., 2021).

In addition to c-MYC, both MCL1 and beta-catenin are eIF4E dependent and their protein levels increase following overexpression of eIF4E (Culjkovic-Kraljacic, et al., 2020). Therefore, the increased protein levels of c-MYC, MCL1 and beta-catenin in this investigation (**Figures 3.9 and 3.14**) can be partially contributed to the release of eIF4E, resulting in increased polysome recruitment of the mRNA. The increased polysome recruitment of c-MYC was shown in this study (**Figure 3.7**). It is important to note that beta-catenin's function is to act as a transcription factor which upregulates c-MYC (Rennoll, et al., 2015). Both c-MYC and beta-catenin therefore show the same trends.

4.2.3 PP2A Inhibitory Subunits Modulate ERK Expression

Previous investigations regarding the kinase ERK have shown that ERK1(p44) and ERK2(p42) proteins are ubiquitously expressed, highly homologous and share multiple binding partners and substrates (Buscà, et al., 2016). ERK2 knockout in murine models is lethal and silencing of ERK2 results in suppression of cell proliferation, properties that are not shared with ERK1. In addition, ERK2 overexpression results in upregulation of ZEB1/2 expression and induction of

epithelial to mesenchymal transition (Shin, et al., 2010). Ectopic expression of ERK2 results in decreased expression of the epithelial marker, E-cadherin and increased mesenchymal marker expression in the breast cell line, MCF-10A (Li, et al., 2008). Also silencing of endogenous ERK2 inhibits RasV12 induced EMT, while ERK1 has no effect on EMT induction.

The transcription factor elk-1 is translocated to the nucleus upon phosphorylation by ERK2 and directly binds CIP2A and MCL1 resulting in transcriptional activation (Liu, et al., 2019). The increased expression of CIP2A, inhibits further PP2A activity resulting in a forward signalling loop promoting transcription activation through ERK/elk-1 pathway, and releasing mTOR/eIF4E translation initiation of c-MYC, MCL1 and beta-catenin. Interestingly, the SET inhibitor TD19 downregulates CIP2A transcription following sequestration of elk-1 in the cytoplasmic complex. Disrupting the oncogenic ERK2/elk-1/CIP2A signal impaired tumour growth of MDA-MB-468 triple negative breast cancer xenograft models (Liu, et al., 2019).

In this research, it was observed that, although total ERK1/2 protein expression did not show a difference in protein expression, a detailed investigation of the ERK isoforms, ERK1(p44) and ERK2(p42), showed that the ratio of p42/p44 increased significantly following overexpression of the PP2A inhibitory subunits (**Figure 3.13**). The ratio of p42/p44 in the originator cell, MDA-MB-453 is 1 as compared to 6, 5.4, and 4.9 following overexpression of CIP2A, SET and IGBP1, respectively. Since previous investigations have proven that ERK2 overexpression induces epithelial to mesenchymal transition (Shin, et al., 2010), the shift towards expression of ERK2(p42) upon overexpression of CIP2A, SET and IGBP1 offers an opportunity to further investigate the role of the PP2A inhibitory subunits in EMT.

4.2.4 PP2A Inhibitory Subunit Overexpression Results in Phosphorylation of PKC Alpha

Previous investigations have shown that PPP2R2A (B55α) dephosphorylates and inactivates PKC alpha (Ruvolo, et al., 2014). Deletions in PPP2R2A resulting in low B55α expression, enhance PKC alpha activity leading to suppression of the PP2A/ B56α complex through phosphorylation of B56α at Serine 41 (S41), and stability of the MYC protein.

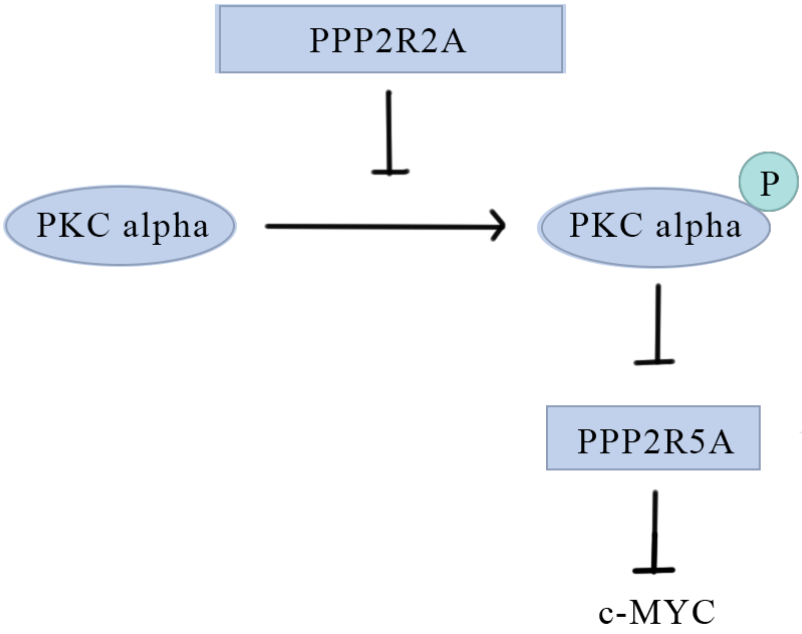

Figure 4.1: PKC alpha activity stabilizes MYC protein. The diagram shows that PPP2RA inactivates PKC alpha, but deletions in PPP2R2A result in activation of PKC alpha, subsequent suppression of the PP2A/ B56α complex by phosphorylation and ultimately stability of the MYC protein.

The results of the investigation show that the presence of the PP2A inhibitory subunits increase the phosphorylation on PKC alpha (**Figure 3.12**). Possibly, there is a complex level of PP2A subunit regulation, and the regulatory subunits target the PP2A activity to different substrates. The DigiWest analysis provides the possibility to investigate this further and hence relate these events to expression of targets and regulatory subunits in the same sample concurrently.

4.2.5 PP2A Inhibitory Subunits Dephosphorylate Ribosomal Protein p70 S6 Kinase

It has been proven that ribosomal protein p70 S6 kinase (S6K) is a downstream target of mTOR signalling. This protein is responsible for cap-dependent translation following activation by phosphorylation, through mTOR (Lee-Fruman, et al., 1999). Phosphorylation occurs at threonine residues 389 and 228. The fully activated kinase in turn phosphorylates the eukaryotic translation initiation factor 4B (eIF4B), causing it to bind with eIF3 (Holz, et al., 2005; Mamane, et al., 2006; Ismail, et al., 2013). The recruitment of the translation initiation complex at the mRNA cap is complex and involves various factors. eIF4E was shown to be released from the suppressive complex eIF4E/4E-BP1 following 4E-BP1 hyperphosphorylation as a result of overexpression of the PP2A inhibitory subunits CIP2A, SET and IGBP1. The results also show that phosphorylation of p70 S6K and eIF4B are decreased. Interestingly, we also show that overexpression of CIP2A, SET and IGBP1 results in enhanced polysome recruitment of competitive mRNA exemplified by c-MYC (**Figure 3.7**). Hence the overall effect is an enhanced efficiency of translation initiation complex. This shows that analysing data obtained on single effector proteins does not generate the collective effect of data on protein networks. The limiting factor of translation initiation is eIF4E and hence in this case a change in the availability of active eIF4E is the driver to promote translation initiation. Thus, the decrease

in p70 S6K and eIF4B (**Table 3.2**), although contradictory to the translation initiation outcome, have a lesser weight in terms of polysome recruitment when compared to activation of the limiting factor, eIF4E. Studies on dephosphorylation of p70 S6K are lacking and according to Mok, et al., 2013, the regulation of S6K is complex and studies on both isoforms would shed more light on the process. It is interesting to note that studies on *Drosophila* PP2A-B' regulatory subunit, which targets PP2A, also dephosphorylated S6K. Knockout of PP2A-B'in these flies caused S6K phosphorylation (Hahn, et al., 2010). This supports our observation, but it is also extremely important to extend studies to cover the simultaneous regulation of proteins in complex networks, including studies on isoforms as in the case of p70 S6K.

4.2.6 PPP2R2A Correlates with Beta-Catenin (CTNNB1) Protein Levels

Using the Breast Invasive Carcinoma (TCGA) datasets, correlation analysis of protein levels between PP2A inhibitory and regulatory subunits, and the protein signature derived from the DigiWest analysis was performed. As expected, AURKA protein levels correlated positively and significantly with the protein levels of CIP2A and SET (**Table 3.5**) with a Spearman coefficient of 0.71 (p-value of 4.5 $X10^{-11}$) and 0.29 (p-value of 0.0224), respectively.

Beta-catenin protein level (DigiWest) increased upon overexpression of CIP2A, SET and IGBP1 and using TCGA datasets we showed a significant inverse correlation with the PP2A regulatory subunit, PPP2R2A with a Spearman coefficient of -0.31 and a p-value of 7.3 $X10^{-3}$ in datasets obtained from TCGA (**Table 3.5**).

In other studies, PPP2R2A, encoding B55α was shown to directly bind beta-catenin resulting in dephosphorylation through the PP2A complex. It is well

established that phosphorylated beta-catenin is degraded, and therefore an active phosphatase brought in direct contact with beta-catenin should stabilise the protein (Zhang, et al., 2009). The regulatory subunit PPP2R2A is therefore responsible for beta-catenin regulation. Knockdown of this regulatory subunit elevates degradation of beta-catenin and decreases Wnt signalling. Although this mechanistic information does not support our findings, regulation of the PP2A activity and shifting of the complex from one substrate to another requires collation of multiple signals converging to the regulation of a specific target. In addition, we also show that the protein expression of beta-catenin in the TCGA dataset positively correlates with epithelial markers, EPCAM and E-cadherin (CDH1), suggesting that mechanisms should be studied in the context of different tumours and their progression. Our experience with DigiWest analysis supports the need to measure protein expression, phospho-profiling and isoforms in the same lysate in a multiplex fashion.

More studies are required to understand this observation, ideally utilising cellular models with modified PP2A regulatory subunits, including PPP2R2A. The latter regulatory subunit is deleted in 17 % of TCGA Breast Invasive Carcinoma patients (**Figure 3.16**) and therefore understanding the mechanisms involved would possibly shed more light on this anomaly.

It is important to consider the variability in end point measurement between protein levels and RNA levels. Comparisons using mRNA datasets provide information on the transcriptional regulation of genes, but lacks post-transcriptional control such as polysome recruitment, protein degradation, and mRNA regulation as exemplified in Figure 4.2.

A

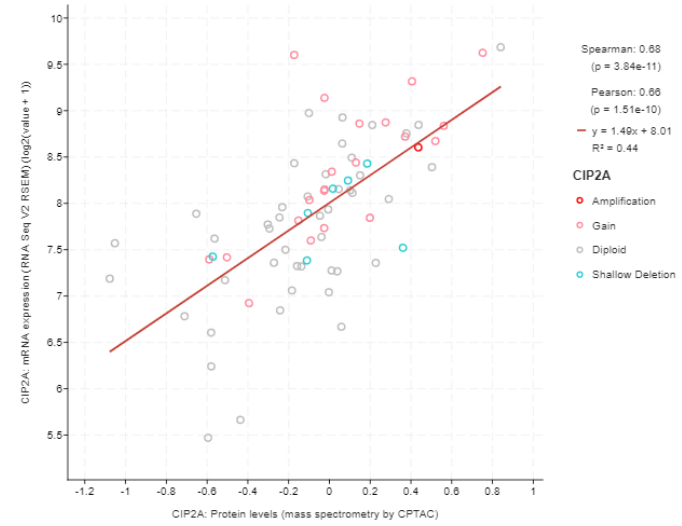

B

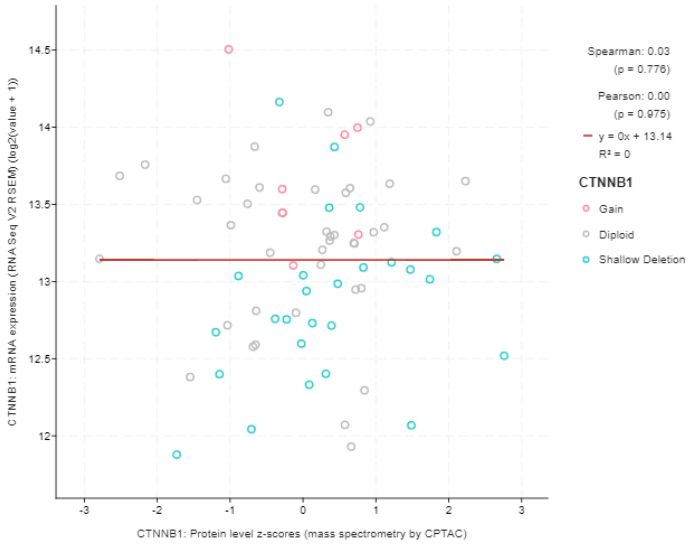

Figure 4.2: Plot showing the correlation between mRNA expression (RNA Seq data) and the Protein expression (z-score level; mass spectrometry) of CIP2A [A] and beta-catenin (CTNNB1) [B]. The figure also provides the Spearman and Pearson correlation coefficient and a key showing Gain (red circle), Diploid (Grey circle) and Deletion (blue circle). Data is taken from https://www.cbioportal.org/. The figure shows that correlations between protein and RNA levels in patient material for the same gene/protein clearly show this discrepancy, exemplified by the positive and significant correlation of CIP2A mRNA/ protein levels and no correlation between mRNA/protein levels of beta-catenin.

4.2.7 PP2A regulation and Metastatic Disease

Collectively, the increased availability of eIF4E through the hyperphosphorylation of 4E-BP1, the higher expression of c-MYC, beta-catenin and MCL1 following overexpression of the PP2A inhibitory subunits support the role of low PP2A activity in breast cancer disease progression. The new insight in the shift of ERK isoforms towards expression of ERK2 and its role in epithelial mesenchymal transition (EMT), supports a potential mechanism of PP2A-dependent mesenchymal transition. Previous studies within our group show the use of AURKA expression as a surrogate marker of low PP2A activity. This is supported by our observation in this investigation that AURKA inversely correlates with PPP2CA (Spearman coefficient of -0.26, p-value = 1.07 $X10^{-17}$) and PPP2R2A (Spearman coefficient of -0.27, p-value = 3.92 $X10^{-19}$) (**Table 3.7**). High expression of AURKA is associated with more than 60 % of triple negative breast cancer (TNBC) patients, representing the poor prognostic basal subtype. To supplement this, Figure 3.17 shows that higher expression of AURKA and deletion in PPP2R2A are common in lymph node metastasis and may require more advanced surgery. In this investigation, high expression of the PP2A inhibitory subunits, CIP2A and SET, was found to correlate with AURKA expression with a Spearman coefficient of 0.71 (p-value = 4.5 $X10^{-11}$) and 0.29 (p-value = 0.0224), respectively (**Table 3.5**). Also, PPP2R2A deletions show significant inverse correlation with SET (Spearman coefficient of -0.18, p-value = 7.04 $X10^{-9}$) and CIP2A (Spearman coefficient of -0.18, p-value = 1.44 $X10^{-9}$) (**Table 3.7**) implying that high expression of these inhibitors results in further inhibitory effect on the phosphatase. These results therefore provide the basis to study the role of PP2A regulation in metastatic disease.

4.3 SELECTION OF RESOURCES AND METHODS

4.3.1 Selection of Suitable Breast Cancer Cell Lines

At the start of the investigation, nine breast cancer cell lines were studied. The ER positive MCF-7 cell line and, even more so, the HER2 positive MDA-MB-453 cell line, both have a low endogenous expression of CIP2A and SET. This was concluded using RT-PCR experiments and results are shown in Figure 3.1. One may argue that the cell line SK-BR-3 could also be considered as a potential candidate for the investigation, as it also possesses low levels of the inhibitors CIP2A and SET. However, this HER2 positive cell line establishes a very strong specific signal which would otherwise interfere with signalling experiments. The use of this cell line was therefore excluded. On the other hand, cell line MDA-MB-453 has been reported to be HER2 amplified, but transcript level and protein level are still low, although higher than normal.

The PP2A inhibitory subunit studies included CIP2A, SET and IGBP1. Quantitative PCR on IGBP1 was not performed since it has been established that the IGBP1 mRNA is regulated at polysome recruitment and hence there is translational control (Grech, et al., 2008). In subsequent experiments, gene expression was measured using polysome bound mRNA levels as well as protein levels. In addition, the protein analysis included phospho-profiling that provided information of the activation of the translation initiation mechanisms, namely the phosphorylation of the mTOR target, eIF4E-binding protein (4E-BP1). mTOR directly phosphorylates 4E-BP1 and releases eIF4E translation initiation factor, the limiting factor for recruitment of cap-dependent mRNA with complex 5'UTR onto polysomes.

The expression of CIP2A, SET and IGBP1 was then assessed using the Immunocytochemistry (ICC) technique. The nine breast cancer cell lines, located on microscope slide cover slips and fixed in paraformaldehyde are available at the Pathology Laboratory. Photographs of the cell lines, exposed to SET, CIP2A and IGBP1 antibody were inspected, and H-scores were calculated, as shown in Table 3.1. Results showed that the expression of IGBP1 in MCF-7 and MDA-MB 453 is low and confirmed that this was also the case for SET and CIP2A. The cell lines MDA-MB-453 and MCF-7 were therefore eligible for ectopic expression studies. They are also adherent cell lines which can be grown in the laboratory with minimal difficulty.

4.3.2 Isolation and Cloning of PP2A Inhibitors

GFP Fusion Technology is a common laboratory technique whereby the protein of interest is tagged with a fluorescent protein, making the former visible under a particular range of wavelengths. This technology was not considered for this investigation, as the interaction of GFP with the protein of interest would possibly compromise and negatively affect the outcome of this experiment. Since the PP2A inhibitory subunits require efficient binding to the PP2A complex, replacing binding of other regulatory subunits, we opted for a short MYC-tag and the expression of GFP as a bicistronic mRNA with an internal ribosome entry site (IRES) (**Figure 2.2**). The bicistronic mRNA express both the MYC-tagged target of interest and the GFP from the same mRNA which is useful to access expression by GFP and at the same time generating a functional protein with minimal interference on its structure. The latter methodology was therefore implemented, as described in Section 2.2. Fluorescent microscopy shows the transfection efficiency (**Figure 3.3**), and Western blotting was used to confirm the expression of the target genes, ensuring the correct size (**Figure 3.4**).

4.3.3 Transfection of Selected Cell Lines

As stated earlier in Section 4.3.1, the ideal cell line for the investigation is MDA-MB-453, as clearly indicated by the results shown in Figure 3.1 and Table 3.1. However, MCF-7 is an ideal candidate for transfection, as this cell line is robust to various methods of transfection. Transfections were therefore carried out for this cell line, as well as the selected MDA-MB-453, to serve as a control. The vector pmaxGFP was also used as another positive control. Like pIRES2-AcGFP1, this vector also contains the GFP gene. Transfection results using this vector on both MCF-7 and MDA-MB-453 are important to compare efficiency of transfection with the three inhibitors (**Figure 3.3**). Upon inspection of transfected cell lines using the Nikon Fluorescent microscope under bright and dark field, using the green filter set-up, it was concluded that transfection of both cell lines with the three inhibitors, was successful with efficiency of 50 to 70 %.

Once the investigation yielded desirable results, another possibility was considered at this stage. The time point at which the desired protein is expressed as well as GFP selection would ensure isolation of positive cell only using the BIOFACS Cell Sorter. An attempt to do so was in fact successful but the idea was discarded as, on a larger scale, it was not practical in terms of chemicals, laboratory ware as well as handling of the experiment itself. Stable transduction is an alternative to sorting, but this requires the use of a viral laboratory facility that was not available at the start of this project. In addition, it would not have added to the requirements of this project. Thus, protein lysates were prepared from the transfected cell lines as described in Section 2.5, and the next phase of the experiment was conducted.

4.3.4 Western Blotting

Western Blotting was carried out as described in Section 2.5. As primary antibody, Myc-Tag 9B11 was used, which recognises the c-MYC tag present in each of the three constructs, thus automatically locating the latter on the polyacrylamide gel. The results of the Western blot are shown in Figure 3.4. GFP was again put into good use as bright green bands of correct size were obtained for both cell lines. In Figure 3.4, one may observe that the band obtained for SET in cell line MDA-MB-453 is weaker than that obtained for the other inhibitors. This tallies with the transfection experiment shown in Figure 3.3, where transfection was less efficient in the case of this target gene and cell line.

4.3.5 Polysome Bound RNA Profiling

The application of polysome bound RNA profiling was the next obvious step in the study, since it is a technique used to study the association of mRNAs with ribosomes. It involves preparation of a cell lysate, consisting of a combination of polysome bound RNA, and free ribosomes/RNA. These different components can be separated using sucrose gradients and high-speed centrifugation and analysis of results conducted using the Aligent 2100 Bioanalyser. Ultimately, the quantity of transcripts that are being translated at a specific time can be investigated. Polysome bound RNA analysis is closer to the protein expression but does not account for mRNA regulation and protein degradation mechanisms.

The original plan for the investigation was to apply polysome bound RNA profiling to transfected cell lines for each inhibitor; namely SET, IGBP1, and CIP2A. Preliminary investigations and optimization experiments were carried

out and results shown in Table 3.8. The methodology adopted was that described by Grech, et al. (2008), as this yielded a high concentration of good quality RNA. One of the main limitations in the preparation of the cell pellets representing the overexpression of target genes is the differential transfection efficiencies and the process to select for the positive cells. As mentioned previously, the use of the bicistronic construct provides the possibility to sort on the basis of fluorescence. During this study, the use of FACS was limiting. The transfection efficiencies between experiments varied from 50 to 70 % positive cells, based on visual and manual microscopy counting. Using bulk cells is possible for direct end-point measurements, such as fluorescence intensity of antibody-antigen interactions as in the case of Western analysis. On the other hand, differences in polysome recruitment measurements between experiments was experienced (**Figure 3.7**). This difference is possibly attributed to the differences in the distribution of free and polysome bound fractions. This difference is amplified in the final calculations due to the generation of a factor required to generate the percent polysome recruitment as described in Section 2.7.6.

To select for positive cells following transfections, the use of the antibiotic G-418 sulphate was also implemented (results not shown). The construct expresses the gene, aminoglycoside 3' phosphotransferase (neomycin resistant gene) under the SV40 promoter. Although there was an improvement in percent positive cells to 70 to 80 % (based on visual microscopy counts), the treatment influenced polysome distribution and pooling the fractions was not possible. Hence, it was decided to utilise the DigiWest technology as a multiplex assay to measure protein expression and phospho-profiles.

4.3.6 Digital Western Technology

Digital Westerns (DigiWest) is a novel technology that allows the interrogation of 200-500 antibodies using one protein lysate. The method involves the separation of proteins on a standard SDS-polyacrylamide gel and transfer of the separated protein fractions onto a blotting membrane. Results are read using the FlexMAP3D Luminex instrument and appear as bar graphs, specific to each antibody (referred to as analyte) showing the intensity of the signal against the molecular weight of the protein (**Figures 3.9 to 3.13**).

With reference to Figure 3.8, one may argue that it would have been ideal to present DigiWest graphs obtained for the control MDA-MB-453 cell line, with the three transfected cell lines, as with the other analytes. Such a run was in fact carried out, and the control and transfected lysates were exposed to analyte CIP2A#1426. However, no peak signals were obtained during this run, showing that the antibody did not function correctly. Therefore only preliminary results were available, which were however, still successful.

As a final step, results obtained from DigiWest technology created the opportunity to compare DigiWest data to patient material, using the Breast Invasive Carcinoma dataset from TCGA (Firehose Legacy, Cerami, et al., 2012; Gao, et al., 2013). Analysis of these results has been described in Section 4.2 with some very interesting findings which support previous research as well as lead us to future experimentation.

4.3.7 Limitations of TCGA Dataset

It is obvious that validation of results obtained in cellular models against patient material is advantageous. However, following the COVID pandemic, it was

almost impossible to conduct retrospective studies. On the other hand, it is not a straightforward task to carry out the same investigations conducted in this research (ratios, phosphorylations etc) in patient material.

Exploration of publicly available databases, specifically the Breast Invasive Carcinoma dataset from TCGA (Firehose Legacy, Cerami, et al., 2012; Gao, et al., 2013) became the next obvious step. This public website utilises data from The Cancer Genome Atlas (TCGA), an NIH-sponsored research project. The dataset used for this particular study is contains a total of 1108 samples (Cerami, et al., 2012; Gao, et al., 2013). Data is obtained from primary and untreated breast tumours. Information about mutations, copy number alterations, mRNA expression and protein levels are available for the dataset. The basic clinic-pathological characteristics and diagnosis age of the cohort are also provided.

Limitations of using TCGA dataset are of course, a reality. Primarily, the data is collected from untreated patients and there is no further information about possible modifications following therapy (Kim, 2017). Another disadvantage is the fact that the dataset does not include T and B cell sequencing information. Today, both immunotherapy and chemotherapy are paramount in cancer research; therefore such information would be invaluable.

Another limitation is that innovative data in the BioPortal becomes available at a very slow pace. (Learned, et al., 2019). Often, the data needs to be published first, and this can postpone research goals. Downloading the data is also a cumbersome task and often needs to be decrypted. TCGA outputs are also difficult to derive and not always straightforward.

All in all, exploration of public databases is still an important aspect of research. Sharing information in the scientific field a necessary and crucial way forward.

4.4 SUMMARY AND CONCLUSION

The results obtained in this investigation have provided us with some very interesting conclusions regarding PP2A and its inhibitory subunits CIP2A, SET and IGBP1.

As expected, the overexpression of the PP2A inhibitory subunits in this study, show significant increase in the protein levels of c-MYC, and in the phosphorylation of 4E-BP1. Both c-MYC and beta-catenin are eIF4E dependent and their protein levels increase following release of eIF4E from the 4E-BP1 suppressive complex. Therefore, the increased protein levels of c-MYC can be partially contributed to the release of eIF4E. The mTOR pathway is directly responsible for inactivation of 4E-BP1, and PP2A is responsible for keeping the mTOR pathway in check (Come, et al., 2009; Junttila, et al., 2007; Mannava, et al., 2011; Niemelä, et al., 2012). Inhibition of PP2A, as is the case in the transfected cell lines, causes an increase in phosphorylation of 4E-BP1 (**Figure 3.10**). Although polysome recruitment of beta-catenin transcript increases, the tight regulation of its protein degradation through its phosphorylation required confirmation at protein level. For instance, analysis of the TCGA dataset showed that protein levels of the PP2A regulatory subunit PPP2R2A inversely correlates with beta-catenin in the TCGA patient dataset (**Table 3.5**). It has been established by previous investigations that PPP2R2A binds to beta-catenin and dephosphorylates it, stabilizing the protein. DigiWest results confirmed an increase in beta-catenin expression at a fold change (log_2) of 1.75, 1.78 and 2.11 following overexpression of IGBP1, SET and CIP2A respectively (**Table 3.3**). Interestingly, an increase in beta-catenin phosphorylation at serine 33/37 and threonine 41 was also observed following overexpression of the PP2A inhibitory subunits. The phospho:total AFI ratio was 0.02 in the control cells and increased to 0.09, 0.07 and 0.09 following overexpression of IGBP1, SET and CIP2A

respectively. Hence the effect on enhanced phosphorylation of beta-catenin, does not overcome the increase in eIF4E-induced polysome recruitment of beta-catenin transcript and increase in protein synthesis. This highlights the importance of measuring both total protein and phospho-profiles in the same lysate.

CIP2A regulates MYC mRNA translation through a PP2A dependent translation initiation pathway. The CIP2A-PP2A axis is crucial for polysome recruitment of c-MYC and stabilisation of c-MYC protein. The results support the role of CIP2A as a regulator of MYC mRNA translation control, through an increased polysome recruitment of the MYC mRNA, and prove that this is mTOR-dependent, as shown by the release of the c-MYC RNA from polysomes following addition of rapamycin, an mTOR inhibitor (McConnell, et al. (2009); **Figure 3.7**). Of interest, one also observes that MYC mRNA polysome recruitment is induced by SET and IGBP1 overexpression. Although overexpression of IGBP1 results in enhanced polysome recruitment of MYC mRNA, addition of rapamycin does not release the RNA from polysomes (**Figure 3.7**), possibly due to the magnitude of enhanced polysome recruitment or indirect mechanisms.

The protein signature and phospho-profile generated from DigiWest data have shown that overexpression of the inhibitory subunits increases protein levels of beta-catenin, MCL1 and RICTOR, and results in downregulation of eIF4B and CREB. On the other hand, there is an increased phosphorylation of 4E-BP1 and PKC alpha, as well as dephosphorylation of p70 S6 kinase (**Figures 3.9 to 3.12**). Using TGCA datasets to correlate expression of various proteins relevant to the study, it was concluded that CIP2A, SET and IGBP1 do not correlate with the protein signature, but CIP2A shows a positive correlation with SET, and with AURKA, the surrogate marker of low PP2A activity (**Table 3.5**). In a

comparison of the correlation between mRNA and protein, it was concluded that translation of protein does not always reflect transcription. CIP2A and AURKA correlate at both RNA and protein level, but this occurs to a lesser extent, with CIP2A and SET (**Figure 3.15**).

This investigation has confirmed that AURKA is the surrogate marker of low PP2A activity and is associated with more than 60 % of triple negative breast cancer (TNBC) patients, representing the poor prognostic basal subtype. The results in Figure 3.17 show that higher expression of AURKA and PPP2R2A is common in lymph node metastasis. Table 3.5 shows that AURKA expression is correlated with CIP2A and SET, and Table 3.7 shows that AURKA inversely correlates with PPP2R2A and PPP2CA. PP2A regulation may therefore also be involved in metastatic disease.

An interesting observation showed that overexpression of CIP2A, SET and IGBP1 caused a significant expression of ERK(p42). Thus, the PP2A inhibitory subunits must also be involved in EMT induction (**Figure 3.13**). Overexpression of CIP2A, SET and IGBP1 also enhanced PKC alpha phosphorylation (**Figure 3.12**). Finally, the overexpressed cell lines caused dephosphorylation of p70 S6 kinase (**Figure 3.11**), prompting further investigation and understanding of the inactivation of this kinase.

4.5 FUTURE EXPERIMENTATION

In this particular investigation, DigiWest technology and analysis of data was conducted for the MDA-MB-453 cell line transfected with the PP2A inhibitory subunits SET, IGBP1 and CIP2A. Future experimentation could be carried out on the MCF-7 transfected cell line and results compared with those obtained in this research. It has been proven in this investigation that both cell lines have low endogenous levels of the three inhibitory subunits.

The potential role of the PP2A complex and its regulation in epithelial mesenchymal transition (EMT) opens a plethora of experiments that are supported by the current findings in this study. The shift towards expression of ERK2(p42) upon overexpression of CIP2A, SET and IGBP1 (**Figure 3.13**) is an interesting observation and supports the use of multiplex analysis combined with size distribution to measure potential isoforms, hence the use of DigiWest analysis. One of the main future experiments is to overexpress the PP2A inhibitory subunits in various cell lines representing epithelial and mesenchymal subtypes, preferably in the TNBC cellular models. The selection of antibodies shall include subtype classifiers, epithelial-mesenchymal markers, PP2A regulatory subunits, AURKA as a surrogate marker of low PP2A activity and the panel of signalling proteins (total and phospho-protein antibodies) used in this study. Currently, the research group is setting up EMT breast cancer models using TGF-β-induced cellular invasion and identified fibronectin, FN1 as an early invasion marker (unpublished data). The PP2A complex shall be measured in such models and compared to the functional assay results following overexpression of the PP2A-inhibitory subunits.

In addition to protein expression and activity measurement, immunoprecipitation studies shall be performed on the overexpressors to measure the binding partners

of the PP2A complex and direct targets. Mass spectrometry analysis shall be used to analyse the binding partners. Of note, to study isoform shifts as in the case of ERK1/2, DigiWest analysis shall also be done, since this information will be lost when mass spectrometry is done.

Studies have shown that expression of CIP2A stabilises beta-catenin via fibronectin, FN1. As indicated above, FN1 was identified as an early invasion marker. FN1 is an adhesive glycoprotein that plays an important role in cell growth, cell cycle progression as well as cell survival and differentiation. Recent studies have shown that this glycoprotein is also associated with tumorigenesis, as its levels are strongly linked to proliferation markers such as AURKA and CIP2A. Although the mechanism behind the relationship between FN1 and tumorigenesis is unclear, a recent study in bladder cancer patients has given some insight to the underlying mechanism (Gao, et al., 2017).

The correlation between stromal FN1, CIP2A and the proliferating cell nuclear antigen (PCNA) using immunofluorescence, revealed that there is a positive correlation between FN1, CIP2A and PCNA in bladder cancer tissues. Bladder cancer cellular models have shown that CIP2A stabilizes beta-catenin through expression of cellular FN1. FN1 and CIP2A shall be included in the panel for future investigation of EMT in breast cancer.

Our research also suggests that protein expression correlations depend on the breast cancer subtype and origin. Regulation of key proteins such as beta-catenin, c-MYC and MCL-1 shall be investigated separately in different tumour types of breast origin. In fact, the data analysis performed on the TCGA datasets shall be performed by filtering specific breast cancer subtypes and EMT markers. Also, primary and metastatic tumour datasets shall be considered separately. An interesting future experiment would involve expression studies and protein

analysis of primary tumour tissue biopsies and matched lymph nodes. The use of Quantigene™ assay for low quality material shall be taken advantage of to run multiplex assays at RNA level (transcript analysis). Further optimisation of Digiwest shall be given good consideration to utilise the technology for FFPE tissues and possibly, plasma-derived exosomes from matched patients. Our research group is currently optimising exosome isolation and multiplex analysis using xMAP technology from Luminex. This is the basis of the DigiWest technology and measuring candidate EMT markers in exosomes is another technology to consider for longitudinal studies. Expression of AURKA was successfully measured in plasma-derived exosomes from metastatic patients.

Another level of analysis includes the generation of datasets for isoform expression at protein level. In this study we find a novel shift in ERK1/2 isoforms associated with overexpression of PP2A inhibitory subunits. The study can be extended to study various isoforms associated with breast cancer disease progression.

REFERENCES

Al-Bazz, Y. O., Underwood, J. C., Brown, B. L., & Dobson, P. R. (2009). Prognostic significance of Akt, phospho-Akt and BAD expression in primary breast cancer. *European Journal of Cancer*, *45*(4), 694–704. https://doi.org/10.1016/j.ejca.2008.11.044

Alessi, D. R., Andjelkovic, M., Caudwell, B., Cron, P., Morrice, N., Cohen, P., & Hemmings, B. A. (1996). Mechanism of activation of protein kinase B by insulin and IGF-1. *The EMBO Journal*, *15*(23), 6541–6551. https://doi.org/10.1002/j.1460-2075.1996.tb01045.x

Alvarez-Fernández, M., Halim, V. A., Aprelia, M., Mohammed, S., & Medema, R. H. (2011). Protein Phosphatase 2A (B55α) Prevents Premature Activation of Forkhead Transcription Factor FoxM1 by Antagonizing Cyclin A/Cyclin-dependent Kinase-mediated Phosphorylation. *Journal of Biological Chemistry*, *286*(38), 33029–33036. https://doi.org/10.1074/jbc.m111.253724

Arnold, H. K., & Sears, R. C. (2006). Protein Phosphatase 2A Regulatory Subunit B56α Associates with c-Myc and Negatively Regulates c-Myc Accumulation. *Molecular and Cellular Biology*, *26*(7), 2832–2844. https://doi.org/10.1128/mcb.26.7.2832-2844.2006

Azuma, H., Takahara, S., Horie, S., Muto, S., Otsuki, Y., & Katsuoka, Y. (2003). Induction of Apoptosis in Human Bladder Cancer Cells In Vitro and In Vivo Caused by FTY720 Treatment. *Journal of Urology*, *169*(6), 2372–2377. https://doi.org/10.1097/01.ju.0000064938.32318.91

Baldacchino, S., Saliba, C., Petroni, V., Fenech, A. G., Borg, N., & Grech, G. (2014). Deregulation of the phosphatase, PP2A is a common event in breast cancer, predicting sensitivity to FTY720. *EPMA Journal*, *5*(1). https://doi.org/10.1186/1878-5085-5-3

Baldacchino, S., Wastall, L., Saliba, C., Hughes, T., Scerri, C., & Berwick, A. et al. (2017). CIP2A expression predicts recurrences of tamoxifen-treated breast cancer. *Tumor Biology*, *39*(10), 101042831772206. https://doi.org/10.1177/1010428317722064

Barford, D., Das, A. K., & Egloff, M. P. (1998). The structure and mechanism of protein phosphatases: insights into catalysis and regulation. *Annual Review of Biophysics and Biomolecular Structure*, *27*(1), 133–164. https://doi.org/10.1146/annurev.biophys.27.1.133

Barjesteh van Waalwijk van Doorn-Khosrovani S, Spensberger D, de Knegt Y, Tang M, Löwenberg B, Delwel R. (2005). Somatic heterozygous mutations in ETV6 (TEL) and frequent absence of ETV6 protein in acute myeloid leukemia. Oncogene. 2005 Jun 9;24(25):4129-37. doi: 10.1038/sj.onc.1208588. PMID: 15806161.

Bartholomeusz, C., Gonzalez-Angulo, A., Liu, P., Hayashi, N., Lluch, A., Ferrer-Lozano, J., & Hortobágyi, G. (2012). High ERK Protein Expression Levels Correlate with Shorter Survival in Triple-Negative Breast Cancer Patients. *The Oncologist*, *17*(6), 766-774. (https://doi.org/10.1634/theoncologist.2011-0377)

Bauman, A. L., & Scott, J. D. (2002). Kinase- and phosphatase-anchoring proteins: harnessing the

dynamic duo. *Nature Cell Biology*, *4*(8), E203–E206. https://doi.org/10.1038/ncb0802-e203

Böckelman, C., Lassus, H., Hemmes, A., Leminen, A., Westermarck, J., Haglund, C., Bützow, R., & Ristimäki, A. (2011). Prognostic role of CIP2A expression in serous ovarian cancer. *British Journal of Cancer*, *105*(7), 989–995. https://doi.org/10.1038/bjc.2011.346

Bonello, D. (2020). High AURKA expression in triple negative breast cancer correlates with expression of CIP2A and PME-1. https://www.um.edu.mt/library/oar/handle/123456789/73532

Buscà, R., Pouysségur, J., & Lenormand, P. (2016). ERK1 and ERK2 Map Kinases: Specific Roles or Functional Redundancy? *Frontiers in Cell and Developmental Biology*, *4*. https://doi.org/10.3389/fcell.2016.00053

Calin, G. A., di Iasio, M. G., Caprini, E., Vorechovsky, I., Natali, P. G., Sozzi, G., Croce, C. M., Barbanti-Brodano, G., Russo, G., & Negrini, M. (2000). Low frequency of alterations of the α (PPP2R1A) and β (PPP2R1B) isoforms of the subunit A of the serine-threonine phosphatase 2A in human neoplasms. *Oncogene*, *19*(9), 1191–1195. https://doi.org/10.1038/sj.onc.1203389

Cerami, E., Gao, J., Dogrusoz, U., Gross, B. E., Sumer, S. O., Aksoy, B. A., Jacobsen, A., Byrne, C. J., Heuer, M. L., Larsson, E., Antipin, Y., Reva, B., Goldberg, A. P., Sander, C., & Schultz, N. (2012). The cBio Cancer Genomics Portal: An Open Platform for Exploring Multidimensional Cancer Genomics Data: Figure 1. *Cancer Discovery*, *2*(5), 401–404. https://doi.org/10.1158/2159-8290.cd-12-0095

Chen, J., Martin, B. L., & Brautigan, D. L. (1992). Regulation of Protein Serine-Threonine Phosphatase Type-2A by Tyrosine Phosphorylation. *Science*, *257*(5074), 1261–1264. https://doi.org/10.1126/science.1325671

Chen, L., Lai, Y., Li, D., Zhu, X., Yang, P., & Li, W. et al. (2011). α4 is highly expressed in carcinogen-transformed human cells and primary human cancers. *Oncogene*, *30*(26), 2943-2953. https://doi.org/10.1038/onc.2011.20

Chen, L., Zhang, Z., Yi, Z., & Li, J. (2017). MicroRNA-211-5p suppresses tumour cell proliferation, invasion, migration and metastasis in triple-negative breast cancer by directly targeting SETBP1. *British Journal Of Cancer*, *117*(1), 78-88. https://doi.org/10.1038/bjc.2017.150

Chiba, K. (2005). FTY720, a new class of immunomodulator, inhibits lymphocyte egress from secondary lymphoid tissues and thymus by agonistic activity at sphingosine 1-phosphate receptors. *Pharmacology & Therapeutics*, *108*(3), 308–319. https://doi.org/10.1016/j.pharmthera.2005.05.002

Chou, H. C., Chen, C. H., Lee, H. S., Lee, C. Z., Huang, G. T., Yang, P. M., Lee, P. H., & Sheu, J. C. (2007). Alterations of tumour suppressor gene PPP2R1B in hepatocellular carcinoma. *Cancer Letters*, *253*(1), 138–143. https://doi.org/10.1016/j.canlet.2007.01.016

Christensen, D. J., Ohkubo, N., Oddo, J., van Kanegan, M. J., Neil, J., Li, F., Colton, C. A., & Vitek, M. P. (2011). Apolipoprotein E and Peptide Mimetics Modulate Inflammation by Binding

the SET Protein and Activating Protein Phosphatase 2A. *The Journal of Immunology*, *186*(4), 2535–2542. https://doi.org/10.4049/jimmunol.1002847

Chrzan, P., Skokowski, J., Karmolinski, A., & Pawelczyk, T. (2001). Amplification of c-myc gene and overexpression of c-Myc protein in breast cancer and adjacent non-neoplastic tissue. *Clinical Biochemistry*, *34*(7), 557-562. https://doi.org/10.1016/s0009-9120(01)00260-0

Cristóbal, I., Manso, R., Rincón, R., Caramés, C., Senin, C., Borrero, A., Martínez-Useros, J., Rodriguez, M., Zazo, S., Aguilera, O., Madoz-Gúrpide, J., Rojo, F., & García-Foncillas, J. (2014). PP2A Inhibition Is a Common Event in Colorectal Cancer and Its Restoration Using FTY720 Shows Promising Therapeutic Potential. *Molecular Cancer Therapeutics*, *13*(4), 938–947. https://doi.org/10.1158/1535-7163.mct-13-0150

Cristóbal I., Blanco F.J., Garcia-Orti L., Marcotegui N., Vicente C., Rifon J. Novo F.J., Bandres E., Calasanz M.J., Bernabeu C., Odero M.D. (2010). SETBP1 overexpression is a novel leukemogenic mechanism that predicts adverse outcome in elderly patients with acute myeloid leukemia. Blood, Volume 115, Issue 3, 2010, Pages 615-625, ISSN 0006-4971, https://doi.org/10.1182/blood-2009-06-227363.

Cohen, P. (2002). Protein kinases — the major drug targets of the twenty-first century? *Nature Reviews Drug Discovery*, *1*(4), 309–315. https://doi.org/10.1038/nrd773

Coleman, L. J., Peter, M. B., Teall, T. J., Brannan, R. A., Hanby, A. M., Honarpisheh, H., Shaaban, A. M., Smith, L., Speirs, V., Verghese, E. T., McElwaine, J. N., & Hughes, T. A. (2009). Combined analysis of eIF4E and 4E-binding protein expression predicts breast cancer survival and estimates eIF4E activity. *British Journal of Cancer*, *100*(9), 1393–1399. https://doi.org/10.1038/sj.bjc.6605044

Côme, C., Laine, A., Chanrion, M., Edgren, H., Mattila, E., Liu, X., Jonkers, J., Ivaska, J., Isola, J., Darbon, J. M., Kallioniemi, O., Thézenas, S., & Westermarck, J. (2009). CIP2A Is Associated with Human Breast Cancer Aggressivity. *Clinical Cancer Research*, *15*(16), 5092–5100. https://doi.org/10.1158/1078-0432.ccr-08-3283

Connor, J. H., Kleeman, T., Barik, S., Honkanen, R. E., & Shenolikar, S. (1999). Importance of the β12-β13 Loop in Protein Phosphatase-1 Catalytic Subunit for Inhibition by Toxins and Mammalian Protein Inhibitors. *Journal of Biological Chemistry*, *274*(32), 22366–22372. https://doi.org/10.1074/jbc.274.32.22366

Culjkovic-Kraljacic, B., Skrabanek, L., Revuelta, M. V., Gasiorek, J., Cowling, V. H., Cerchietti, L., & Borden, K. L. B. (2020). The eukaryotic translation initiation factor eIF4E elevates steady-state m ^{7} G capping of coding and noncoding transcripts. *Proceedings of the National Academy of Sciences*, *117*(43), 26773–26783. https://doi.org/10.1073/pnas.2002360117

Denk, S., Schmidt, S., Schurr, Y., Schwarz, G., Schote, F., Diefenbacher, M., Armendariz, C., Dejure, F., Eilers, M., & Wiegering, A. (2020). CIP2A regulates MYC translation (via its 5′UTR) in colorectal cancer. *International Journal of Colorectal Disease*, *36*(5), 911–918. https://doi.org/10.1007/s00384-020-03772-y

Fenton, T. R., & Gout, I. T. (2011). Functions and regulation of the 70kDa ribosomal S6 kinases. *The International Journal of Biochemistry & Cell Biology*, *43*(1), 47–59. https://doi.org/10.1016/j.biocel.2010.09.018

Gao, F., Xu, T., Wang, X., Zhong, S., Chen, S., Zhang, M., Zhang, X., Shen, Y., Wang, X., Xu, C., & Shen, Z. (2017). CIP2A mediates fibronectin-induced bladder cancer cell proliferation by stabilizing β-catenin. *Journal of Experimental & Clinical Cancer Research*, *36*(1). https://doi.org/10.1186/s13046-017-0539-8

Gao, J., Aksoy, B. A., Dogrusoz, U., Dresdner, G., Gross, B., Sumer, S. O., Sun, Y., Jacobsen, A., Sinha, R., Larsson, E., Cerami, E., Sander, C., & Schultz, N. (2013). Integrative Analysis of Complex Cancer Genomics and Clinical Profiles Using the cBioPortal. *Science Signaling*, *6*(269). https://doi.org/10.1126/scisignal.2004088

GeneCards - The Human Gene Compendium. (2013, 19 March 2013). Retrieved 21 September 2013, 2013, from www.genecards.org

Geyer, F., Lacroix-Triki, M., Savage, K., Arnedos, M., Lambros, M., & MacKay, A. et al. (2010). β-Catenin pathway activation in breast cancer is associated with triple-negative phenotype but not with CTNNB1 mutation. *Modern Pathology*, *24*(2), 209-231. https://doi.org/10.1038/modpathol.2010.205

Gray, K. A., Daugherty, L. C., Gordon, S. M., Seal, R. L., Wright, M. W., & Bruford, E. A. (2012). Genenames.org: the HGNC resources in 2013. *Nucleic Acids Research*, *41*(D1), D545–D552. https://doi.org/10.1093/nar/gks1066

Grech, G., Baldacchino, S., Saliba, C., Grixti, M. P., Gauci, R., Petroni, V., Fenech, A. G., & Scerri, C. (2016). Deregulation of the protein phosphatase 2A, PP2A in cancer: complexity and therapeutic options. *Tumor Biology*, *37*(9), 11691–11700. https://doi.org/10.1007/s13277-016-5145-4

Grech, G., Blázquez-Domingo, M., Kolbus, A., Bakker, W. J., Müllner, E. W., Beug, H., & von Lindern, M. (2008). Igbp1 is part of a positive feedback loop in stem cell factor–dependent, selective mRNA translation initiation inhibiting erythroid differentiation. *Blood*, *112*(7), 2750–2760. https://doi.org/10.1182/blood-2008-01-133140

Gu, P., Qi, X., Zhou, Y., Wang, Y., & Gao, X. (2011). Generation of Ppp2Ca and Ppp2Cb conditional null alleles in mouse. *Genesis*, *50*(5), 429–436. https://doi.org/10.1002/dvg.20815

Hahn, K., Miranda, M., Francis, V. A., Vendrell, J., Zorzano, A., & Teleman, A. A. (2010). PP2A Regulatory Subunit PP2A-B′ Counteracts S6K Phosphorylation. *Cell Metabolism*, *11*(5), 438–444. https://doi.org/10.1016/j.cmet.2010.03.015

Hahn W.C., Dessain S.K, Brooks M.W., King J.E., Elenbaas B., Sabatini D.M., DeCaprio J.A., Weinberg R.A. (2002). Enumeration of the simian virus 40 early region elements necessary for human cell transformation. Mol Cell Biol. 2002 Apr;22(7):2111-23. doi: 10.1128/MCB.22.7.2111-

2123.2002. Erratum in: Mol Cell Biol 2002 May;22(10):3562. PMID: 11884599; PMCID: PMC133688.

Han, W., Zhang, C., Shi, C., Gao, X., Zhou, M., & Shao, Q. et al. (2020). Roles of eIF3m in the tumorigenesis of triple negative breast cancer. *Cancer Cell International*, *20*(1). https://doi.org/10.1186/s12935-020-01220-z

Hatsell S, Rowlands T, Hiremath M, Cowin P. (2003). Beta-catenin and Tcfs in mammary development and cancer. *J Mammary Gland Biol Neoplasia*;8:145–158.

Hemmings, B. A., Adams-Pearson, C., Maurer, F., Mueller, P., Goris, J., Merlevede, W., Hofsteenge, J., & Stone, S. R. (1990). .Alpha.- and .beta.-forms of the 65-kDa subunit of protein phosphatase 2A have a similar 39 amino acid repeating structure. *Biochemistry*, *29*(13), 3166–3173. https://doi.org/10.1021/bi00465a002

Hendrix P, Mayer-Jackel R.E., Cron P., Goris J., Hofsteenge J., Merlevede W., Hemmings B.A. (1993). Structure and expression of a 72-kDa regulatory subunit of protein phosphatase 2A. Evidence for different size forms produced by alternative splicing. Journal of Biological Chemistry, Volume 268, Issue 20, 1993, Pages 15267-15276, ISSN 0021-9258 https://doi.org/10.1016/S0021-9258(18)82465-6.

Heuberger, J., & Birchmeier, W. (2009). Interplay of Cadherin-Mediated Cell Adhesion and Canonical Wnt Signaling. *Cold Spring Harbor Perspectives In Biology*, *2*(2), a002915-a002915. https://doi.org/10.1101/cshperspect.a002915

Holz, M. K., Ballif, B. A., Gygi, S. P., & Blenis, J. (2005). mTOR and S6K1 Mediate Assembly of the Translation Preinitiation Complex through Dynamic Protein Interchange and Ordered Phosphorylation Events. *Cell*, *123*(4), 569–580. https://doi.org/10.1016/j.cell.2005.10.024

Ismail, H. M., Myronova, O., Tsuchiya, Y., Niewiarowski, A., Tsaneva, I., & Gout, I. (2013). Identification of the general transcription factor Yin Yang 1 as a novel and specific binding partner for S6 Kinase 2. *Cellular Signalling*, *25*(5), 1054–1063. https://doi.org/10.1016/j.cellsig.2013.02.002

Janssens, V., Goris, J., & van Hoof, C. (2005). PP2A: the expected tumor suppressor. *Current Opinion in Genetics & Development*, *15*(1), 34–41. https://doi.org/10.1016/j.gde.2004.12.004

Junttila, M. R., Puustinen, P., Niemelä, M., Ahola, R., Arnold, H., Böttzauw, T., Ala-aho, R., Nielsen, C., Ivaska, J., Taya, Y., Lu, S. L., Lin, S., Chan, E. K., Wang, X. J., Grènman, R., Kast, J., Kallunki, T., Sears, R., Kähäri, V. M., & Westermarck, J. (2007). CIP2A Inhibits PP2A in Human Malignancies. *Cell*, *130*(1), 51–62. https://doi.org/10.1016/j.cell.2007.04.044

Kloeker, S., Reed, R., McConnell, J. L., Chang, D., Tran, K., Westphal, R. S., Law, B. K., Colbran, R. J., Kamoun, M., Campbell, K. S., & Wadzinski, B. E. (2003). Parallel purification of three catalytic subunits of the protein serine/threonine phosphatase 2A family (PP2AC, PP4C, and

PP6C) and analysis of the interaction of PP2AC with alpha4 protein. *Protein Expression and Purification*, *31*(1), 19–33. https://doi.org/10.1016/s1046-5928(03)00141-4

Laine, A. (2013). The role of an oncoprotein CIP2A in breast carcinoma. Doctorate, University of Turku, Turku.

LaMontagne, K., Littlewood-Evans, A., Schnell, C., O'Reilly, T., Wyder, L., Sanchez, T., Probst, B., Butler, J., Wood, A., Liau, G., Billy, E., Theuer, A., Hla, T., & Wood, J. (2006). Antagonism of Sphingosine-1-Phosphate Receptors by FTY720 Inhibits Angiogenesis and Tumor Vascularization. *Cancer Research*, *66*(1), 221–231. https://doi.org/10.1158/0008-5472.can-05-2001

Lazar, D. F., & Saltiel, A. R. (2006). Lipid phosphatases as drug discovery targets for type 2 diabetes. *Nature Reviews Drug Discovery*, *5*(4), 333–342. https://doi.org/10.1038/nrd2007

Learned K., Durbin A., Currie R. et al. (2019). Barriers to accessing public cancer genomic data. *Sci Data* **6**, 98 (2019). https://doi.org/10.1038/s41597-019-0096-4

Lee, Y., Lee, J., Ho, C., Hong, Q., Yu, S., & Tzeng, C. et al. (2011). miRNA-34b as a tumor suppressor in estrogen-dependent growth of breast cancer cells. *Breast Cancer Research*, *13*(6). https://doi.org/10.1186/bcr3059

Lee-Fruman, K. K., Kuo, C. J., Lippincott, J., Terada, N., & Blenis, J. (1999). Characterization of S6K2, a novel kinase homologous to S6K1. *Oncogene*, *18*(36), 5108–5114. https://doi.org/10.1038/sj.onc.1202894

Li L., Fang C., Xu D., Xu Y., Fu H., Li J. (2016). Cardiomyocyte specific deletion of PP2A causes cardiac hypertrophy. *Am. J. Transl. Res.*;8:1769–1779.

Li Q, Mattingly R.R. (2008). Restoration of E-cadherin cell-cell junctions requires both expression of E-cadherin and suppression of ERK MAP kinase activation in Ras-transformed breast epithelial cells. Neoplasia. 2008 Dec;10(12):1444-58. doi: 10.1593/neo.08968. PMID: 19048123; PMCID: PMC2586695.

Li, Y., Yue, P., Deng, X., Ueda, T., Fukunaga, R., Khuri, F., & Sun, S. (2010). Protein Phosphatase 2A Negatively Regulates Eukaryotic Initiation Factor 4E Phosphorylation and eIF4F Assembly through Direct Dephosphorylation of Mnk and eIF4E. *Neoplasia*, *12*(10), 848-855. https://doi.org/10.1593/neo.10704

Liu, J., Farmer, J. D., Lane, W. S., Friedman, J., Weissman, I., & Schreiber, S. L. (1991). Calcineurin is a common target of cyclophilin-cyclosporin A and FKBP-FK506 complexes. *Cell*, *66*(4), 807–815. https://doi.org/10.1016/0092-8674(91)90124-h

Liu, C., Li, Y., Semenov, M., Han, C., Baeg, G., & Tan, Y. et al. (2002). Control of β-Catenin Phosphorylation/Degradation by a Dual-Kinase Mechanism. *Cell*, *108*(6), 837-847. https://doi.org/10.1016/s0092-8674(02)00685-2

Liu, C. Y., Huang, T. T., Chen, Y. T., Chen, J. L., Chu, P. Y., Huang, C. T., Wang, W. L., Lau, K. Y., Dai, M. S., Shiau, C. W., & Tseng, L. M. (2019). Targeting SET to restore PP2A activity disrupts an oncogenic CIP2A-feedforward loop and impairs triple negative breast cancer progression. *EBioMedicine, 40*, 263–275. https://doi.org/10.1016/j.ebiom.2018.12.032

Liu, H., Qiu, H., Song, Y., Liu, Y., Wang, H., & Lu, M. et al. (2016). Cip2a promotes cell cycle progression in triple-negative breast cancer cells by regulating the expression and nuclear export of p27Kip1. *Oncogene*, *36*(14), 1952-1964. https://doi.org/10.1038/onc.2016.355

Lucas, C. M., Harris, R. J., Giannoudis, A., Copland, M., Slupsky, J. R., & Clark, R. E. (2011). Cancerous inhibitor of PP2A (CIP2A) at diagnosis of chronic myeloid leukemia is a critical determinant of disease progression. *Blood*, *117*(24), 6660–6668. https://doi.org/10.1182/blood-2010-08-304477

Lyon, M. A., Ducruet, A. P., Wipf, P., & Lazo, J. S. (2002). Dual-specificity phosphatases as targets for antineoplastic agents. *Nature Reviews Drug Discovery*, *1*(12), 961–976. https://doi.org/10.1038/nrd963

Mamane, Y., Petroulakis, E., LeBacquer, O., & Sonenberg, N. (2006). mTOR, translation initiation and cancer. *Oncogene*, *25*(48), 6416–6422. https://doi.org/10.1038/sj.onc.1209888

Mannava, S., Omilian, A. R., Wawrzyniak, J. A., Fink, E. E., Zhuang, D., Miecznikowski, J. C., Marshall, J. R., Soengas, M. S., Sears, R. C., Morrison, C. D., & Nikiforov, M. A. (2011). PP2A-B56α controls oncogene-induced senescence in normal and tumor human melanocytic cells. *Oncogene*, *31*(12), 1484–1492. https://doi.org/10.1038/onc.2011.339

Markova, B., Albers, C., Breitenbuecher, F., Melo, J. V., Brümmendorf, T. H., Heidel, F., Lipka, D., Duyster, J., Huber, C., & Fischer, T. (2009). Novel pathway in Bcr-Abl signal transduction involves Akt-independent, PLC-γ1-driven activation of mTOR/p70S6-kinase pathway. *Oncogene*, *29*(5), 739–751. https://doi.org/10.1038/onc.2009.374

McConnell, J. L., & Wadzinski, B. E. (2009). Targeting Protein Serine/Threonine Phosphatases for Drug Development. *Molecular Pharmacology*, *75*(6), 1249–1261. https://doi.org/10.1124/mol.108.053140

Mok, K. W., Mruk, D. D., & Cheng, C. Y. (2013). Regulation of Blood–Testis Barrier (BTB) Dynamics during Spermatogenesis via the "Yin" and "Yang" Effects of Mammalian Target of Rapamycin Complex 1 (mTORC1) and mTORC2. *International Review of Cell and Molecular Biology*, 291–358. https://doi.org/10.1016/b978-0-12-407704-1.00006-3

Mumby, M. (2007). PP2A: Unveiling a Reluctant Tumor Suppressor. *Cell*, *130*(1), 21–24. https://doi.org/10.1016/j.cell.2007.06.034

Mukhopadhyay, A., Saddoughi, S. A., Song, P., Sultan, I., Ponnusamy, S., Senkal, C. E., Snook, C. F., Arnold, H. K., Sears, R. C., Hanniui, Y. A., & Ogretmen, B. (2008). Direct interaction between the inhibitor 2 and ceramideviasphingolipid-protein binding is involved in the regulation of protein phosphatase 2A activity and signaling. *The FASEB Journal*, *23*(3), 751–763.

https://doi.org/10.1096/fj.08-120550

Neviani, P., Santhanam, R., Trotta, R., Notari, M., Blaser, B. W., Liu, S., Mao, H., Chang, J. S., Galietta, A., Uttam, A., Roy, D. C., Valtieri, M., Bruner-Klisovic, R., Caligiuri, M. A., Bloomfield, C. D., Marcucci, G., & Perrotti, D. (2005). The tumor suppressor PP2A is functionally inactivated in blast crisis CML through the inhibitory activity of the BCR/ABL-regulated SET protein. *Cancer Cell*, *8*(5), 355–368. https://doi.org/10.1016/j.ccr.2005.10.015

Neviani, P., Santhanam, R., Oaks, J. J., Eiring, A. M., Notari, M., Blaser, B. W., Liu, S., Trotta, R., Muthusamy, N., Gambacorti-Passerini, C., Druker, B. J., Cortes, J., Marcucci, G., Chen, C. S., Verrills, N. M., Roy, D. C., Caligiuri, M. A., Bloomfield, C. D., Byrd, J. C., & Perrotti, D. (2007). FTY720, a new alternative for treating blast crisis chronic myelogenous leukemia and Philadelphia chromosome–positive acute lymphocytic leukemia. *Journal of Clinical Investigation*, *117*(9), 2408–2421. https://doi.org/10.1172/jci31095

Niemelä, M., Kauko, O., Sihto, H., Mpindi, J. P., Nicorici, D., Pernilä, P., Kallioniemi, O. P., Joensuu, H., Hautaniemi, S., & Westermarck, J. (2012). CIP2A signature reveals the MYC dependency of CIP2A-regulated phenotypes and its clinical association with breast cancer subtypes. *Oncogene*, *31*(39), 4266–4278. https://doi.org/10.1038/onc.2011.599

O'Connor, C. M., Perl, A., Leonard, D., Sangodkar, J., & Narla, G. (2018). Therapeutic targeting of PP2A. *The International Journal of Biochemistry & Cell Biology*, *96*, 182–193. https://doi.org/10.1016/j.biocel.2017.10.008

O'Hare, T., Deininger, M. W., Eide, C. A., Clackson, T., & Druker, B. J. (2010). Targeting the BCR-ABL Signaling Pathway in Therapy-Resistant Philadelphia Chromosome-Positive Leukemia. *Clinical Cancer Research*, *17*(2), 212–221. https://doi.org/10.1158/1078-0432.ccr-09-3314

Orsulic, S., Huber, O., Aberle, H., Arnold, S., & Kemler, R. (1999). E-cadherin binding prevents beta-catenin nuclear localization and beta-catenin/LEF-1-mediated transactivation. *Journal Of Cell Science*, *112*(8), 1237-1245. https://doi.org/10.1242/jcs.112.8.1237

Petritsch, C., Beug, H., Balmain, A., & Oft, M. (2000). TGF-β inhibits p70 S6 kinase via protein phosphatase 2A to induce G1 arrest. *Genes & Development*, *14*(24), 3093–3101. https://doi.org/10.1101/gad.854200

Petroulakis, E., Mamane, Y., le Bacquer, O., Shahbazian, D., & Sonenberg, N. (2005). mTOR signaling: implications for cancer and anticancer therapy. *British Journal of Cancer*, *94*(2), 195–199. https://doi.org/10.1038/sj.bjc.6602902

Peyssonnaux, C., & Eychène, A. (2001). The Raf/MEK/ERK pathway: new concepts of activation. *Biology of the Cell*, *93*(1–2), 53–62. https://doi.org/10.1016/s0248-4900(01)01125-x

Polakis, P. (2012). Wnt Signaling in Cancer. *Cold Spring Harbor Perspectives In Biology*, *4*(5), a008052-a008052. https://doi.org/10.1101/cshperspect.a008052

Puustinen, P., Junttila, M. R., Vanhatupa, S., Sablina, A. A., Hector, M. E., Teittinen, K., Raheem, O., Ketola, K., Lin, S., Kast, J., Haapasalo, H., Hahn, W. C., & Westermarck, J. (2009). PME-1 Protects Extracellular Signal-Regulated Kinase Pathway Activity from Protein Phosphatase 2A–Mediated Inactivation in Human Malignant Glioma. *Cancer Research*, *69*(7), 2870–2877. https://doi.org/10.1158/0008-5472.can-08-2760

Nien, W., Dauphinee, S., Moffat, L., & Too, C. (2007). Overexpression of the mTOR alpha4 phosphoprotein activates protein phosphatase 2A and increases Stat1α binding to PIAS1. *Molecular And Cellular Endocrinology*, *263*(1-2), 10-17. https://doi.org/10.1016/j.mce.2006.08.015

Pettersson, F., Yau, C., Dobocan, M., Culjkovic-Kraljacic, B., Retrouvay, H., & Puckett, R. et al. (2011). Ribavirin Treatment Effects on Breast Cancers Overexpressing eIF4E, a Biomarker with Prognostic Specificity for Luminal B-Type Breast Cancer. *Clinical Cancer Research*, *17*(9), 2874-2884. https://doi.org/10.1158/1078-0432.ccr-10-2334

Qi, Z., Yang, W., Liu, Y., Cui, T., Gao, H., Duan, C., Lu, L., Zhao, C., Zhao, H., & Yang, H. (2011). Loss of PINK1 function decreases PP2A activity and promotes autophagy in dopaminergic cells and a murine model. *Neurochemistry International*, *59*(5), 572–581. https://doi.org/10.1016/j.neuint.2011.03.023

Rennoll, S. (2015). Regulation of MYC gene expression by aberrant Wnt/β-catenin signaling in colorectal cancer. *World Journal of Biological Chemistry*, *6*(4), 290. https://doi.org/10.4331/wjbc.v6.i4.290

Ruediger, R., Hentz, M., Fait, J., Mumby, M., & Walter, G. (1994). Molecular model of the A subunit of protein phosphatase 2A: interaction with other subunits and tumor antigens. *Journal of Virology*, *68*(1), 123–129. https://doi.org/10.1128/jvi.68.1.123-129.1994

Ruediger, R., Ruiz, J., & Walter, G. (2011). Human Cancer-Associated Mutations in the Aα Subunit of Protein Phosphatase 2A Increase Lung Cancer Incidence in Aα Knock-In and Knockout Mice. *Molecular and Cellular Biology*, *31*(18), 3832–3844. https://doi.org/10.1128/mcb.05744-11

Ruvolo, P. P., Ruvolo, V. R., Jacamo, R., Burks, J. K., Zeng, Z., Duvvuri, S. R., Zhou, L., Qiu, Y., Coombes, K. R., Zhang, N., Yoo, S. Y., Pan, R., Hail, N., Konopleva, M., Calin, G., Kornblau, S. M., & Andreeff, M. (2014). The protein phosphatase 2A regulatory subunit B55α is a modulator of signaling and microRNA expression in acute myeloid leukemia cells. *Biochimica et Biophysica Acta (BBA) - Molecular Cell Research*, *1843*(9), 1969–1977. https://doi.org/10.1016/j.bbamcr.2014.05.006

Sablina, A. A., Hector, M., Colpaert, N., & Hahn, W. C. (2010). Identification of PP2A Complexes and Pathways Involved in Cell Transformation. *Cancer Research*, *70*(24), 10474–10484. https://doi.org/10.1158/0008-5472.can-10-2855

Sears, R., Nuckolls, F., Haura, E., Taya, Y., Tamai, K., & Nevins, J. (2000). Multiple Ras-dependent phosphorylation pathways regulate Myc protein stability. *Genes &Amp;*

Development, *14*(19), 2501-2514. https://doi.org/10.1101/gad.836800

Sefidbakht S, Saeedipour H, Saffar H, Mirzaian E. (2021). Determination of β-catenin Expression in Breast Cancer and Its Relationship with Clinicopathologic Parameters. Asian Pac J Cancer Prev. 2021 Nov 1;22(11):3493-3498. doi: 10.31557/APJCP.2021.22.11.3493. PMID: 34837904; PMCID: PMC9068189.

Sents, W., Ivanova, E., Lambrecht, C., Haesen, D., & Janssens, V. (2012). The biogenesis of active protein phosphatase 2A holoenzymes: a tightly regulated process creating phosphatase specificity. *FEBS Journal*, *280*(2), 644–661. https://doi.org/10.1111/j.1742-4658.2012.08579.x

Seshacharyulu, P., Pandey, P., Datta, K., & Batra, S. K. (2013). Phosphatase: PP2A structural importance, regulation and its aberrant expression in cancer. *Cancer Letters*, *335*(1), 9–18. https://doi.org/10.1016/j.canlet.2013.02.036

Shin S., Dimitri C.A., Yoon S.O., Dowdle W., Blenis J. (2010). ERK2 but not ERK1 induces epithelial-to-mesenchymal transformation via DEF motif-dependent signaling events. Mol Cell. 2010 Apr 9;38(1):114-27. doi: 10.1016/j.molcel.2010.02.020. PMID: 20385094; PMCID: PMC2854677.

Silverstein, A. M., Barrow, C. A., Davis, A. J., & Mumby, M. C. (2002). Actions of PP2A on the MAP kinase pathway and apoptosis are mediated by distinct regulatory subunits. *Proceedings of the National Academy of Sciences*, *99*(7), 4221–4226. https://doi.org/10.1073/pnas.072071699

Slupe, A. M., Merrill, R. A., & Strack, S. (2011). Determinants for Substrate Specificity of Protein Phosphatase 2A. *Enzyme Research*, *2011*, 1–8. https://doi.org/10.4061/2011/398751

Sontag, J. M., Nunbhakdi-Craig, V., Mitterhuber, M., Ogris, E., & Sontag, E. (2010). Regulation of protein phosphatase 2A methylation by LCMT1 and PME-1 plays a critical role in differentiation of neuroblastoma cells. *Journal of Neurochemistry*, *115*(6), 1455–1465. https://doi.org/10.1111/j.1471-4159.2010.07049.x

Stål, O., Pérez-Tenorio, G., Åkerberg, L., Olsson, B., Nordenskjöld, B., Skoog, L., & Rutqvist, L. E. (2003). Akt kinases in breast cancer and the results of adjuvant therapy. *Breast Cancer Research*, *5*(2). https://doi.org/10.1186/bcr569

Stanevich, V., Jiang, L., Satyshur, K. A., Li, Y., Jeffrey, P. D., Li, Z., Menden, P., Semmelhack, M. F., & Xing, Y. (2011). The Structural Basis for Tight Control of PP2A Methylation and Function by LCMT-1. *Molecular Cell*, *41*(3), 331–342. https://doi.org/10.1016/j.molcel.2010.12.030

Stebbing, J., Lit, L. C., Zhang, H., Darrington, R. S., Melaiu, O., Rudraraju, B., & Giamas, G. (2013). The regulatory roles of phosphatases in cancer. *Oncogene*, *33*(8), 939–953. https://doi.org/10.1038/onc.2013.80

Switzer, C. H., Ridnour, L. A., Cheng, R. Y. S., Sparatore, A., del Soldato, P., Moody, T. W., Vitek, M. P., Roberts, D. D., & Wink, D. A. (2009). Dithiolethione compounds inhibit Akt

signaling in human breast and lung cancer cells by increasing PP2A activity. *Oncogene*, *28*(43), 3837–3846. https://doi.org/10.1038/onc.2009.244

Switzer, C. H., Cheng, R. Y. S., Vitek, T. M., Christensen, D. J., Wink, D. A., & Vitek, M. P. (2011). Targeting SET/I2PP2A oncoprotein functions as a multi-pathway strategy for cancer therapy. *Oncogene*, *30*(22), 2504–2513. https://doi.org/10.1038/onc.2010.622

Takagi, Y. (2000). Alterations of the PPP2R1B gene located at 11q23 in human colorectal cancers. *Gut*, *47*(2), 268–271. https://doi.org/10.1136/gut.47.2.268

Takayama, T., Shiozaki, H., Shibamoto, S., Oka, H., Kimura, Y., Tamura, S., Inoue, M., Monden, T., Ito, F., Monden, M. (1996). Beta-catenin expression in human cancers. *American Journal of Pathology*, *148*(1):39-46. PMID: 8546224; PMCID: PMC1861624.

Teng, H. W., Yang, S. H., Lin, J. K., Chen, W. S., Lin, T. C., Jiang, J. K., Yen, C. C., Li, A. F. Y., Chen, P. C. H., Lan, Y. T., Lin, C. C., Hsu, Y. N., Wang, H. W., & Chen, K. F. (2012). CIP2A Is a Predictor of Poor Prognosis in Colon Cancer. *Journal of Gastrointestinal Surgery*, *16*(5), 1037–1047. https://doi.org/10.1007/s11605-012-1828-3

Tonks, N. K. (2006). Protein tyrosine phosphatases: from genes, to function, to disease. *Nature Reviews Molecular Cell Biology*, *7*(11), 833–846. https://doi.org/10.1038/nrm2039

Tsiakou, A., Zagouri, F., Zografos, E., Samelis, G., Gazouli, M., & Kalapanida, D. et al. (2019). Prognostic significance of miR-34 rs4938723 T > C polymorphism in triple negative breast cancer patients. *Clinical Biochemistry*, *68*, 9-14. https://doi.org/10.1016/j.clinbiochem.2019.03.009

The Cancer Genome Atlas (TCGA) Society for Translational Oncology Fellows Forum, Kim Summaries (2017)

Vaarala, M. H., Väisänen, M. R., & Ristimäki, A. (2010). CIP2A expression is increased in prostate cancer. *Journal of Experimental & Clinical Cancer Research*, *29*(1). https://doi.org/10.1186/1756-9966-29-136

Vural, H., Kurar, E., Avcı, E., Eroğlu, C., Çelen, E., Çınar, L., ŞIrin, S., & Elagöz, A. (2018). KRAS Mutations: A Possible Biomarker for Advanced Prostate Cancer. *Cancer Science & Research*, *1*(4). https://doi.org/10.33425/2639-8478.1019

Wang, J., Li, W., Li, L., Yu, X., Jia, J., & Chen, C. (2011). CIP2A is over-expressed in acute myeloid leukaemia and associated with HL60 cells proliferation and differentiation. *International Journal of Laboratory Hematology*, *33*(3), 290–298. https://doi.org/10.1111/j.1751-553x.2010.01288.x

Wang, S. S., Esplin, E. D., Li, J. L., Huang, L., Gazdar, A., Minna, J., & Evans, G. A. (1998). Alterations of the PPP2R1B Gene in Human Lung and Colon Cancer. *Science*, *282*(5387), 284–287. https://doi.org/10.1126/science.282.5387.284

Watt, L., Panicker, N., Mannan, A., Copeland, B., Kahl, R., & Dun, M. et al. (2017). Functional importance of PP2A regulatory subunit loss in breast cancer. *Breast Cancer Research And Treatment*, *166*(1), 117-131. https://doi.org/10.1007/s10549-017-4403-5

Westphal, R., Coffee, R., Marotta, A., Pelech, S., & Wadzinski, B. (1999). Identification of Kinase-Phosphatase Signaling Modules Composed of p70 S6 Kinase-Protein Phosphatase 2A (PP2A) and p21-activated Kinase-PP2A. *Journal Of Biological Chemistry*, *274*(2), 687-692. https://doi.org/10.1074/jbc.274.2.687

Xiang, T., Ohashi, A., Huang, Y., Pandita, T. K., Ludwig, T., Powell, S. N., & Yang, Q. (2008). Negative Regulation of AKT Activation by BRCA1. *Cancer Research*, *68*(24), 10040–10044. https://doi.org/10.1158/0008-5472.can-08-3009

Xiang, T., Jia, Y., Sherris, D., Li, S., Wang, H., Lu, D., & Yang, Q. (2011). Targeting the Akt/mTOR pathway in Brca1-deficient cancers. *Oncogene*, *30*(21), 2443–2450. https://doi.org/10.1038/onc.2010.603

Xu, J., Lu, Y., Liu, Q., Xia, A., Zhao, J., & Xu, X. et al. (2020). Long noncoding RNA GMAN promotes hepatocellular carcinoma progression by interacting with eIF4B. *Cancer Letters*, *473*, 1-12. https://doi.org/10.1016/j.canlet.2019.12.032

Xu, Y., Xing, Y., Chen, Y., Chao, Y., Lin, Z., Fan, E., Yu, J. W., Strack, S., Jeffrey, P. D., & Shi, Y. (2006). Structure of the Protein Phosphatase 2A Holoenzyme. *Cell*, *127*(6), 1239–1251. https://doi.org/10.1016/j.cell.2006.11.033

Zhang, Q., & Claret, F. X. (2012). Phosphatases: The New Brakes for Cancer Development? *Enzyme Research*, *2012*, 1–11. https://doi.org/10.1155/2012/659649

Zhang, X., Farrell, A., Daniel, C., Arnold, H., Scanlan, C., & Laraway, B. et al. (2011). Mechanistic insight into Myc stabilization in breast cancer involving aberrant Axin1 expression. *Proceedings Of The National Academy Of Sciences*, *109*(8), 2790-2795. https://doi.org/10.1073/pnas.1100764108

Zhang, W., Yang, J., Liu, Y., Chen, X., Yu, T., Jia, J., & Liu, C. (2009). PR55α, a Regulatory Subunit of PP2A, Specifically Regulates PP2A-mediated β-Catenin Dephosphorylation. *Journal of Biological Chemistry*, *284*(34), 22649–22656. https://doi.org/10.1074/jbc.m109.013698

Appendix A:

Raw Data

The Immunocytochemistry Technique (Section 2.2.4)

A: MCF-7:
vehicle control (lack of antibody)

B: MCF-7:
exposed to anti-IGBP1 antibody

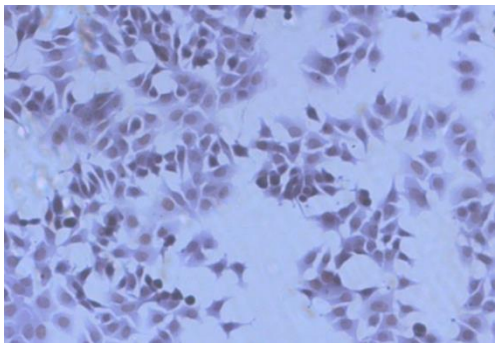

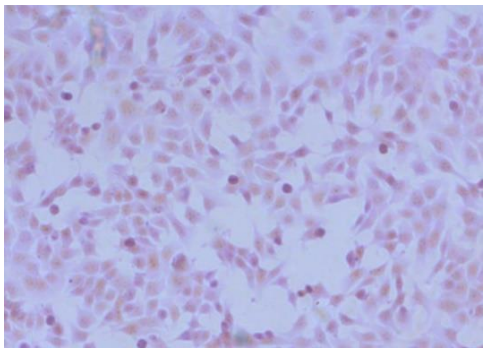

Photographic results of the immunocytochemistry technique carried out on the MCF-7 cell line. A panel of breast cancer cell lines, located on cover slips and fixed in paraformaldehyde were subjected to the immunocytochemistry (ICC) technique, using the protocol documented by the CSA II Biotin-Free Tyramide Signal Amplification System. The cell lines were subjected to anti-CIP2A, SET and IGBP1 antibodies in the final step of the procedure. Photographic images of the results obtained were taken and inspected. The presence and location of the protein of interest is indicated by a brown stain. Photograph A in Figure 3.2 shows the vehicle control for the MCF-7 cell line, where the cells lacked exposure to the antibody of interest, while photograph B shows the same cell line exposed to anti- IGBP1 antibody. A brown stain in the cytoplasm shows that the cell contains the IGBP1 protein. Similar photographs were inspected for all three inhibitors CIP2A, SET and IGBP1, and for the nine selected cell lines (Figure 3.1).

Double Digestion of pIRES2 and pDBLeu vectors (Section 2.3.5)

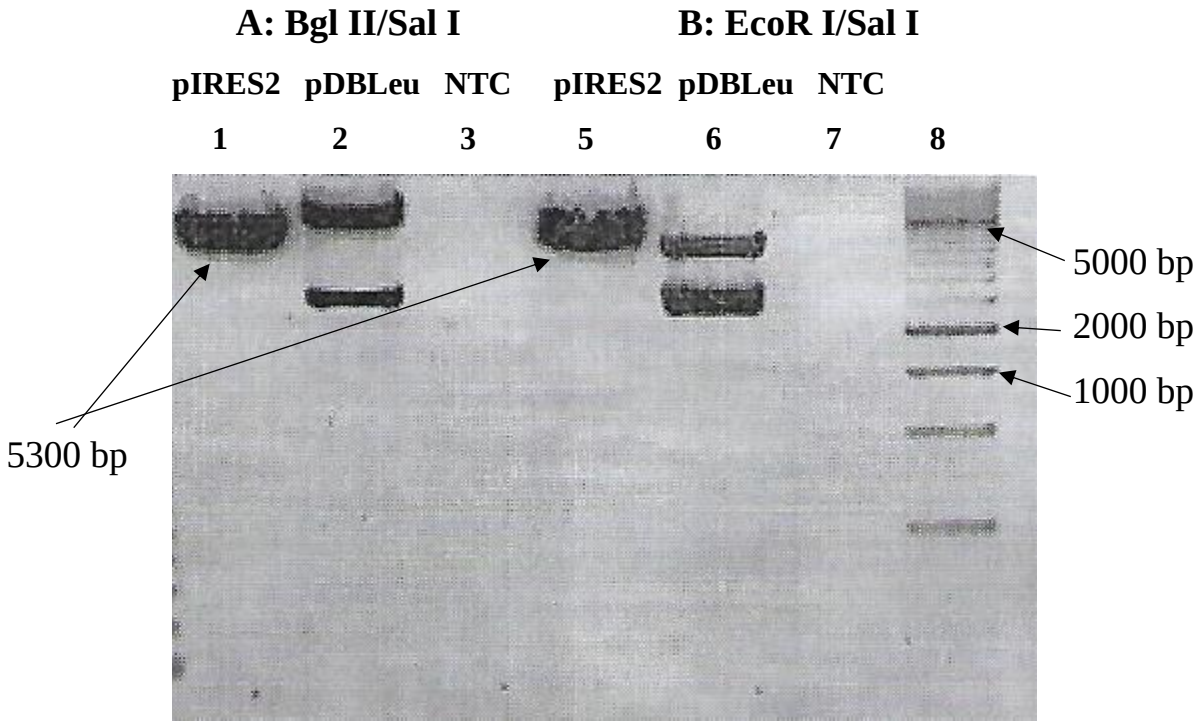

Double Digestion of pIRES2-AcGFP1 using restriction enzymes Bgl II/Sal I and EcoRI/Sal I. The figure shows a photograph of the gel electrophoresis experiment, following double digestion of the vector pIRES2-AcGFP1 with the selected enzymes; Bgl II/Sal I in **A** and EcoR I/Sal I in **B**, as described in Section 2.3.2. Each lane contains 2 µl of reaction mixture. In both cases, the vector is linearised, as the enzymes cut at the multiple cloning site (MCS), producing a fragment size about 5300 bp. This is shown in lanes 1 and 5. The pDBLeu digestion, using the same enzyme pairs, shown in lanes 2 and 6, produces two fragments and serves as a positive control. The NTC shown in lanes 3 and 7 serves as a blank and does not show any bands. Lane 8 is the DNA molecular weight marker (ProMega-Marker® Lambda Ladder).

Bradford Protein Assay (Section 2.5.3)

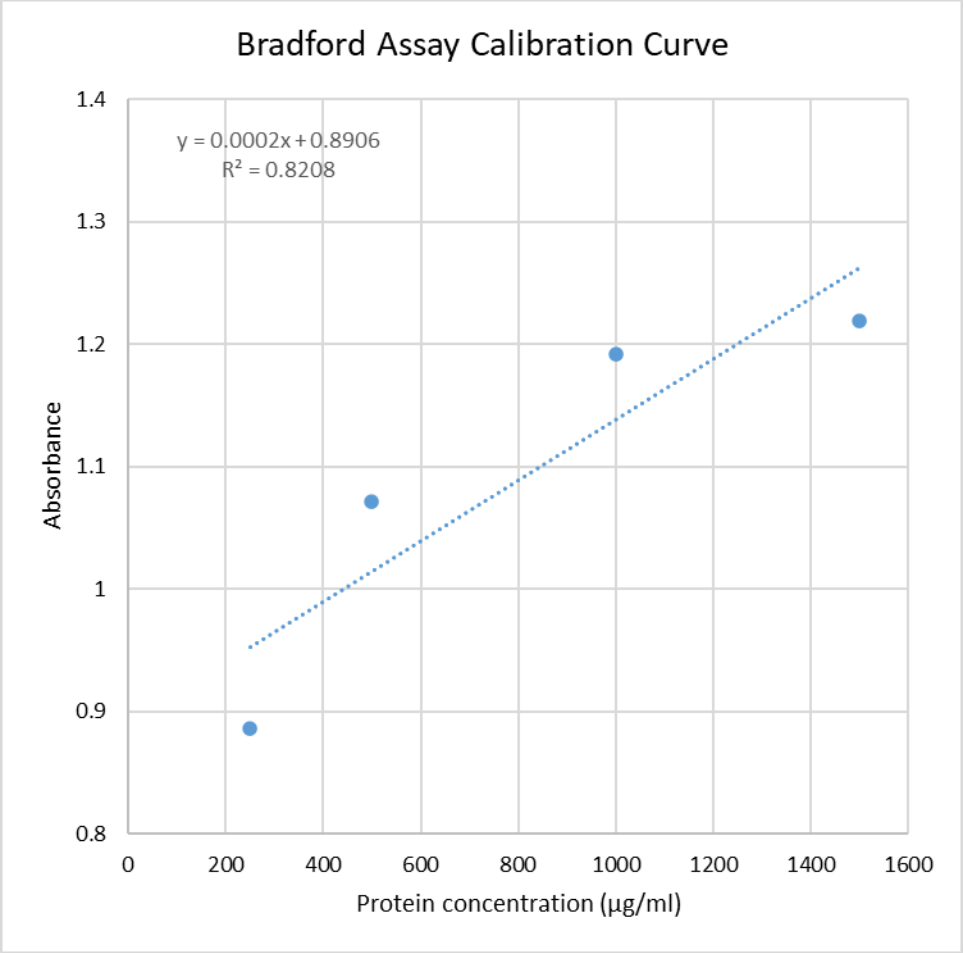

Bradford assay calibration curve for protein quantification. The figure shows absorbance (measured at 598 nm) on the y-axis against protein concentration (µg/ml) on the x-axis and is generated by the spectrophotometer instrument. This calibration curve was prepared using a series of standards. Only the range of protein concentrations used in the experiment is shown, as well as the linear trendline (shown as a dotted line). The graph was then used to determine the concentration of the protein lysates, by extrapolation. This is a necessary step prior to Western Blotting, required to quantify the amount of protein present in the lysate (Concentrations obtained were about 4000 µg/ml, and were diluted accordingly).

Electropherograms of Clones (Section 2.3.6)

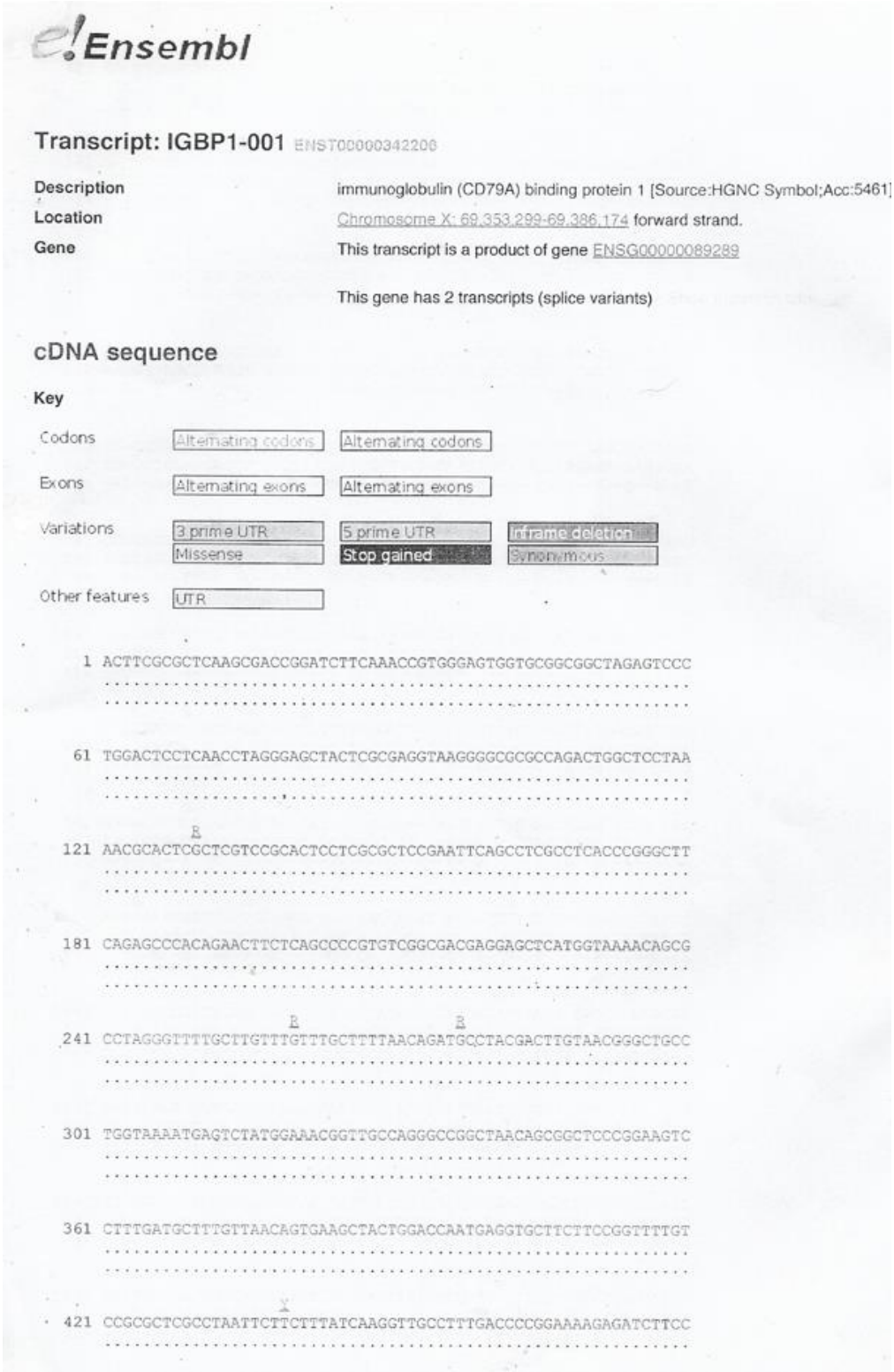

Ensembl

Transcript: IGBP1-001 ENST00000342200

Description	immunoglobulin (CD79A) binding protein 1 [Source:HGNC Symbol;Acc:5461]
Location	Chromosome X: 69,353,299-69,386,174 forward strand.
Gene	This transcript is a product of gene ENSG00000089289
	This gene has 2 transcripts (splice variants)

cDNA sequence

Key

Codons: Alternating codons | Alternating codons

Exons: Alternating exons | Alternating exons

Variations: 3 prime UTR | 5 prime UTR | Inframe deletion | Missense | Stop gained | Synonymous

Other features: UTR

```
   1 ACTTCGCGCTCAAGCGACCGGATCTTCAAACCGTGGGAGTGGTGCGGCGGCTAGAGTCCC
     ............................................................
     ............................................................

  61 TGGACTCCTCAACCTAGGGAGCTACTCGCGAGGTAAGGGGCGCGCCAGACTGGCTCCTAA
     ............................................................
     ............................................................

 121 AACGCACTCGCTCGTCCGCACTCCTCGCGCTCCGAATTCAGCCTCGCCTCACCCGGGCTT
     ............................................................
     ............................................................

 181 CAGAGCCCACAGAACTTCTCAGCCCCGTGTCGGCGACGAGGAGCTCATGGTAAAACAGCG
     ............................................................
     ............................................................

 241 CCTAGGGTTTTGCTTGTTTGTTTGCTTTTAACAGATGCCTACGACTTGTAACGGGCTGCC
     ............................................................
     ............................................................

 301 TGGTAAAATGAGTCTATGGAAACGGTTGCCAGGGCCGGCTAACAGCGGCTCCCGGAAGTC
     ............................................................
     ............................................................

 361 CTTTGATGCTTTGTTAACAGTGAAGCTACTGGACCAATGAGGTGCTTCTTCCGGTTTTGT
     ............................................................
     ............................................................

 421 CCGCGCTCGCCTAATTCTTCTTTATCAAGGTTGCCTTTGACCCCGGAAAAGAGATCTTCC
     ............................................................
```

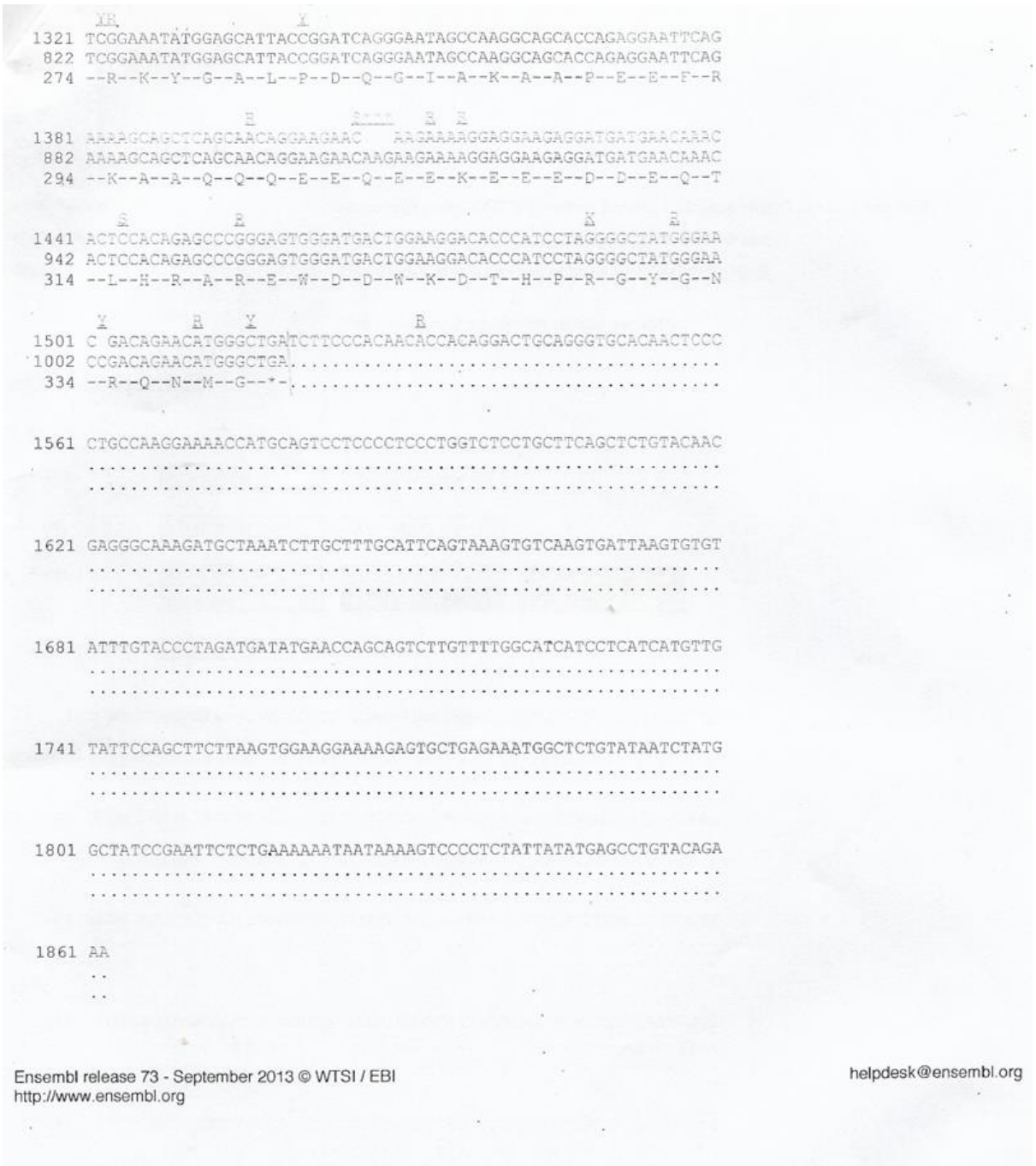

Ensembl

Transcript: SET-001 ENST00000372692

Description	SET nuclear oncogene [Source:HGNC Symbol;Acc:10760]
Location	Chromosome 9: 131,445,934-131,458,679 forward strand.
Gene	This transcript is a product of gene ENSG00000119335
	This gene has 11 transcripts (splice variants)

cDNA sequence

Key

Codons	Alternating codons	Alternating codons	
Exons	Alternating exons	Alternating exons	
Variations	3 prime UTR	5 prime UTR	Frameshift
	Inframe deletion	Missense	Stop gained
	Synonymous		
Other features	UTR		

```
  1 GTGCCCCTGCAGAGCGAGGCAGAGAGCAACTAAAAGAAATTTCTCCTGATTGGAGGGTGG
    ............................................................
    ............................................................

 61 GTGGGATGAGGCTGGGGGAGGGGGCCGGGGTGTGTGTCCCACTGTCATGTAAATATCCCT
    ............................................................
    ............................................................

121 TCCAGGCAGGGCGGCTCCAGTGCAGATTTAAGCCGCTGGCACCTGGGGCAGTCTCAGTGT
    ............................................................
    ............................................................

      Y
181 TCAGCCTGCTTCCGGACGGGCGAGGAGACTCGTGGTCTGGTTCTGGGACTTCCCTAACAG
    ............................................................
    ............................................................

                                      R Y
241 CATGGCCCCTAAACGCCAGTCTCCACTCCCGCCTCAAAAGAAGAAACCAAGACCACCTCC
    .ATGGCCCCTAAACGCCAGTCTCCACTCCCGCCTCAAAAGAAGAAACCAAGACCACCTCC
    .M--A--P--K--R--Q--S--P--L--P--P--Q--K--K--K--P--R--P--P--P

       YK
301 TGCTCTGGGACCGGAGGAGACATCGGCCTCTGCAGGCTTGCCGAAGAAGGGAGAAAAAGA
 60 TGCTCTGGGACCGGAGGAGACATCGGCCTCTGCAGGCTTGCCGAAGAAGGGAGAAAAAGA
 20 --A--L--G--P--E--E--T--S--A--S--A--G--L--P--K--K--G--E--K--E

361 ACAGCAAGAAGCGATTGAACACATTGATGAAGTACAAAATGAAATAGACAGACTTAATGA
120 ACAGCAAGAAGCGATTGAACACATTGATGAAGTACAAAATGAAATAGACAGACTTAATGA
 40 --Q--Q--E--A--I--E--H--I--D--E--V--Q--N--E--I--D--R--L--N--E

                                                      Y       R
421 ACAAGCCAGTGAGGAGATTTTGAAAGTAGAACAGAAATATAACAAACTCCGCCAACCATT
```

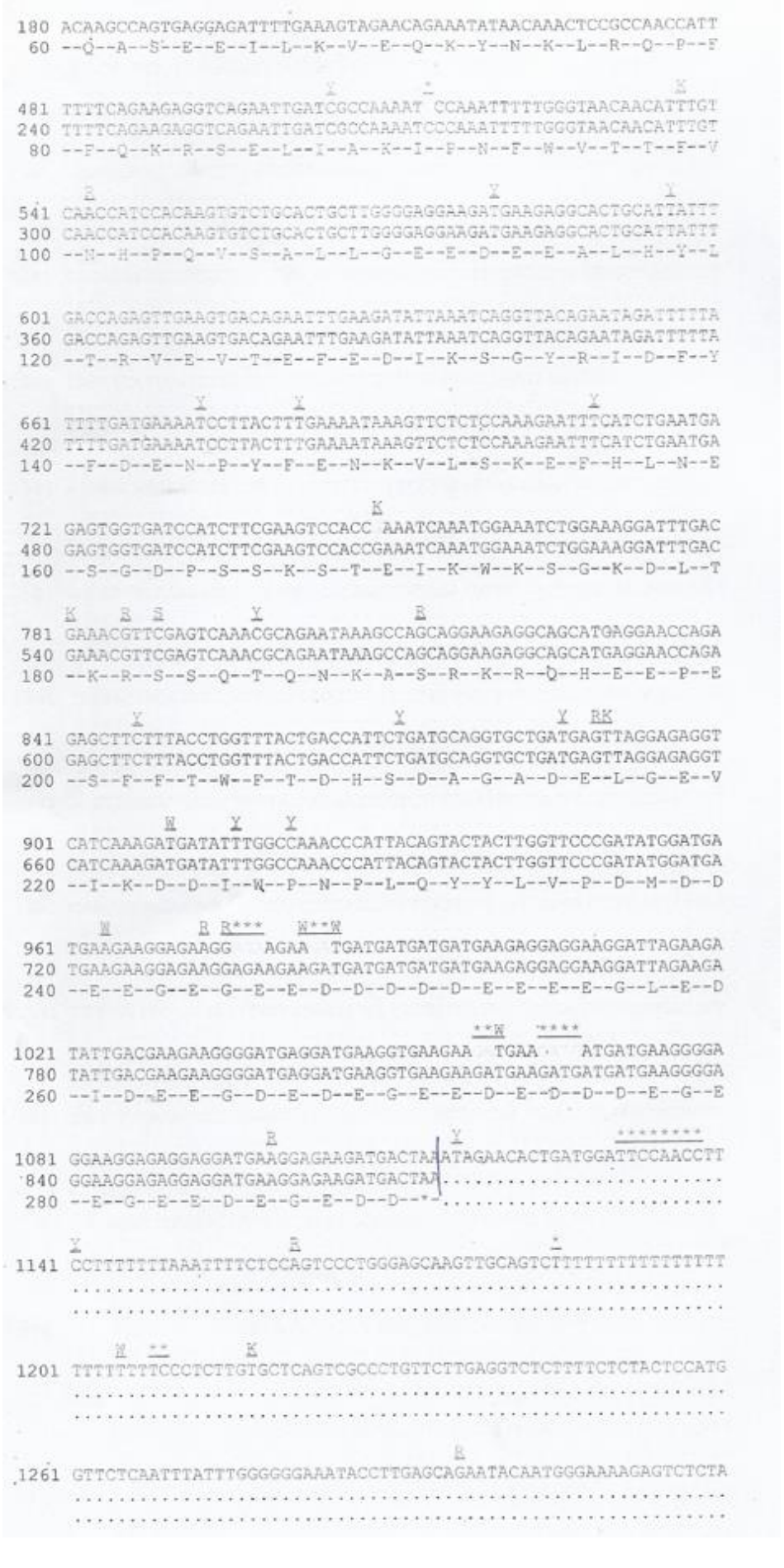

e!Ensembl

Transcript: KIAA1524-001 ENST00000295746 (CIP2A)

Description	KIAA1524 [Source:HGNC Symbol;Acc:29302]
Location	Chromosome 3: 108,268,716-108,308,299 reverse strand.
Gene	This transcript is a product of gene ENSG00000163507
	This gene has 6 transcripts (splice variants)

cDNA sequence

Key

Codons	Alternating codons	Alternating codons	
Exons	Alternating exons	Alternating exons	
Variations	3 prime UTR	5 prime UTR	Frameshift
	Initiator codon	Missense	Splice region
	Stop gained	Synonymous	
Other features	UTR		

```
                                        Y RR  Y Y           Y
    1 AAAAAAAGCGCGGCGAAAGCTAAAGGCCGGCGCACGCTGGGCGGTGGTGGTCCCTAAGCC
      ............................................................
      ............................................................

      S               W         Y                       Y     ****
   61 GGGCCGCGGCCGGTGCAATGGACTCCACTGCCTGCTTGAAGTCCTTGCTCCTGAC    A
      ..............  ATGGACTCCACTGCCTGCTTGAAGTCCTTGCTCCTGACTGTCA
      ..............  -M--D--S--T--A--C--L--K--S--L--L--L--T--V--

                 Y              S                       Y
  121 GTCAGTACAAAGCCGTGAAGTCAGAGGCGAACGCCACTCAGCTTTTGCGGCACTTGGAGG
   44 GTCAGTACAAAGCCGTGAAGTCAGAGGCGAACGCCACTCAGCTTTTGCGGCACTTGGAGG
   15 S--Q--Y--K--A--V--K--S--E--A--N--A--T--Q--L--L--R--H--L--E--

            S                       W Y
  181 TAATTTCTGGACAGAAACTCACACGACTATTTACATCAAATCAGATATTAACAAGTGAAT
  104 TAATTTCTGGACAGAAACTCACACGACTATTTACATCAAATCAGATATTAACAAGTGAAT
   35 V--I--S--G--Q--K--L--T--R--L--F--T--S--N--Q--I--L--T--S--E--

            K                           M
  241 GCTTGAGTTGCCTTGTAGAGCTACTTGAAGACCCCAACATAAGTGCTTCACTGATCTTAA
  164 GCTTGAGTTGCCTTGTAGAGCTACTTGAAGACCCCAACATAAGTGCTTCACTGATCTTAA
   55 C--L--S--C--L--V--E--L--L--E--D--P--N--I--S--A--S--L--I--L--

            R               R           Y               Y
  301 GTATTATCGGTTTGCTGTCTCAACTAGCAGTAGACATTGAAACCAGAGATTGTCTTCAGA
  224 GTATTATCGGTTTGCTGTCTCAACTAGCAGTAGACATTGAAACCAGAGATTGTCTTCAGA
   75 S--I--I--G--L--L--S--Q--L--A--V--D--I--E--T--R--D--C--L--Q--

            W       R                           S
  361 ATACATATAATCTGAATAGTGTGCTGGCGGGAGTGGTTTGTCGGAGCAGCCACACTGATT
  284 ATACATATAATCTGAATAGTGTGCTGGCGGGAGTGGTTTGTCGGAGCAGCCACACTGATT
   95 N--T--Y--N--L--N--S--V--L--A--G--V--V--C--R--S--S--H--T--D--

                       M                   R
  421 CGGTGTTTTTGCAGTG ATTCAACTTCTACAGAAGTTAACATATAATGTCAAAATTTTCT
```

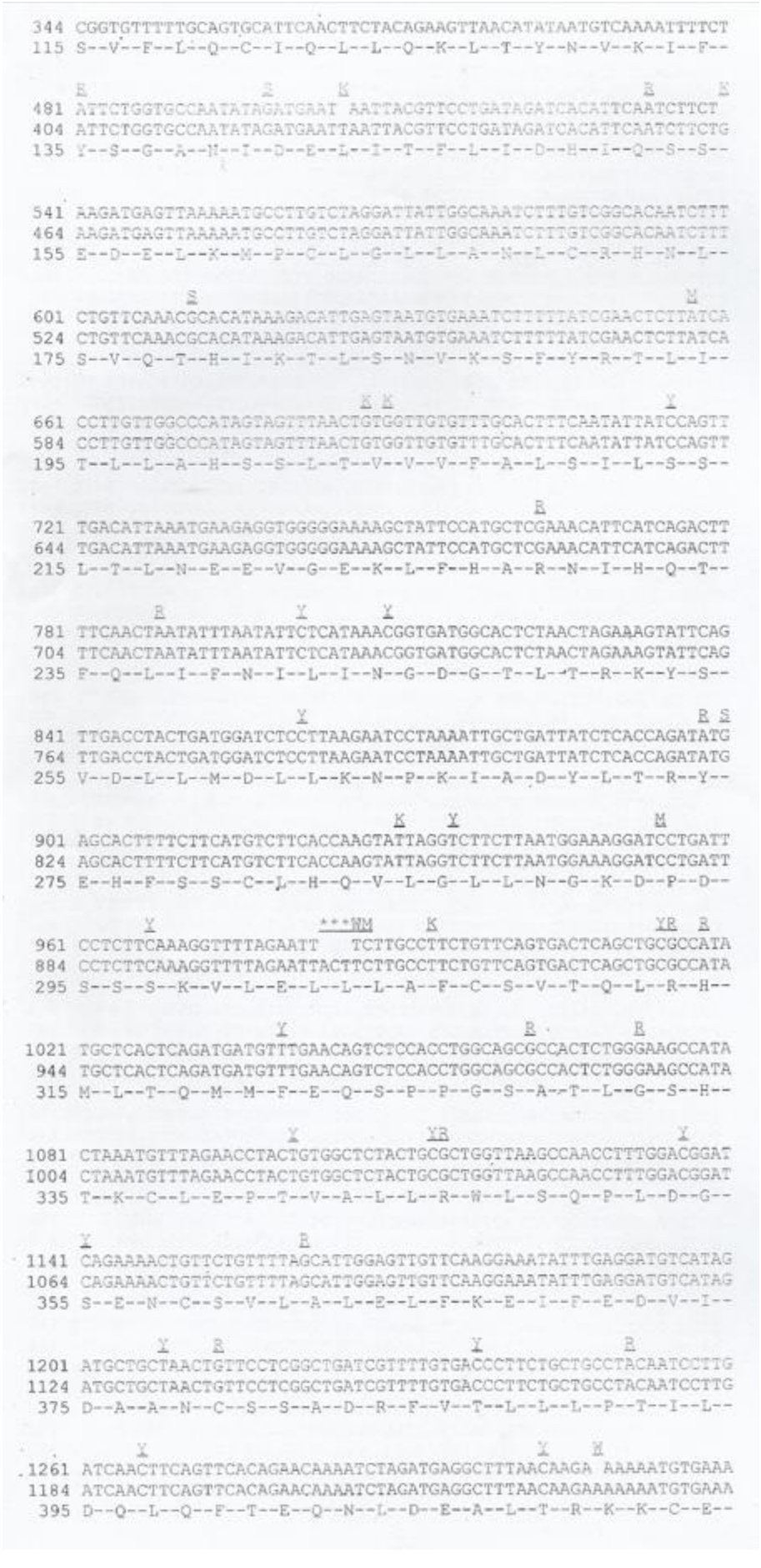

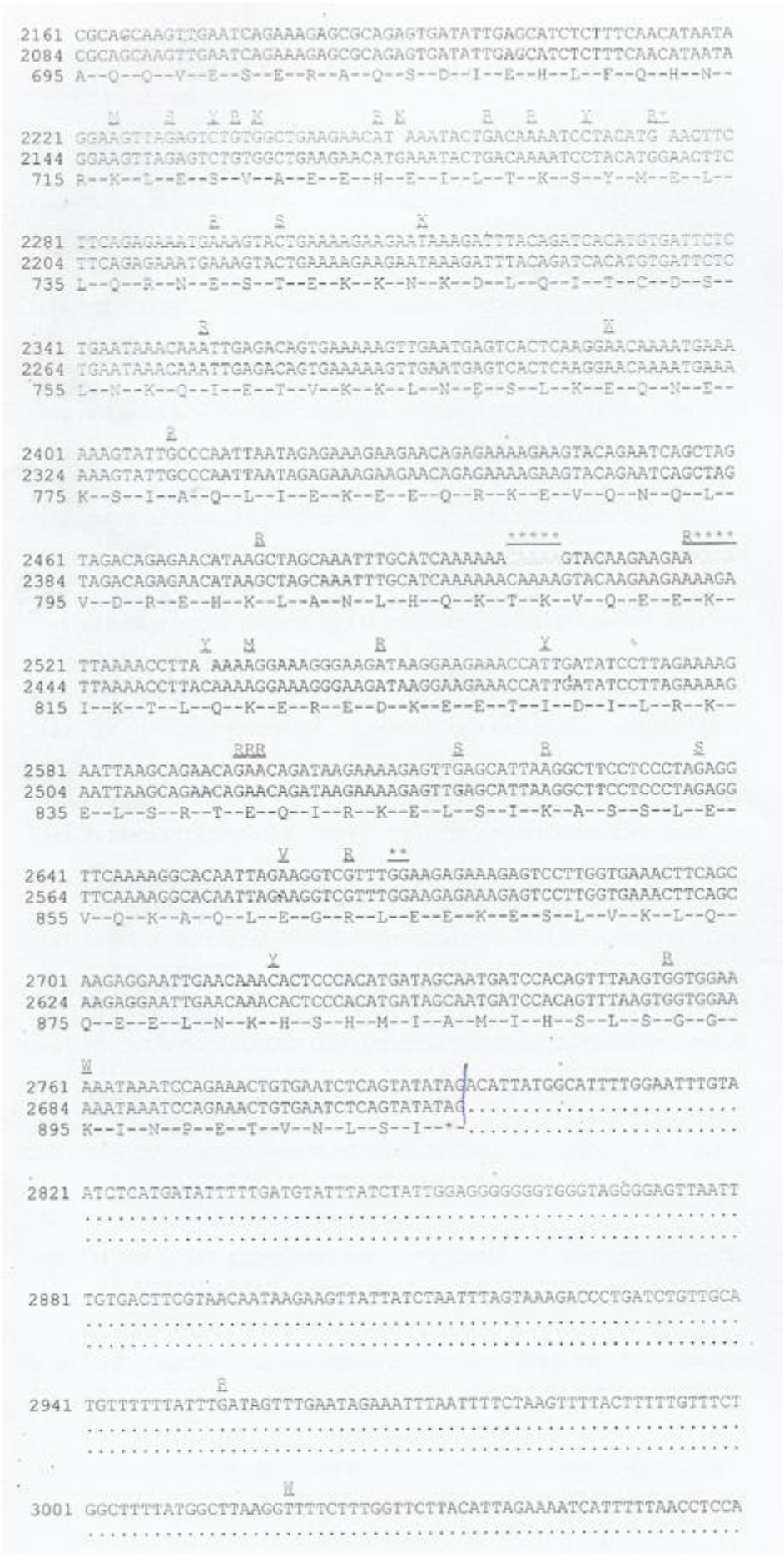

Paired t-test (Section 2.7.6)

		Mean	Std. Deviation	Std. Error Mean	Sig. (2-tailed)
Pair 1	plRESMCF7 - MCF7cip2a	-19.13333	3.17228	1.83151	.009
Pair 2	plRESHCC - HCCcip2a	-9.73333	.83267	.48074	.002
Pair 3	plRES453 - cip2a453	-26.41667	3.90011	2.25173	.007
Pair 4	MCF7plRESs - MCF7SET	-40.47000	1.16820	.67446	.000
Pair 5	HCCplRESs - HCCSET	2.68000	.58924	.34020	.016
Pair 6	plRES453s - SET453	-20.28667	1.55773	.89936	.002
Pair 7	MCF7plRESi - MCF7lgbp1	-13.29000	1.55155	.89579	.005
Pair 8	HCCplRESi - HCClgbp1	-8.62333	.54372	.31392	.001
Pair 9	plRES453i - IGBP1453	-6.97667	1.00082	.57782	.007
Pair 10	plRESHCC - HCCplRESs	-47.92333	6.10013	3.52191	.005
Pair 11	plRESHCC - HCCplRESi	11.08333	5.10008	2.94453	.064
Pair 12	HCCplRESs - HCCplRESi	59.00667	1.00007	.57739	.000
Pair 13	MCF7cip2a - MCF7cip2aRAPA	15.10667	2.07464	1.19779	.006
Pair 14	HCCcip2a - HCCcip2aRAPA	3.38333	5.04389	2.91209	.365
Pair 15	cip2a453 - Cip2a453RAPA	16.00667	5.00001	2.88676	.031
Pair 16	MCF7SET - MCF7setRAPA	16.89667	1.82812	1.05547	.004
Pair 17	HCCSET - HCCsetRAPA	14.15667	1.67285	.96582	.005
Pair 18	SET453 - SET453RAPA	15.61667	2.74234	1.58329	.010
Pair 19	MCF7lgbp1 - MCF7igbpRAPA	2.71667	1.62795	.93990	.102
Pair 20	HCClgbp1 - HCCigbpRAPA	-.48667	1.41426	.81652	.612
Pair 21	IGBP1453 - IGBP453RAPA	2.99333	1.25496	.72455	.054

Data used for Figure 3.1

CELL LINE	CIP2A CNRQ	CIP2A SEM (CNRQ)	SET CNRQ	SET SEM (CNRQ)	RPL13A CNRQ	RPL13A SEM (CNRQ)	normalization factor
MCF-7	2.14E-01	1.58E-02	1.22E+00	5.57E-02	1.32E+00	1.25E-01	6.07E-01
MDA-MB-453	7.13E-02	1.98E-02	4.63E-01	4.73E-02	9.68E-01	4.17E-02	1.16E+00
SK-BR3	5.09E-01	1.13E-02	1.78E+00	5.32E-02	1.32E+00	4.31E-02	1.42E+00
BT-474	1.80E+00	4.48E-02	5.21E+00	2.54E-01	8.15E-01	9.58E-03	1.53E+00
BT-20	1.11E+00	6.32E-02	3.15E+00	1.37E-01	1.13E+00	7.24E-02	2.76E-01
Hs578T	1.93E+00	1.90E-01	7.10E-01	5.83E-02	7.27E-01	7.93E-02	1.12E+00
MDA-MB-468	1.51E+00	3.59E-02	1.45E+00	7.80E-02	8.17E-01	3.66E-02	2.87E+00
MDA-MB-436	1.30E+01	4.19E-01	9.48E+00	2.10E-01	1.97E+00	4.36E-02	4.38E-01
HCC-1937	4.89E+00	1.07E+00	4.35E+00	6.18E-01	5.89E-01	8.31E-02	1.16E+00
MCF10-A	1.00E+00	3.36E-02	1.00E+00	8.41E-02	1.00E+00	2.43E-02	8.47E+00

Data used for Figure 3.4

CELL LINE	pIRES-GFP	CIP2A overexpression	ST error	plus rapamycin	ST error
MCF-7	4.099	22.800	1.541	8.987	1.990
HCC1937	26.127	36.534	5.687	32.355	1.243
MDA-MB-453	1.552	28.105	0.106	11.982	0.245

CELL LINE	pIRES-GFP	SET overexpression	ST error	plus rapamycin	ST error
MCF-7	9.859	49.468	1.944	33.774	0.327
HCC1937	74.067	71.302	2.500	57.761	5.933
MDA-MB-453	6.308	27.664	1.155	11.316	0.177

CELL LINE	pIRES-GFP	IGBP1 overexpression	ST error	plus rapamycin	ST error
MCF-7	2.715	16.072	0.594	13.424	0.751
HCC1937	15.054	23.927	2.411	24.376	3.359
MDA-MB-453	3.137	10.069	0.646	7.576	2.562

Data used for Tables 3.2 and 3.3

© Fridolin Treindl	Sample 1			Sample 2			Sample 3			Sample 4		
Data exported 2020-04-13/16:27	CONTROL			IGBP1			SET			CIP2A		
	Sample 1	Sample 1	Sample 1	Sample 2	Sample 2	Sample 2	Sample 3	Sample 3	Sample 3	Sample 4	Sample 4	Sample 4
	Peak 1	Peak 2	Peak 1+2	Peak 1	Peak 2	Peak 1+2	Peak 1	Peak 2	Peak 1+2	Peak 1	Peak 2	Peak 1+2
Analyte	[AFI]	[AFI]	[AFI]	[AFI]	[AFI]	[AFI]	[AFI]	[AFI]	[AFI]	[AFI]	[AFI]	[AFI]
4E-BP1 - phosphoSer65# 1202	80			233			254			219		
4E-BP1 - phosphoThr37/Thr46# 1203	295			534	560	1095	653	653	1306	455	609	1065
4E-BP1 - phosphoThr70# 2345	229	115	344	231	295	527	402	292	694	356	335	691
Bcl236# 1821												
beta-Catenin# 1783	886			8859			7967			9193		
beta-Catenin - phosphoSer552# 1862	54			347			256			466		
beta-Catenin (non-pospho Ser33/37/Thr41; active) # 2323				797			616			801		
CIP2A# 1426												
c-myc# 1717	375			32209			20456			31907		
c-myc - phosphoThr58# 2398	782			1209			1173			1146		
c-myc - phosphoThr58/Ser62# 1240				104			62			54		
CREB# 1827	50											
CREB - phosphoSer133# 1920				94			308			113		
DEPTOR/DEPDC6# 2355	310			551			727			376		
eIF4B# 2189	176											
eIF4B - phosphoSer406# 2356										52		
eIF4B - phosphoSer422# 2188	120						89					
eIF4E# 1820	7219			13350			12211			9635		
eIF4E - phosphoSer209# 1904	174			756			673			397		
GRB10# 2364												
GRB10 - phosphoSer476# 2365										87		
GSK3 beta# 1835	3491			5477			7384			7030		
GSK3 beta - phosphoSer9# 2073										128		
Mcl-1# 0702				124	222	346		567			548	
Mcl-1 - phosphoSer159/Thr163# 0698				60								
p70 S6 kinase# 1566	66	1112	1178		889		85	816	901	112	617	729
p70 S6 kinase - phosphoThr389# 1211	63											
p70 S6 kinase - phosphoThr421/Ser424# 2094												
PKC (pan) - phosphoSer660# 1218	499			309			207			346		
PKC (pan) gamma - phosphoThr514# 2378	1792	921	2714	2602	1864	4466	2135	1539	3674	2542	1103	3645
PKC alpha# 1583										69		
PKC alpha - phosphoSer657# 2340	228			278			304			288		
PKC alpha - phosphoThr497# 2341				1542			1381			1289		
PKC alpha/beta II - phosphoThr638/Thr641TK # 092				456			486			471		
PRAS40# 2081	1510			2912			3830			3058		
PRAS40 (AKT1S1) - phosphoThr246# 2487				70								
Raptor# 1167	253			693			814			447		
Raptor - phosphoSer792# 1467				153			128			55		
Rictor# 1468				207			175			99		
S6 ribosomal protein# 1836	2477			17545			13306			11567		
S6 ribosomal protein - phosphoSer235/236# 2079	9665			19102			23292			24838		
S6 ribosomal protein - phosphoSer240/Ser244BG/MP # 055	3372			6793			7828			9106		
SGK1 - phosphoSer78# 2387	348			142			65			90		
ULK1# 1649												
ULK1 - phosphoSer555# 2396												
zzms-blk												
zzrb-blk												
zzstrep	550332			1628791			1434903			1316890		
Median strep	1375896.5											
Correction factor	0.39998067	0.39998067	0.39998067	1.18380343	1.18380343	1.18380343	1.04288586	1.04288586	1.04288586	0.95711414	0.95711414	0.95711414

Data used for Figure 3.13

© Fridolin Treindl	Sample 1			Sample 2			Sample 3			Sample 4		
Data exported 2020-03-11/10:56	CONTROL			IGBP1			SET			CIP2A		
	Sample 1	Sample 1	Sample 1	Sample 2	Sample 2	Sample 2	Sample 3	Sample 3	Sample 3	Sample 4	Sample 4	Sample 4
	Peak 1	Peak 2	Peak 1+2	Peak 1	Peak 2	Peak 1+2	Peak 1	Peak 2	Peak 1+2	Peak 1	Peak 2	Peak 1+2
Analyte	[AFI]	[AFI]	[AFI]	[AFI]	[AFI]	[AFI]	[AFI]	[AFI]	[AFI]	[AFI]	[AFI]	[AFI]
4E-BP1	272	1091	1363	1091	1984	3075	779	2293	3072	1015	1269	2284
Actin beta	134622			213861			247582			239385		
Aurora A (AIK)				55			52					
Aurora A (AIK) - phosphoThr288												
Cytokeratin Pan (most acidic, all basic)	11456			177363			160487			184228		
Erk1/2 (MAPK p44/42)	8598	8625	17223	2805	13655	16460	2462	13238	15701	2094	12636	14730
ERK1/2 (MAPK) - phosphoThr202/Tyr204												
GAPDH	191557			250694			256973			217923		
Her2	130											
HSP 27				896			929			1042		
HSP 27 - phosphoSer78										91		
HSP 90	354959			1008101			629548			190069		
mTOR (FRAP)	654			1681			2108			1124		
mTOR (FRAP)- phosphoSer2448							348					
PP2A C	3471			6297			8754			6755		
PP2A C - phospho Tyr307	399			186			336			198		
ms-blk												
rb-blk												
strep	540809			1628253			1402899			1307809		
Median strep	1355354											
Correction factor	0.399017	0.399017	0.399017	1.201349	1.201349	1.201349	1.035079	1.035079	1.035079	0.964921	0.964921	0.964921

Appendix B:

Ethical Approval

L-UNIVERSITÀ TA' MALTA
Msida – Malta

Fakulta` tal-Mediċina u l-Kirurġija

UNIVERSITY OF MALTA
Msida – Malta

Faculty of Medicine and Surgery

Prof. Helen Grech
Chairperson
University of Malta Research Ethics Committee
University of Malta

Through

Dr. Mario Vassallo
Chairperson
Faculty of Medicine & Surgery Research Ethics Committee
University of Malta

11th September, 2017

Requesting approval for a PhD student to work on an ongoing ethically approved project.

With reference to the **"Biomarker-driven therapeutic groups sensitive to pp2a activators in Cancer patients" Ref: 22/2012**, we are requesting approval for Ms Maria Pia Grixti to work on this project for her PhD.

During the course of the project that started in October of 2011, we have discovered novel biomarkers that provide valuable information in defining therapeutic groups that are sensitive to pp2a activators, mainly in the Triple Negative subset of breast cancer. We would like to further investigate these biomarkers in a larger retrospective patient cohort of triple negative breast cancer cases through Dorianne's M.Sc entitled: "The Phosphatase PP2A Complex Regulates Cell Cycle in Breast Cancer Subtypes". The duration of the M.Sc is from October 2016 to October 2018 and falls within the dates of project Ref 22/2012.

Maria Pia agrees to and will abide by all data protection and UREC conditions outlined in this project.

Thanking you in advance

Dr Shawn Baldacchino
169989M
Faculty of Medicine & Surgery
University of Malta
Tel.: 9929 2530

Ms Maria Pia Grixti
ID number 316569M
Email mp.grixti@gmail.com
Tel: 79911055

Prof Godfrey Grech
Project Supervisor
Faculty of Medicine & Surgery
University of Malta

Dr James Degaetano
Consultant Hisopathologist
Department of Pathology
Mater Dei Hospital

Appendix C:

Publication

Deregulation of the protein phosphatase 2A, PP2A in cancer: complexity and therapeutic options

Godfrey Grech, Shawn Baldacchino, Christian Saliba, Maria Pia Grixti, Robert Gauci, Vanessa Petroni, Anthony G. Fenech, et al.

Tumor Biology
Tumor Markers, Tumor Targeting and Translational Cancer Research

ISSN 1010-4283

Tumor Biol.
DOI 10.1007/s13277-016-5145-4

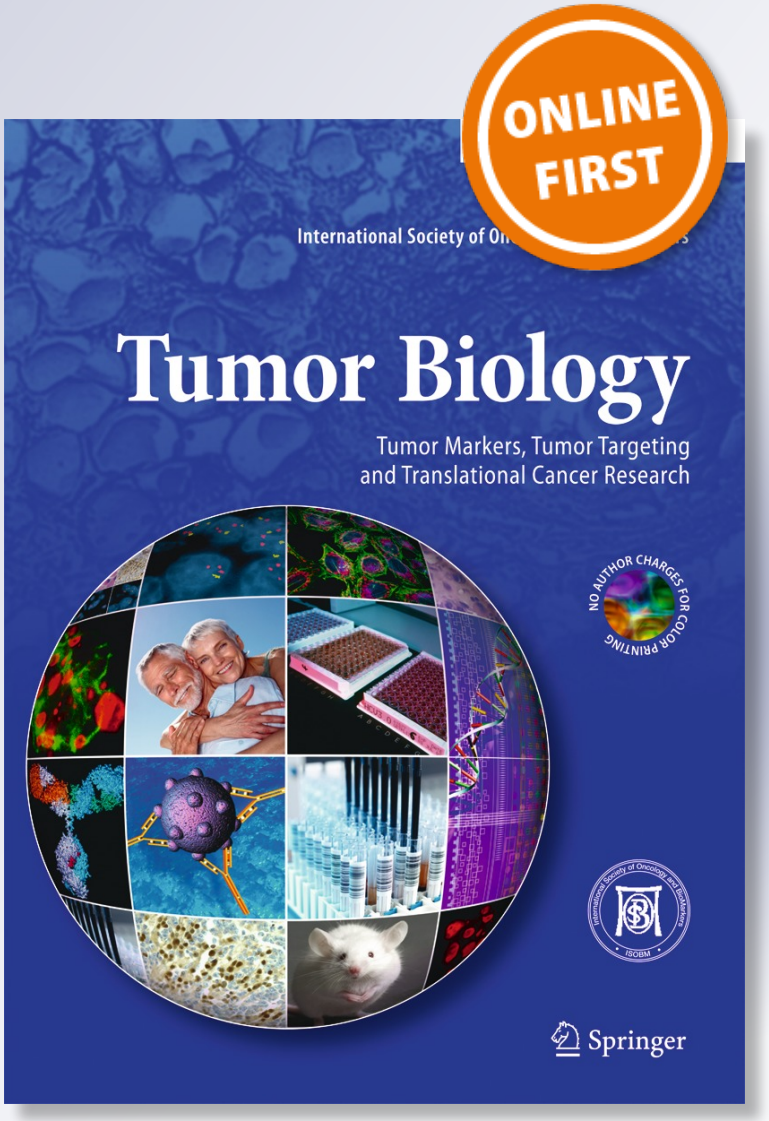

Springer

Tumor Biol.
DOI 10.1007/s13277-016-5145-4

REVIEW

Deregulation of the protein phosphatase 2A, PP2A in cancer: complexity and therapeutic options

Godfrey Grech[1] · **Shawn Baldacchino**[1] · **Christian Saliba**[2] · **Maria Pia Grixti**[1] · **Robert Gauci**[1] · **Vanessa Petroni**[3] · **Anthony G. Fenech**[4] · **Christian Scerri**[5,6]

Received: 22 March 2016 / Accepted: 11 July 2016

Abstract The complexity of the phosphatase, PP2A, is being unravelled and current research is increasingly providing information on the association of deregulated PP2A function with cancer initiation and progression. It has been reported that decreased activity of PP2A is a recurrent observation in many types of cancer, including colorectal and breast cancer (Baldacchino et al. EPMA J. 5:3, 2014; Cristobal et al. Mol Cancer Ther. 13:938–947, 2014). Since deregulation of PP2A and its regulatory subunits is a common event in cancer, PP2A is a potential target for therapy (Baldacchino et al. EPMA J. 5:3, 2014). In this review, the structural components of the PP2A complex are described, giving an in depth overview of the diversity of regulatory subunits. Regulation of the active PP2A trimeric complex, through phosphorylation and methylation, can be targeted using known compounds, to reactivate the complex. The endogenous inhibitors of the PP2A complex are highly deregulated in cancer, representing cases that are eligible to PP2A-activating drugs. Pharmacological opportunities to target low PP2A activity are available and preclinical data support the efficacy of these drugs, but clinical trials are lacking. We highlight the importance of PP2A deregulation in cancer and the current trends in targeting the phosphatase.

Keywords Molecular targets · Phosphatase activation · PP2A complex · Breast cancer · Colorectal cancer · Kinase inhibitors · Novel therapeutics

Godfrey Grech, Shawn Baldacchino and Christian Saliba contributed equally to this work.

✉ Godfrey Grech
godfrey.grech@um.edu.mt

[1] Department of Pathology, Faculty of Medicine & Surgery, Medical School, University of Malta, Msida MSD2090, Malta

[2] Centre for Molecular Medicine and Biobanking, University of Malta, Msida, Malta

[3] Department of Anatomy, Faculty of Medicine & Surgery, University of Malta, Msida, Malta

[4] Department of Clinical Pharmacology & Therapeutics, Faculty of Medicine & Surgery, University of Malta, Msida, Malta

[5] Department of Physiology and Biochemistry, Faculty of Medicine & Surgery, University of Malta, Msida, Malta

[6] Molecular Genetics Clinic, Mater Dei Hospital, Msida, Malta

Protein phosphatase 2 (PP2 or PP2A) is a member of the PPP family which is involved in the feedback of diverse signalling pathways, affecting cell growth and proliferation, cell cycle progression, apoptosis, transcription, DNA replication and translation [1–5]. PP2A is considered to be a tumour suppressor that regulates pathways crucial for cellular transformation, supported by malignant transformation of cells following inactivation of PP2A, using a simian virus 40 small t (SV40ST) mutant that specifically inactivates the phosphatase [6].

The PP2A complex is the main serine/threonine phosphatase, regulating multiple signals in mammalian cells. PP2A is a negative regulator of several signalling pathways promoting cell growth, proliferation and survival, including the phosphoinositide-3-kinase (PI3K)/Akt/mTOR, Wnt/β-catenin, c-Myc and the Ras-Raf-mitogen-activated protein (MAP)/extracellular signal-regulated kinase (ERK) family of kinases [1, 4, 6, 7]. PP2A dephosphorylates Cdc25, controlling the major DNA-responsive G2/M checkpoint, restricting entry of cells from G2 to M phase [8]. PP2A also dephosphorylates and inactivates the forkhead transcription factor, FoxM1, that controls expression of genes required for cell cycle progression through G2 phase [9]. PP2A was also shown to sustain p53-dependent apoptosis through enhanced stability of the p53 protein [10]. The apoptotic genes Bcl-2

Published online: 21 July 2016

and caspase-3 are also regulated by the PP2A complex [1, 4]. The tumour suppressor, PP2A, is important to attenuate proliferative and survival pathways, regulates cell cycle checkpoints and maintains the apoptotic capacity of the cell (Table 1). Hence, decreased activity of PP2A promotes cellular transformation.

Decreased activity of PP2A is a recurrent observation in many types of cancer, including colorectal cancer (CRC) and breast cancer [16, 17]. In fact, recent research on patients with CRC have shown that PP2A is frequently inactivated in such patients. Interestingly, the activity of PP2A is restored using FTY720, an activator of PP2A, resulting in suppressed proliferation of CRC cells, suggesting that PP2A represents a potential therapeutic target for this disease [17]. Understanding the dynamics of the PP2A complex, regulation of the endogenous inhibitors and the post-translational modifications that specifies binding of regulatory subunits will provide the means to understand the mechanisms of deregulation and targeting of the complex.

PP2A: a diversely heterogeneous complex

The predominant PP2A complex is a heterotrimer composed of an active core dimer that can exist independently, consisting of a catalytic subunit (C subunit—36 kDa), a scaffold A subunit (65 kDa) and a variable regulatory B subunit. There are two different transcripts of the A and C subunits, which are coded by different genes. The structural subunit A has two transcripts, PPP2R1A (Aα) and PPP2R1B (Aβ), that share 87 % homology and are also ubiquitously expressed and coded by genes on chromosome bands 19q13.41 and 11q23.2, respectively. Their high homology suggests similar structure and function. The α form is more abundant (90 %) than the β form (10 %), although *Xenopus* studies have shown that there are very high levels of PPP2R1B in oocytes up to fertilisation and early stages of embryogenesis. The ratio of PPP2R1B to PPP2R1A is then restored in late embryogenesis indicating a possible role in early development [18, 19]. The A subunit is composed of 15 tandem repeats of Huntington/elongation/A subunit/TOR (HEAT) making it a stable protein with an elongated architecture [20, 21].

Similarly, the α and β isoforms of the C subunit (PP2Ac) share 97 % of their sequence, and although they are both ubiquitously expressed, the α isoform is about ten times more abundant than the β isoform. The α and β isoforms are coded by the genes PPP2CA and PPP2CB on chromosome bands 5q23-q31 and 8p12-p11.2, respectively. Although the C subunit transcripts are almost identical, knockout of the PPP2CA gene leads to early embryonic death in mice, indicating that PPP2CB does not rescue this loss [22]. The C-terminus of the catalytic subunit spans residues 294–309 [18], containing two main regulated residues in this motif: the tyrosine 307 (Y307) and leucine 309 (L309), which when phosphorylated or demethylated, respectively, results in inactivation of PP2A [23–25]. Residue L309 of PP2Ac is demethylated by the phosphatase methylesterase (PME-1) and methylated by leucine carboxyl methyltransferase 1 (LCMT-1). Thus, post-translational modification of this region on PP2Ac has a role in determining the composition of the PP2A complex [26].

The B subunit is categorized into four unrelated families: B (B55/PR55), B′ (B56/PR61), B″ (PR48/72/130) and B‴ (PR93/110) which are encoded by distinct genes that give rise to various structurally related isoforms (α, β, γ, δ and ε) (Table 2). The type of B subunit bound to the core dimer determines both the substrate specificity and cellular localisation of PP2A holoenzyme complexes [30]. The B subunits of PP2A share the same binding site or have overlapping binding sites on the PP2A structural subunit A, hence explaining why the binding of one B subunit is mutually exclusive for the binding of other B subunits [20]. Substrate specificity is determined by selective recruitment of B subunits to the core dimer (A/C) [7, 31]. The variety of B subunits, encoded from all over the human genome, can form a myriad of different PP2A complexes. Different regulatory subunits are often tissue-specific. As exemplified by the B55 family, the B55α and B55β have a widespread tissue expression, whereas the B55γ and B55δ are mainly restricted to the

Table 1 Targets of PP2A and their role in carcinogenesis

Targets of PP2A	Cellular role	Reference
p53, Cdc25	Cell cycle checkpoints and regulation	[1]
PI3K/Akt	Cell proliferation and survival	[6, 11]
RAF, MAPK, ERK	Cell proliferation and survival	[4, 12, 13]
p70 S6K, mTOR	Cell proliferation, survival and translation initiation	[7, 14]
c-Myc	Tumourigenesis	[6, 15]
Wnt/β-catenin	Tumourigenesis	[1, 6]
FoxM1	Transcription factor that control expression of genes involved in the cell cycle	[9]
Bcl-2, caspase-3	Apoptosis	[4]

Table 2 The different subunits of the PP2A trimeric enzyme complex [18, 21, 27–29]

PP2A subunits					
Structural subunits, A	Regulatory subunits, B				Catalytic subunits, C
	Regulatory subunit family B	Regulatory subunit family B′	Regulatory subunit family B″	Regulatory subunit family B‴	
PPP2R1A (Aα or P65α)	PPP2R2A (B55α or PR55α)	PPP2R5A (B′56α or PR61α)	PPP2R3A (B″α or PR72α)	PPP2R4 (B‴ or PR53)	PPP2CA
PPP2R1B (Aβ or P65β)	PPP2R2B (B55β or PR55β)	PPP2R5B (B′56β or PR61β)	PPP2R3B (B″β or PR70β)	Striatin (STRN or PR110)	PPP2CB
	PPP2R2C (B55γ or PR55γ)	PPP2R5C (3 isoforms: B′56γ1, B′56γ2 and B′56γ2 or PR61γ1, PR61γ2 and PR61γ3)	PPP2R3B (PR48)	Striatin-3SG2NA (STRN3 or PR93)	
	PPP2R2D (B55δ or PR55δ)	PPP2R5D (B′56δ or PR61δ)	PPP2R3C (B″γ or PR72γ)	Striatin-4 (STRN4)	
		PPP2R5E (B′56ε or PR61ε)			

brain environment. Moreover, each distinct subunit is localised to specific areas of the brain, and furthermore shows different subcellular localisation (nuclear versus cytoplasmic).

The PPP2R5A, PPP2R5B and PPP2R5E genes of the B′56 subunit family have a nuclear export signal in the C-terminus that causes the PP2A complex to migrate to the cytoplasm. In contrast, PPP2R5C and PPP2R5D are found mainly in the nucleus as they lack the signal sequence on the C-terminus [31]. This provides evidence that compartmental PP2A activity is determined by the B subunits [21]. There may be other B subunits interacting with PP2A although some are still not adequately characterised. The S/G2 nuclear autoantigen (SG2NA) is one of these potential new members possibly in the B‴ family and is suspected to interact with the PP2A active core dimer [21].

The binding of the B subunits to the PP2A active dimer is post-translationally controlled through methylation or phosphorylation at the residues L309 and Y307, respectively. The recruitment of the B and some members of the B′ family to the active core dimer is inhibited by phosphorylation of Y307, while B″ subunit binding is unaffected. The effect of L309 methylation of the catalytic subunit of PP2A on B (B55) subunit binding is still unclear although the recruitment of B′ or B″ subunits is unaffected [31, 32]. Of interest, methylated C subunit promotes binding of the core dimer to PR55α/B [33], determining substrate specificity in vitro and the subcellular localisation of the complex in vivo [3, 6]. Suppressed methylation of the C subunit following overexpression of PME-1 or silencing of LCMT-1 results in activation of the Akt/mTOR pathway, promoting cellular transformation [34].

Aberrations of core PP2A subunits in malignancies

Scaffold subunit (PP2AA)

Genetic variations in the scaffold subunit may inhibit binding of the C and B subunits, hindering PP2A activity. PPP2R1A and PPP2R1B missense mutations or loss of heterozygosity (through homozygous deletions) has been observed in breast, lung, ovarian, colon, liver and melanoma malignancies. Loss of heterozygosity is observed in a considerable percentage of these patients and also in non-Hodgkin's lymphomas and chronic lymphocytic leukaemia although to a lesser extent [21, 35–39]. Somatic missense mutations were also detected in PPP2R1A in high-grade serous endometrial tumours [13]. A higher frequency of PPP2R1B mutations was identified in lung and breast (13 %) cancers resulting in defective attachment of the B and C subunits. In addition, low expression or loss of PPP2R1B in breast cancer contributes to transformation events [21, 40].

Regulatory subunit (PP2AB)

PPP2R2A/B55α

PPP2R2A deletions were found in 67 % of prostate cancers [41] and also reported in breast cancer and myeloma. Haploinsufficiency results in perturbed binding of B55α to the PP2A core dimer, decreasing the stability of p53, and in reduced dephosphorylation of Akt at threonine 308. In addition, inhibition of the myelocytomatosis viral oncogene (v-Myc) is suppressed, resulting in accumulation of the oncogene [42].

PPP2R5A/B'56α

Decreased expression of PPP2R5A in melanoma cells suppresses v-Myc transcriptional factor activity leading to a reduction in cellular proliferation. Dephosphorylation of v-Myc destabilizes it and leads to its rapid degradation [15].

PPP2R5C/B'56γ

Lack of adequate PP2A localisation due to the presence of a truncated form of PPP2R5C leads to an aggressive phenotype and increased metastatic potential in melanoma [15]. This is probably mediated through dephosphorylation of p70 S6K by PPP2R5C.

Catalytic subunit (PP2Ac)

Despite being very similar, the two isoforms of PP2Ac are coded by different genes and have an apparently very distinct function. Expression of the PPP2CA subunit is decreased in prostate cell lines and cancers, when compared to neighbouring normal or benign tissues [13]. Expression of a mutated PP2Ac has also been described in breast tumours positive for human epidermal growth factor 2 (HER2). This mutation, associated with phosphorylated Y307, significantly correlates with disease progression and loss of PP2A activity. Apoptosis was induced upon reactivation of PP2A activity [13].

Regulation of PP2A through binding of endogenous inhibitors

Since PP2A has an effect on a variety of cell processes, it needs to be tightly regulated. This is achieved mainly by binding of endogenously expressed inhibitory proteins. Binding of endogenous inhibitors to PP2A leads to decreased PP2A activity. Overexpression of these inhibitors is recurrently found to play a role in malignancy. The main inhibitory subunits are immunoglobin (CD79A) binding protein 1 (IGBP1; also known as α4), the nuclear oncogene SET, SET binding protein 1 (SETBP1) and cancerous inhibitor of protein phosphatase 2A (CIP2A).

IGBP1

IGBP1 is a regulatory subunit that binds and interacts with PP2A altering its activity and substrate specificity [3]. It binds to the catalytic subunit of PP2A causing its displacement from the structural A and variable B PP2A subunits. The study of Kong et al. in 2004 reported that IGBP1 deletion caused rapid cellular apoptosis, implying that IGBP1 binding attenuates PP2A activity. The interaction of IGBP1 with PP2Ac also inhibits its methylation [43].

Studies using murine erythroblast cell model resulted in identification of the key role of specific pathways to regulate the balance between proliferation and differentiation of haematopoietic progenitors. The results identified IGBP1 to be a major contributor to block erythroid differentiation. IGBP1 exerts the differentiation block by binding and suppressing the phosphatase PP2A. Interestingly, mTOR activity is maintained and, as a result, polysome recruitment of IGBP1 and hence its expression is induced [44].

SET and SETBP1

Nuclear oncogene, SET, was identified as inhibitor 2 of PP2A (I2PP2A) and has been widely implicated in leukaemogenesis. In chronic myeloid leukaemia (CML) patients, the phosphatase activity of PP2A is inhibited by the expression of the PP2A inhibitor SET. SET is overexpressed in a number of solid tumours, in CML and potentially other leukaemias. Induced suppression of SET has been reported to lead to the restoration of PP2A activity [45].

It has been shown that the reactivation of PP2A activity in these cells promoted dephosphorylation of key regulators involved in cell survival and proliferation and induced a reduction in the activity and degradation of tyrosine kinase inhibitor BCR-ABL. Hence, PP2A activation led to growth suppression, enhanced apoptosis, restored differentiation and decreased in vivo leukaemogenesis of BCR-ABL positive cells [45]. The BCR-ABL fusion is characterised by the t(9;22) translocation. BCR-ABL has been shown to enhance mTOR in an Akt-independent manner [46] and drives other pathways as MAPK and STAT5/JAK2 among other mechanisms [47] potentially through PP2A deregulation. The BCR-ABL expression is also correlated with maintenance of phosphorylation at Y307 (Y307-P) of the PP2Ac, resulting in PP2A inhibition [45]. The persistence of the PP2A Y307-P facilitates and sustains the BCR-ABL kinase activity [48].

The SET-binding protein (SETBP1 or SEB) binds to SET without hindering binding of SET to PP2A. SETBP1 protects SET from protease cleavage leading to an increase in the

availability of active full-length SET protein. SETBP1 is thus implicated in the reduction of PP2A activity and confers growth advantage in haematopoietic progenitors. It is overexpressed in acute myeloid leukaemia (AML) cases due to the t(12;18) translocation that involves the ETV6 gene [49].

SETBP1 has been found in mutated forms in colorectal carcinomas or lost in the common chromosomal aberrations at 18q21. More than 60 % of 18q21 aberrations are deletions [50] and are associated with malignant lymphoma, acute leukaemia, pancreatic carcinoma and colorectal cancer.

CIP2A

The PP2A inhibitor, CIP2A, is encoded by the KIAA1524 gene on chromosome 3q13.13. CIP2A overexpression correlates with high-grade or advanced tumour stages in breast, colon, prostate, ovarian cancers and head and neck squamous cell carcinoma [29, 51–56]. The mechanism of PP2A inhibition by CIP2A is not well annotated although some suggest that CIP2A binds to PP2Ac allosterically at its B subunit binding interface, thus altering substrate specificity and/or limiting activity [32, 36, 51, 56].

CIP2A acts by preventing PP2A-mediated dephosphorylation of the c-Myc oncoprotein leading to an increase in progenitor cell proliferation and cell renewal. PP2A dephosphorylates Myc at serine 62 which results in its ubiquitination and proteolytic degradation. CIP2A-mediated PP2A inhibition results in the stabilization of the Myc protein, resulting in increased availability of this oncoprotein [42, 51, 55, 57]. Knockdown of CIP2A led to increased PP2A activity which in turn reduces c-Myc levels.

Phosphatases as therapeutic targets in cancer

The therapeutic targeting of phosphatases exploits the cell's own mechanisms of growth suppression and promotes negative feedback mechanisms to attenuate sustained signalling. The PP2A negative feedback regulates a number of major molecules in central pathways involved in carcinogenesis (Table 1). Phosphatases are abundantly expressed in normal cells, and hence the activity of phosphatases is relatively high when compared to malignant cells with suppressed PP2A activity. Targeting malignant cells with the low PP2A activity phenotype is attractive, since the drugs have minimal effect on cells with normal phosphatase activity, providing selective tumour targeting.

Therefore, targeting a phosphatase is expected to have an effect on cellular growth and survival. This led to the development of phosphatase targets, several of which have undergone clinical trials [58–60]. However, the only FDA-approved drugs are the immunosuppressants cyclosporin A (CsA) and tacrolimus (FK506). CsA, a fungal metabolite from the fungus *Tolypocladium inflatum*, and FK506 are commonly used as immunosuppressants to prevent the rejection of organ transplants. Similar to CsA, FK506 blocks the activation of calcineurin through the formation of complexes with immunophilins [61].

The PP2A complex as a target for drug development

Suppression of PP2A activity promotes malignant transformation through various mechanisms of deregulation. Molecules that result in a decrease in the endogenous inhibitors of PP2A, inhibition of the phosphorylation and demethylation of the C-terminus of the catalytic subunit or resulting in activation of the PP2A complex in any other way are candidates for targeting tumours that are characterised with a decreased activity of PP2A (Fig. 1).

Targeting chemical modification of catalytic subunit

Inhibition of protein methylesterase 1 (PME-1) maintains methylation of the C-terminus of the catalytic subunit and hence an active PP2A heterotrimer. The aza-β-lactam, ABL127, and the sulfonyl acrylonitrile, AMZ-30, are commercially available covalent inhibitors of PME-1 [62, 63] that result in decreased cell proliferation and invasion in in vitro models of endometrial cancer [64].

The alkylating agent chloroethylnitrosourea (CENU) used as chemotherapy in various types of cancers induces PP2A methylation. CENU is a mustard gas-related β-chloronitrosourea compound. The compound eventually leads to Akt dephosphorylation, consequently reducing cell proliferation in melanoma [65].

Targeting endogenous inhibitors

SET

Apolipoprotein E (ApoE) is a major protein involved in lipid, vitamin and cholesterol transport. It also has anti-inflammatory effects and suppresses T-cell proliferation [66]. Recent studies on mitogen-treated lymphocytes and monocytes have shown that an ApoE mimetic peptide has an effect on PP2A activity [67]. This occurs via inhibitory binding to SET, thereby enhancing endogenous PP2A activity. This in turn reduces levels of phosphorylated kinases, signalling and inflammatory responses.

Fingolimod (FTY720) is a small molecule immunosuppressant which is being implemented for organ transplantation and multiple sclerosis [68]. It is an analogue of the natural compound myriocin, an amino fatty acid antibiotic derived from the thermophylic fungus *Mycelia sterilia*. FTY720 binds the sphingosine-1-phosphate receptors (S1PR) resulting in internalisation and potently decrease the movement of T-

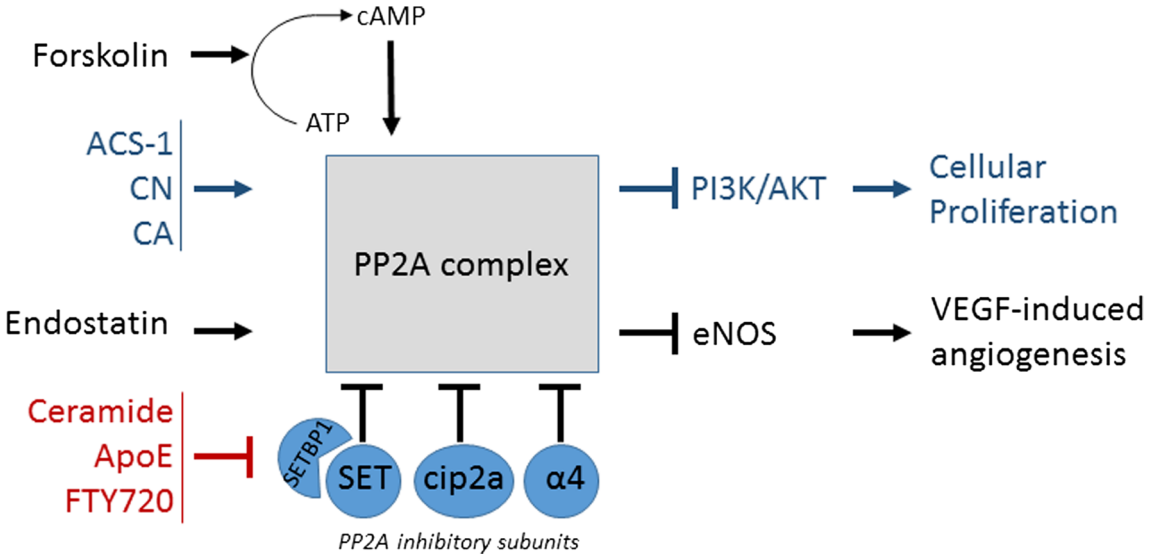

Fig. 1 Physiological inhibitory subunits suppress the activity of PP2A resulting in enhanced cellular proliferation and VEGF-induced angiogenesis. Various therapeutic options reactivate the PP2A phosphatase by acting on different subunits of the complex. *CN* chloroethylnitrosourea, *CA* carnosic acid, *eNOS* endothelial nitric oxide synthase, *ATP* adenosine triphosphate, cAMP cyclic adenosine monophosphate, *Akt* protein kinase B, *SET* Set nuclear oncogene, *CIP2A* cancerous inhibitor of protein phosphatase 2A, *α4* immunoglobin (CD79A) binding protein 1, *VEGF* vascular endothelial growth factor

lymphocytes into the freshly transplanted organs, thus preventing rejection [69]. FTY720 directly binds and disrupts repressive SET/PP2A complexes, resulting in the reactivation of the PP2A activity [70]. Studies on colorectal cancer (CRC) cell lines show that the activity of PP2A is restored using FTY720, resulting in suppressed proliferation of CRC cells [17]. Other sensitive cell lines include leukemic cell lines [71], human bladder cancer cells [72], ovarian cancer cells [73], gastric cancer cells [74] and breast cancer cells [16]. Sensitivity to FTY720 was also observed in cancer cells that are resistant to conventional chemotherapy, exemplified by sensitivity of imatinib-resitant gastrointestinal stromal tumour and myeloid cells positive for cKit mutants [75]. Of interest, OSU-2S, a non-immunosuppressive analogue of FTY720, was developed, lacking the capacity to bind to S1PR, exhibiting higher potency as an antitumour drug in hepatocellular carcinoma [76].

The phosphorylation of FTY720, a process which occurs in vivo, allows it to inhibit vascular endothelial growth factor (VEGF), consequently reducing tumour-associated angiogenesis as well as tumour cell proliferation. Of interest, FTY720 does not induce apoptosis in non-transformed cells and normal bone marrow cells. FTY720-treated leukaemia cells exhibit increased PP2A activity, leading to the dephosphorylation of various compounds, including Akt, eventually causing cell death [68].

Ceramide is known to interact with SET [77], resulting in increased PP2A activity. It is also worth considering using ceramide as a pharmacological agent, although this molecule is very quickly metabolised. However, agents that stimulate ceramide biosynthesis, such as vitamin D3, should theoretically enhance PP2A activation [78].

CIP2A

Bortezomib, a proteasome inhibitor, induced apoptosis in triple negative breast cancer (TNBC) cells and in in vivo xenograft models of TNBC, mediated by downregulation of CIP2A mRNA levels [79]. The compound celastrol directly binds and sequestrates CIP2A into a complex targeted to the ubiquitin proteasome degradation pathway, in non-small cell lung cancer cells [80]. Decreased expression of CIP2A following celastrol addition/administration induced apoptosis in cells and suppressed tumour growth in murine models. Similarly, the natural compound, ethoxysanguinarine (ESG), inhibits proliferation in lung cancer cells through the downregulation of CIP2A [81].

Molecules that upregulate expression of the catalytic and regulatory subunits

The glucocorticoid methylprednisolone has pharmacological similarity to the natural hormone produced by mammalian adrenal glands and may be used as replacement therapy in adrenal insufficiency. Its potent anti-inflammatory activity makes it useful for the management of certain forms of arthritis; skin, blood, kidney, eye, thyroid and intestinal disorders including colitis; severe allergies and asthma. Methylprednisolone is also used to treat certain types of

cancer, namely myeloid leukaemia, since it upregulates PP2A B subunits, causing cell differentiation [82].

The adenoviral E1A mediates sensitization to a variety of anticancer drug, inducing apoptosis in different cancer cell models. The mechanisms by which this takes place occur via multiple pathways. However, studies in human breast cancer cell lines have shown that E1A upregulates PP2A C subunits, eventually leading to apoptosis [83].

Activators of PP2A with unknown mechanism

The recent research on oestrogen receptor (ER) negative breast cancer has shown that nitric oxide (NO) promotes cancer progression by activating various signalling pathways, including the PI3K/Akt pathway [84] and VEGF-induced angiogenesis [85]. Of interest, endostatin activates PP2A, which is known to directly dephosphorylate endothelial NO synthase (eNOS) at Ser1177, a phosphorylation event promoted by VEGF. Hence, endostatin suppresses endothelial cell (EC) migration, acting as an anti-angiogenic factor. Such findings shed light on the possibility of targeting PP2A with therapeutic agents. Various agents are being described and illustrated in Fig. 1.

A plausible therapeutic agent for PP2A activation is forskolin, a labdane diterpene produced by the Indian coleus plant *Coleus forskohlii*. Forskolin resensitizes cell receptors by increasing the intracellular levels of cAMP. The latter is an important signal carrier necessary for the proper biological response of cells to hormones and other extracellular signals. Forskolin also has an effect on PP2A. It leads to PP2A activation, effectively antagonizing leukaemogenesis in both in vitro and in vivo models of these cancers [86].

Dithiolethiones are a well-known class of cancer chemopreventive agents, found commonly in vegetables, including broccoli. Although the clinical application of oltipraz, a typical dithiolethione, in smokers, revealed adverse side effects, anethole dithiolethione (ADT) proved to be a safer compound and is now clinically used for xerostomia [87]. A dithiolethione compound, closely related in structure to ADT, is ACS-1. The latter was found to inhibit Akt signalling in human breast and lung cancer cells by increasing PP2A activity and consequently inhibiting cell proliferation, suggesting the use of this molecule as a therapeutic agent for cancer therapy.

Carnosic acid is a natural polyphenolic diterpene found in rosemary (*Rosmarinus officinalis*) and common sage (*Salvia officinalis*). Dried leaves of rosemary or sage contain 1.5 to 2.5 % carnosic acid, which is recognised to be a potent antioxidant and exerts a protective effect on skin cells against UV-A radiation. Studies carried out in prostate cancer in vitro showed that carnosic acid also activates PP2A and consequently downregulates Akt [88].

Of interest, a novel class of small molecule activators of PP2A (SMAPs) developed by reverse engineering of tricyclic neuroleptic drugs, directly bind and activate PP2A and showed favourable antitumour properties in preclinical models of prostate cancer and lung cancer [89].

Conclusion

Inhibition of kinases has been utilised extensively as therapeutic agents in the oncology field. The occurrence of acquired resistance of tyrosine kinase inhibitors prompts for alternative drug development strategies. This review provides the knowledge base for considering the use of phosphatase activators in a subset of cancer patients classified on the basis of a suppressed activity of the PP2A phosphatase. This review focused on potential therapeutic agents that reactivate suppressed PP2A activity. Potentially therapeutic groups include a subset of tumours with haploinsufficiency due to mutations in the PP2A core complex, deactivation of the PP2A complex due to phosphorylation and demethylation of the catalytic subunit or increased expression of endogenous inhibitors of the PP2A complex. Considering the knowledge gained in modulating the activity of PP2A, the lack of clinical trials utilising PP2A activators in cancer is disappointing. Of interest, inhibition of PP2A as a potential therapeutic option is currently being investigated and a clinical trial is recruiting patients resistant to conventional treatments. The rationale towards using PP2A inhibitors stems from the function of PP2A to attenuate RAS signalling during G2 phase, promoting stable quiescence [90]. Hence, inhibition of PP2A using a small molecular inhibitor, LB-100, overcomes quiescence and sensitizes mitotic cells to combinatory treatment [91].

The future challenges include the definition of biomarker panels required to classify potential therapeutic groups, followed by well-structured clinical trials.

Compliance with ethical standards

Conflicts of interest None.

References

1. Zhang Q, Claret FX. Phosphatases: the new brakes for cancer development? Enzym Res. 2012;2012:1–11.
2. Qi Z, Yang W, Liu Y, Cui T, Gao H, et al. Loss of PINK1 function decreases PP2A activity and promotes autophagy in dopaminergic cells and a murine model. Neurochem Int. 2011;59:572–81.
3. Kloeker S, Reed R, McConnell JL, Chang D, Tran K, et al. Parallel purification of three catalytic subunits of the protein serine/threonine phosphatase 2A family (PP2AC, PP4C, and PP6C) and

analysis of the interaction of PP2AC with alpha4 protein. Protein Expr Purif. 2003;31:19–33.
4. Silverstein AM. Actions of PP2A on the MAP kinase pathway and apoptosis are mediated by distinct regulatory subunits. Proc Natl Acad Sci. 2002;99:4221–6.
5. Peyssonnaux C, Eychene A. The Raf/MEK/ERK pathway: new concepts of activation. Biol Cell. 2001;93:53–62.
6. Sablina A, Hector M, Colpaert N, Hahn WC. Identification of PP2A complexes and pathways involved in cell transformation. Cancer Res. 2010;70:10474–84.
7. Hahn K, Miranda M, Francis VA, Vendrell J, Zorzano A, et al. PP2A regulatory subunit PP2A-B′ counteracts S6K phosphorylation. Cell Metab. 2010;11:438–44.
8. Margolis SS, Perry JA, Forester CM, Nutt LK, Guo Y, et al. Role for the PP2A/B56delta phosphatase in regulating 14-3-3 release from Cdc25 to control mitosis. Cell. 2006;127:759–73.
9. Alvarez-Fernandez M, Halim VA, Aprelia M, Mohammed S, Medema RH. Protein phosphatase 2A (B55) prevents premature activation of forkhead transcription factor FoxM1 by antagonizing cyclin A/cyclin-dependent kinase-mediated phosphorylation. J Biol Chem. 2011;286:33029–36.
10. Jin Z, Wallace L, Harper SQ, Yang J. PP2A:B56{epsilon}, a substrate of caspase-3, regulates p53-dependent and p53-independent apoptosis during development. J Biol Chem. 2010;285:34493–502.
11. Alessi DR, Andjelkovic M, Caudwell B, Cron P, Morrice N, et al. Mechanism of activation of protein kinase B by insulin and IGF-1. EMBO J. 1996;15:6541–51.
12. Puustinen P, Junttila MR, Vanhatupa S, Sablina AA, Hector ME, et al. PME-1 protects extracellular signal-regulated kinase pathway activity from protein phosphatase 2A-mediated inactivation in human malignant glioma. Cancer Res. 2009;69:2870–7.
13. Stebbing J, Lit LC, Zhang H, Darrington RS, Melaiu O, et al. (2013) The regulatory roles of phosphatases in cancer. Oncogene.
14. Ismail HMS, Myronova O, Tsuchiya Y, Niewiarowski A, Tsaneva I, et al. Identification of the general transcription factor Yin Yang 1 as a novel and specific binding partner for S6 kinase 2. Cell Signal. 2013;25:1054–63.
15. Mumby M. PP2A: unveiling a reluctant tumor suppressor. Cell. 2007;130:21–4.
16. Baldacchino S, Saliba C, Petroni V, Fenech AG, Borg N, et al. Deregulation of the phosphatase, PP2A is a common event in breast cancer, predicting sensitivity to FTY720. EPMA J. 2014;5:3.
17. Cristobal I, Manso R, Rincon R, Carames C, Senin C, et al. PP2A inhibition is a common event in colorectal cancer and its restoration using FTY720 shows promising therapeutic potential. Mol Cancer Ther. 2014;13:938–47.
18. Seshacharyulu P, Pandey P, Datta K, Batra SK. Phosphatase: PP2A structural importance, regulation and its aberrant expression in cancer. Cancer Lett. 2013;335:9–18.
19. Ruediger R, Hentz M, Fait J, Mumby M, Walter G. Molecular model of the A subunit of protein phosphatase 2A: interaction with other subunits and tumor antigens. J Virol. 1994;68:123–9.
20. Hemmings BA, Adams-Pearson C, Maurer F, Mueller P, Goris J, et al. Alpha- and beta-forms of the 65-kDa subunit of protein phosphatase 2A have a similar 39 amino acid repeating structure. Biochemistry. 1990;29:3166–73.
21. Janssens V, Goris J, Van Hoof C. PP2A: the expected tumor suppressor. Curr Opin Genet Dev. 2005;15:34–41.
22. Gu P, Qi X, Zhou Y, Wang Y, Gao X. Generation of Ppp2Ca and Ppp2Cb conditional null alleles in mouse. Genesis. 2012;50:429–36.
23. Chen J, Martin BL, Brautigan DL. Regulation of protein serine-threonine phosphatase type-2A by tyrosine phosphorylation. Science. 1992;257:1261–4.
24. Sontag J-M, Nunbhakdi-Craig V, Mitterhuber M, Ogris E, Sontag E. Regulation of protein phosphatase 2A methylation by LCMT1 and PME-1 plays a critical role in differentiation of neuroblastoma cells. J Neurochem. 2010;115:1455–65.
25. Sents W, Ivanova E, Lambrecht C, Haesen D, Janssens V. The biogenesis of active protein phosphatase 2A holoenzymes: a tightly regulated process creating phosphatase specificity. FEBS J. 2013;280:644–61.
26. Stanevich V, Jiang L, Satyshur KA, Li Y, Jeffrey PD, et al. The structural basis for tight control of PP2A methylation and function by LCMT-1. Mol Cell. 2011;41:331–42.
27. (2013) GeneCards—The human gene compendium.
28. Gray KA, Daugherty LC, Gordon SM, Seal RL, Wright MW, et al. Genenames.org: the HGNC resources in 2013. Nucleic Acids Res. 2013:41.
29. Laine A. The role of an oncoprotein cip2a in breast carcinoma. Turku: University of Turku; 2013.
30. Kong M, Fox CJ, Mu J, Solt L, Xu A, et al. The PP2A-associated protein alpha4 is an essential inhibitor of apoptosis. Science. 2004;306:695–8.
31. Slupe AM, Merrill RA, Strack S. Determinants for substrate specificity of protein phosphatase 2A. Enzym Res. 2011;2011:1–8.
32. Xu Y, Xing Y, Chen Y, Chao Y, Lin Z, et al. Structure of the protein phosphatase 2A holoenzyme. Cell. 2006;127:1239–51.
33. Yu XX, Du X, Moreno CS, Green RE, Ogris E, et al. Methylation of the protein phosphatase 2A catalytic subunit is essential for association of Balpha regulatory subunit but not SG2NA, striatin, or polyomavirus middle tumor antigen. Mol Biol Cell. 2001;12:185–99.
34. Jackson JB, Pallas DC. Circumventing cellular control of PP2A by methylation promotes transformation in an Akt-dependent manner. Neoplasia. 2012;14:585–99.
35. Calin GA, Iasio MG, Caprini E, Vorechovsky I, Natali PG, et al. Low frequency of alterations of the α (PPP2R1A) and β (PPP2R1B) isoforms of the subunit A of the serine-threonine phosphatase 2A in human neoplasms. Oncogene. 2000;19:1191–5.
36. Ruediger R, Ruiz J, Walter G. Human cancer-associated mutations in the A α subunit of protein phosphatase 2A increase lung cancer incidence in A α knock-in and knockout mice. Mol Cell Biol. 2011;31:3832–44.
37. Wang SS, Esplin ED, Li JL, Huang L, Evans GA. Alterations of the PPP2R1B gene in human lung and colon cancer. Science. 1998;282:284–7.
38. Takagi Y, Futamura M, Yamaguchi K, Aoki S, Takahashi T, et al. Alterations of the PPP2R1B gene located at 11q23 in human colorectal cancers. Gut. 2000;47:268–71.
39. Chou H-C, Chen C-H, Lee H-S, Lee C-Z, Huang G-T, et al. Alterations of tumour suppressor gene PPP2R1B in hepatocellular carcinoma. Cancer Lett. 2007;253:138–43.
40. Sablina AA, Chen W, Arroyo JD, Corral L, Hector M, et al. The tumor suppressor PP2A Aβ regulates the RalA GTPase. Cell. 2007;129:969–82.
41. Cheng Y, Liu W, Kim S-T, Sun J, Lu L, et al. Evaluation of PPP2R2A as a prostate cancer susceptibility gene: a comprehensive germline and somatic study. Cancer Genet. 2011;204:375–81.
42. Niemelä M, Kauko O, Sihto H, Mpindi JP, Nicorici D, et al. CIP2A signature reveals the MYC dependency of CIP2A-regulated phenotypes and its clinical association with breast cancer subtypes. Oncogene. 2012;31:4266–78.
43. Migueleti DLS, Smetana JHC, Nunes HF, Kobarg J, Zanchin NIT. Identification and characterization of an alternatively spliced isoform of the human protein phosphatase 2A catalytic subunit. J Biol Chem. 2011;287:4853–62.
44. Grech G, Blazquez-Domingo M, Kolbus A, Bakker WJ, Mullner EW, et al. Igbp1 is part of a positive feedback loop in stem cell factor-dependent, selective mRNA translation initiation inhibiting erythroid differentiation. Blood. 2008;112:2750–60.

45. Neviani P, Santhanam R, Trotta R, Notari M, Blaser BW, et al. The tumor suppressor PP2A is functionally inactivated in blast crisis CML through the inhibitory activity of the BCR/ABL-regulated SET protein. Cancer Cell. 2005;8:355–68.
46. Markova B, Albers C, Breitenbuecher F, Melo JV, Brümmendorf TH, et al. Novel pathway in Bcr-Abl signal transduction involves Akt-independent, PLC-γ1-driven activation of mTOR/p70S6-kinase pathway. Oncogene. 2009;29:739–51.
47. O'Hare T, Deininger MWN, Eide CA, Clackson T, Druker BJ. Targeting the BCR-ABL signaling pathway in therapy-resistant Philadelphia chromosome-positive leukemia. Clin Cancer Res. 2010;17:212–21.
48. Lucas CM, Harris RJ, Giannoudis A, Copland M, Slupsky JR, et al. Cancerous inhibitor of PP2A (CIP2A) at diagnosis of chronic myeloid leukemia is a critical determinant of disease progression. Blood. 2011;117:6660–8.
49. Barjesteh van Waalwijk van Doorn-Khosrovani S, Spensberger D, de Knegt Y, Tang M, Lowenberg B, et al. Somatic heterozygous mutations in ETV6 (TEL) and frequent absence of ETV6 protein in acute myeloid leukemia. Oncogene. 2005;24:4129–37.
50. Minakuchi M, Kakazu N, Gorrin-Rivas MJ, Abe T, Copeland TD, et al. Identification and characterization of SEB, a novel protein that binds to the acute undifferentiated leukemia-associated protein SET. Eur J Biochem. 2001;268:1340–51.
51. Junttila MR, Puustinen P, Niemelä M, Ahola R, Arnold H, et al. CIP2A inhibits PP2A in human malignancies. Cell. 2007;130:51–62.
52. Vaarala MH, Väisänen M-R, Ristimäki A. CIP2A expression is increased in prostate cancer. J Exp Clin Cancer Res. 2010;29:136.
53. Böckelman C, Lassus H, Hemmes A, Leminen A, Westermarck J, et al. Prognostic role of CIP2A expression in serous ovarian cancer. Br J Cancer. 2011;105:989–95.
54. Teng H-W, Yang S-H, Lin J-K, Chen W-S, Lin T-C, et al. CIP2A is a predictor of poor prognosis in colon cancer. J Gastrointest Surg. 2012;16:1037–47.
55. Come C, Laine A, Chanrion M, Edgren H, Mattila E, et al. CIP2A is associated with human breast cancer aggressivity. Clin Cancer Res. 2009;15:5092–100.
56. Wang J, Li W, Li L, Yu X, Jia J, et al. CIP2A is over-expressed in acute myeloid leukaemia and associated with HL60 cells proliferation and differentiation. Int J Lab Hematol. 2011;33:290–8.
57. Mannava S, Omilian AR, Wawrzyniak JA, Fink EE, Zhuang D, et al. PP2A-B56α controls oncogene-induced senescence in normal and tumor human melanocytic cells. Oncogene. 2011;31:1484–92.
58. Lazar DF, Saltiel AR. Lipid phosphatases as drug discovery targets for type 2 diabetes. Nat Rev Drug Discov. 2006;5:333–42.
59. Lyon MA, Ducruet AP, Wipf P, Lazo JS. Dual-specificity phosphatases as targets for antineoplastic agents. Nat Rev Drug Discov. 2002;1:961–76.
60. Tonks NK. Protein tyrosine phosphatases: from genes, to function, to disease. Nat Rev Mol Cell Biol. 2006;7:833–46.
61. Liu J, Farmer Jr JD, Lane WS, Friedman J, Weissman I, et al. Calcineurin is a common target of cyclophilin-cyclosporin A and FKBP-FK506 complexes. Cell. 1991;66:807–15.
62. Bachovchin DA, Zuhl AM, Speers AE, Wolfe MR, Weerapana E, et al. Discovery and optimization of sulfonyl acrylonitriles as selective, covalent inhibitors of protein phosphatase methylesterase-1. J Med Chem. 2011;54:5229–36.
63. Bachovchin DA, Mohr JT, Speers AE, Wang C, Berlin JM, et al. Academic cross-fertilization by public screening yields a remarkable class of protein phosphatase methylesterase-1 inhibitors. Proc Natl Acad Sci U S A. 2011;108:6811–6.
64. Pusey M, Bail S, Xu Y, Buiakova O, Nestor M, et al. (2016) Inhibition of protein methylesterase 1 decreased cancerous phenotypes in endometrial adenocarcinoma cell lines and xenograft tumor models. Tumour Biol.
65. Madhunapantula SV, Robertson GP. Therapeutic implications of targeting AKT signaling in melanoma. Enzyme Res. 2011;2011:327923.
66. Hwang YY, Liang RH. An update in management of noncutaneous T-cell lymphomas. Adv Hematol. 2010;2010:424786.
67. Christensen DJ, Ohkubo N, Oddo J, Van Kanegan MJ, Neil J, et al. Apolipoprotein E and peptide mimetics modulate inflammation by binding the SET protein and activating protein phosphatase 2A. J Immunol. 2011;186:2535–42.
68. Neviani P, Santhanam R, Oaks JJ, Eiring AM, Notari M, et al. FTY720, a new alternative for treating blast crisis chronic myelogenous leukemia and Philadelphia chromosome-positive acute lymphocytic leukemia. J Clin Invest. 2007;117:2408–21.
69. Chiba K. FTY720, a new class of immunomodulator, inhibits lymphocyte egress from secondary lymphoid tissues and thymus by agonistic activity at sphingosine 1-phosphate receptors. Pharmacol Ther. 2005;108:308–19.
70. Pippa R, Dominguez A, Christensen DJ, Moreno-Miralles I, Blanco-Prieto MJ, et al. Effect of FTY720 on the SET-PP2A complex in acute myeloid leukemia; SET binding drugs have antagonistic activity. Leukemia. 2014;28:1915–8.
71. Cristobal I, Garcia-Orti L, Cirauqui C, Alonso MM, Calasanz MJ, et al. PP2A impaired activity is a common event in acute myeloid leukemia and its activation by forskolin has a potent anti-leukemic effect. Leukemia. 2011;25:606–14.
72. Azuma H, Takahara S, Horie S, Muto S, Otsuki Y, et al. Induction of apoptosis in human bladder cancer cells in vitro and in vivo caused by FTY720 treatment. J Urol. 2003;169:2372–7.
73. Zhang N, Qi Y, Wadham C, Wang L, Warren A, et al. FTY720 induces necrotic cell death and autophagy in ovarian cancer cells: a protective role of autophagy. Autophagy. 2010;6:1157–67.
74. Zheng T, Meng X, Wang J, Chen X, Yin D, et al. PTEN- and p53-mediated apoptosis and cell cycle arrest by FTY720 in gastric cancer cells and nude mice. J Cell Biochem. 2010;111:218–28.
75. Dumont AG, Reynoso DG, Trent JC. Essential requirement for PP2A inhibition by the oncogenic receptor c-KIT suggests PP2A reactivation as a strategy to treat c-KIT+ cancers—letter. Cancer Res. 2011;71:2403 .author reply 2404
76. Omar HA, Chou CC, Berman-Booty LD, Ma Y, Hung JH, et al. Antitumor effects of OSU-2S, a nonimmunosuppressive analogue of FTY720, in hepatocellular carcinoma. Hepatology. 2011;53:1943–58.
77. Mukhopadhyay A, Saddoughi SA, Song P, Sultan I, Ponnusamy S, et al. Direct interaction between the inhibitor 2 and ceramide via sphingolipid-protein binding is involved in the regulation of protein phosphatase 2A activity and signaling. FASEB J. 2009;23:751–63.
78. Switzer CH, Cheng RY, Vitek TM, Christensen DJ, Wink DA, et al. Targeting SET/I(2)PP2A oncoprotein functions as a multi-pathway strategy for cancer therapy. Oncogene. 2011;30:2504–13.
79. Tseng LM, Liu CY, Chang KC, Chu PY, Shiau CW, et al. CIP2A is a target of bortezomib in human triple negative breast cancer cells. Breast Cancer Res. 2012;14:R68.
80. Liu Z, Ma L, Wen ZS, Hu Z, Wu FQ, et al. Cancerous inhibitor of PP2A is targeted by natural compound celastrol for degradation in non-small-cell lung cancer. Carcinogenesis. 2014;35:905–14.
81. Liu Z, Ma L, Wen ZS, Cheng YX, Zhou GB. Ethoxysanguinarine induces inhibitory effects and downregulates CIP2A in lung cancer cells. ACS Med Chem Lett. 2014;5:113–8.
82. Uzunoglu S, Uslu R, Tobu M, Saydam G, Terzioglu E, et al. Augmentation of methylprednisolone-induced differentiation of myeloid leukemia cells by serine/threonine protein phosphatase inhibitors. Leuk Res. 1999;23:507–12.
83. Liao Y, Hung MC. A new role of protein phosphatase 2a in adenoviral E1A protein-mediated sensitization to anticancer drug-induced apoptosis in human breast cancer cells. Cancer Res. 2004;64:5938–42.

84. Switzer CH, Glynn SA, Ridnour LA, Cheng RY, Vitek MP, et al. Nitric oxide and protein phosphatase 2A provide novel therapeutic opportunities in ER-negative breast cancer. Trends Pharmacol Sci. 2011;32:644–51.
85. Urbich C, Reissner A, Chavakis E, Dernbach E, Haendeler J, et al. Dephosphorylation of endothelial nitric oxide synthase contributes to the anti-angiogenic effects of endostatin. FASEB J. 2002;16: 706–8.
86. Perrotti D, Neviani P. Protein phosphatase 2A (PP2A), a drugable tumor suppressor in Ph1(+) leukemias. Cancer Metastasis Rev. 2008;27:159–68.
87. Switzer CH, Ridnour LA, Cheng RY, Sparatore A, Del Soldato P, et al. Dithiolethione compounds inhibit Akt signaling in human breast and lung cancer cells by increasing PP2A activity. Oncogene. 2009;28:3837–46.
88. Kar S, Palit S, Ball WB, Das PK. Carnosic acid modulates Akt/IKK/NF-kappaB signaling by PP2A and induces intrinsic and extrinsic pathway mediated apoptosis in human prostate carcinoma PC-3 cells. Apoptosis. 2012;17:735–47.
89. McClinch K, Avelar R, Callejas D, Kastrinsky D, Ohlmeyer M, Plymate S, et al. Therapeutic reactivation of PP2A for prostate cancer treatment; 2015 Nov 5–9; Boston, MA. Philadelphia (PA): Molecular targets and cancer therapeutics.
90. Naetar N, Soundarapandian V, Litovchick L, Goguen KL, Sablina AA, et al. PP2A-mediated regulation of Ras signaling in G2 is essential for stable quiescence and normal G1 length. Mol Cell. 2014;54:932–45.
91. Hong CS, Ho W, Zhang C, Yang C, Elder JB, et al. LB100, a small molecule inhibitor of PP2A with potent chemo- and radiosensitizing potential. Cancer Biol Ther. 2015;16:821–33.